ECHO PATTERN FORMATION IN A HIGH RESOLUTION MULTISTATIC SONAR

By

David Morris M.Sc.

A Doctoral Thesis

Submitted in partial fulfilment of the requirements

for the award of

Doctor of Philosophy of the Loughborough University of Technology

July 1979

Supervisor: I. A. Dempster, B.Sc., Ph.D

Department of Electronic and Electrical Engineering

ACKNOWLEDGEMENTS

This work was conducted while the author was a postgraduate student in the Department of Electronic and Electrical Engineering, Loughborough University of Technology, Loughborough, Leicestershire.

The author would like to sincerely thank his supervisor Dr I A Dempster, for the continuous help and assistance given by him, which came in the form of many useful discussions, guidance and suggestions throughout the project. The author would also like to thank Professor J W R Griffiths for guidance and suggestions during the early part of the project, and for support and facilities throughout.

Many colleagues in the Department also contributed immeasurably, through discussion groups and private talks, to the success of the work.

TABLE OF CONTENTS

SYNOPSIS

More emphasis is falling on sonar systems to display the data received from the underwater environment in a form which enables the observer to classify the echo patterns as being due to a particular target shape. In high resolution monostatic sonar systems, where the resolution cell is smaller than the target dimensions, difficulties arise because the echo patterns formed tend to be specular in nature and show only the acoustic highlights of the target.

In this thesis, echo formation is examined in terms of the angular distribution of reflected energy in the medium. The way in which echoes are formed results in a less than optimum display in terms of the number of samples of the target outline. An increase in the number of resolution cells displaying the target outline and an improvement in target shape portrayal can be obtained by using a multistatic sonar system, but it is shown that this improvement is dependent on a number of factors.

An experimental, high resolution multistatic sonar system is described which was used to verify and measure the improvement in target shape portrayal. Selected echo patterns obtained with this equipment are shown and the measured performance compared with the predicted performance. An empirical equation, which was derived from the measurements, relates the improvement in the displayed echo patterns to the number of bistatic receivers employed.

LIST OF SYMBOLS

CHAPTER I

$s(t)$ – transmitted signal.

$R_t(t)$ – target impulse response.

$y(t)$ – reflected signal.

D – rectangular surveillance area.

N – number of resolution cells in D.

T – area of target.

C_t – target outline enclosing T.

CHAPTER II

Q – area of a resolution cell.

m – number of resolution cells coinciding with the outline C_t, and called the 'display magnification'.

I – information level in bits of the surveillance area.

b – the number of detected cells in the surveillance area ($b < m$).

L – the display loss factor, relating the number of detected cells to the 'display magnification'.

L_{Max} – the maximum loss factor, defined by the 'display magnification'.

A_I – incident plane wave complex amplitude.

θ_I – angle of incidence between A_I and reflecting plane.

$f_I(x)$ – complex amplitude and phase function across reflecting plane, set up by A_I.

R – reflection coefficient.

$f_R(x)$ – reflected amplitude and phase function across reflection plane.

$A_R(\theta)$ – reflected plane wave complex angular spectrum.

$F_R(S)$ – reflected plane wave complex angular spectrum identical to $A_R(\theta)$ but expressed in terms of sin (θ).

$G(S)$ – allpass propagation function for a lossless, uniform medium.

CHAPTER III

$H(f)$ – receiver frequency response.

$S(f)$ – signal frequency response.

$b(t)$ – output of bias network.

$q(t)$ – output of receiver filters.

B – positive dc bias voltage.

V_t – positive threshold voltage.

X_I, Y_I – input echo co-ordinates.

X_R, Y_R – reference echo co-ordinates having the same azimuth bearing as X_I, Y_I.

X_D, Y_D – a difference vector formed from X_I, Y_I and X_R, Y_R.

T_x, T_y – a tolerance used to test X_D, Y_D.

PL – total path length travelled by a transmitted pulse from transmitter to target to receiver.

DB – length of data base from transmitter to receiver.

Φ – angle between transmitter beam and the data base.

LIST OF TABLES

LIST OF FIGURES

CHAPTER I

INTRODUCTION

1.1 The sonar system functions

Sonar systems have evolved from early sets employing audio detection methods for target recognition, to present day systems employing highly sophisticated time domain correlation receivers and a variety of information display techniques. Throughout these progressive stages of development, the functions of the sonar equipment have remained the same and can be stated as,

(a) detection of target like echoes,

(b) localisation of detected echoes,

and (c) classification of detected echoes.

These three objectives are self explanatory. However, the processes involved in achieving them are related and interdependent. An overlapping of the operations occurs which means that the performance of a particular post-detection echo classification scheme depends to a large extent on the performance of the receiver or initial detection device. For example, if an increase in the receiver signal processing gain of say 3 dB is achieved, then the subsequent classification process can operate with a 3 dB increase in signal dynamic range. This, in turn, means that additional echoes which would normally be undetected against background noise can now be utilised in the classification process. In this thesis, echo classification is regarded as an overall system function rather than as the final operation in the signal processing chain, and in the work to be presented echo pattern formation by the sonar is considered from a system performance viewpoint.

1.2 Sonar displays

The sonar display is usually the final link in the signal processing chain and refers to the device or devices which interface to the human

observer in the system. All displays have the objective of aiding the observer in interpreting the information about the underwater environment which the sonar system provides. Emphasis is falling increasingly on the display techniques and signal processing to extract and present data to the observer in a form which optimises not simply the process of detecting targets in noisy backgrounds, but in addition, the correct classification of the detected echo pattern as being due to a particular shape or form.

The information which is presented to the observer can usually be placed in one or more of the three categories below.

(a) Geometrical or spatial information. For example the plan position indicator (ppi) display.

(b) Time series information. For example a simple A-scan range display.

(c) Frequency domain information. For example a power spectrogram for a passive sonar.

Of various ways in which the data can be presented to the observer, the visual display, in the form of a ppi or B-scan, is the most widely used. There are slight differences between the ppi and B-scan type of displays, but in general the information presented on this type of display is in the form of echo patterns which are displayed in the relative spatial locations in which they actually occur in the medium. This method of displaying the data is an attempt to present the echo patterns in a form which is similar to a horizontal section of the environment when illuminated by the more familiar lightwaves. Such a display is the natural choice if it is desired to utilise the pattern recognition capabilities of the human observer.

The work to be described here is concerned mainly with the presentation of geometrical data to the observer. Use is made exclusively of the familiar ppi display for this purpose as the main output device in the experimental system to be described.

1.3 Echo patterns on the display

The phrase 'echo patterns' has been used in the preceding section in conjunction with a brief discussion on the output information display. In a wide sense the echo pattern can refer to the ensemble of 'paints' on a ppi display occurring during one complete transmission cycle, ie the time between successive 'pings'. In the context of this work however the term refers to a much more localised event. Namely, the cluster of echoes which are considered to arise due to one isolated target. Implicit in this meaning of the phrase is the assumption that the sonar is capable of producing a cluster of echoes from one target. In other words, it must be capable of resolving individual echo producing regions on the target.

The resolving power of any sonar is an important parameter. It is usually expressed in terms of the resolution cell dimensions for the system. The resolution cell can be a four-dimensional volume describing the range, doppler, horizontal and vertical angular resolutions available at the output of the sonar, and is a function of the receiver bandwidth, transmitted signal parameters, and sound projector and receiver dimensions. In this work only static targets were studied, and no attempt was made to resolve in the vertical plane for the reasons given in section 1.6 below. The four-dimension resolution cell therefore reduced to a two-dimensional area defined by the range and azimuthal resolution of the system.

In order that the sonar be capable of producing a cluster of independent echoes from one target, a large number of resolution cells must be contained within or overlay the area of the target. If the target lies entirely within a resolution cell, neglecting for the moment possible range and bearing ambiguity, then a single echo can be expected from the corresponding cell. As the cell size is decreased in relation to the target, always assuming that the echoes are detected, more echoes will

appear and ideally, the target shape will be displayed with increasing clarity.

An example of an idealised echo pattern display is shown in figure 1.1. This sequence of displays was synthesised from a plan projection of two target shapes as shown in figure 1.1(a). The set of figures 1.1(a) to 1.1(d) illustrate the effect of a relative decrease in the total number of picture elements, or resolution cells, in the target area. A transition can be seen between a well defined display of two distinct shapes to an ambiguous display with no target shape portrayal. The displays are binary in nature, each cell is either on or off, in keeping with the type of display used in the experiments to be described. The two ends of the sequence (a) and (d) highlight respectively, the high resolution and low resolution cases in terms of the number of spatial samples of the target area. No attempt has been made to define the absolute spatial dimensions involved because the problem of classification shown here is one of relative resolution rather than absolute resolution. In other words, if the targets which it is desired to classify or differentiate are sufficiently unrelated in terms of their geometric shapes then it is possible that they could be classified at level (c) for example. The absolute definition of a target echo pattern does, of course, depend upon the absolute spatial sampling rate in the target area. Additionally, an important aspect is the ratio of target surface roughness to the wavelength of the acoustic energy. If it is desired to resolve small surface irregularities on a target in order to classify it, then a correspondingly high bandwidth and short wavelength must be employed.

However, in traversing the scale of events from (d) to (a), by increasing the range and angular resolution, the response of the system does not necessarily conform to that depicted in this idealised sequence for a number of reasons. Firstly, the range and bearing ambiguities

THIS SYNTHETIC DISPLAY SEQUENCE SHOWS THE APPROX. RESOLUTION OF THE EXPERIMENTAL SYSTEM COMPARED TO OTHERS REFERRED TO IN THE TEXT

(a)

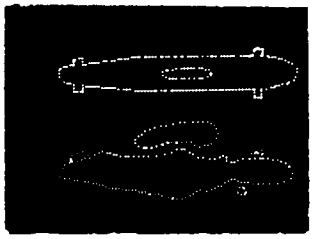

THIS DEPICTS THE MAX. DISPLAY ACCURACY AVAILABLE FROM THE DISPLAY FORMATTING PROGRAM (SEE CHAPTER 3)

(b)

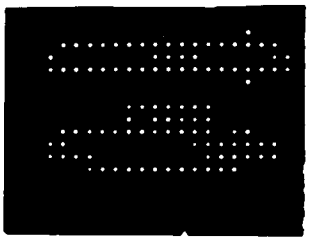

THIS DEPICTS THE RELATIVE RESOLUTION CELL SIZE USED IN THIS WORK

(c)

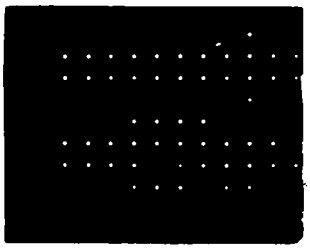

THIS DEPICTS THE RELATIVE RESOLUTION CELL SIZE USED IN REFERENCE 1

(d)

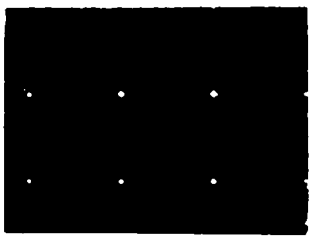

THIS DEPICTS THE RELATIVE RESOLUTION CELL SIZE USED IN REFERENCE 4

FIG. 1·1 THE EFFECT OF INCREASING THE SYSTEM RESOLUTION CELL SIZE (FROM (a) TO (d)) ON TARGET SHAPE PORTRAYAL

caused by finite bandwidth and aperture size for the signal and beamformer respectively, are present at all levels of resolution and manifest as additional false echoes on the display. The relationship between the target surface roughness and geometry with respect to the incident energy bandwidth and beam width affects the formation of echoes. In particular, where the target surface is acoustically smooth the resulting echoes are highly specular, or directional, and result in discrete echo regions on the display, which, under these conditions, bear little resemblance to the actual target shape. This aspect of echo formation is discussed in CHAPTER II which deals more fully with this topic.

A D Dunsiger (1) showed that under conditions of high resolution, back-scattered acoustic echoes characteristically exhibit a wide dynamic amplitude range, typically 80 dB or more from one target. This in turn makes stringent demands on the signal processing equipment in terms of dynamic operating range and signal to noise ratio which, if not met, mean that certain low level echoes are not detected against background noise and reverberation. This feature of the echo formation process is a consequence of the specular nature of the echoes from the target surface.

Certain areas of the target surface will not receive any direct insonification and will reside in the acoustic shadow region. The all round look of figure 1.1 (a) must be replaced by a more realistic situation in which a large part of the outline is obscured due to shadowing.

The sum total of these various effects is that in a high resolution system, in which a narrow acoustic beam and a wide band signal are used to produce a large number of spatial samples of the surveillance area, the resulting echo patterns fall short of that expected from a consideration of the transmitted signal energy and resolution cell size alone with respect to target shape portrayal.

1.4 The background to the present work

The preceding sections have briefly described the important limitations of high resolution sonar systems and displays in general terms and the overall problem area with which this thesis is concerned. This section describes some relevant previous work and studies which relate to the project.

An understanding of the echo formation processes in the underwater environment is obviously mandatory for the efficient use of the available transmitted and reflected signal energy. Consequently, a great deal of effort has been directed at gaining such an understanding. A wealth of published material exists dealing with the analysis and synthesis of the time series signals reflected from target and other surfaces of varying roughness and complexity (see for example references 1, 2, 4).

A large proportion of the published work deals with the estimation of the backscattered and forward scattered power levels of signals reflected from non-deterministic surfaces; for example, the surface of the sea and the sea bed. In these instances the reflecting surface is both time varying and random in nature and its acoustic properties can only be described in terms of a set of statistical parameters.

This present work is concerned with reflecting surfaces which do not change with time in the manner of the sea surface and sea bed examples above. A representation of the reflected signal can therefore be obtained in the terms of linear network theory. Thus, the reflected time signal is assumed to be the result of convoluting the transmitted signal $s(t)$ with a target impulse response $R_t(t)$. Written formally the reflection is:-

$$y(t) = \int_{-\infty}^{+\infty} s(t)\, R_t\,(t - \tau)\, d\tau \quad - \quad 1.1$$

In his work on acoustic echo formation A Freedman [4, 5] presented a detailed account which described the response $y(t)$ as being composed of a number of echoes whose amplitudes and phases are functions of the target surface geometry. The reflected signal $y(t)$ is the result of convoluting the transmitted signal $s(t)$ with a response function $R_t(t)$ which is calculated directly from the target parameters. The response function obtained by this method consist of a set of weighted impulses, the weighting and physical separation of these impulses being proportional to the strengths and physical separations of the reflecting regions on the target surface.

An important aspect of A Freedman's studies discussed the portrayal of the target shape by the sonar system [6] . The echo patterns, as displayed on a ppi, which resulted from the insonification of some basic target shapes were examined and related to the echo forming mechanism at the target surface. A general conclusion was that, due to the localised or specular nature of the echoes, and the effects of the sonar beam side-lobes, the portrayal of target shape was poor and made classifications of even simple shapes difficult. At this point it is useful to consider some of the basic parameters of the equipment used in the study mentioned above. Freedman used only range resolution in his experiments. The test targets were resolved into a number of range discontinuities, but the width of the main lobe of the insonifying beam was such that the whole of the target was enveloped by the beam. In most cases the targets were sampled by a limited number of resolution cells and the angular resolution was such as to produce only one unambiguous bearing or azimuthal response for the target. Figure 1.1(d) shows an analogous effect where the target is sampled by only a few resolution cells.

Visual classification of the ppi displays was made difficult because the theoretical maximum number of target samples was small, eg two to three cells. Different target shapes could produce essentially the same echo patterns as far as the observer was concerned.

In a subsequent study A D Dunsiger [1, 7] considered the target recognition problem in detail. By employing the image echo technique used by Freedman, Dunsiger predicted the variation in amplitude and physical location of echoes from simple target shapes, ie cones, spheres, rectangular blocks and cylinders, with changing target aspect and position. By establishing experimentally whether measurable differences existed between the echo patterns, he was then able to attempt target classification. The hypothesis was that, if differences in echo patterns existed and could be reliably predicted and measured, this would allow a classification procedure to be proposed which utilised these differences.

An important aspect of these experiments was that a model sonar system was employed in which the resolution cell was very much smaller than the targets used; Dunsiger pointed out that current trends in beamformer design enabled increasingly narrow beams to be produced. In the experiments a very narrow sound beam of 2.2 degrees between the 6 dB points was used in the horizontal plane, together with a range resolution of approximately 5mm, which was achieved by using a 2.4 MHz cw pulse of 6 μs duration. At the mean ranges quoted of about 59 cm this resulted in the targets being overlayed by approximately 50-60 resolution cells, compared with Freeman's experiments in which a much larger resolution cell was employed. Figures 1.1(c) and (d) show qualitatively the differences in the two systems in terms of cell sizes.

However, even with the much improved resolution of the system, the echo patterns which Dunsiger obtained on a ppi display exhibited a similar specular nature and did not provide the classification potential which might have been expected from a consideration of the number of resolution cells overlaying the targets.

Parts of the insonified areas of the targets did not show any echo structure, a feature which was attributed to the highly localised or specular nature of the sound reflection mechanism. Note that these results referred to the measurement of backscattered signals at the transmitter location.

One other result from this study, which is relevant from the classification viewpoint, was that the variation in amplitude of echoes measured at the sound transmitter position due to changes in target aspect and position, was very large. Even from one location on a particular target, variations of 100 dB were recorded due to slight changes in aspect. The implications of this are that firstly, a very large dynamic range is required in the signal processing equipment to accommodate such variations and secondly, since the display device is unable to cope with such a range (a typical CRO screen has 12-15 dB of intensity variation before saturation) a dynamic range compression device must be incorporated to match the display.

If the only differentiating echoes between two otherwise similar target responses lie at the low amplitude end of the scale, or if they are characterised by small amplitude differences, then in either case the classification potential of these echoes is likely to be marginal. The inadequate dynamic range of the display and the ambient noise level in the system will mask these marginal echoes unless special precautions are taken.

Summarising so far, in order to improve the portrayal of target shape and reduce the ambiguities in the echo pattern produced by a sonar system in which the target produces a single response, basic changes in the system parameters must be made. The number of resolution cells which sample the target surface must be increased above the single response situation, but an increase in the number of resolution cells in the surveillance area may not, per se, solve the classification problem or remove the ambiguities between different target responses. All the cells which coincide with insonified areas may not contain a corresponding target response. The number of independent data samples of the target surface is, at least in part, limited by the specular nature of echoes generated by the target. It is against this background that the present work is set and it takes its origins from the target shape portrayal problems discussed briefly above.

In order to obtain the desired number of resolution cells in relation to the target size without recourse to using large targets and a large experimental tank, a high frequency model sonar system was used. The use of a relatively high transmission frequency of 2.5 MHz enabled the desired narrow sound beam to be generated with a small aperture, whilst good range resolution was achieved by utilising the short wavelength of sound at these high frequencies.

1.5 Aims of the project

The area of research has been discussed above, and some work conducted by other researchers briefly outlined. The results of these previous studies influenced the course of the present work. In particular, the limitations of high resolution sonar systems in fulfilling their purpose regarding target classification, prompted further study of the mechanisms of acoustic echo pattern formation when the resolution cell is much smaller than the target dimensions.

Reducing display ambiguities was the overall general aim of the present study. In one sense this was quite a specific objective, but in another sense, because the study of echo patterns on a ppi display tends towards the subjective end rather than the objective end of the scale of things, it was also a somewhat open ended study.

One of the needs which emerged at an early stage in the project, was to evolve a technique for assessing the improvements in the echo pattern displayed which, as far as possible, did not require a human observer to make any subjective judgements. As a consequence of this need, one result of this work was a more objective, graphical means of quantifying ppi display improvements which enabled an optimum display to be specified for a particular system, and improvements evaluated in terms of how closely they approached this optimum.

The aims can therefore be summarised in the following terms. The characteristic highlight structure of the target response gives rise to poor target shape portrayal. Consequently, it was intended that a study be made which would result in improvements in terms of an increased number of independent samples of the target outline. Such an increase should immediately improve the intrinsic target classification potential of the high resolution sonar by providing a ppi display which more closely approached the optimum display for the particular system. In this context,

it was proposed to investigate the use of additional acoustic sensors in the form of a bistatic or multistatic arrangement of receivers and transmitter, as a means of increasing the number of detected echoes providing independent data about the target outline. This neglected area of study seemed to offer the possibility of a fresh approach to this topic. By attacking the problems to do with target shape portrayal from a different direction, it was hoped that some of the difficulties outlined above could be circumvented, or an avenue opened which would lead to their solution.

1.6 Assumptions and limitations of the work

Some simplifying assumptions are discussed briefly below because they affected both the theoretical and experimental aspects of this study.

As already mentioned, A D Dunsiger [1] showed that the range of amplitudes obtained from the same target can vary by 100 dB, a non-linear dynamic range compression device was therefore necessary between the receiver output and the Z-modulation input of the display. Such a device compresses the dynamic range at its input to match the limited intensity range of the display tube and consequently distorts the amplitude relationships between adjacent and neighbouring echoes.

Dunsiger also performed a series of subjective tests with a number of observers to measure the classification potential of the high resolution ppi displays. His results indicated that, although predictable amplitude relationships existed between echoes, very careful observation would be required to utilise this information because of the large variations in amplitude possible from the same echoing region. The geometrical relationships of the echoes on the display gave the strongest clues to the observer as to the target shape.

Collectively, these factors resulted in a decision by the author to exclude amplitude information from the ppi displays. A simple threshold test was performed on all received data to determine whether the corresponding display resolution cells were either filled or empty. The displays used were therefore of a binary nature, with cells corresponding to a detection or non-detection of target echoes. As far as the experimental equipment was concerned this gave the additional advantage of reducing the number of degrees of freedom in the system with a corresponding reduction in the amount of information input to the display formatting processor (see CHAPTER III). The nature of the binary display has been shown in the synthetic displays in figure 1.1.

In the analysis and experimental work which is to be described a two dimensional model for the targets and sonar system was assumed throughout. The system as a whole was considered to possess only range and angular resolutions. The targets used in the experimental part of the work were constructed to present a vertical reflecting surface to the incident energy as far as possible. By this means it was hoped to exclude secondary echoes formed by a convex surface reflecting via the water-air interface directly above. It should be noted, however, that such echoes can in certain circumstances provide a differentiating echo between otherwise similar echo patterns; for example, from a cylinder and rectangular block with the same plan outlines. Nevertheless, because of the additional time delay incurred due to the non-direct reflection path, these echoes do not correspond to the physical target outline. Furthermore, they are also very dependent upon the scattering properties of the water-air interface. For these reasons this type of echo was excluded from the display in the manner described above.

As mentioned previously, the information from the surveillance area was presented on the ppi display in the form of a binary echo pattern. A method of measuring the information content was required in order to evaluate and compare the performance of the experimental system under different operating conditions and with changing target aspects and location. If the final decision and evaluation of available data is performed by a human observer, it would seem reasonable to measure the classification potential of the display by requiring the observer to differentiate the echo patterns as being due to one of a set of n targets. This method of display evaluation has been used in the past and has provided informative results particularly regarding the importance of the geometrical correspondence of target shape and echo pattern. The drawback with this technique is the amount of a priori information which the observer is given. If the observer is told to look for one of a class of n shapes, then an infinity of possible target shapes is immediately excluded from consideration. In many cases this may be a valid assumption, however in subjective tests of this nature it becomes difficult to separate basic information due to the echo pattern from a priori knowledge applied by the observer. The classical example of this dilemma concerns the Rayleigh resolution criteria for two closely spaced target time responses. This argues that, since the response of one target will always differ from the response of two, in the absence of any noise the two targets can be resolved to any level of separation. The point about this statement is that the observer has already been given an infinte amount of information in the fact that the response is that of two targets. If the bandwidth of the signal observed is say W Hz, then the number of degrees of freedom or amount of independent data provided by the signal is fixed by the well known sampling theorem as being inversely proportional to twice the bandwidth 2W Hz. A detailed discussion of the correspondence

between resolving power and information is given in reference 8.

A direct parallel between this example and the ppi display situation is not possible and was not intended, however the situation in which a priori knowledge obscures the absolute information presented is a factor to be considered and the above example was quoted to illustrate this.

In order to remove this factor as far as possible in the evaluation of the ppi displays shown in CHAPTER V, an alternative method of measuring the information presented on the display was used. By utilising a basic parameter of the system, namely the two dimensional resolution cell discussed earlier, it was hoped to obviate the need for subjective assessment of the displays using a human observer.

Consider a fixed rectangular surveillance area D. Let this area D be sampled by a two dimensional sampling function comprising a total of N resolution cells. If the output of every resolution cell is subjected to a simple threshold test then a binary display can be generated of the form shown in figure 1.1.

The maximum amount of information which can be presented on the display is N picture elements or bits per scan. If a target occupies an area, T say, within the surveillance area D, the amount of independent data which can be displayed about the target is NT/D bits per scan. In this present work it was assumed that no internal echoes would be received from targets, although A D Dunsiger [7] reported that such echoes can be used to separate a class of solid targets from those which are hollow. Thus the target area T must be replaced by a contour C_t representing the sampled target outline in the manner shown in figure 1.1(a). The maximum amount of independent target data displayed is now equal to the number of cells in the contour and is C_t bits per scan. This simple measurement is independent of the observer since the number of filled cells depends upon the performance and parameters of the system only. However, there is an obvious danger in applying this technique without due care. In general

the echo patterns presented on a display contain redundant information in the form of range and bearing ambiguities. These manifest as beam-former side-lobes for example. The above technique cannot differentiate on a resolution cell basis between these ambiguous responses and the real target. The tendency would therefore be to over estimate the amount of independent target data displayed. For this reason it was considered necessary to employ what knowledge was available about the target in a controlled manner. In particular, if a contour C_t was available for display, together with the measured response, a quantitative evaluation could be made in terms of this reference. Such a technique was employed to study the displays obtained experimentally and is discussed further in CHAPTER V.

1.7 Organisation of the thesis

In this introductory chapter, the overall problem area, the background to the work, its main aims and objectives together with the assumptions made, have been briefly described. The hurried reader requiring only a brief overview of the work and its conclusions should begin with the synopsis, then skip directly to a summary of the work in CHAPTER VII, section 7.6. A more detailed account of the work, including the main objectives, achievements and suggestions for future work can be obtained by reading this chapter followed by CHAPTER VII.

In CHAPTER II a method of evaluating the display and the performance of the system is presented. This method is then used to predict the performance of a high resolution multistatic sonar system via an example. Echo formation is discussed in terms of the spatial characteristics of the echoes, and the sonar system is viewed as a spatial sampling device which samples the target co-ordinates.

In CHAPTER III a description is given of the experimental system constructed together with an account of its operation. Where possible, the features of its construction and operation which affected the overall performance are quantified and isolated as artifacts of the system. This chapter can be skipped by the hurried reader who is not interested in the details of how the multistatic sonar system was implemented.

CHAPTER IV briefly describes the objectives of the experimental work carried out, catalogues the actual records taken, and also describes some experiments necessary to calibrate the system. This chapter can also be skipped in the interests of brevity.

In CHAPTER V some experimental results obtained with the sonar system are presented and briefly discussed.

In CHAPTER VI, these results are analysed and presented in terms of the display loss curves discussed in CHAPTER II, and comparisons are made where possible with the simulation also described in CHAPTER II. CHAPTER VII discusses the achievements of the work and the extent to which the intial objectives were fulfilled. In addition, the limitations of the work are summarised and suggestions made for improvements and possible future work in this field. Finally, APPENDIX A includes the transmitter beam pattern plot and detailed circuit diagrams of the analogue sonar described in CHAPTER III.

CHAPTER II

ECHO PATTERN FORMATION AND PERFORMANCE PREDICTION IN MULTISTATIC SYSTEMS

2.1 Introduction

CHAPTER I briefly discussed the background and outlined the problem areas which formed the basis of this work. The need for a method of evaluating the performance of the sonar system in a more objective manner suited to this study was also briefly discussed.

This theme is developed in this chapter. A simple measure of performance is described in an attempt to obviate the need for the subjective assessment of the observed echo patterns. A mechanism of echo formation is then outlined which suited the requirements of this work in terms of predicting the response of the sonar when additional sensors are incorporated into the system.

The likely gains from this increase in system complexity are shown using the measure of performance developed. They are also related, via some examples, to the parameters of the system which affect the performance in terms of target shape portrayal.

2.2 A method of measuring the performance of the system

It was mentioned above that some previous relevant work utilised the judgement of human observers to differentiate between echo patterns due to targets insonified from various orientations. In an attempt to remove at least part of this subjective aspect of assessment, the amount of independent data samples of the target which were displayed was evaluated. The method used was based on a cell by cell count of the data on the display.

The concept of the resolution cell is a familiar one, and it will not be discussed in detail here. In this work it was considered to be a two dimensional area defined by the beamwidth of the projected sound beam

between the 3 dB response points on the beam pattern, and ideally, the width of the signal autocorrelation function.

In practice, the factor which determined the number of range bins in the sweep time was the inadequate data processing rate of the system and not the signal autocorrelation function. However this is discussed further in CHAPTER III, and for the purposes of this chapter it is assumed that no such limitation applies.

Consider a surveillance area, D say, as depicted in figure 2.1. The sonar system is assumed to sample this area into non-overlapping resolution cells each of area Q and N in number. If the range to the surveillance area is large compared to its dimensions, then the cells can be considered as approximately rectangular in shape.

Into this surveillance area is placed a target described by its two-dimensional contour C_t, representing the boundary between the target and the medium supporting the sonar transmissions. If the target is larger than a single resolution cell, then the display will ideally be composed of a maximum of say, m cells which coincide with the contour C_t. In other words, the target is larger than a single cell by some 'display magnification factor' m.

For any of these display cells to contain information about the contour C_t, a number of conditions must be fulfilled:-

(a) The target must be insonified in the region of a particular cell, and energy must impinge upon the contour C_t within the particular cell.

(b) A reflection of all or part of this incident energy back into the medium must occur.

(c) The sonar system must detect the presence of this energy and localise its source as being a particular cell.

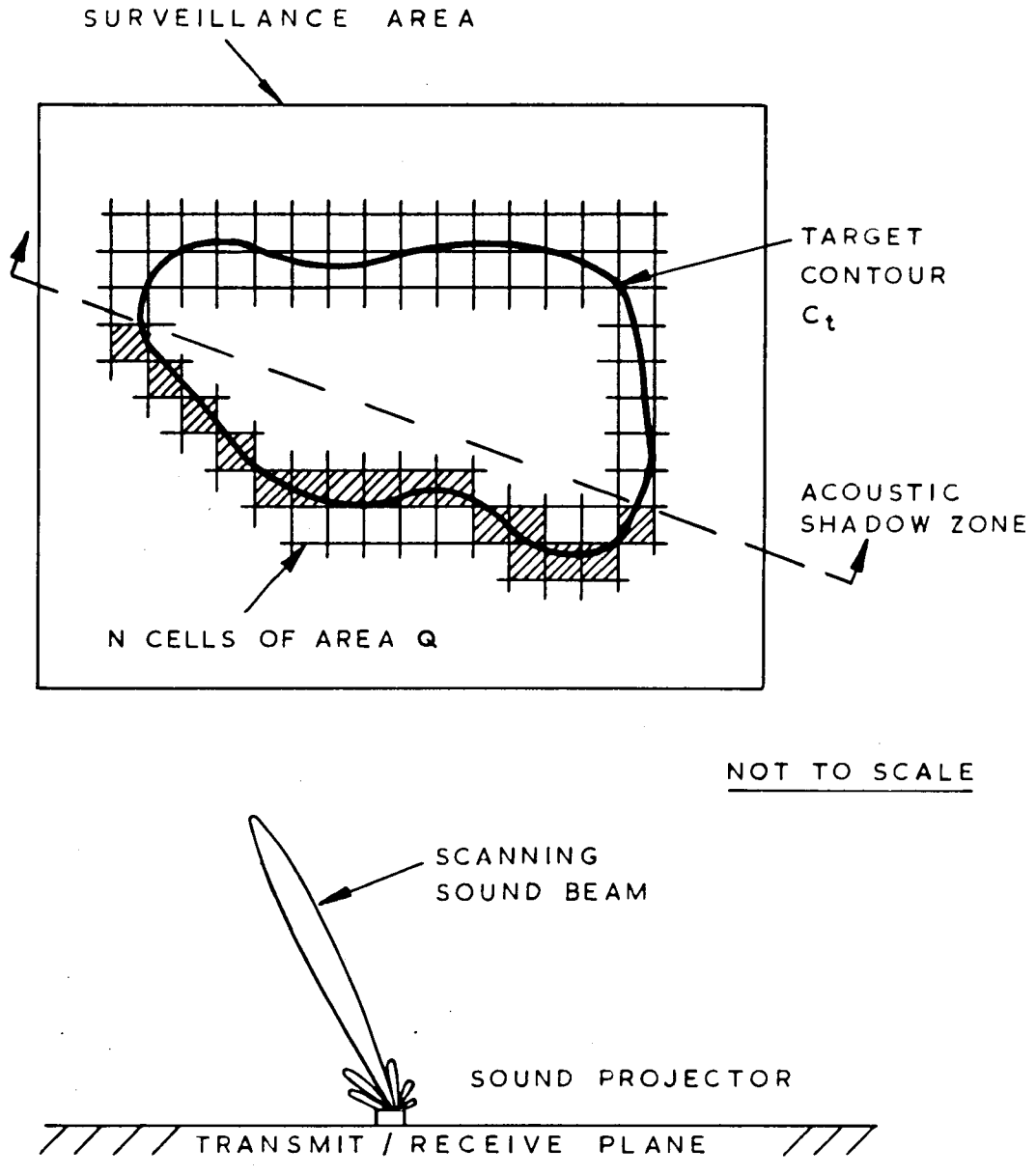

FIG. 2·1 SCHEMATIC OF THE GENERAL SONAR SCENARIO, SHOWING SURVEILLANCE AREA D OVERLAYED BY N CELLS.

Insonification of the target is the function of the sound projector, which in this case scans a narrow sound beam across the contour C_t. The target will not be completely insonified because of the conditions which are assumed to apply (see CHAPTER I, Section 1.6). Only that part of C_t which faces the sound projector will receive energy from the transmissions, and the target will therefore have associated shadow zones. Only those cells shown shaded in figure 2.1 can display any information about C_t.

Reflection of the sound impinging on the target is necessary for an echo to be detected at all, and the general topics of sound reflection and scattering have received, and still do receive, a great deal of attention in the literature. Of the many techniques and methods proposed for calculating the reflected sound components [eg refs 9, 10, 11, 12, 13], a particular method was selected to describe the reflection process, and is discussed later.

However, for the purpose of the present discussion, consider the maximum information displayed to an observer from an area D as described above. Let the basic measure of this information be:-

$$I = \log_2 (\text{ number of possibilities}), \quad \ldots\ldots\ldots \quad 2.1$$

where I is the information level in bits. For the simple case when the contour C_t occupies only one binary resolution cell, the information on the display is:-

$$I = \log_2 (2)$$

$$= 1 \text{ bit.}$$

When C_t is overlayed by m binary resolution cells, as assumed here, then the maximum information is given by:-

$$I = m \log_2 (2)$$

$$= m \text{ bits.} \quad \ldots\ldots\ldots\ldots\ldots\ldots\ldots \quad 2.2$$

It is tacitly assumed that a cell must be 'on' in the sense that a bright spot appears on the display before any useful information is presented to the observer. However, decisions will be made as to whether an echo is present or not at some fixed probability of detection P_d, whilst the sonar is actively scanning the surveillance area. Under these conditions, only a quantity of b cells, where $b < m$ will be detected in all likelihood. Then the information displayed is defined as b bits and a loss has occurred.

For convenience a loss factor, L, can be defined as:-

$$L = 10 \log_{10} (m/b) \text{ in dB re 1 cell} \quad \ldots\ldots\ldots\ldots \quad 2.3$$

For example, if L = + 3dB, then only 50 percent of the total number of cells overlaying the target contour C_t contain echoes.

It can be seen that L is a normalised quantity and imparts no information about the parameters of the system to which it refers. A system in which the target contour C_t lies entirely within one resolution cell ($m = 1$), will have a loss factor L = 0 dB if any detection is made in that cell. A system in which $m \gg 1$ will have a loss factor $L > 0$ dB if less than m cells are detected when scanning the same contour. However, from the point of view of target shape portrayal, then the latter system will certainly be better as long as L is less than a maximum loss defined by:-

$$L_{max} = 10 \log_{10} (m) \quad \ldots\ldots\ldots\ldots\ldots\ldots \quad 2.4$$

Note that even in a system in which m = 1, a loss of 0 dB is still sensible because it indicates that the maximum amount of data is being presented on the display with respect to C_t.

These cases illustrate that in applying this technique, cognisance must be taken of the fact that the loss factor L does not indicate the fidelity of target shape portrayal. Rather, it indicates the performance of the system in presenting independent spatial samples of C_t.

The main disadvantage with this scheme is that there is no intrinsic discrimination between cells filled by either noise exceeding the detection threshold or by side-lobe interference from the main transmission, and cells filled by echoes from the contour C_t. All cells are equally weighted regarding their information content. In the experimental phase of this project, an attempt was made to resolve this difficulty by using a priori knowledge of C_t available in a bit map format, to remove the spurious echoes from the display. The bit map was used to form a reference display against which the real display was correlated. The technique is explained further in CHAPTER V and the result was that a better estimate of the value of L was obtained from the experimental results.

In conclusion, this display evaluation technique provided a basic measure of the information displayed by the sonar system, and allowed quantitative comparisons to be made of the performance of the monostatic and multistatic systems investigated. But there remains the drawback that all filled cells are equally weighted when calculating L. This is irrespective of the reason for detection or their relative position on the display.

2.3 The formation of echoes within a resolution cell

A model was needed which described the echo formation process within a resolution cell in a way which was relevant to a multistatic environment, and would enable estimates to be made of the parameter L.

H G Booker and P C Clemmow [14] were perhaps the first workers to demonstrate that a Fourier transform relationship existed between the far-field response or Fraunhoffer diffraction region, and the aperture or excitation function of an antenna or array. This fundamental relationship has been widely used by array designers for synthesising and analysing far-field beam patterns due to complex amplitude distributions across the arrays in question.

In the field of underwater acoustics, and in particular in connection with the problems of acoustic echo formation, this relationship has been used to describe the beam patterns due to particular amplitude distributions at boundaries and reflecting surfaces (see reference 10 for example).

The way in which an aperture distribution can be transformed into an angular spectrum makes this method of analysis attractive here, because the response at receivers outside the surveillance area can be written in terms of the angular spectrum at the echo formation point. Consequently, in this section a way of describing the echo created within a resolution cell in terms of its angular spectrum is briefly discussed. This method is then applied to the problem of modelling the multistatic sonar environment so that the performance of the system can be assessed in terms of the loss factor L, which was discussed in the previous section.

The notation used here follows that of J A Ratcliffe [9] who applied this method to a similar problem concerning diffraction and reflection of E-M waves by the Ionosphere. However, there exists a great deal of published material describing the mathematical principles involved, and only a brief non-rigorous description is given here.

As mentioned in CHAPTER I, the problem of sound reflection considered was confined to a 2-dimensional (X, Y) system, with no variation in the Z direction. Throughout this discussion capital letters X, Y have been used to denote distances measured in terms of the unit of length (metres) and small letters x, y to denote distances normalised in terms of the wavelength λ.

To further simplify the discussion at this stage, the time variations of the sound field have been omitted and only CW signals are considered. It is shown below in section 2.10.1 that under certain conditions this is a reasonable and justifiable simplification.

Consider therefore the 2-dimensional situation shown schematically in figure 2.2(a). A reflecting surface at Y = 0 is insonified by an infinite plane wave of complex amplitude A_I which makes an angle θ_I with the Y axis as shown. At the reflecting boundary this wave sets up a distribution $f_I(X)$, which describes the amplitude and phase of the incident wave field as a function of position X across the boundary.

If the surface at Y = 0 is a simple pressure release type, the reflection coefficient R equals -1. For example, an air-water interface has this characteristic. To satisfy the energy equation, a reflected wave f_R is set up with an associated surface distribution so that:-

$$f_R(X) + f_I(X) = 0$$

This wave propagates outwards from the surface at an angle θ_R with respect to the Y axis as shown in diagram (a).

Let a set of these outgoing plane waves, each having the same temporal frequency, and travelling in directions making angles θ_R with the Y axis, constitute an angular spectrum of plane waves.

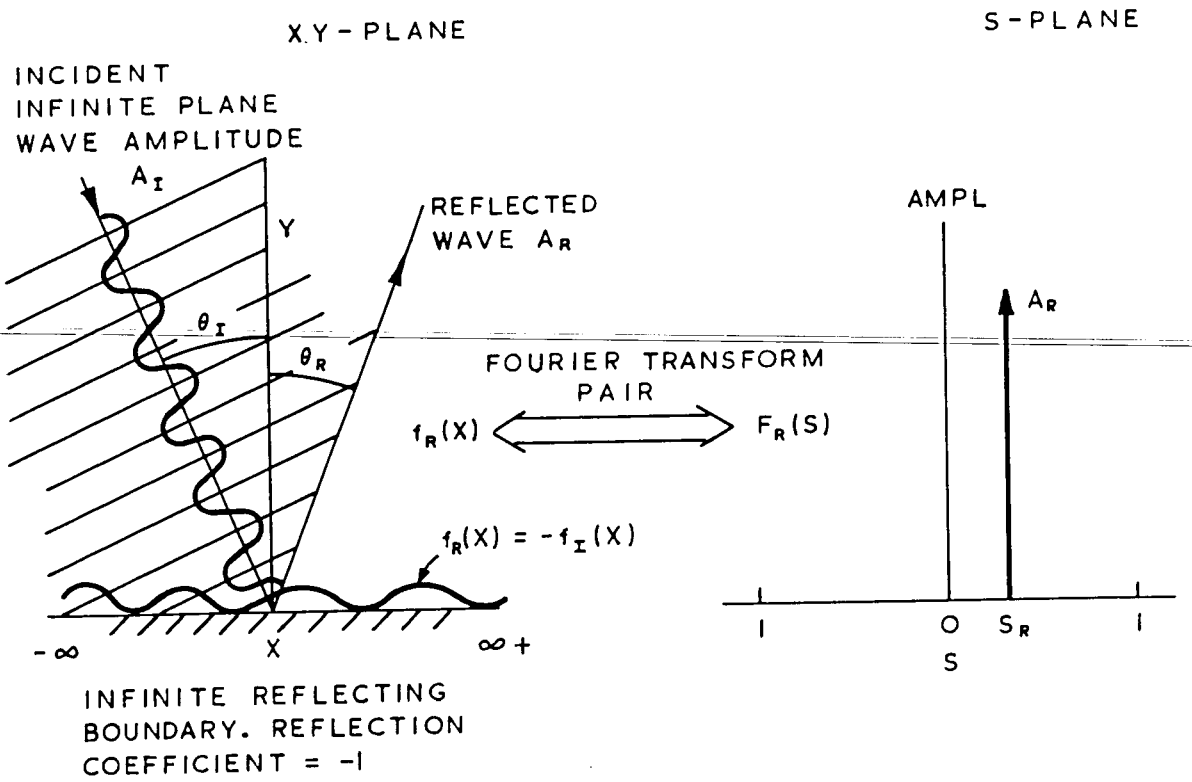

FIG. 2·2a

FIG. 2·2b

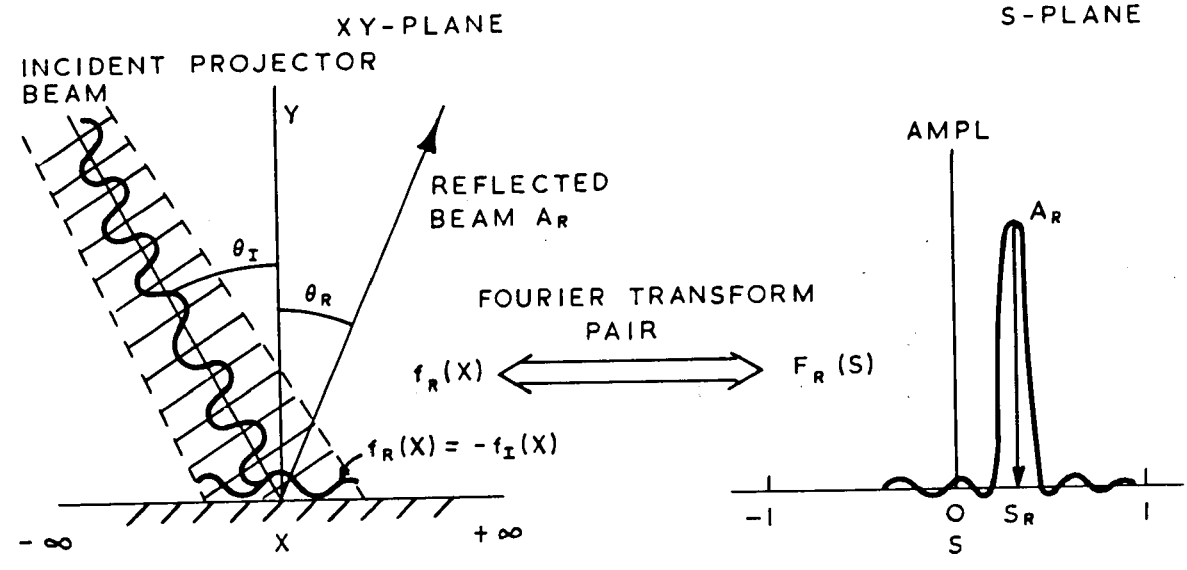

FIG. 2·2c

FIG. 2·2d

FIG. 2·2. A DIAGRAMATIC REPRESENTATION OF THE RELATIONSHIP BETWEEN THE XY - PLANE AND THE ANGULAR SPECTRUM (S - PLANE) FOR AN INFINITE PLANE WAVE (2·2 a AND b) AND AN APERTURE LIMITED CASE (2·2 c AND d) AS REFERRED TO IN THE TEXT

By using superposition, any general wave field propagating away from the reflecting boundary can now be synthesised from a distribution of uniform plane waves as described above. Each component wave travels in a different direction Θ_R with a particular complex amplitude A_R, and the resultant complex amplitude of waves propagating in directions lying between Θ_R and $\Theta_R + d\Theta_R$ is assumed to be $A_R(\Theta)d\Theta_R$. The variation with X and Y is given by,

$$A_R(\Theta)d\Theta_R \quad \exp(jk(X \sin \Theta + Y \cos \Theta)) \quad \ldots\ldots\ldots\ldots \quad 2.5$$

where $k = 2\pi/\lambda$ and is called the wavenumber. The field at co-ordinates x, y is found by integrating equation 2.5 with respect to Θ, thus,

$$f_R(x,y) = \int_{-\pi/2}^{\pi/2} A_R(\Theta) \cos \Theta \exp (2\pi j(x \sin \Theta + y \cos \Theta))d\Theta \qquad 2.6$$

where $x = X/\lambda$ and $y = Y/\lambda$.

By expressing the angles in terms of sin Θ and cos Θ, and substituting a function $F_R(S)$ for the function $A_R(\Theta)$,

where $S = \sin \Theta$, $C = \cos \Theta$ and $F_R(S) \equiv A_R(\Theta)$,

equation 2.6 can be re-written in the form below. Thus,

$$f_R(x,y) = \int_{-1}^{+1} F_R(S) \quad \exp (2\pi j(Sx + Cy)) \, dS \quad \ldots\ldots\ldots \quad 2.7$$

Equation 2.7 is simply a representation of the wave field at spatial co-ordinates x,y in terms of an angular spectrum $F_R(S)$. At the plane Y = 0, the distribution $f_R(x)$ is given by the Fourier transform of the spectrum $F_R(S)$, apart from the limits of the integral which should be $\pm \infty$. This discrepancy can be resolved by noting that values of $|S| > 1$ correspond to pure imaginary values of $\cos \Theta = (1-S^2)^{\frac{1}{2}}$, and equation 2.7 then contains an exponential attenuation factor corresponding to propagation

in the Y direction. No energy is transmitted in this direction by these waves which are called evanescent modes and such waves are not important in this context. However, strictly speaking, if the limits of equation 2.7 are extended to $\pm\infty$ then they are included.

By including these modes, and invoking the inversion theorem of Fourier transforms, the transform pair written below can be obtained.

$$\left.\begin{aligned} f_R(x) &= \int_{-\infty}^{+\infty} F_R(S) \exp(2\pi j\, Sx)\, dS \\ F_R(S) &= \int_{-\infty}^{+\infty} f_R(x) \exp(-2\pi j\, Sx)\, dx \end{aligned}\right\} \quad \ldots\ldots\ldots\ldots \quad 2.8$$

This familiar result says that a distribution $f_R(x)$ over the plane $Y = 0$ will produce an angular spectrum $F_R(S)$, where $f_R(x)$ and $F_R(S)$ are a Fourier transform pair.

In this case the distribution $f_R(x)$ results from the reflection of an incident wave $f_I(x)$ at a reflecting boundary, and it is the reflected spectrum $F_R(S)$ which is of interest.

2.4 Propagation of the echo into the far field

Propagation of the angular spectrum $F_R(S)$ through a lossless and uniform medium involves phase retardation of the individual plane wave components of $F_R(S)$. The new angular spectrum, $P_R(S)$ say, at some distant plane (Y = constant) is found by multiplying $F_R(S)$ by an allpass propagation function which results from a solution of the wave equation [9]. For non-evanescent modes, this function reduces to a simple form,

$$G(S) = \exp(jk\, Cy) \quad \ldots\ldots\ldots\ldots\ldots\ldots \quad 2.9$$

and propagation is an entirely linear phenomenon as expected. The angular spectrum $P_R(S)$ can now be written as,

$$P_R(S) = F_R(S).\, G(S) \quad \ldots\ldots\ldots\ldots\ldots\ldots \quad 2.10$$

Important modifications of equation 2.10 are obtained by applying the Fresnel (near field) and Frauenhoffer (far field) approximations to the propagation function G(S).

Let,

$$G(S) = \exp(j\, ky(1-S^2)^{\frac{1}{2}}) \quad \ldots\ldots\ldots\ldots \quad 2.11$$

now a binomial expansion of the square root part allows the Fresnel approximation to be applied, thus,

$$(1-S^2)^{\frac{1}{2}} \simeq \left(1 - \frac{S^2}{2}\right) \quad \ldots\ldots\ldots\ldots \quad 2.12$$

Also, if $y \gg \frac{kx^2}{2}$, in other words, that the field point is a sufficiently large number of wavelengths from Y = 0, then the phase factor becomes approximately constant. This stronger Frau nhoffer approximation means that the observed far field distribution $P_R(S)$, can be found directly from the Fourier transform of the distribution $f_R(x)$ at Y = 0, thus,

$$P_R(S) = K.\ F_R(S) \quad \ldots\ldots\ldots\ldots \quad 2.13$$

where K is a complex constant depending upon the range y to the plane in question.

2.5 Examples of echo formation

2.5.1 The infinite reflecting aperture

Consider the example shown in figure 2.2(a) in which an infinite plane wave is incident at an angle $-\theta_i$ upon a reflecting boundary at Y = 0. The incident distribution across the boundary is,

$$f_I(x) = A_I \exp(-2\pi\, jx(-S_I)), \quad \ldots\ldots\ldots\ldots \quad 2.14$$

where A_I is a complex amplitude function dependent upon the angle of incidence, and $-S_I = -\sin\theta_I$. For the case of a pressure release boundary the distribution $f_R(x)$ is given by

$$f_R(x) = -A_I \exp\left(-2\pi jx(-S_I)\right) \quad \text{2.15}$$

where the minus sign attached to A_I indicates reflection.

The reflected angular spectrum set up by this distribution is found by evaluating the integral transform,

$$F_R(S) = \int_{-\infty}^{\infty} f_R(x)\exp[-2\pi jxS]dx,$$

which upon substitution of the appropriate $f_R(x)$ is,

$$F_R(S) = \int_{-\infty}^{+\infty} -A_I \exp[-2\pi jxS] \exp[-2\pi jx(-S_I)]\,dx \quad \text{2.16}$$

In this simple example, the spectral shift theorem of Fourier transforms can be invoked to show that equation 2.16 evaluates to a unit impulse of amplitude A_I shifted by an amount $+S_I$ along the S-plane axis. This corresponds to an outgoing infinite plane wave making an angle $\theta_R = \theta_I$ with the Y axis. This result is of course expected from a straightforward consideration of the rule of equal angles of incidence and reflection from a plane surface and the situation is shown diagrammatically in figure 2.2(b).

2.5.2 The spatially limited aperture

In the example above the distribution $f_I(x)$ was considered to be unbounded in the x direction in keeping with the description of A_I being due to a uniform, infinite plane wave. If the distribution $f_I(x)$ is spatially limited to a region defined by $|x| \leq L$, the effect upon the angular spectrum is analogous to the effect on the frequency spectrum of a time waveform which has limited temporal extent. Such a transient waveform produces a non-band limited frequency spectrum and similarly, the limited aperture extent results in a non-band limited angular spectrum.

For example, let the distribution across the boundary be:-

$$f_R(x) = \begin{cases} -A_I \cdot \exp\ -2\pi jx(-S_I) , & |x| \leq L \\ 0 , & |x| > L , \end{cases}$$

as shown in figure 2.2(c). Now,

$$F_R(S) = -A_I \int_{-L}^{+L} \exp[-2\pi jx(S-S_I)]\, dx$$

which gives a familiar result,

$$F_R(S) = -2LA_I \left\{ \frac{[\sin 2\pi L(S-S_I)]}{2\pi L(S-S_I)} \right\} \quad \ldots\ldots\ldots\ldots \quad 2.17$$

This function still has a maximum in the specular direction, but the reflected energy has now been distributed across the S-plane as shown in figure 2.2(d).

In this present context, this situation can arise due to two reasons,

(a) because of a spatial limitation of the reflecting surface; the insonified region contains either a discontinuity or a boundary in C_t,

or (b) because the sound projector has a narrow beam pattern and the resolution cell dimensions are smaller than the extent of C_t (ie m >>1).

Thus, subject to certain limitations, the concept of the angular spectrum $F_R(S)$, formed within a resolution cell by the aperture distribution $f_R(x)$, can be utilised to describe the spatial distribution of the echo from that cell.

2.6 Echo levels at the receiving plane

It has been stated above that provided observations are made at a sufficiently large distance from the reflecting boundary, the measured signal can be obtained from a consideration of the Fourier transform of the aperture distribution within the resolution cell. To investigate the effects of insonification of a contour C_t by a scanning sound beam, a computer program was written to evaluate the far field response by utilising the well known Fast Fourier Transform algorithm [15, 16] to compute the angular spectrum $F_R(S)$ from equation 2.8. This program had as its input a sequence representing the complex amplitude distribution within the resolution cell (see figures 2.3(a) and (b)). The output was in the form of an angular spectrum which was then used to produce the familiar polar diagram representing the angular distribution of the reflected sound.

Both outputs, ie the angular spectrum and its corresponding polar diagram, were subjected to an amplitude threshold test which resulted in amplitudes less than the particular threshold being discarded. The effect of this thresholding was to produce an arc of detection as shown in figure 2.4 within which a detection of the echo from that cell would be made at a suitable placed receiver.

The reason for such a threshold can be seen by examining the active sonar equation,

$$EL = SL - 2PL + TS - NL, \quad \ldots\ldots\ldots \quad 2.18$$

where EL = the signal or echo level at the transducer face in dB re 1 μPa,

SL = the projector source level in dB re 1 μPa.

PL = the transmission loss of the signal in dB,

TS = the target strength in dB which is defined below, and

NL = the equivalent noise and other interference level in dB.

Normally monostatic target strength is defined as ten times the log ratio of the echo intensity along the direction of insonification at a

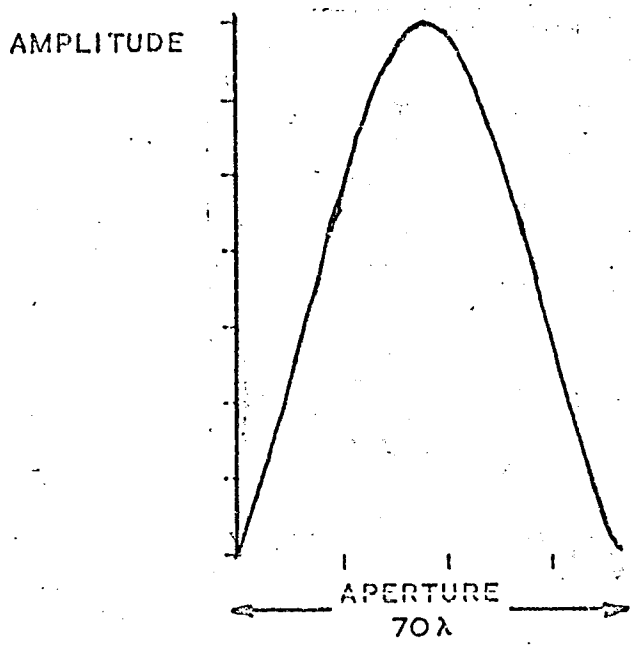

FIG 2·3 (a)

THE AMPLITUDE FN USED AS THE I/P TO THE SIMULATION PROGRAM. TAKEN FROM THE MAIN LOBE OF THE MEASURED PROJECTOR BEAM PATTERN

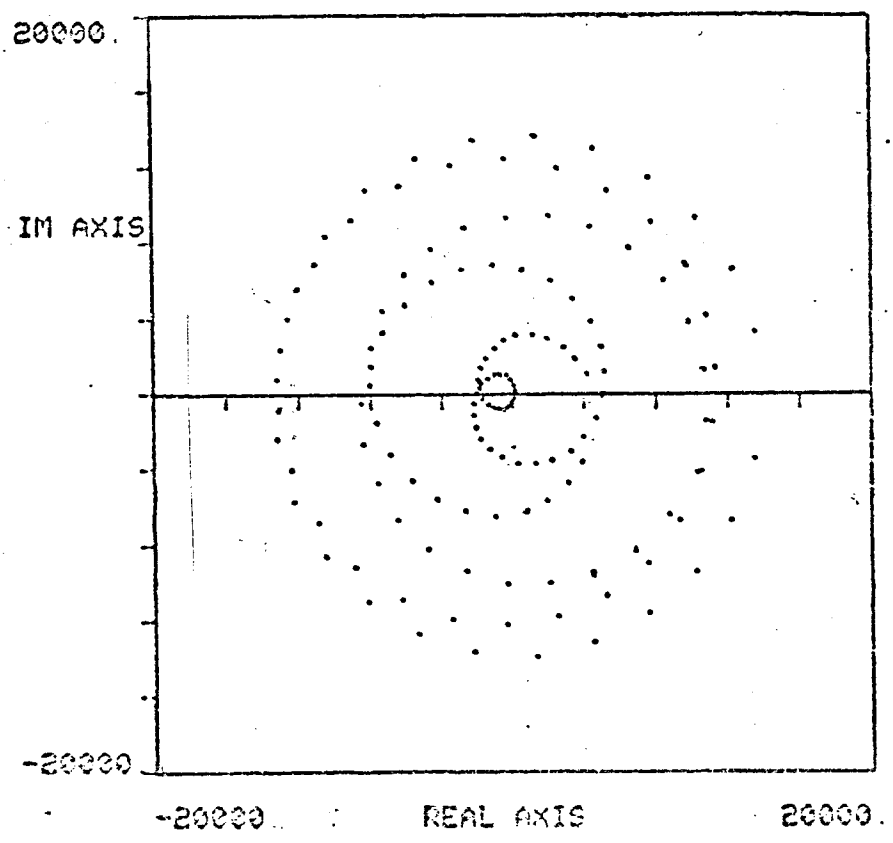

FIG. 2·3 (b)

FIG. 2·3 AN EXAMPLE OF THE COMPLEX I/P SEQUENCE TO THE SIMULATION PROGRAM WHEN THE INCIDENT BEAM IS GIVEN A 4° STEER . SEE FIG. 2·5 FOR THE CORRESPONDING O/P FROM THE PROGRAM

nominal range of 1 yd, to the incident intensity.

Thus,

$$TS = 10 \log_{10} \left\{ \frac{\text{Echo intensity } (I_r)}{\text{Incident intensity } (I_i)} \right\}$$

The incident intensity I_i is the source level minus the propagation loss to the target so,

$$I_i = SL - PL, \text{ in dB.}$$

From this can be obtained a pressure p_i in microPascals (μPa), which is the pressure across the reflecting boundary due to the source, and which is the realisation of the function $f_I(x)$ in this context. From this the angular spectrum $F_R(S)$ can be found, and if there are no losses upon reflection (R = 0dBs), then the echo intensity in a particular direction S is found from

$$I_r = 10 \log_{10} [F_R(S)]^2$$

Target strength can now be written as

$$TS = 10 \log_{10} [F_R(S)]^2 - 10 \log_{10} (I_i),$$

so that in the particular case where the resolution cell is very much smaller than the target,

$$TS = 10 \log_{10} [F_R(S)]^2 - (SL - PL).$$

Substituting this into equation 2.18 gives

$$EL = 10 \log_{10} [F_R(S)]^2 - PL - NL, \quad \ldots\ldots\ldots \quad 2.19$$

which represents the situation at the receiver when the insonified region or resolution cell is much smaller than the target dimensions.

A threshold applied to the function $F_R(S)$ is therefore equivalent to specifying a minimum echo level at the receiver, required for detection.

For the purposes of this study it was assumed for the case of a resolution cell at a given range, and at normal incidence with respect to the sound projector, that the specular echo from this cell exceeded the minimum required echo level. This echo excess depends upon the source level, propagation losses and the background or reverberation level, and is found by substituting the appropriate numbers into equation 2.19 above. As the insonified cell moves away from normal incidence with respect to the sound projector, due to the scanning of the sound beam across the contour C_t, the echo level will change in any direction S in accordance with the function $F_R(S)$. A detection will only be made at a receiver coincident with the projector if the echo level in that direction exceeds the threshold value, ie lies within the detection arc determined by the threshold. In this study a number of threshold values were used corresponding to echo excesses of 30 dB, 40 dB, 50 dB and 60 dB.

The discussion so far has been limited to a consideration of each resolution cell being insonified by a narrow sound beam without any side-lobes. The existence of side-lobes in the far field means that the region of the target insonified during a transmission sequence can exceed the extent of the resolution cell coinciding with the beam pointing direction. However, any increase in the reflecting aperture size resulting from incorporating the side-lobe effects into $f_R(x)$ would result in an increased specularity of the resulting echo and a reduction in the detection arc for a given threshold. Usually, the angular separation of the side-lobes from the main response means that they can be treated as separate insonifications of the target. To prevent side-lobes confusing the target shape portrayal, the echo excess must be reduced by an amount equal to the difference between the main-lobe and side-lobe levels. This further limits the detection arc for a given situation, and no matter from which point of view they are considered, side-lobes degrade the performance of the system, as of course they must.

2.7 Echoes from a simple target contour

In order to quantify the various effects described above, the computer program was used to simulate echoes from a simple contour C_t which was a linear reflecting surface of finite dimension in the x axis of 20 resolution cells. The amplitude function shown in figure 2.3(a) was used to form a complex amplitude distribution representing the insonification on this contour. The phase being that due to a linear delay across the aperture due to an angle of incidence of the sound beam - S_i. For the purposes of this simulation the range to the receiver plane in wavelengths was taken as approximately 2000, and the beamwidth θ was taken as approximately 2-3 degrees to the first zero crossing (1.5 degrees to 3 dB points), both of these parameters being chosen to coincide with values of beamwidth and range proposed for the experimental work. With these parameters, the insonified region on the target due to the angular extent of the main-lobe of the transmitter beam is approximately 70 wavelengths, neglecting side-lobes. Thus a sampled version of $f_R(x)$ with samples every half wavelength was constructed and is shown diagrammatically in figure 2.3(b) as a set of samples on the complex plane. The polar diagram obtained from the angular spectrum due to a normally incident sound beam is shown in figure 2.4. On this diagram a 50 dB dynamic range has been applied and reflections below this value have been suppressed. This value of threshold was considered a reasonable one under these conditions, and represents the echo excess required in the specular direction in order that an echo be detected at a receiver anywhere within the corresponding detection arc.

The beamwidth of the transmitter determines the scan increment, (which is approximately 2 degrees), required to insonify the next resolution cell on the contour C_t. A series of plots was therefore

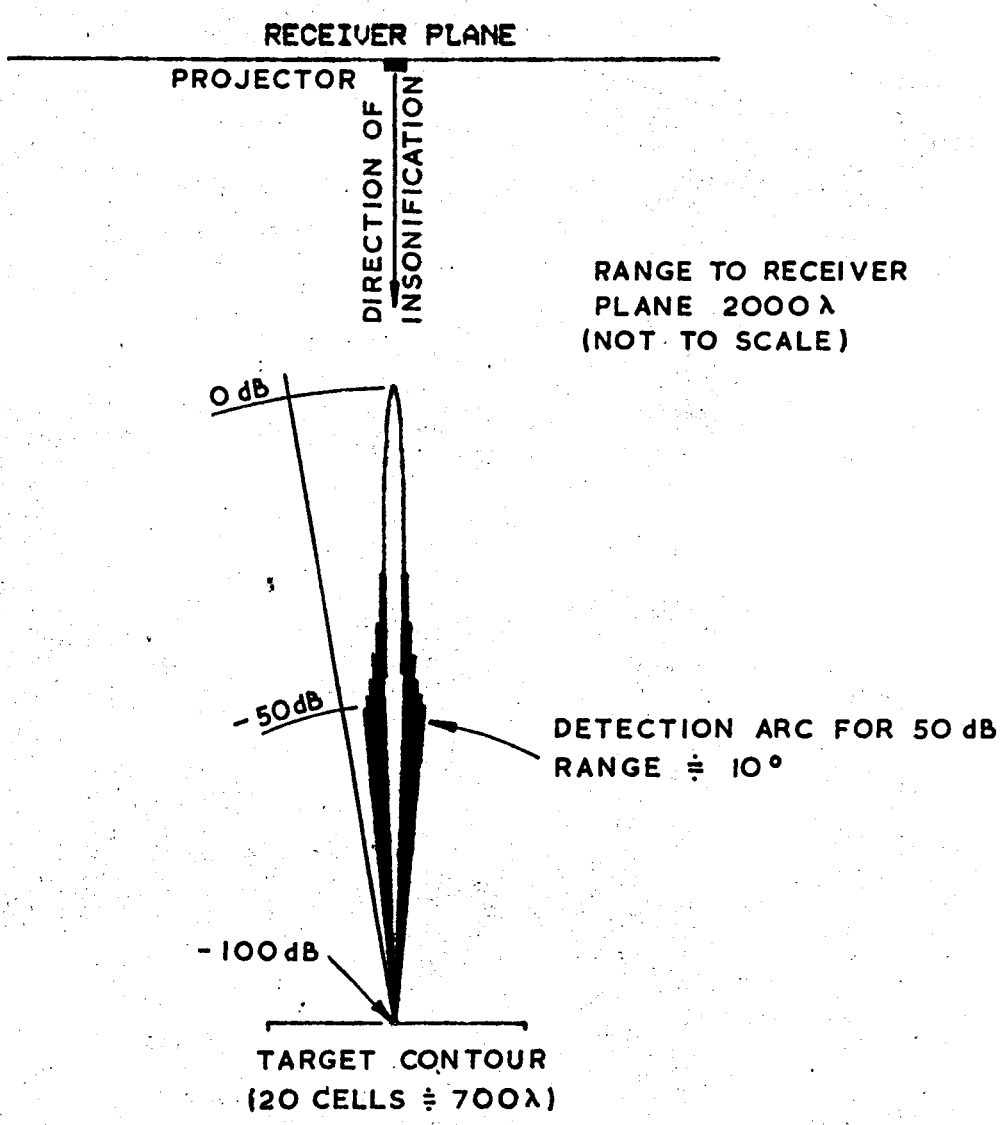

FIG. 2·4. 50dB REFLECTION POLAR RESPONSE DUE TO NORMALLY INCIDENT BEAM AND AMPLITUDE TAPER SHOWN IN FIG 2·3(a). THIS FIG. ALSO SHOWS THE ARRANGEMENT OF THE TARGET AND RECEIVER PLANE ASSUMED IN THE SIMULATION

constructed showing the reflection polar diagram at each cell as the transmitter beam was incremented by 2 degrees. For brevity only the salient plots are reproduced here, corresponding to those beam steers at which the echo is just lost and falls below the 50 dB threshold. For the region around normal incidence the transition occurs at about $\pm$ 4 degrees of steer. In other words after moving away from the normal incidence cell by an amount $\pm$ 1 cell the echo is no longer visible at the monostatic receiver. This transition is shown in figure 2.5.

At this transition point the outer edge of the detection arc is approximately 8 degrees away from normal incidence. At the receiver plane this corresponds to a region around the transmitter position given by $\pm$ 2R tan θ, where θ is 8 degrees here.

When considering the placement of additional receivers along the receiver plane to form a multistatic environment, cognisance must be taken of this region. Receivers should not be placed inside this region because at least one echo co-ordinate from this multistatic receiver will not be independent data. The same resolution cell can be detected by the monostatic receiver at the edge of the corresponding detection arc.

At the limits of the scanned contour C_t, the aperture function $f_R(x)$ undergoes a spatial limitation due to the physical limits of the reflecting surface. The effect on the angular spectrum $F_R(S)$ is to cause an increase in angular bandwidth as the reflecting aperture is spatially limited. This situation was simulated by changing the sequence $f_R(x)$ to model the effect of scanning across the target boundary. A number of polar plots were made assuming an angle of incidence of approx 20 degrees which corresponded to the target contour of $\pm$ 10 cells (m = 20). The transition point at which an echo exceeding the 50 dB threshold is reflected or scattered back towards the monostatic receiver is shown in figure 2.6. A reduction in signal level in the specular direction occurs

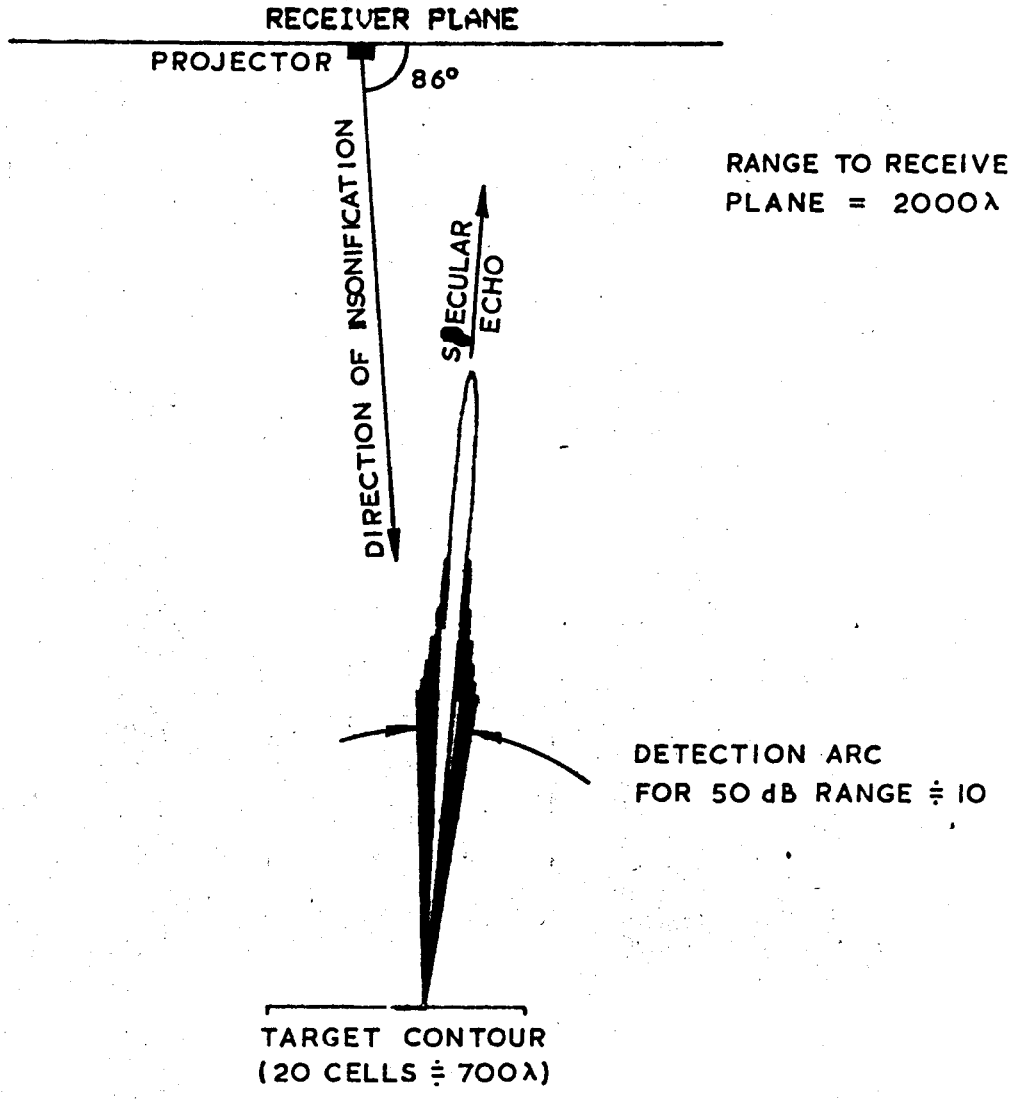

FIG. 2·5. 50 dB REFLECTION POLAR RESPONSE AT 4° OF PROJECTOR BEAM STEER SHOWING THE TRANSITION TO NON-DETECTION OF THE CORRESPONDING CELL. THE TARGET STRENGTH IS < REQUIRED FOR DETECTION. FOR CORRESPONDING PROGRAM I/P SEE FIG. 2·3 (b)

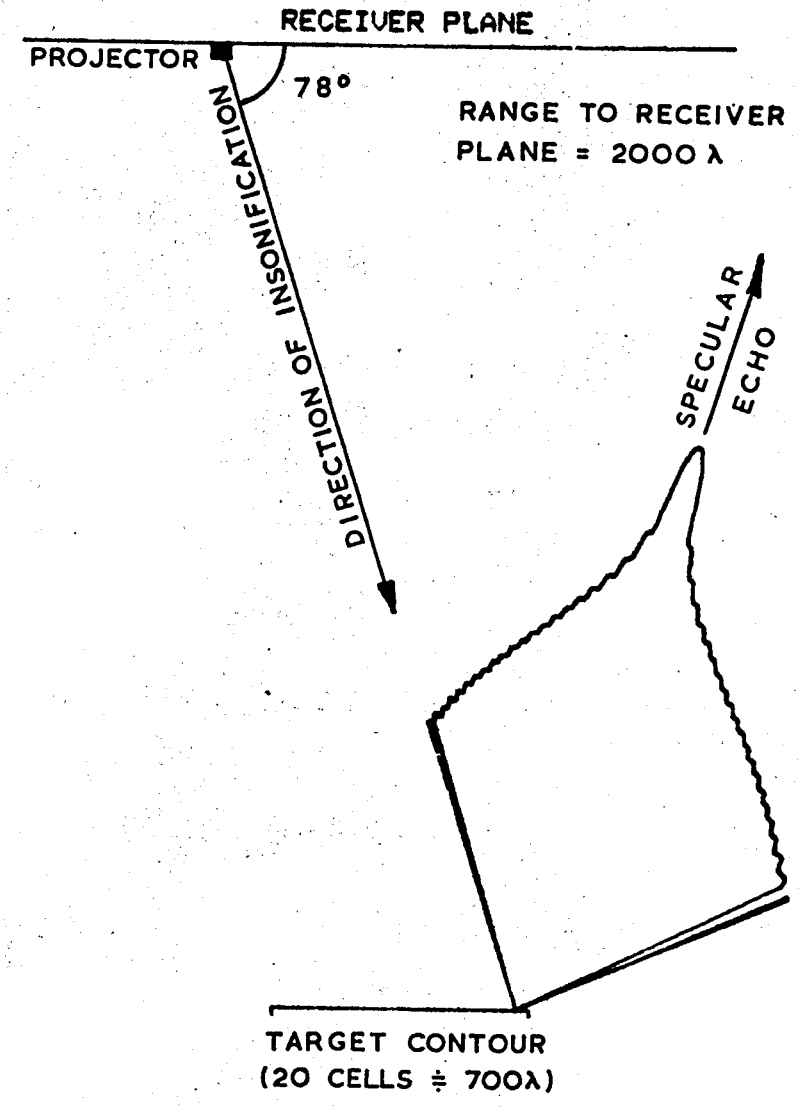

FIG 2·6 50dB REFLECTION POLAR RESPONSE AT PROJECTOR BEAM STEER CORRESPONDING TO 50% APERTURE REDUCTION (≃ 18°) SHOWING TRANSITION TO DETECTION OF THE CELL CORRESPONDING TO THE TARGET BOUNDARY

because the total reflected energy has been redistributed and limited by the reduction in aperture size. In this particular example this transition from no detection to detection occurred when the full aperture or resolution cell was reduced by about 50 percent.

Scanning of this simple contour is now complete and an estimate of the number of detections or filled cells can be made for this target on the basis of this simulation.

2.8 Estimation of the loss factor for this target

At normal incidence a detection arc of approximately 8.5 degrees ensured that a total of 3 cells were detected with a 50 dB echo excess. Because of the angular distribution of reflected energy away from normal incidence no more detections are made until the target boundary discontinuity causes an increase in angular bandwidth. The symmetrical nature of the scan either side of normal incidence therefore means that 5 cells are detected out of a total of 20 for this monostatic situation.

Substitituing this value for b in equation 2.3 gives a value of +6dB for $L_{monostatic}$, and this point is shown plotted as the first point on curve **2** in figure 2.7.

Consider now the effect of introducing an additional receiver onto the receiving plane. In this particular case it has been shown that the existence of an arc of detection at each resolution cell for the monostatic case meant that the receiver should not be placed within such a region if the best use is to be made of the extra degree of freedom in the system. Two such regions exist for this example; one at normal incidence and the other at the edges of the contour. Assume that the receiver is placed at a position corresponding to a transmitter steer angle of 10 degrees. Figure 2.8 shows the polar diagram of the reflection from the corresponding cell at this steer. The detection arc spans approximately 12 degrees, corresponding to a region of about $\pm$ 4 cells on the receiver plane within

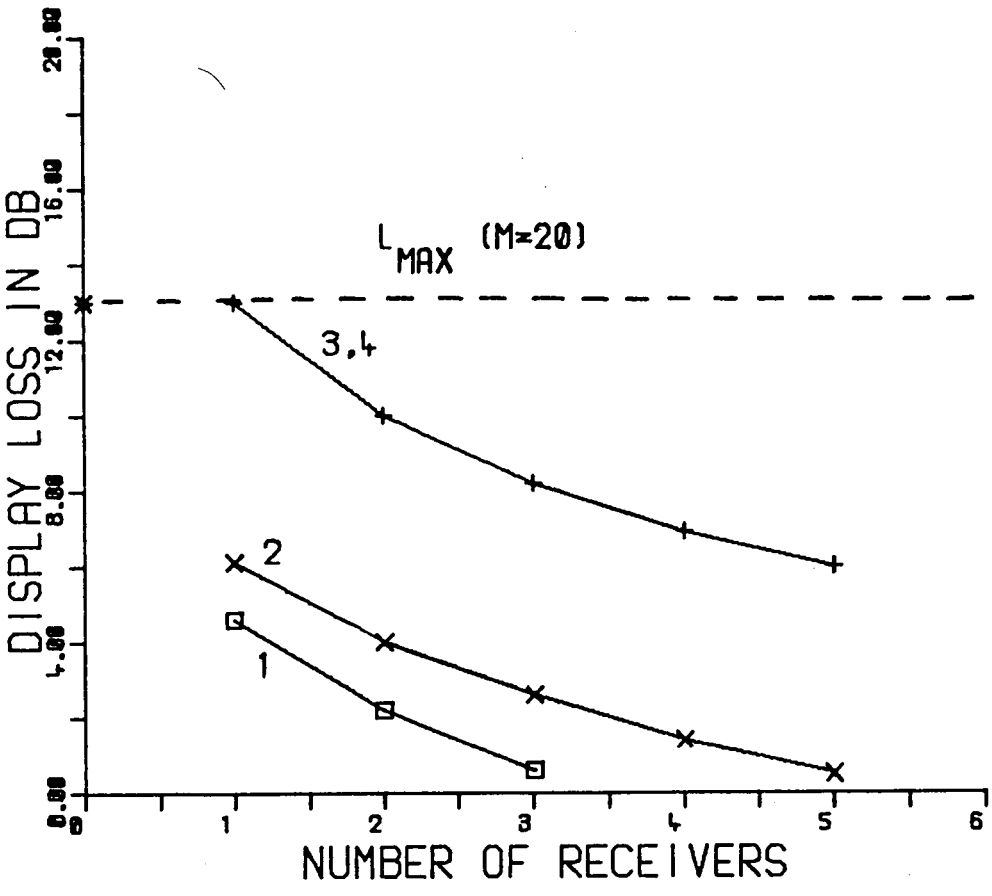

PARAMETERS 1=60DB ECHO EXCESS
2=50DB ECHO EXCESS
3=40DB ECHO EXCESS
4=30DB ECHO EXCESS

. BEAM WIDTH =1.5DEG TO 3DB POINTS
RANGE =2000 WAVELENGTHS

FIG 2.7 DISPLAY LOSS AS A FUNCTION OF THE NUMBER OF RECEIVERS.

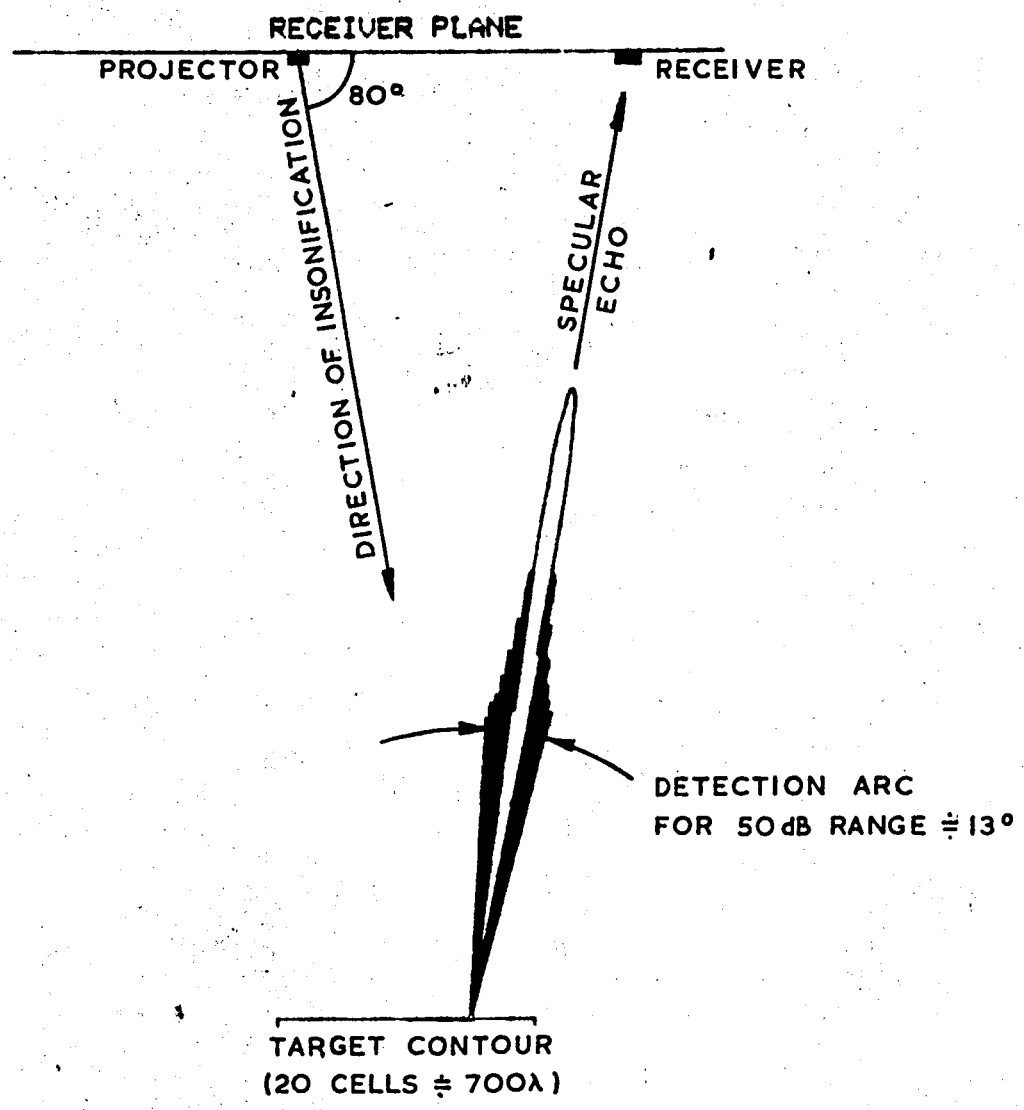

FIG. 2·8. 50dB REFLECTION POLAR RESPONSE AT A PROJECTOR BEAM STEER OF 10°, SHOWING THE RESPONSE AT A SUITABLY PLACED BISTATIC RECEIVER. A RECEIVER IN THE SPECULAR ECHO POSITION WILL DETECT THE CORRESPONDING CELL AND ONE EITHER SIDE

which a detection will be made. This in turn means that the bistatic receiver will detect echoes from approximately 3 resolution cells as the beam increments across the target.

With this additional receiver the value of b increases to 8 and the value of L becomes + 4dB after making the appropriate substitutions. A sensible arrangement for another bistatic receiver would take advantage of the symmetry of the geometry about the transmitter position to reduce L to +2.6 dB.

Finally, with a total of 5 bistatic receivers properly situated on the receiver plane L reduces to +0.46 dB. These points are shown plotted on figure 2.7 as curve 1.

An equivalent set of calculations was performed assuming threshold values of 30 dB, 40 dB and 60 dB. The results are plotted on figure 2.7 as curves **4** (30 dB), 3 (40 dB) and **1** (60 dB).

The 40 dB detection arc at normal incidence has an angular extent of 4 degrees, and at 2 degrees of steer of the transmitter beam the echo is already outside the detection range of the receiver. At the target boundary the spatial limitation of the aperture causes an increase in the angular bandwidth as before. However the reflections back towards the monostatic position never exceed the required 40 dB threshold. Further reduction in the aperture only serves to reduce the amplitude of the specular echo. The situation is shown in figure 2.9 which shows the polar response after the aperture has been reduced by 35 percent.

Therefore the monostatic system results in a loss factor of + 13 dB. This is a limiting case because the required receiver density on the receiver plane for detection of individual cells approaches the number of cells on the target contour itself. In other words, each additional bistatic receiver only detects one additional resolution cell, except at the target boundary where the corresponding receiver will detect both

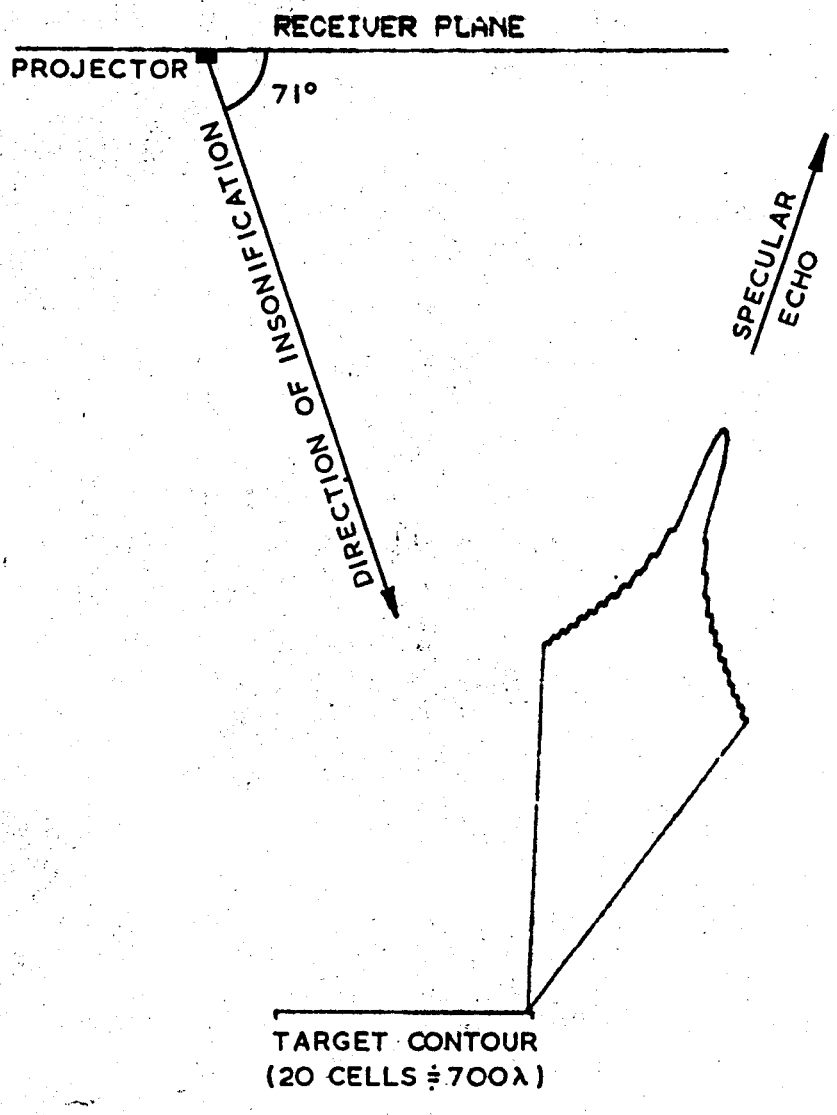

FIG. 2·9 40dB REFLECTION POLAR RESPONSE AT PROJECTOR BEAM STEER CORRESPONDING TO 35% APERTURE REDUCTION. NO DETECTIONS ARE MADE WITH THIS ECHO EXCESS AND FURTHER APERTURE REDUCTIONS ONLY REDUCE THE SPECULAR ECHO AT LEAST 50 dB ECHO EXCESS IS NEEDED FOR A DETECTION (SEE FIG. 2·6)

the specular echo from the resolution cell adjacent to the boundary and also the echo from the diffracting boundary. However, in plotting curve 3 in figure 2.7 it was considered more appropriate to show the case where a small number of additional receivers were included in the system. This was on the assumption that for any given contour, C_t, the bistatic receivers would not necessarily be at such fortuitous points on the receiver plane, and that the system bandwidth might limit the number of receivers (this point is discussed further in CHAPTER III).

If the echo excess is further reduced to 30 dB, then a smaller detection arc will be delineated on the receiver plane, but this region will still be finite and detections made as per the 40 dB case. The 40 dB case therefore represents an upper bound on performance, and the curve for the 30 dB echo excess is the same as the curve for the 40 dB echo excess. A performance threshold has been reached at 40 dB, and further reduction in echo excess will not affect the loss factor curve. This is true at least until the echo excess is below some arbitrary recognition differential for the system. Stated the other way around, for a given number of receivers no improvement in performance (as defined here) will result as the echo excess is increased, until the 40 dB threshold is reached. What will change is the false alarm rate on the display, but this is not being considered here. This situation is shown as curve 4 in figure 2.7.

In contrast to this, at the other end of the scale, the calculation with a 60 dB echo excess showed that when two bistatic receivers were added to the system (placed one either side of the monostatic position) the loss factor was at a minimum. No significant increase in performance could be achieved by adding more receivers.

2.9 The effects of parameter changes on the performance of a multistatic system

Because of the difficulties of generalisation in this situation, in particular with regard to the target contour, the discussion in the previous section necessarily dealt with a specific case involving a simple linear target model. Nevertheless, it illustrated certain aspects relating to the performance of a multistatic system which must be considered when assessing likely improvements in target shape portrayal provided by the system. These are summarised here under the following general headings:-

(a) The echo excess available at the monostatic receiver for the normally incident specular echo.

(b) The value of 'display magnification' chosen for the likely class of targets to be portrayed,

and (c) the effect of changing the width of the scanning sound beam with respect to a given target.

Considering the first of these, if other parameters such as projector beamwidth, range to the surveillance area and the value of 'display magnification' for a given target remain constant, then figure 2.7 shows the changes in the loss factor or performance index L for a 30 dB range of echo excess.

The worst case considered at 30 dB was shown in curve 4 and represented an upper limit in terms of L. Further reduction in the echo excess, always provided it is sufficient for any detections at all, does not alter the performance curve. A system operating at this end of the range will gain most from increasing system complexity by incorporating a number of bistatic receivers.

At the other end of the scale, when a large (60 dB) echo excess exists at the monostatic receiver, much less improvement is seen by incorporating bistatic receivers. The 30 dB range which separates these extremes might be considered small compared with the large changes in echo amplitude reported for small changes in target aspect [1]. However, it does mean that a trade-off between echo excess and the number of bistatic receivers needed to reach a given level of performance is possible at the system design stage. The nature of this trade-off, ie the shape of the curves shown in figure 2.7, will depend upon the nature of C_t. For example, on how many discontinuities are encountered during the scan, and only one example has been considered here.

The value of the 'display magnification' m chosen for the system and class of targets combination changes the performance curves by moving them up or down according to whether m is decreased or increased. In other words, the more cells which overlay C_t, the more there is to be gained by increasing the number of bistatic receivers. A more quantitative evaluation can be obtained by constructing a set of curves, as per the example above, for the likely targets under surveillance.

If m was doubled in the example above then all the curves shown in figure 2.7 would be moved up away from the X axis by approximately 3 dB per curve, but it should be noted that this applies if m is increased by introducing correspondingly larger targets into the surveillance area whilst keeping the system parameters constant. If m was increased by reducing the projector beamwidth and thereby changing the size of the basic resolution cell in terms of the number of wavelengths across the reflecting region, a different effect would occur. The aperture function $f_R(x)$ would be reduced in spatial extent and the reflected angular spectrum $F_R(S)$ would increase in spatial bandwidth. Assuming a constant power input to the projector, then its source level would be

increased by 3 dB. The increased spatial bandwidth would reduce the peak specular return by a corresponding 3 dB which in turn means that the same echo excess would result at the monostatic receiver. In the example above this means that a comparison can be made between the two systems with different beamwidths using a common 50 dB threshold, for example. Figure 2.10 shows the polar response of the specular reflection from an aperture which has been reduced by 50 percent by reducing the projector beamwidth. The detection arc is now 14 degrees at the 50 dB threshold level. At a projector steer of approximately 4 degrees the transition occurs from detection to non-detection of the corresponding insonified resolution cell. A count of the number of detected cells on the contour reveals that the monostatic receiver detected four cells either side of the normal incidence cell, making a total of nine. At the contour boundaries, when the reflecting aperture is reduced by about 14 percent, a detection is made at the monostatic receiver. Therefore the monostatic system can be expected to display a total of eleven cells scanning the same contour. A bistatic receiver placed outside the delineated regions defined by the detection arcs at the boundary and at normal incidence of the sound beam detected five cells when the simulation program was run with the new parameters. The resulting performance curve is shown in figure 2.11, which also shows the corresponding curve for 50 dB threshold taken from figure 2.7 for comparison. The conclusion is that the performance index L has not been changed significantly by doubling the value of m in this way. A similar argument applies if m is reduced for a given contour C_t by increasing the projector beamwidth.

What has deliberately not been discussed here, and what the figures do not convey, is the likely value of L at which satisfactory portrayal of target shape is achieved. Changes in the value of m for a fixed contour will involve information rate changes and also subjective changes to do with target recognition factors.

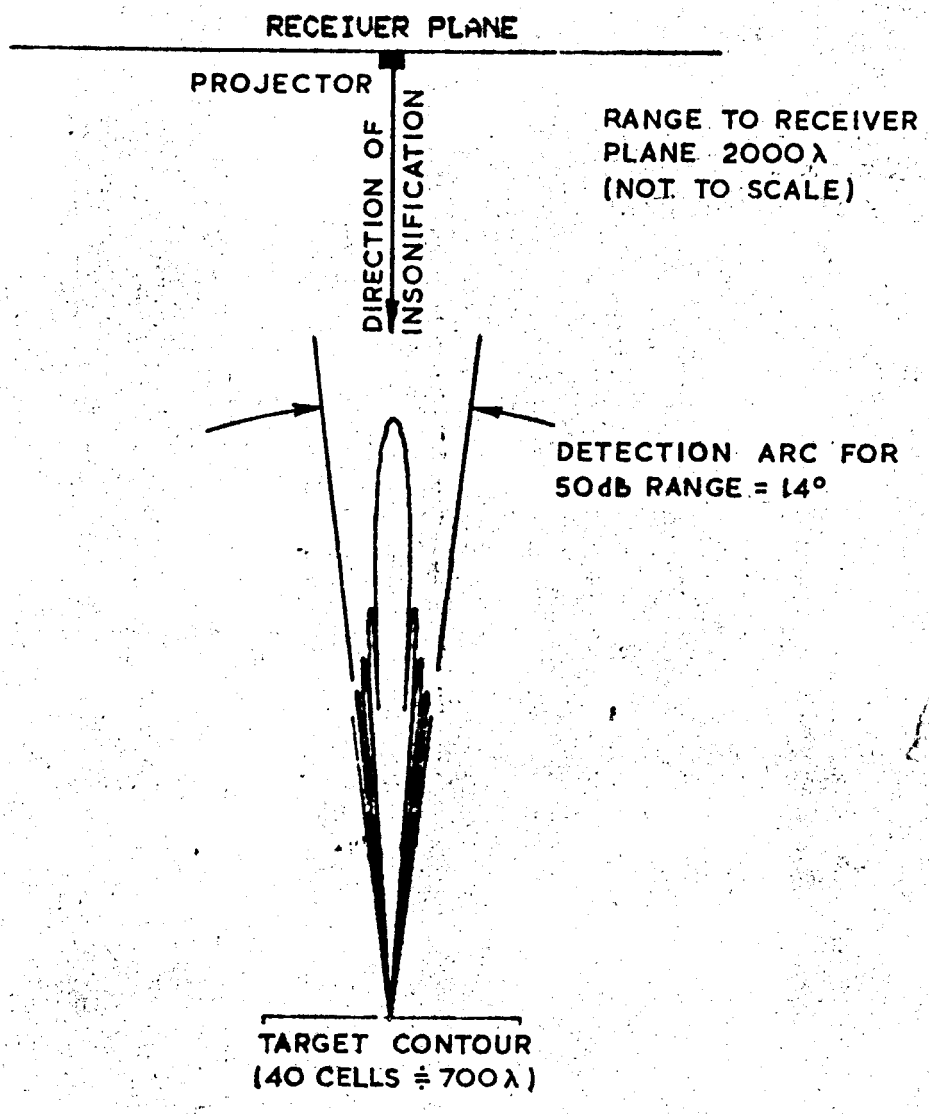

FIG 2·10. 50dB REFLECTION POLAR RESPONSE AT NORMAL INCIDENCE SHOWING INCREASE IN DETECTION ARC DUE TO A 50% REDUCTION IN PROJECTOR BEAMWIDTH. THE NUMBER OF RESOLUTION CELLS IN THE TARGET CONTOUR HAS BEEN DOUBLED

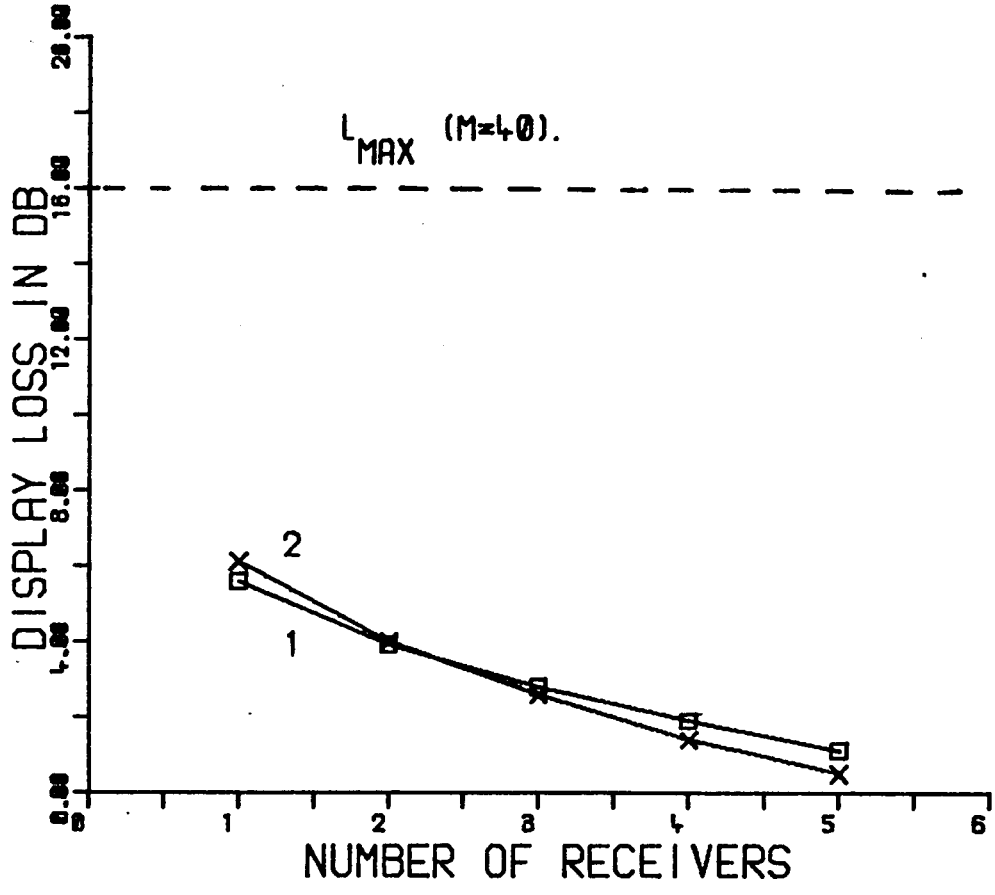

PARAMETERS 1=50DB ECHO EXCESS
2=50DB ECHO EXCESS (FROM FIG 2.7)
BEAM WIDTH =0.75DEG (1)
=1.5DEG (2)
RANGE =2000 WAVELENGTHS

FIG 2.11 EFFECT OF CHANGING THE VALUE OF M ON THE DISPLAY LOSS.

No conclusions can be drawn from the discussion here concerning the choice of m for recognisable target shape portrayal, but it is significant that the performance of the system does not seem to be a function of the projector beamwidth, provided that the 'display magnification' m, lies between sensible limits for a given contour. By this is meant that,

(a) m is sufficiently greater than unity to justify any additional receivers, and the situation with m = 1 and L = 0 dB does not apply, and

(b) m is not so large that the Fourier transform method no longer applies (see section 2.10.1 below).

2.10 Limitations of the method used to predict system performance

2.10.1 Applicability of the Fourier transform technique

The transformation of an aperture function into a far field beam pattern is an accepted method of dealing with the problems of beam pattern anaylysis and synthesis. In order to apply this technique here it was assumed that the aperture function $f_R(x)$ was well behaved with a linear phase shift due to the angle of incidence of the sound beam being the only disturbing feature.

In practice the reflecting surface is rarely smooth and usually possesses surface irregularities which contribute random changes in $f_R(x)$. These surface features can be described by their RMS height about a mean and if the RMS height is less than $\frac{1}{4}$ wavelength, then Rayleigh's criteria says that their effect on scattering is small. An average smooth surface can be postulated onto which is superimposed a function describing the distance of perturbations from this average in fractions of the wavelength of interest. The phase distribution across the aperture is now described in terms of a phase slope due to the angle of incidence plus a randon phase due to surface roughness. In a similar fashion, changes in reflectivity can be incorporated into the amplitude function so modifying $f_R(x)$ in its two degrees of freedom.

The effect of these perturbations will be generally to widen the angular bandwidth of the reflection from each cell and thereby increase the detection arc for each cell. This mitigates against the gains from adding multistatic receivers to the system by moving the performance curves in figure 2.7 downwards towards the 0 dB line. However, this was not the object of the exercise and a target can always be chosen with a sufficiently rough surface to cause wide angular spectrum bandwidth on reflection. The problem studied here was concerned with how to improve the performance of a system which was already limited by scanning a sufficiently smooth target surface to cause highly specular and narrow

band angular reflections.

Eventually, as surface roughness increases to the point where acoustic shadowing occurs within an individual resolution cell the transform approach as described here becomes no longer applicable. However in this case the situation has again changed from the consideration of straightforward reflection to that of sound scattering by each resolution cell.

An important simplification was made initially by assuming that the narrow band nature of the transmissions allowed the time variations to be omitted from equations 2.5 to 2.17 for the purposes of clarity. Finite bandwidth in the transmitted signal is of course necessary if the resolution cell is to include the range resolution dimension. The extension to the method used here to include finite bandwidth signals is based on the assumption that the processes of propagation and reflection are linear so that superposition can be applied. The transmitted signal is therefore Fourier analysed into its component sinusoids and each component then treated as above. The echo at the receiver plane is then found by a synthesis of the reflected components.

If time variations are included in the transform equations 2.8, the angular spectrum can be re-written as:-

$$F_R(S,f) = \int_{-\infty}^{\infty} \int_{-\infty}^{\infty} f_R(x,t).\ \exp(-jkXS).\ \exp(-j2\pi ft)\ dxdt \quad . \ . \ . \qquad 2.20$$

If $f_R(x,t)$ is written as the product of two functions $f_R(x)$ and $f_R(t)$, where $f_R(t)$ represents the time variations, the double integral above can be written as the product of two single integrals thus:-

$$F_R(S,f) = \int_{-\infty}^{\infty} f_R(x).\ \exp(-jkXS)dx \int_{-\infty}^{\infty} f_R(t).\ \exp(-j2\pi ft)dt \qquad 2.21$$

. . . . . .

where $k = w/c$,

$w = 2\pi f$,

c = velocity of sound,

and f = temporal frequency in Hz.

Independence of the two integrals is a function of the magnitude of the change in k with frequency. In this work a Q-factor of 10 was used in the transmission and reception circuit filters which implies an effective aperture with modulation of about 10 percent. Applied to the example used above in section 2.7, the nominal aperture of 70 wavelengths was changed by 10 percent and changes in the detection arc for a 50 dB echo excess evaluated with the simulation program. The result was that the detection arc at the monostatic position (normal incidence) changed from 8.5 to 9.5 degrees. This 1.0 degree change did not materially affect the performance curves shown because the scan increment exceeded this, and it was concluded that for Q-factors of 10 or more, independence of the two integrals can be assumed in this situation. Range resolution can therefore be considered separately.

2.10.2 The target contour C_t

Of necessity a very simple example was chosen to illustrate the effects on system performance of a multistatic environment. Targets are not generally so well defined in terms of C_t, and the performance of a multistatic system when portraying a more complex contour is not so easily determined. The technique described above in section 2.6 must be applied with care if a sensible prediction of performance is to be obtained. The experimental work described in CHAPTERS IV and V was an attempt to evaluate a real world situation and compare results with the general predictions made.

An important aspect of the target contour to be considered in any event is the number of discontinuities likely to cause aperture function changes as described in section 2.6 above. The word discontinuity is taken here to mean some departure from linearity of the contour. Two cases can be enumerated,

(a) If the change in the contour occurs over a number of resolution cells, then the curvature within any cell will be small by definition. Each cell can therefore be given an average phase slope in addition to that due to the angle of incidence of the sound beam. The total phase slope will steer the direction of specular echoes in the normal way, but will not cause any increase in the angular bandwidth due to aperture limiting for example.

(b) The second case has already been mentioned in section 2.7.1 which discussed the applicability of the transform technique. It concerns changes in the contour which occur within the resolution cell, and one case in which a discrete range change occurred was considered in 2.7.1, where a physical limit on aperture size was caused by a target boundary. Reiterating what was stated previously, this case can be treated by incorporating an average phase slope plus a random component into the function $f_R(X)$.

The first case (a) is unlikely to mitigate against the multistatic environment, but the second case (b) has been shown to reduce the likely gains from such an environment.

CHAPTER III

AN EXPERIMENTAL HIGH RESOLUTION MULTISTATIC SONAR SYSTEM

3.1 Introduction

This chapter describes the sonar system which was constructed in order to observe and study the acoustic echo patterns from specularly reflecting targets placed in a multistatic sonar environment.

In common with any sonar system, the experimental equipment included certain basic components, namely a beamformer or scanning system, a receiver and transmitter subsystem and an echo pattern display device. The beamforming and scanning was performed by mechanically sweeping a narrow beam of ultra-sound across the surveillance area and measuring the angular position of the beam. Echoes from the targets used were detected by three acoustic hydrophones suitably positioned in the experimental tank. Their outputs were threshold processed and used to trigger the transmission of data to a small digital computer for display and analysis.

A schematic diagram of the complete system is shown in figure 3.1 and it can be seen that the sonar comprised two functionally and geographically separate parts linked by a data cable. The analogue sonar end generated the data necessary for the digital computer to format and produce the echo pattern displays. It comprised the mechanical components such as the scanner and hydrophones, and all the electronics needed to perform its function.

Some photographs of the various equipments which were constructed by the author are shown in the accompanying figures. With reference to these, figure 3.2 shows the mechanical scanner arrangement, which included the sound projector transducer. This also doubled as one of the three receiver hydrophones via a transmit-receive switch in the

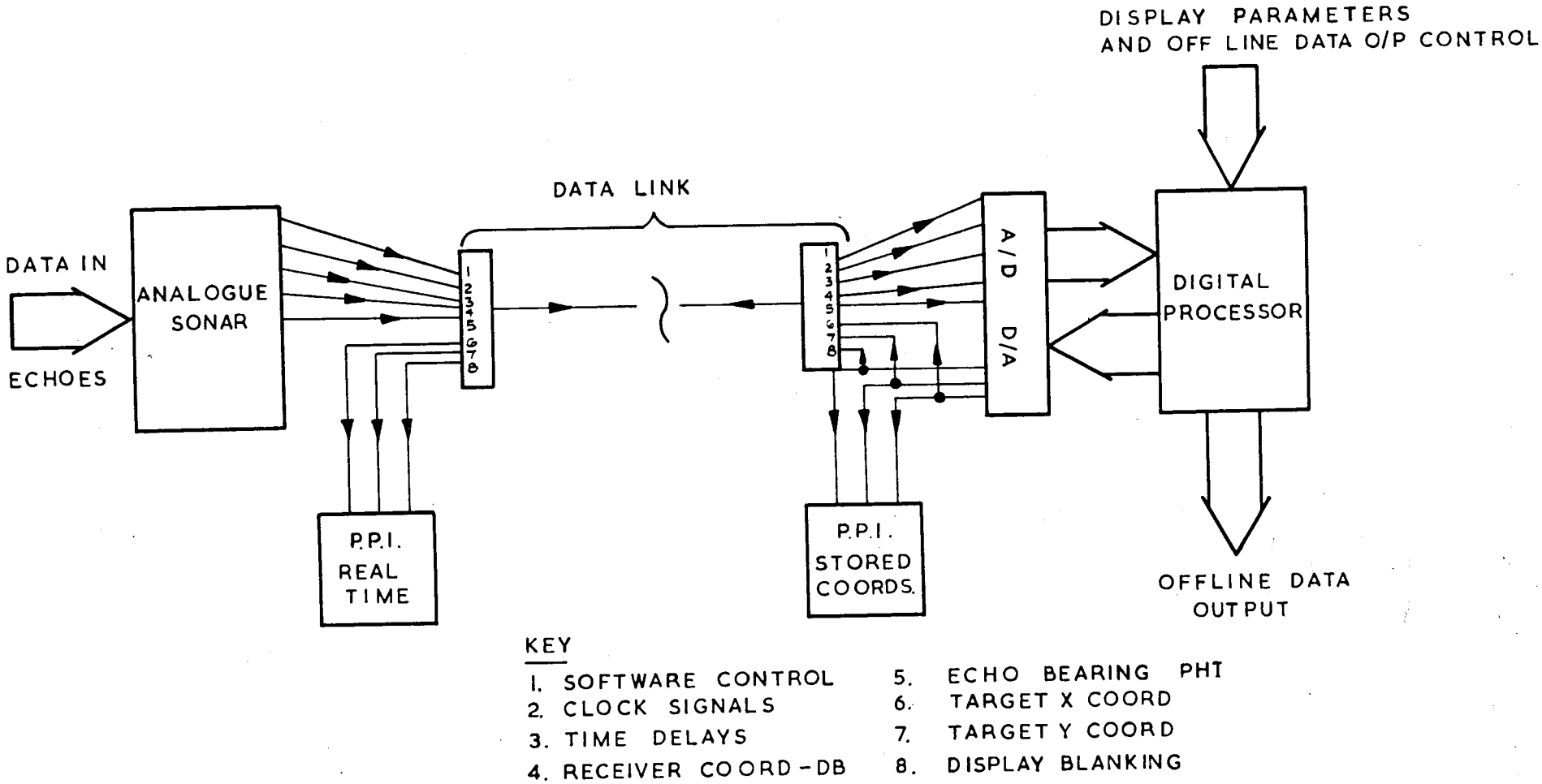

FIG.3·1 HIGH RESOLUTION SONAR SYSTEM.

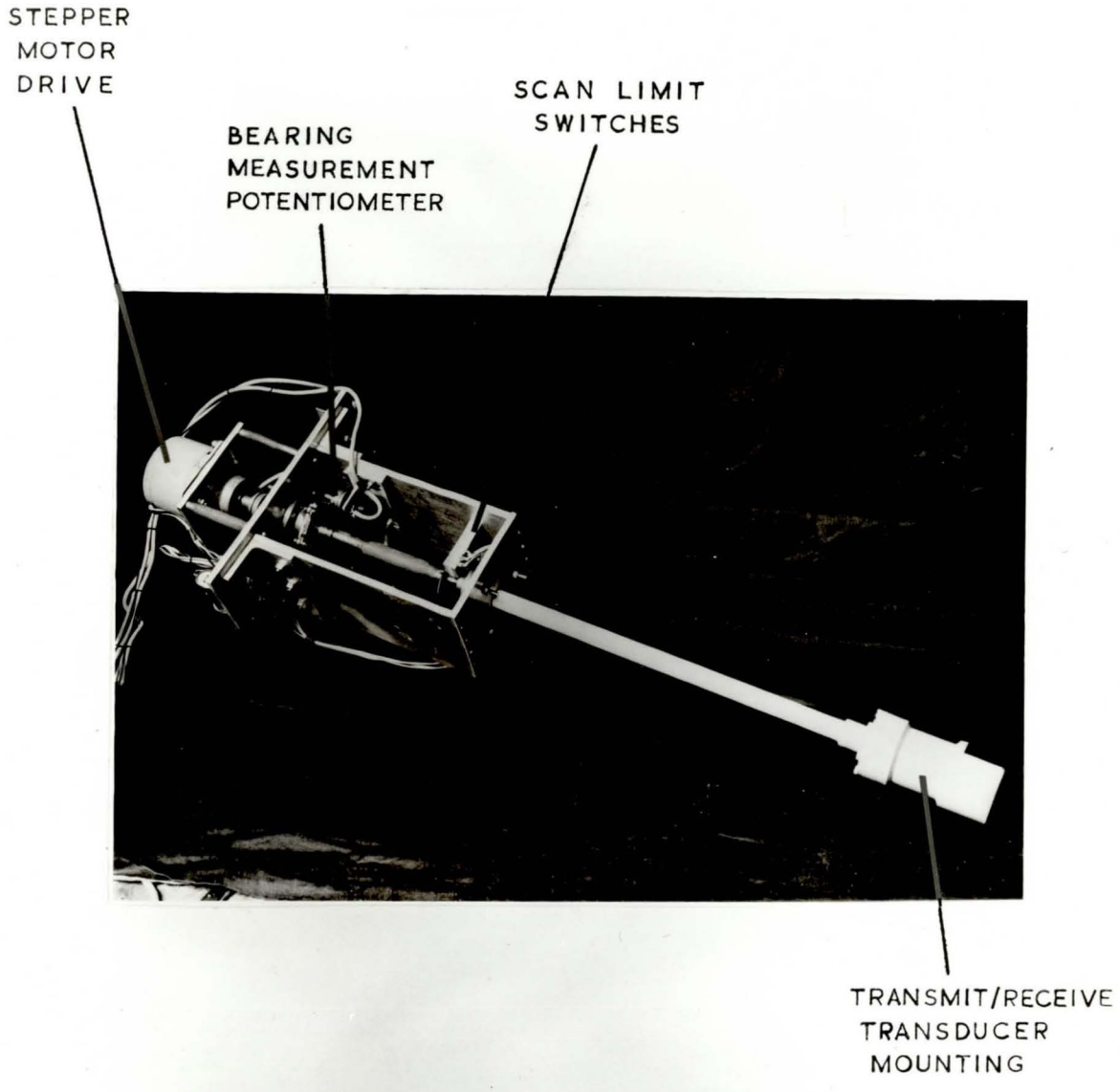

FIG. 3·2 PHOTOGRAPH SHOWING THE MECHANICAL SCANNER ARRANGEMENT INCLUDING DRIVE MOTOR LIMIT SWITCHES, BEARING MEASUREMENT AND TRANSMIT/RECEIVE TRANSDUCER

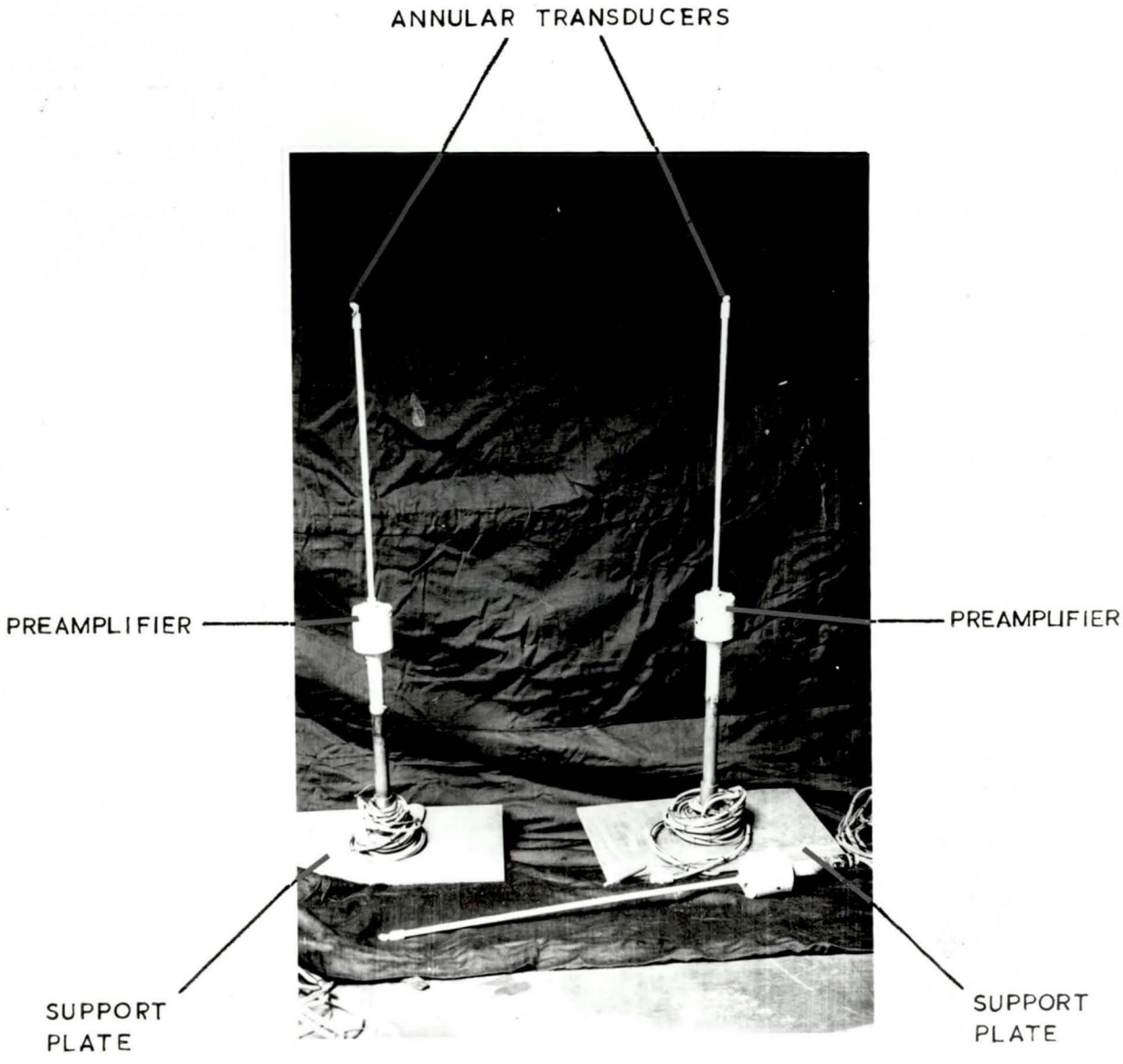

FIG. 3·3. PHOTOGRAPH SHOWING THE HYDROPHONES AND INTEGRAL PREAMPLIFIER ASSEMBLY

FIG 3.4

FIG 3.4 A PHOTOGRAPH SHOWING THE ANALOGUE SONAR.

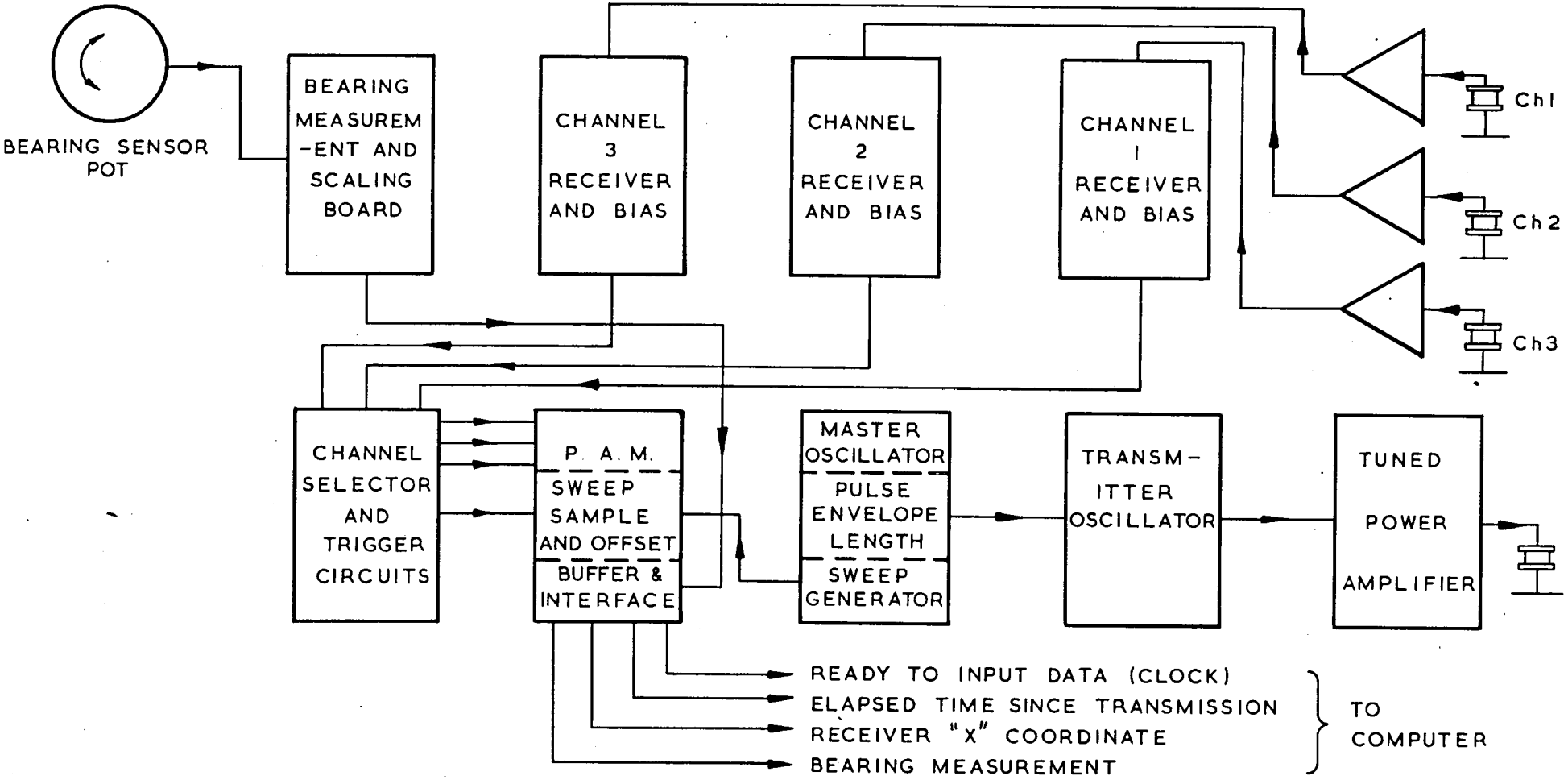

FIG.3·5 HIGH RESOLUTION SONAR SYSTEM INFORMATION FLOW AND INTERCONNECTIONS

electronics. Figure 3.3 shows the additional hydrophones, mounted on support plates, which were needed to form the multistatic environment. Finally, figure 3.4 shows the double layer electronic rack which was used to house the various circuit cards constructed. The function of each of these cards together with the signal flow and interconnections between them is shown in figure 3.5, and a description of the operation is given in the next section.

The digital processor end accepted the analogue data sent by the sonar and processed this data to produce the ppi displays shown in CHAPTER V. Certain other utility functions were included in the program as indicated in figure 3.1. These are explained in section 3.3 below which describes the operation of this part of the system.

A description of the operation of the complete system divides naturally into two parts dealing firstly with the analogue sonar, and secondly with the digital display processor. The remainder of this chapter is consequently devoted to this description and then a brief analysis of the performance and errors introduced by the equipments.

3.2 Operation of the high resolution analogue sonar

3.2.1 General

As stated above the function of the sonar was to provide data to enable the digital computer to format and provide a ppi display of the target echo patterns. This data was input to the computer via an analogue to digital converter (ADC) interface designed specifically for operation with the computer. The salient parameters of the ADC, ie resolution, dynamic range, timing and mode of operation, influenced the design of the equipment because it was necessary to provide analogue data which was compatible with the specification of this device. These parameters are listed briefly for reference purposes in table 3.1.

TABLE 3.1: SALIENT PARAMETERS OF ANALOG INPUT MODULE

TYPE 1.722 FOR MODULAR ONE COMPUTER

Clocked Input Mode	
Input Range	-5.120V to +5.115V (±15V overload)
Input Accuracy	±5mV
Number of Bits	10 plus sign bit
Timing	
Transfer Data from Old Conversion	0.2 μs
Set Multiplexer to new channel	5 μs
Hold and Digitise Signal	11.2 μs
Total Time (excluding variable track time)	16.4 μs

The most important aspects were, as mentioned, the time for conversion of one data channel, the accuracy or value of the least significant bit, and the maximum input voltage magnitude before overload.

Operation of the system can be understood by reference to figure 3.5 which shows information flow and interconnections, and by reference to figure 3.6 which is a schematic timing diagram for the equipment. Four output signals can be identified in figure 3.5 which are transmitted to the computer. These signals are also shown in figure 3.6 as traces K, C, M, and N respectively. An explanation of the generation of these signals will describe the operation of the complete system and is given briefly below.

3.2.2 Generation of the clock pulse (RID) trace K in figure 3.6

Generation of this signal will be described first because it was the control signal which informed the computer that data was available, and initiated the sequence of events culminating in an echo 'paint' on the ppi display.

The periodic sequence of events shown in figure 3.6 was controlled by the master timing oscillator shown as trace A in figure 3.6. The positive going edge of this waveform triggered the transmitter oscillator, which generated a fixed number of oscillations controlled by the pulse length circuit. The output from this circuit was fed via an impedance matching network to the transmitter power amplifier driving the piezo-electric transducer used for transmission.

Echoes from the target were received on one or more of the three hydrophones employed in the system, and after an initial amplification stage were processed in the receivers of which figure 3.7 is a schematic diagram of one channel.

FIG .3·6

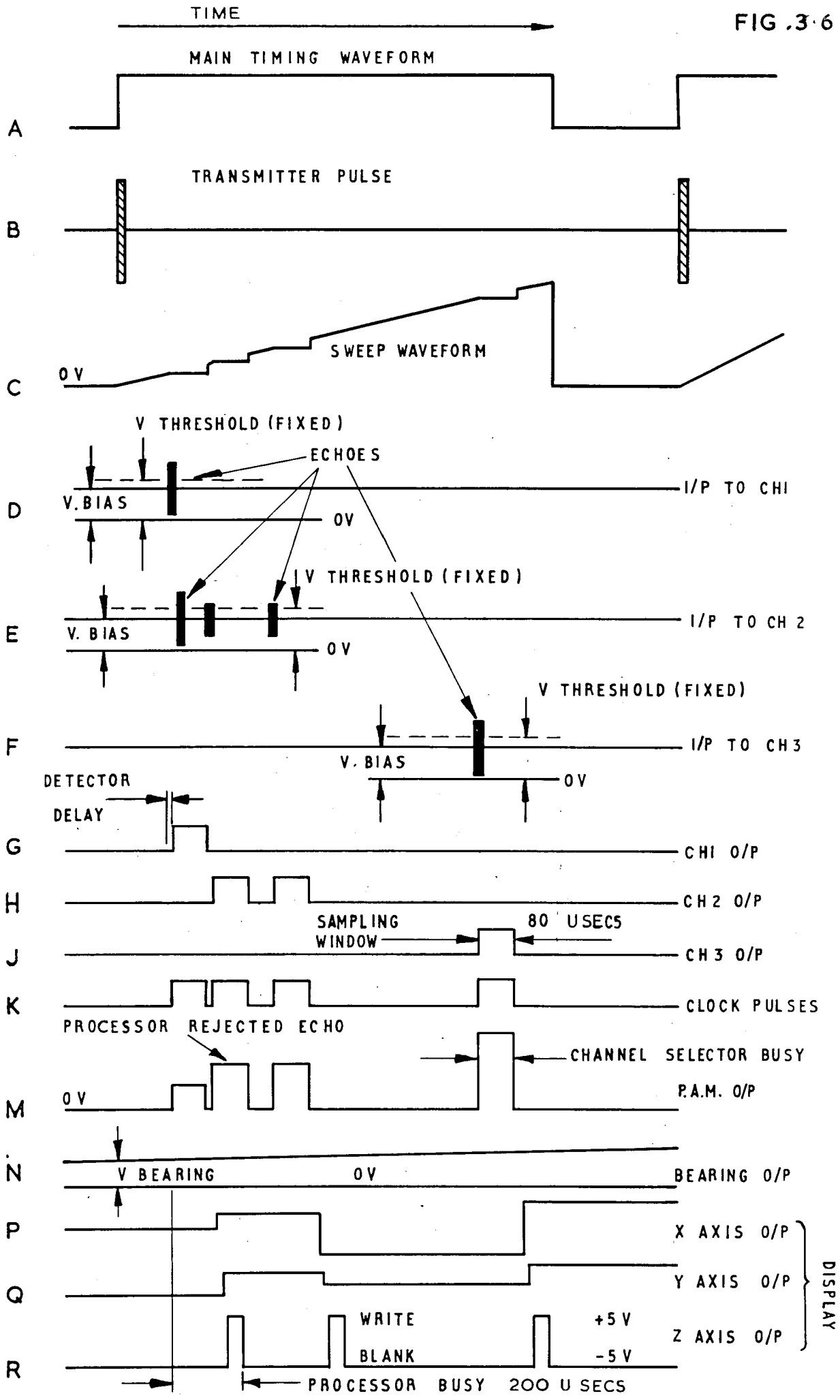

FIG.3·6 HIGH RESOLUTION SONAR OPERATION.

The receiver consisted of a simple two-stage cascaded tuned amplifier followed by a buffer stage, and finally a bias network. The output of the bias network, shown as traces D, E and F, formed the input to a threshold detector in the form of a temperature compensated Schmitt trigger. When the signal plus the bias exceeded the preset threshold voltage the Schmitt trigger generated a pulse at its output corresponding in time to the duration of the signal above the threshold. The output from each detector was input to a channel selector circuit which generated a unique 80 μs output pulse corresponding to the input channel and also inhibited the generation of any other outputs during the 80 μs period. These outputs are shown as traces G, H, and J. The outputs from all channels were logically combined by an OR function to provide the clock pulse, which was then used as the sampling pulse for the ADC and the sweep sampling circuit which is described below.

3.2.3 Generation of the time delay (PL) trace C in figure 3.6

The positive-going edge of the master timing oscillator also triggered a linear time base circuit which is shown as trace C in figure 3.6.

This sweep generator provided a linear ramp voltage in the range 0 – 5 volts which was proportional to the elapsed time after transmission. The linearity of the sweep was designed to be compatible with the resolution of the ADC, and the time period of the sweep determined the maximum range of the sonar and therefore the size of the range bins. This was because the number of range bins was fixed by the sweep amplitude which always corresponded to a digital range of 0 – 1000 in unit cell increments. Thus a maximum of 1000 range bin increments were possible within the sweep period.

A track and hold circuit continuously monitored the sweep output and when a clock pulse was generated, as described above, the sweep voltage, at the instant of the front edge of the clock pulse, was held on a buffer capacitor for the 80 μs duration of the clock pulses. This voltage, suitably buffered, was then transmitted to the ADC at the digital computer as shown in figures 3.5 and 3.6.

3.2.4 Generation of the receiver x co-ordinate (DB) trace M in figure 3.6

The output of the receiver bias circuit was fed to the Schmitt trigger corresponding to that channel and information about which receiver had generated the particular signal was implicit in the particular Schmitt trigger circuit which was stimulated. Consequently, the outputs from each pulse - stretching monostable (one per Schmitt trigger), were input to a simple operational weighting network in which each input was weighted according to the physical separation of the transmitter and receiver. The output of this pulse-amplitude modulator (PAM) was a time series of weighted pulses and formed the input to the ADC which corresponded to the receiver x co-ordinate.

Weighting of the pulses was on the same scale as the range sweep and was affected by adjustment of the summing resistors in the circuit (see APPENDIX A for details). The calibration of this circuit is described in the next chapter which deals with experimental procedure.

3.2.5 Generation of the bearing voltage (ϕ), trace N in figure 3.6

The information concerning the azimuthal angle of the sound projector was coded into a slowly varying dc voltage. The whole transmitter and monostatic receiver arrangement was mounted on a mechanically scanned rig driven by a stepper motor, and the angular position of the transducers was coupled to a linear potentiometer by a mechanical linkage which can be seen in figure 3.2.

A voltage was applied across the potentiometer and the slider output was then proportional to angle. This output was fed into a high impedance buffer circuit for amplification and rescaling before being transmitted to the ADC interface; note that since the rate of change of bearing voltage was small during the sampling period of 80 μs no sample and hold circuit was employed here.

Typically, the scanner speed was approximately 14 rpm for a traverse of 0 - 90 degrees. The triangular output voltage was scaled from 0 to 4.5V and in the 80 μs sampling period the change in bearing voltage was calculated as approximately 0.33 mV. Since the ADC least significant bit value was 5 mV no holding circuit was deemed necessary.

The voltage range quoted above gave an accuracy of 0.1 degrees, which was consistent with the requirements of minimising errors in the bearing measurement (see section 3.4.2). In practice the angular resolution of the equipment was much less than this figure, being defined by the beam pattern of the transmitter.

3.2.6 The receiver and threshold detector

As mentioned in section 3.2.2 above, the received echoes were required to exceed a preset threshold before causing data to be strobed into the digital computer.

The transmitted signal was a simple pulsed continuous wave (PCW) signal at a carrier frequency of 2.5 MHz. This signal s(t) can be represented as,

$$s(t) = A(t) \sin (\omega_o t + \theta), \qquad 3.1$$

where $A(t) = A$ for $0 \leq t \leq T$

$= 0$ for $t > T$

A(t) is the envelope function which was ideally a rectangular pulse of duration T seconds and amplitude A volts.

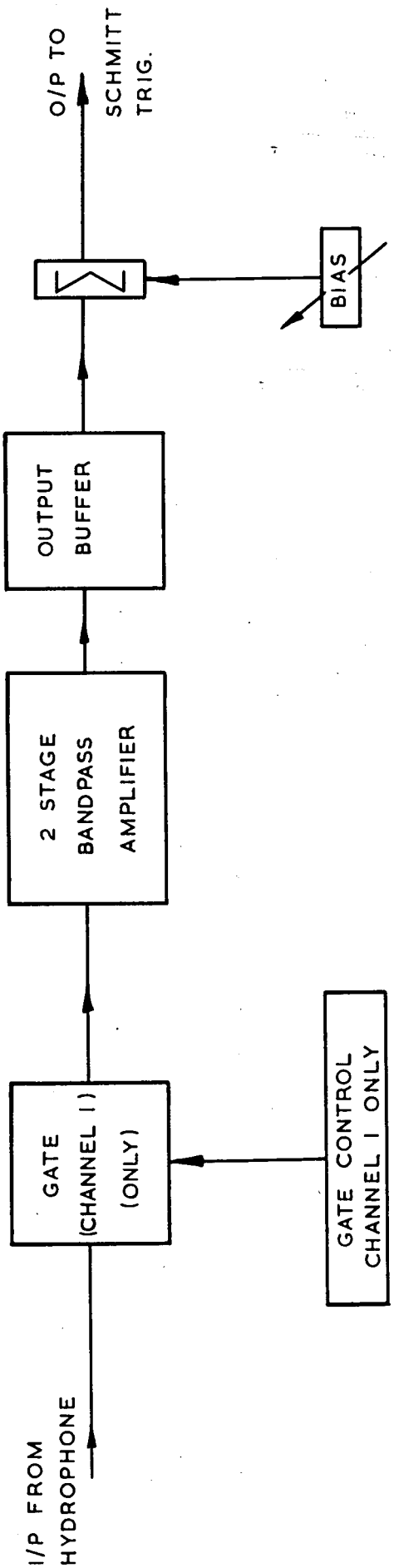

FIG 3·7 RECEIVER SCHEMATIC

Assuming the linearity of the echo formation process as described in CHAPTER I and the absence of reverberation interference, then the received signal at any one hydrophone will, in general, be a linear combination of signals of the form of equation 3.1 above. This combination process is the convolution of the target impulse response $R_t(t)$ and the incident signal $s(t)$.

Thus $y(t) = s(t) * R_t(t) + n(t)$,

where $y(t)$ represents the received signal,

'*' represents the convolution integral, and

$n(t)$ represents an unwanted noise component in the received signal.

If the noise $n(t)$ is stationary, white and Gaussian distributed, G L Turin [17] shows that the signal to noise ratio at the output of the receiver is maximised by a receiver whose frequency response $H(f)$, is the complex conjugate of the transmitted signal $S(f)$, ie a matched filter. However, in the case where the signal is of a simple form then it is the bandwidth of the receiver which is important and M Schwartz [18] shows that for a simple rectangular signal of the form equation 3.1 above then the loss in SNR for a first order network is of the order +1.0 dB relative to the matched filter. This augurs well for the use of a simple receiver, and a tuned bandpass network was employed here with a centre frequency and bandwidth corresponding to that of the signal $s(t)$.

The output from the tuned filter was input to a bias network which introduced a positive dc offset voltage into the signal. The output from the bias network was therefore $b(t) = q(t) + B$, where $q(t)$ was the output of the filter and B is the dc bias. This signal formed the input to the threshold detector which operated on a fixed positive threshold value V_t. The output of the detector was,

$$m(t) = 1 \text{ for } b(t) > V_t$$

$$= 0 \text{ for } b(t) \leq V_t.$$

The way in which this scheme worked is shown diagrammatically in figure 3.8 where it can be seen that a variation in bias B was equivalent to a variable threshold. The detector effectively operated on the sum of rectified cosine shaped signal pulses and noise. This would give a false indication of the number of targets for a finite length bandpass signal as shown. If the detector output is used to trigger a pulse lengthening circuit or monostable, then this problem does not occur since the first half-cycle of the signal to exceed the threshold causes a fixed length pulse to be output from the monostable. Provided this is not a retriggerable monostable, then only one detection can ensue. In this case the monostable circuit was incorporated in the channel selector circuit as described above, and the pulse length was dictated by the needs of the ADC interface rather than being matched to the length of the signal envelope after filtering.

3.3 The digital processor

3.3.1 General

The digital processor which was interfaced to the analogue sonar system, described above, was a type 'CTL Modular One', sixteen-bit, parallel-arithmetic computer with hardware multiply and divide logic. System peripherals included two teleprinters and an analogue input/analogue output converter module as described above.

The primary reason for incorporating the digital computer into the system was to format the analogue data from the sonar into a rectangular co-ordinate system suitable for display and analysis purposes. Study and assessment of the performance of high resolution sonars revolves around the final display to the operator, and the digital computer and software programs used provided an easily controlled display which enabled analysis of the system to be made. The format of the output X,Y co-ordinates was arranged to provide a display of the scanned area

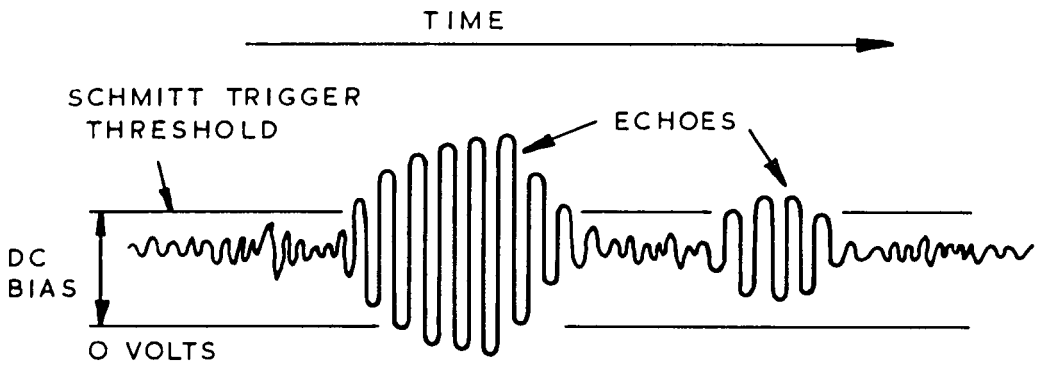

OUTPUT OF BANDPASS AMP. AND
INPUT TO SCHMITT TRIGGER CIRCUIT

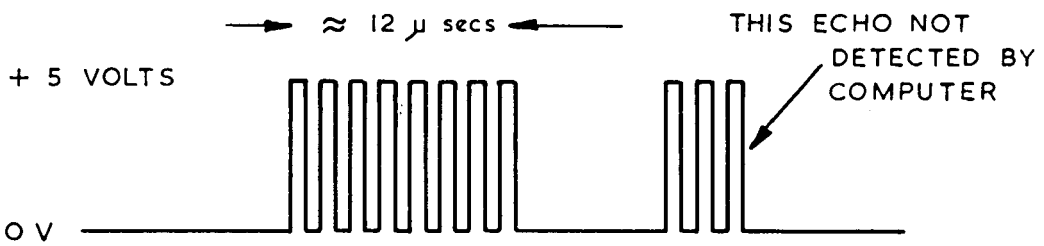

OUTPUT OF SCHMITT TRIGGER AND
INPUT TO PULSE STRETCHING MONOSTABLE

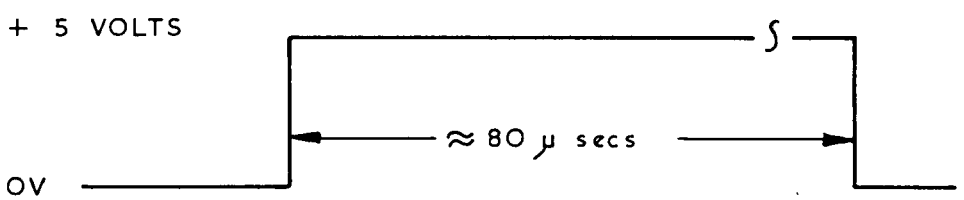

OUTPUT OF MONOSTABLE AND INPUT TO CLOCK
PULSE AND CHANNEL INHIBIT CIRCUITS

FIG. 3·8 SCHEMATIC DIAGRAM SHOWING THE OPERATION OF THE RECEIVER – DETECTOR CIRCUITS

of 1000 by 1000 range increments, thus providing a resolution of 10^6 picture elements or cells. Each of these cells was given a weighting of '1' or '0' according to whether a signal was present or not in each cell. As mentioned in CHAPTER I, the binary nature of the display simplified the formatting of data, reduced the quantity of data input to the computer and also the amount of storage required to store a data frame per scan by approximately 30 percent.

Since the display was of a binary nature, target echoes were defined by their X,Y co-ordinates and occupied two words of storage. However, even with this order of data reduction the total storage requirements were clearly far greater than the available memory of some 16K words (K = 1024). Under these circumstances it is sometimes more efficient to store the display as a bit pattern which in this case would require 10^6 bits of store. The disadvantage with this technique is the increased complexity associated with decoding and coding the display in the computer and in the interests of simplicity this method was rejected (even assuming that less than 10^6 bits are stored) in favour of storing the co-ordinates as 2 word vectors. In practice, most of the total scanned area contained no echoes at all and the display was confined to a small cluster of echoes around the target. It was found experimentally that on average only approximately 100 echoes occurred per scan so that 16K of memory was more than adequate.

The actual method of data storage used was based on an angular addressing mode which made subsequent retrieval of target data a matter of defining an angular sector only. Associated with each detected echo which was input to the computer was a bearing word which was quantised into the range 0 - 900 decimal. This corresponded to a scanned sector of 0 - 90 degrees and thus gave the accuracy of 0.1 degree quoted previously. This bearing word was used as an angular bin address into

which the computed co-ordinates were placed. The stored display was therefore represented as a maximum of 901 segments in the range 0 - 90 degrees, and the echo co-ordinates were represented as the elements of a two-dimensional array with subscript B, where B was the echo azimuth bearing. The total storage required was thus 1802 words for a 90 degree sector.

The disadvantage with this method was that multiple echoes occurring in the same azimuthal segment, but at different ranges, were overlaid in the memory such that only the last occurring echo was retained. In other words, if three echoes, E_1, E_2, and E_3 occurred at times t_1, t_2, t_3, (where $t_1 < t_2 < t_3$), but each had the same bearing address B say, then only E_3 would remain at the end of the epoch $t_1 - t_3$.

It was stated in CHAPTER I, that the targets used in the experiments were constructed with hollow air filled interiors. This was specifically to present a unity reflection coefficient and avoid the generation of internal echoes. These multiple internal echoes would by definition all occur with the same bearing address B and therefore only the last echo would be retained. However, two other possibilities existed regarding the loss of data due to overlaid echoes. Firstly, random noise in the system could occur at any range and on any bearing with equal probability. Target echoes would be overlaid by noise generated false echoes which occurred at greater ranges than the target, but on the same bearing addresses as the stored echo co-ordinates. Secondly, because the transmitter beam pattern had side-lobes of finite amplitude, there was the possibility of spurious echoes due to side-lobes occurring at greater ranges than the current main-lobe echo. Because the bearing address was the same for the side-lobes and main-lobe, the wanted echo could be over-written by the side-lobe response.

3.3.2 Display noise reduction

Returning to the first possibility mentioned above, ie noise-generated false echoes, a simple display noise reducing feature was built into the software programs which utilised the physical stationarity of the target.

The noise was assumed to be Gaussianly distributed and stationary (statistically), so that there was an equal chance of noise exceeding the signal threshold at any range and bearing. Noise on the display will therefore be evenly distributed spatially and will change from scan to scan. By spatially correlating each scan with a reference display by some means, only those echoes which consistently remain in the same geometrical location will be retained as genuine echoes. The effects of noise overwrite described above could then be reduced by allowing a sufficient number of scans to integrate in the display store.

The correlation process was simplified by the method of data storage which assigned a unique location for each echo. To perform the spatial correlation, the reference X,Y data with address subscript, B, corresponding to the bearing of the current echo co-ordinates $(X_I\ Y_I)$, was used to calculate a difference vector

$$\begin{bmatrix} X_D \\ Y_D \end{bmatrix} = \begin{bmatrix} X_R \\ Y_R \end{bmatrix} - \begin{bmatrix} X_I \\ Y_I \end{bmatrix} \quad \ldots\ldots \quad 3.1$$

where X_R and Y_R are the reference co-ordinates with the same address B.

Then

$$\begin{bmatrix} X_o \\ Y_o \end{bmatrix} = \begin{bmatrix} X_I \\ Y_I \end{bmatrix}, \qquad X_D \leq T_X \text{ and } Y_D \leq T_y$$

$$\begin{bmatrix} 0 \\ 0 \end{bmatrix}, \qquad X_D > T_X \text{ or } Y_D > T_y \qquad 3.2$$

where X_o, Y_o are the displayed echo co-ordinates and T_x, T_y are spatial tolerances. In other words, the echo was displayed if it lay within an association area defined by T_x T_y, otherwise it was rejected.

This was a straightforward method which required only a small number of operations in the processor. In order to work successfully however, a suitable reference display was required. Since no a priori knowledge of the target echo patterns was available, the reference display was itself a representation of the actual surveillance area. The reference display was the accumulation of a number of scans chosen to ensure that good target echoes were present and also that undue saturation of the reference by noise was avoided. During the course of the experimental work with the sonar, the problem of noise on the display was found to be less severe than was anticipated. This was attributed to the near ideal operating conditions in the experimental tank, ie uniform temperature, freedom from turbulence and surface and bottom echoes etc. Nevertheless, this feature illustrated the flexibility introduced by the programmable computer which enabled this sort of sophistication to be introduced by straightforward modification to the software, and without the need for additional hardware.

3.3.3 Brief description of program operation

The computer formatted the input data derived from the monostatic and bistatic receivers and placed echoes obtained from this data into the corresponding display cells.

Calculation of the display, X,Y co-ordinates of the echo was made using the transformation from cylindrical to rectangular co-ordinates where,

$$\left.\begin{aligned} X &= R \cos \Phi \\ \text{and } Y &= R \sin \Phi \end{aligned}\right\} \qquad 3.3$$

In equation 3.3,

$$R = \frac{PL}{2} \text{ for the monostatic case and,}$$

$$R = \frac{(PL^2 - DB^2)}{2(PL - DB\cos\Phi)} \text{ for the bistatic case} \quad [19]$$

The bistatic range was the solution of the triangle formed between the transmitter, receiver, and target echoing location or cell. PL represents the total path length travelled by the signal from the transmitter via reflection to the receiver, and DB represents the receiver-transmitter separation or data base. The angle between the data base and the transmit direction is represented as Φ .

The data input to the computer was defined by these relationships and was discussed above in section 3.2.

A flow diagram which illustrates program operation is shown in figure 3.9.

When the program is started a number of resolution parameters are entered from the keyboard. These parameters set up the quantizing step size for the range delay and bearing word. Quantisation of the input data has the effect of combining a number of input cells to form one new cell. This process was illustrated schematically in CHAPTER I, figure 1.1, and gives a measure of control over the output display definition. However, in the experimental work the most used parameters were unity range and bearing quantising, ie maximum definition, and nearly all the display results presented are with these values.

A cosine table is then generated in the form of a 901 elements corresponding to values of cosine from 0 - 90 degrees in 0.1 degree steps. The sine-cosine functions required in the program are extracted from the look up table by generating an indirect address from the bearing word. This standard method enables high speed sine-cosine

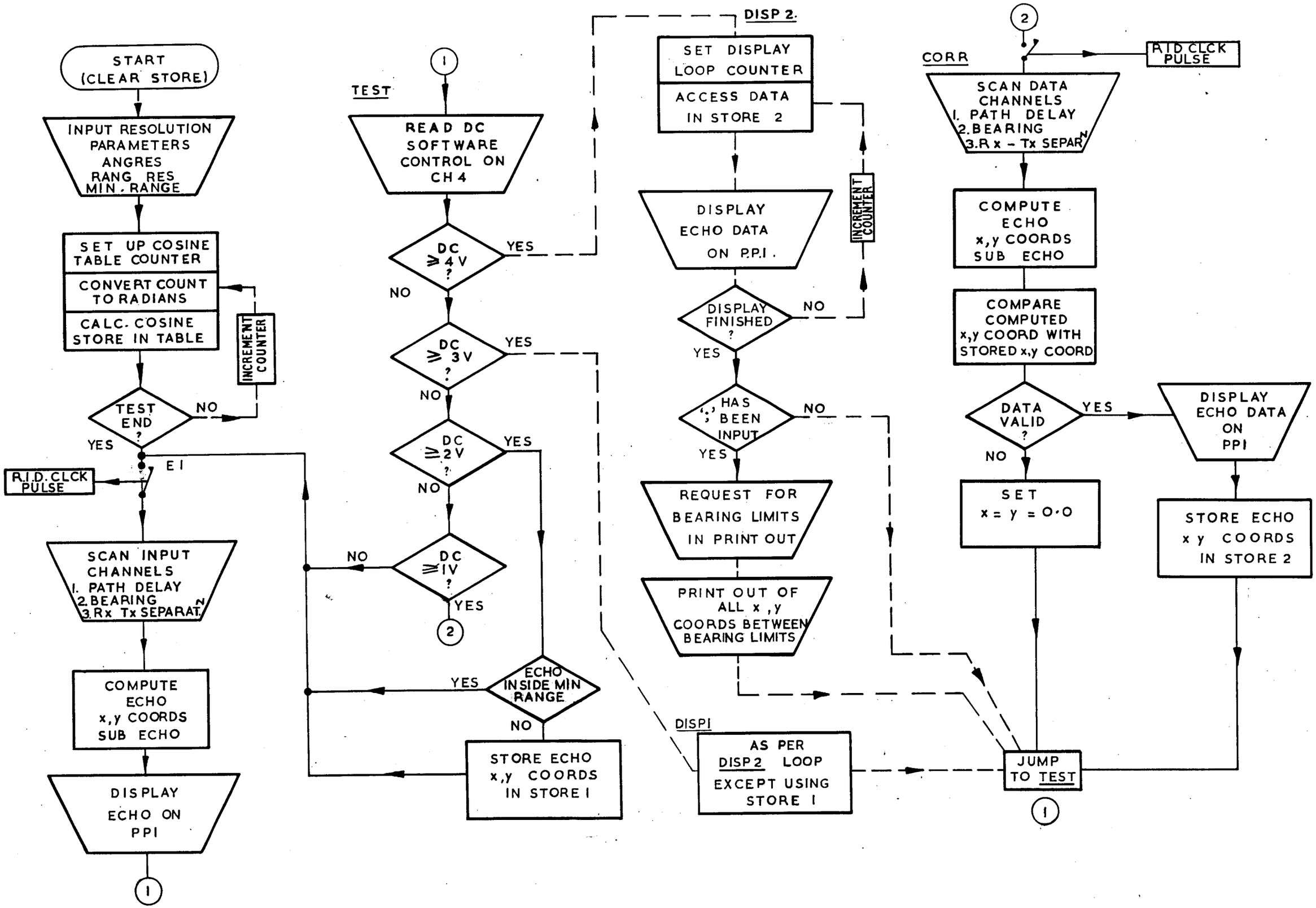

FIG. 3·9 FLOW DIAGRAM OF SONAR DATA PROCESSING PROGRAM

KEY : (——►——) REAL TIME OPERATIONS, (— ► —) NON-REAL TIME OPERATIONS.

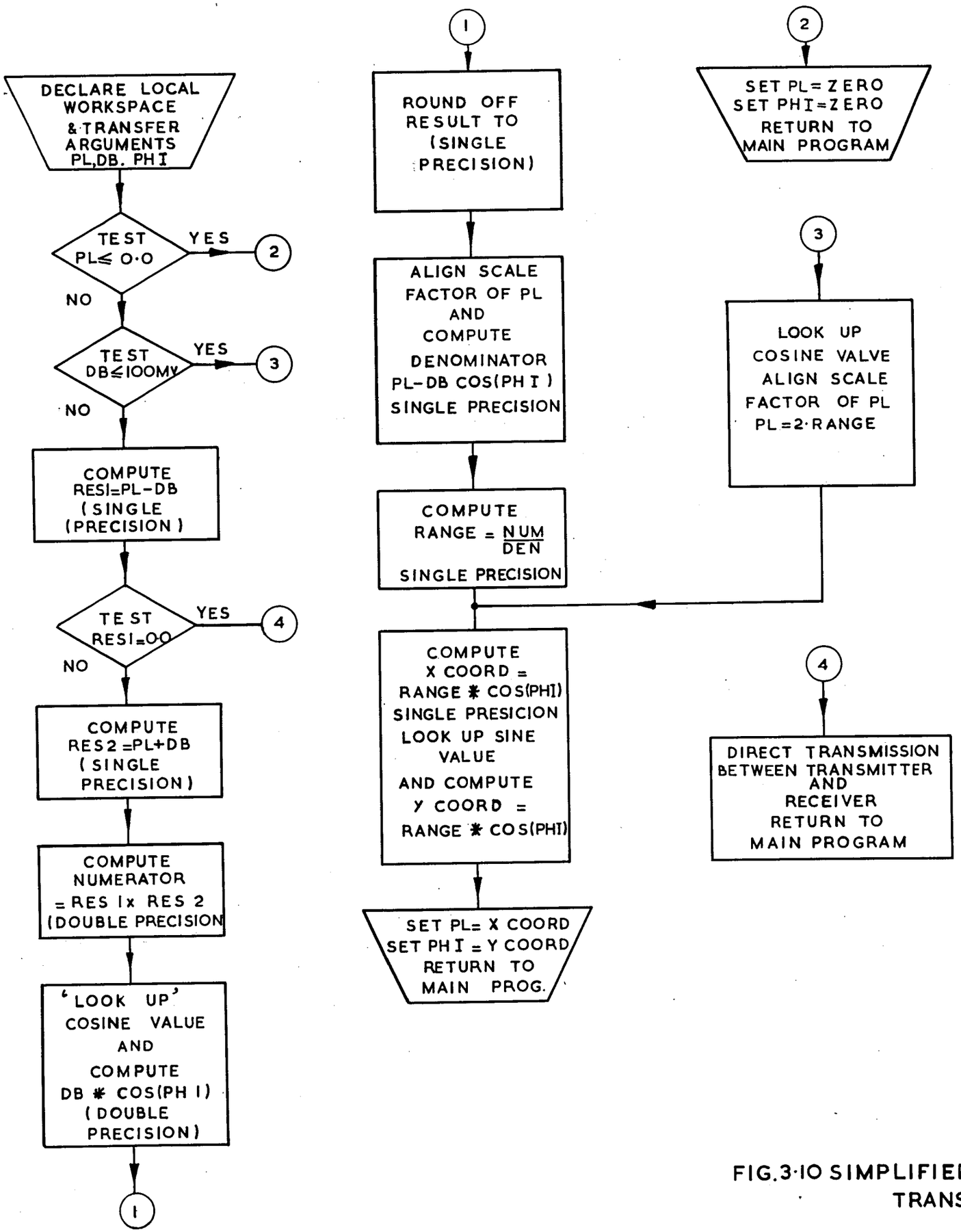

FIG.3·10 SIMPLIFIED FLOW DIAGRAM OF COORDINATE TRANSFORM SUBROUTINE (ECHO)

generation from a simple address offset at the expense of increased core storage.

At this point the program enters the real-time segment proper and initiates the input ADC to the track/clocked mode of operation. The program now reverts to a quiescent or suspended mode until triggered by the clock pulse from the analogue sonar which causes the program to sequentially scan and store the selected input channels. When the scan is completed the digitised parameter values are passed back as arguments to the calling segment, and the data is converted to X,Y co-ordinates by the subroutine 'Echo' which is shown in flow diagram form in figure 3.10. The X,Y data pairs are then output to the display drive together with a write pulse as shown in figure 3.6.

A measure of remote control of the program is achieved by sampling a fourth input channel and conditionally branching dependent upon the value of the dc voltage impressed on the channel input (see figure 3.9 location TEST). This dc control is a simple switch incorporated in the analogue sonar which gives five options in the software. These options are:-

(a) to stop any more data coming into the computer and display in core refresh mode echo patterns stored in the working array,

(b) to stop any more data coming into the computer and display in core refresh mode echoes stored in the reference array (noise reduction process),

(c) to enter currently computed echo co-ordinates into the reference arrays for the purpose of building up a reference display,

(d) to compare currently computed echo co-ordinates with the reference array as per equations 3.1, 3.2 and store or reject these depending on the result, and lastly,

(e) to compute the echo co-ordinates as they occur and output these in real-time to the ppi display.

During the experimental work a typical sequence was to start with option (e), in order to orientate the target and equalise the receivers (see next chapter for details of this procedure), then a switch to (c) to store a reference display followed by a return to (d) when a suitable reference display was available, or alternatively to (b). Options (a) and (b) provided stable ppi displays for visual examination and recording, in addition, in order to obtain a punched tape containing all stored echo co-ordinates it was necessary to enter either of these non real-time modes. This facility was used to produce data for the off-line analysis which is described in CHAPTER V.

Whatever option was chosen, the program eventually returned to its quiescent stage of tracking the input data channels of the ADC module. The implications of this synchronous mode of operating are discussed further below in section 3.4.4.

3.4 Analysis of the performance and errors introduced by the system

3.4.1 General

Assuming all signals exceeding the receiver thresholds V_t are treated as valid echo data, the performance of the system can be described in terms of its ability to display the echoes in precisely the right resolution cell on the ppi. Any shortcomings in terms of either echo data being placed into the wrong cell, or data being rejected due to insufficient throughput rate in the computer will obviously affect the evaluation of the multistatic environment as a shape portrayal system of superior capabilities compared with the monostatic system. It was therefore important to quantify those shortcomings due to the system alone, as distinct from those attributable to the general hypothesis.

The performance can be discussed in terms of:-

(a) the errors introduced by the system, which result in incorrectly placed echo 'paints' on the ppi, and

(b) the throughput data rate of the system and the implications of insufficient bandwidth in the processing side.

With regard to (a) above, the system divides naturally into the digital and analogue parts shown in figure 3.1.

Firstly, it was assumed that the analogue data transmitted to the computer was the sum of the correct signals plus error terms. Secondly, it was assumed that the computer, in processing this data, introduced further errors in the form of roundoff and truncation of intermediate results as the data was processed by the program.

3.4.2 Sensitivity of the range equations to measurement errors

The outputs from the system were the X,Y co-ordinates of the target which were computed using the range equations 3.3. The way in which these echo co-ordinates were affected by errors in the independent variables was important, both during the initial system design stage, and during the actual experiments. An analysis of this dependence was therefore carried out to determine the effect of such errors on the performance of the system. The X,Y co-ordinates were functions of three independent variables, thus,

$$X = f_x(PL, \Phi, DB) \text{ , and } Y = f_y(PL, \Phi, DB).$$

If the individual errors in PL, Φ and DB are small, the total derivatives of f_x and f_y relate the per unit errors in X,Y to the per unit errors in PL, Φ and DB. The total derivatives are, for small errors,

$$\frac{df_x}{f_x} = \frac{\partial f_x}{\partial PL} \cdot \frac{dPL}{PL} \cdot \frac{PL}{f_x} + \frac{\partial f_x}{\partial \Phi} \cdot \frac{d\Phi}{\Phi} \cdot \frac{\Phi}{f_x} + \frac{\partial f_x}{\partial DB} \cdot \frac{dDB}{DB} \cdot \frac{DB}{f_x} \quad \ldots \quad 3.4$$

and

$$\frac{df_y}{f_y} = \frac{\partial f_y}{\partial PL} \cdot \frac{dPL}{PL} \cdot \frac{PL}{f_y} + \frac{\partial f_y}{\partial \Phi} \cdot \frac{d\Phi}{\Phi} \cdot \frac{\Phi}{f_y} + \frac{\partial f_y}{\partial DB} \cdot \frac{dDB}{DB} \cdot \frac{DB}{f_y} \quad \ldots \quad 3.5$$

where $\frac{df_x}{f_x}$ is the per unit or relative error in X,

$\frac{\partial f_x}{\partial PL}$ etc are the partial derivatives of X with respect to PL etc.,

$\frac{dPL}{PL}$ etc are the per unit or relative errors in the variable PL etc, and

f_x is the value of the function of X for a set of inputs PL, Φ and DB. Similarly for Y,

$\frac{df_y}{f_y}$ is the per unit or relative error in Y etc.

By setting two of the relative error terms to zero for the independent variables, the error in X,Y due to errors in the third variable can be easily calculated. For example, if $d\Phi$ and dDB are set to zero, equations 3.4 and 3.5 reduce to,

$$\frac{df_x}{f_x} = \frac{\partial f_x}{\partial PL} \cdot \frac{dPL}{PL} \cdot \frac{PL}{f_x}, \quad \text{and}$$

$$\frac{df_y}{f_y} = \frac{\partial f_y}{\partial PL} \cdot \frac{dPL}{PL} \cdot \frac{PL}{f_y}.$$

The relative errors in X,Y were then calculated as PL was varied by assuming fixed values for DB, Φ and the relative error in PL. An equivalent calculation was carried out for the other two variables DB and Φ. In order to be representative of the system itself, the ranges of PL, Φ and DB were chosen to be the same as the expected measured values, ie,

$1500 < PL < 2500$ range units

$250 < DB < 1000$ range units

and $30 < \Phi < 60$ degrees.

For each of the three separate evaluations of the relative errors in X,Y, a per unit error of one percent was assumed for the appropriate variable as being the worst case.

For clarity only a representative set of plots of the relative error in X is reproduced here in figure 3.11. The three plots show the error in X as a function of each of the independent variables in turn, with appropriate constant values of the other two variables. Similar behaviour was obtained for the Y component. Figure 3.11(a) shows that the effect of bearing errors on the computed echo X co-ordinate is

RELATIVE ERROR
IN X COORDINATE
FOR .01 PER UNIT ERROR

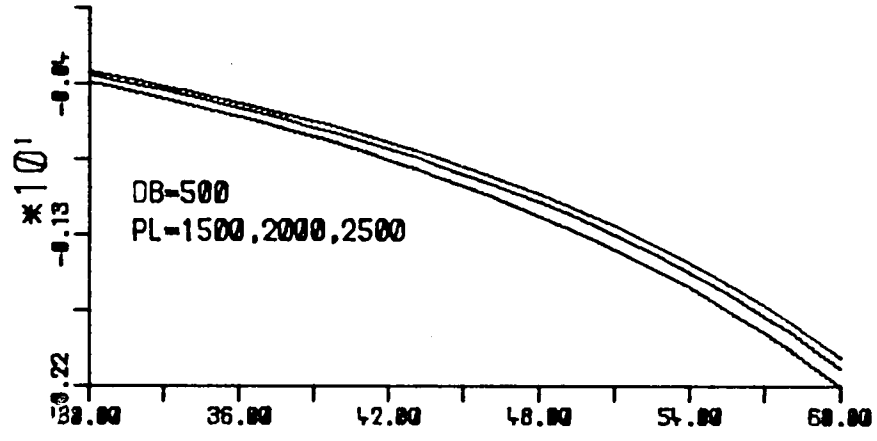

(A)

PHI IN DEGREES

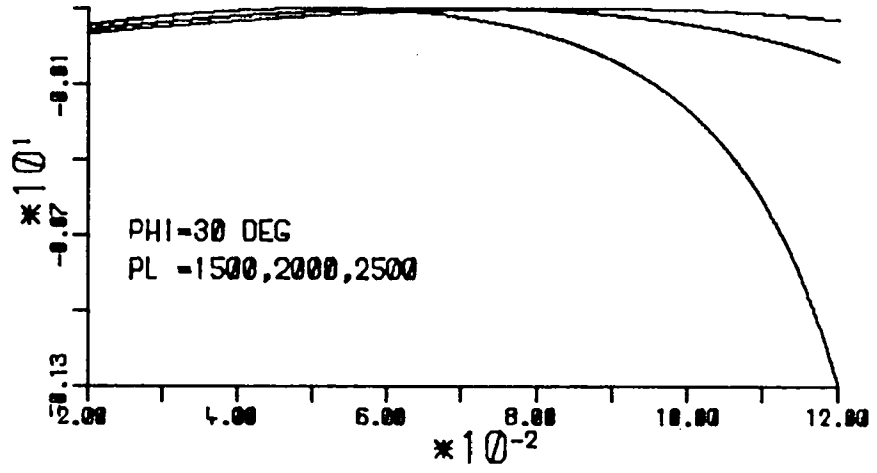

(B)

DB IN RANGE UNITS

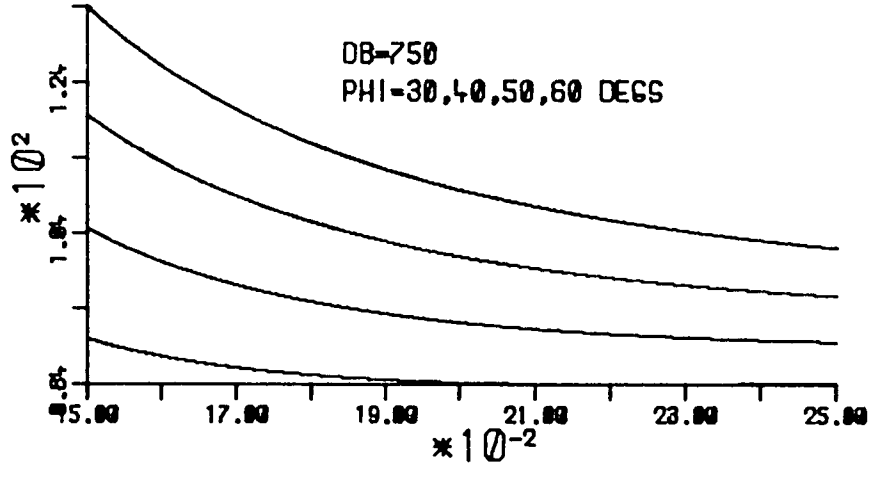

(C)

. PL IN RANGE UNITS

FIG 3.11 GRAPHS SHOWING THE RELATIVE ERROR IN THE ECHO X COORDINATE AS FUNCTIONS OF THE INDEPENDENT VARIABLES.

largely independent of the total path length travelled by the echo over the range considered. It was also largely independent of the value of transmitter-receiver separation DB. A one percent error in DB and PL represented an actual error of about 10-20 range units, which was considered a pessimistic estimate for both. However a one percent bearing error was not considered pessimistic and the conclusion was that the system was much more sensitive to azimuth bearing errors than to linear range unit errors. In descending order of priority, figure 3.11(b) shows that at large values of DB of about 1000 range units, the relative error changed rapidly from PL = 1500 to PL = 2500. Significant echo co-ordinate errors would therefore result from errors in DB when DB was large and approaching the value of PL.

This analysis showed that in designing the system, great care needed to be directed towards making accurate azimuth bearing measurements and this variable was quantised to an accuracy of 0.1 degrees. To an approximately equal degree, distortions in the echo co-ordinates due to errors could be expected at large values of DB and when PL approached DB in magnitude, although errors due to these causes were more dependent on azimuth, as can be seen in figure 3.11(c) for example.

Despite taking suitable precautions in respect of the measurement of PL, Φ and DB, displacement of echo co-ordinates from their true position occurred in the displayed echo patterns and accounted for at least some of the 'jitter' in the position of adjacent echo co-ordinates. The only remedy at this stage was to allow a tolerance in the echo positions on the display when comparing them with the reference display, and later on during the analysis of the results, with the reference contour C_t. This latter aspect is discussed further in CHAPTER V.

3.4.3 Display formatting program accuracy

Notwithstanding any errors introduced into the measurement of the parameters input to the computer, there remained the fact that the combination of software program and computer hardware was only capable of a finite dynamic range. The software program itself used integer arithmetic throughout and this was confined to single precision except in certain operations, as indicated in the schematic flow diagram figures 3.9 and 3.10, when double precision (ie double word length) was used.

In order to check the accuracy of the main display formatting program, a separate program was used to compare the output X and Y co-ordinates produced by a floating-point computation and the integer or fixed-point algorithm used. The inputs to this simulation program consisted of a set of random values of bearing, path length and separation. First, three random numbers, with a flat probability distribution in the range 0 - 1.0, were generated and then suitably scaled and truncated to represent the correct range of data values normally input by the ADC converter. Using these three values, two computations were performed to produce the display co-ordinates; firstly using the floating-point algorithm and secondly using the fixed-point routine. After each calculation the differences between the two sets of co-ordinates were computed and averaged, together with their RMS difference and standard deviation.

After N such calculations the final mean errors and standard deviation of the fixed point co-ordinates with respect to the floating point co-ordinates were printed out.

The average error in the displayed X and Y co-ordinates with respect to the floating point calculations after 1000 such iterations were:-

$E_X = -0.35$, and $E_Y = -0.27$,

measured in range cell units, whilst the standard deviation about the mean for the X and Y outputs were:-

$\sigma_X = 0.95$, and $\sigma_Y = 0.36$.

The X co-ordinate output has both a greater mean and standard deviation error than the Y output. This was a result of the bias towards the X-direction of the echo points. In other words, for a particular error in the calculation of the range vector from the transmit position, the X component tends to be the larger. The negative mean or bias in the X and Y outputs indicated that the fixed-point algorithm tended to produce echo ranges which were smaller than the more accurate floating-point range. The conclusion was that for the X direction the displayed output could be in error by up to approximately 1.3 cells (standard deviation plus mean) whilst the Y direction could be in error by approximately 1 cell.

3.4.4 Computer processing speed limitations

For a monostatic sonar the information rate at the receiver output along a fixed bearing is defined by the sampling theorem which states that the resolution or independent sampling interval is given by $1/2W$, where W is the system bandwidth. For such a single receiver system, any signal processor capable of accepting data samples at a rate of $1/2W$ at each bearing increment will be capable of processing all the independent data available from the medium.

In the system being described here, the data from the analogue sonar was the total of three separate channels, and an extension of the single channel case suggested that three times the bandwidth would be required to process the information on a continuous basis. Two things helped to alleviate this situation. Firstly, the thresholding of data at the receivers reduced the data input to bursts of signals associated with

target echo clusters, interspersed with periods of inactivity. Secondly, in cases of simultaneous detection in more than one receiver, since by definition the echo must have originated in the same cell, it was only necessary for one channel to pass data to the processor to properly fill the cell on the display.

Even so, difficulties were encountered in trying to ensure that sufficient system bandwidth was available to process all the detected echoes. Each receiver channel had a theoretical resolution equivalent to approximately 6 μs in time delay, corresponding to approximately 150 KHz of bandwidth. The cpu and software program combination were not capable of this processing speed, 5 μs being the order of one instruction time in the cpu. There was therefore a known upper limit on the data rate into the cpu which resulted in the rejection of a percentage of target echoes. The response time of the system was measured from the front edge of the clock-pulse to the trailing edge of the Z axis modulation (see figure 3.3) and was approximately 180 to 200 μ secs.

This meant that echoes would only be accepted provided they were separated by more than 200 μs in time, ie > approximately 15.0 cm in range. Only approximately 3 percent of the total possible resolvable echoes occurring during a ping cycle could be processed by the system. This is a small percentage, however, the targets were constructed in a way to ensure that only one discontinuity echo could occur on each bearing scan. Under these conditions the data throughput rate would therefore only need to be less than the time between successive pings.

In practice, side-lobe and noise echoes could occur before receipt of the target echo on a particular bearing, and if the time difference between echoes was less than 200 μs, then the true target echo would be rejected.

This effect is considered further in CHAPTER V, when an attempt is made to quantify the magnitude of the data rejected by the system for the above reason.

CHAPTER IV

EXPERIMENTAL PROCEDURES

4.1 The objectives of the experimental work

The main purpose of the experimental phase of the project was to observe and record the echo patterns obtained with the sonar system, so that comparisons could be made with the expected results where possible. In addition, the differences between the bistatic and monostatic systems, in terms of target shape portrayal, were to be observed under various target orientations and system configurations. This would enable quantitative measurements of the performance of the sonar to be made and also point the way for future improvements and modifications.

Some of the runs with the sonar were also intended to highlight errors and limitations in the displayed echo patterns, due to inaccuracies in the analogue sonar and in the display program.

4.2 The venue for the experiments

All of the experimental work was carried out in a small tank measuring approximately 3 metres long by 2 metres wide by 1.5 metres deep, constructed from concrete blocks and lined with a tough, waterproof, plastic membrane bonded to the sides and bottom. The tank itself was housed in a small laboratory in which the analogue sonar circuitry and measurement equipment described in CHAPTER III was also laid out. After suitable conditioning, signals produced by the equipments were transmitted via a multicore cable to the remotely situated digital computer which was housed in another part of the Electrical Engineering Building. Figure 4.1 shows a schematic diagram of the tank layout together with transmitter and receiver hydrophones and other equipments. It can be seen from this diagram that the transmitter and receiver transducers were arranged at one end of the tank with the transmitter in one corner and the hydrophones spaced across the tank. These transducers were supported on a rigid framework which provided the

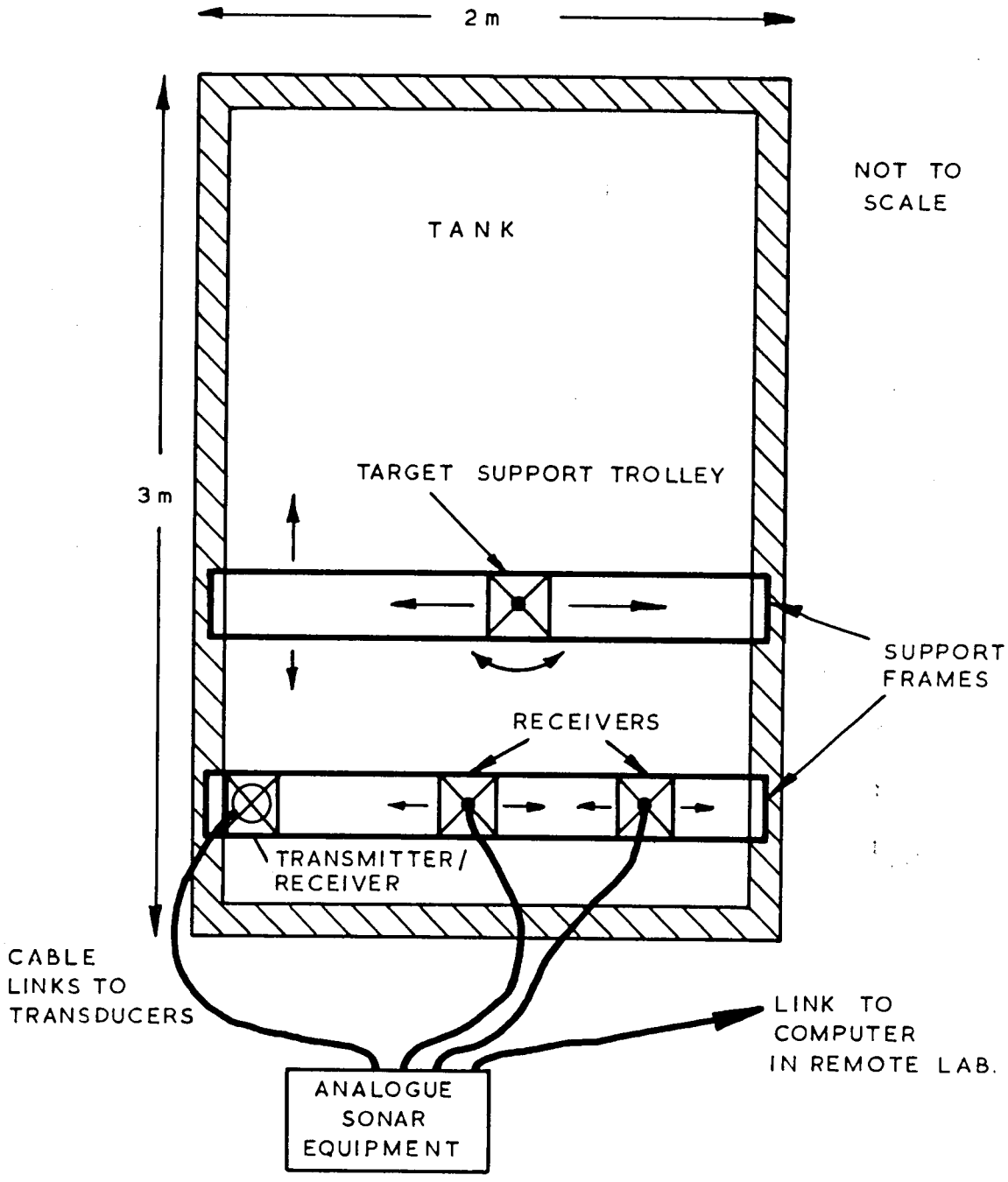

FIG. 4·1 SCHEMATIC OF EXPERIMENTAL AREA SHOWING LAYOUT OF EQUIPMENT IN THE TANK LAB FOR EXPERIMENTAL WORK. PHOTOGRAPHS OF EQUIPMENT COMPONENTS ARE SHOWN IN FIG. 3·1

required stability for both the mechanical scanner and hydrophone supports, as well as providing a linear base line reference for the receiver plane. The targets used in the experiments were suspended below a moveable trolley which ran on a similar rigid framework positioned laterally on the tank above the designated surveillance area. This arrangement allowed both lateral movement of the target parallel to the receiver plane and rotation of the target about its support axis in 5 degree steps.

4.3 Target models

Figure 4.2 is a photograph of the three targets used in the experimental part of the work.

As already mentioned, the targets were constructed in a manner so as to exclude as far as possible:-

(a) air-water reflections from the surface of the tank,

and (b) internal reflections caused by acoustic energy penetrating the body of the target and being internally refracted then re-radiated.

If the target is constructed such that it always presents a vertical reflector to the incident sound, then the echo will be reflected normally to this surface and back to the receiver via the direct water path. To ensure that this was the case for the main-lobe of the transmission at least, it was necessary to ensure sufficient depth in the construction of the targets. With a main-lobe of approximately 2 degrees at the 3 dB points the required depth at 1 metre range is approximately 3.5 cms, and the targets used therefore all exceeded this depth.

The results presented in the next chapter also indicated that no echoes were received from the targets other than via the direct path.

Internal reflections from within the target can be prevented by ensuring a near unity reflection coefficient at the target-water interface and high attenuation of energy penetrating the target volume.

FIG 4.2

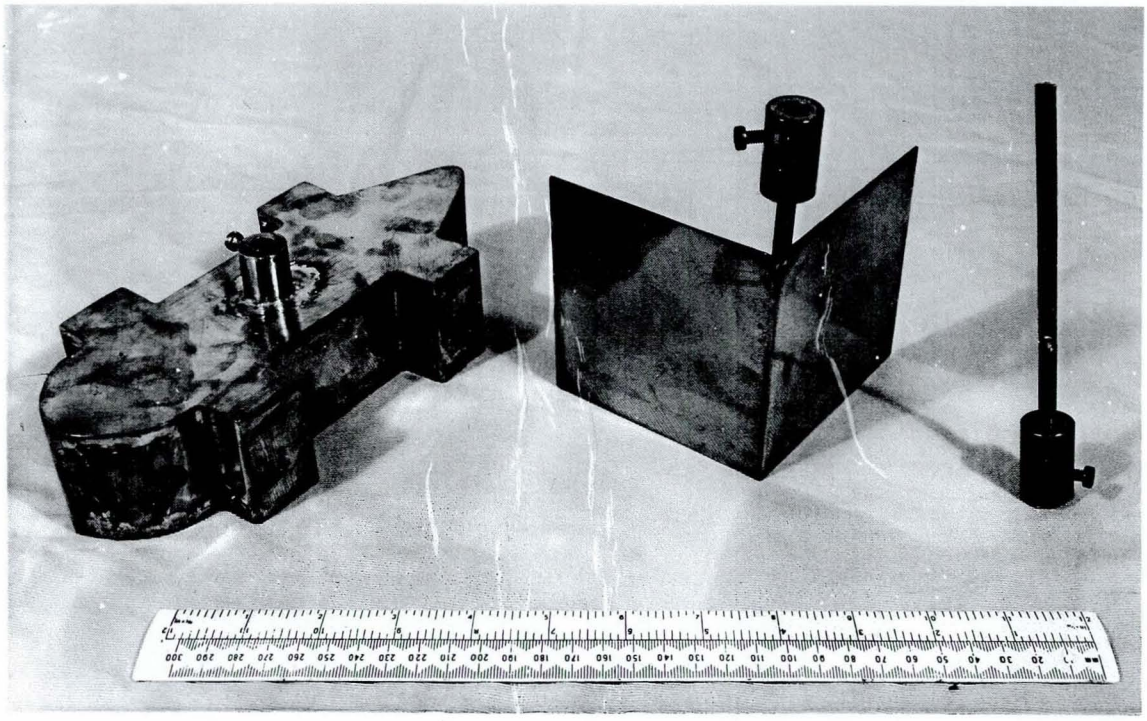

FIG 4.2 A PHOTOGRAPH SHOWING THE TARGETS USED IN THE EXPERIMENTAL WORK.

Hollow air-filled targets provide these characteristics and target 1 was constructed from thin brass sheet with soldered joints to ensure a watertight construction. Target 2 being a flat plate reflector was first covered with a thin layer of polystyrene sheet, then finally a thin polythene covering was applied to form an air-water interface. Again the results indicated that the only echoes received from the targets were due to water-target boundary reflections as desired.

Regarding the choice of target outline, in the past the tendency has been to use very simple geometric shapes such as cubes, cylinders, etc. These are useful in developing basic theories about reflection mechanisms from target surfaces and discontinuities, and whilst it can be argued that real world targets are composed of these basic shapes, it was felt that a more complex shape could be used to advantage in this phase of the project.

It has been stated that one of the objectives of the experimental work was an evaluation of the system as an improved target shape portrayal scheme, therefore a more varied structure was proposed for the main investigation. With reference to figure 4.3 which gives a full-size plan outline of targets 1 and 2, target 1 embodies the rectangular and curved reflecting surfaces into an outline which was intended to represent, schematically at least, a submarine contour. Examination of the echo patterns obtained from this target revealed the characteristic structure attributable to these various types of surfaces, and provided the opportunity to observe the system performance when a reasonable number of discontinuity echoes were present in the echo patterns.

4.4 Equalisation of the receivers

The calculations performed in CHAPTER II to produce the multistatic system performance curves were made with the assumption that both the monostatic and multistatic receive sub-systems were of equal overall

FIG. 4.3

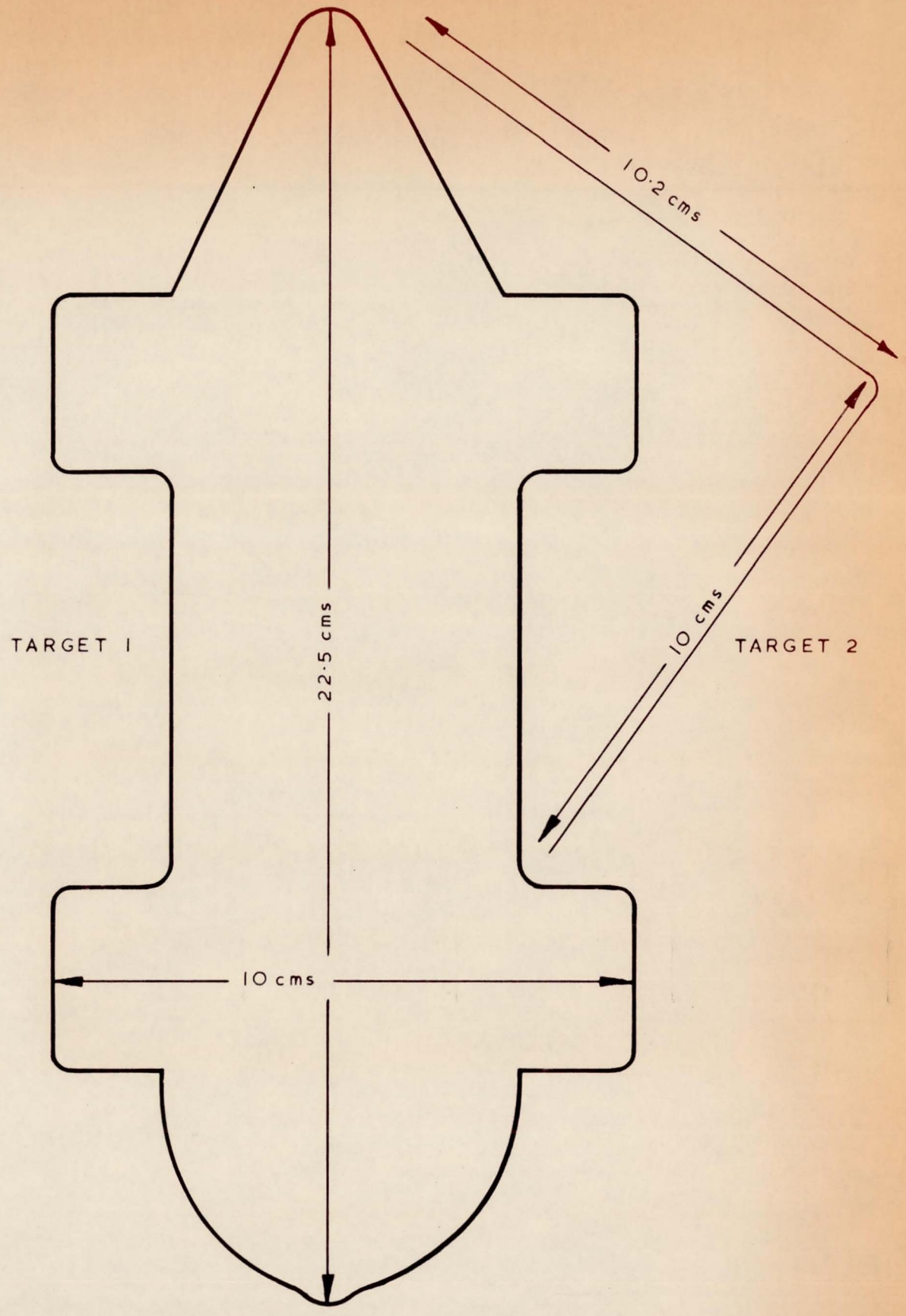

FIG. 4.3 FULL SIZE PLAN OUTLINE OF TARGETS 1 & 2 USED TO PRODUCE REFERENCE DISPLAYS FOR PPI DISPLAY PROCESSING PROGRAMS

sensitivity. Furthermore, it was assumed that both receiver systems had equal directivity indices (DI's).

This was not true in both cases in practice, firstly because different transducers were used for the monostatic and bistatic receivers, and secondly because the transducers were of different sizes. It was convenient to use the same transducer for both transmission and reception in the monostatic system, but this meant that with the same source level the monostatic receiver, with its narrow receive beam, operated with a larger echo excess than the omnidirectional bistatic receivers.

Whether or not it was a justifiable approach, an attempt was made to redress this imbalance by making an estimate of the difference in sensitivity and DI of the two systems. This in turn allowed corrections to be applied to the results of CHAPTER V which are consequently presented in both corrected and uncorrected form. A difficulty encountered during the experimental work was the lack of suitable apparatus and calibrated transducers to enable absolute sensitivity and beam pattern measurements to be made. This meant that estimates of the different sensitivities had to be made in terms of relative measurements between the monostatic and multistatic systems.

Two sets of measurements were made, the first resulted in a comparative plot of receiver sensitivities in terms of the required threshold settings for a 100 percent detection rate, and the second involved obtaining a measurement of the number of echo co-ordinates detected by the monostatic system as the receiver threshold was varied.

For the first of these, a flat plate reflector shown as target 2 figure 4.2 was introduced into the surveillance area and an attenuator incorporated into the transmitter feed so that the source level could be varied. The assumption was made that the target strengths in the monostatic and bistatic modes were equal, provided the reflector was

orientated to direct the specular echo at the receiver. This meant adjusting the target until the signal at each receiver was a maximum in turn.

At the two orientations, a plot was made of the receiver threshold setting required versus source level for 100 percent detection rates. This was achieved by monitoring the respective channel selector outputs over a large time interval to ensure that no pulse dropouts occurred during any transmission. If any were detected, the source level was increased by 1 dB and the pulse train again monitored for missed detections. This procedure resulted in the relative sensitivity plot shown in figure 4.4.

For the second measurement, target 1 was placed midway along the receiver plane and at an orientation of zero degrees relative to the receiver plane. A measurement of the number of XY co-ordinates produced during a scan as the threshold of the monostatic receiver was varied was made with the source level set at that used during the experiments. The results of this test are shown plotted in figure 4.5, and in conjunction with the plot of figure 4.4 an estimate of the correction factor was obtained as described below.

Most of the runs shown in CHAPTER V were performed with the receive sub-system relative thresholds constant at approximately 14-15 dB. With this assumption, figure 4.4 showed that with a constant relative source level of about 35 dB, the difference in performance or echo excess was approximately 3 dB. This situation is indicated by the dotted line on the graph. This same situation was also found to be approximately correct over the threshold range 10-16 dB, increasing to about 5-6 dB at a 6 dB threshold setting. In other words, it was found that the bistatic system was typically 3 dB less sensitive in terms of the required receiver threshold or echo excess than the monostatic system,

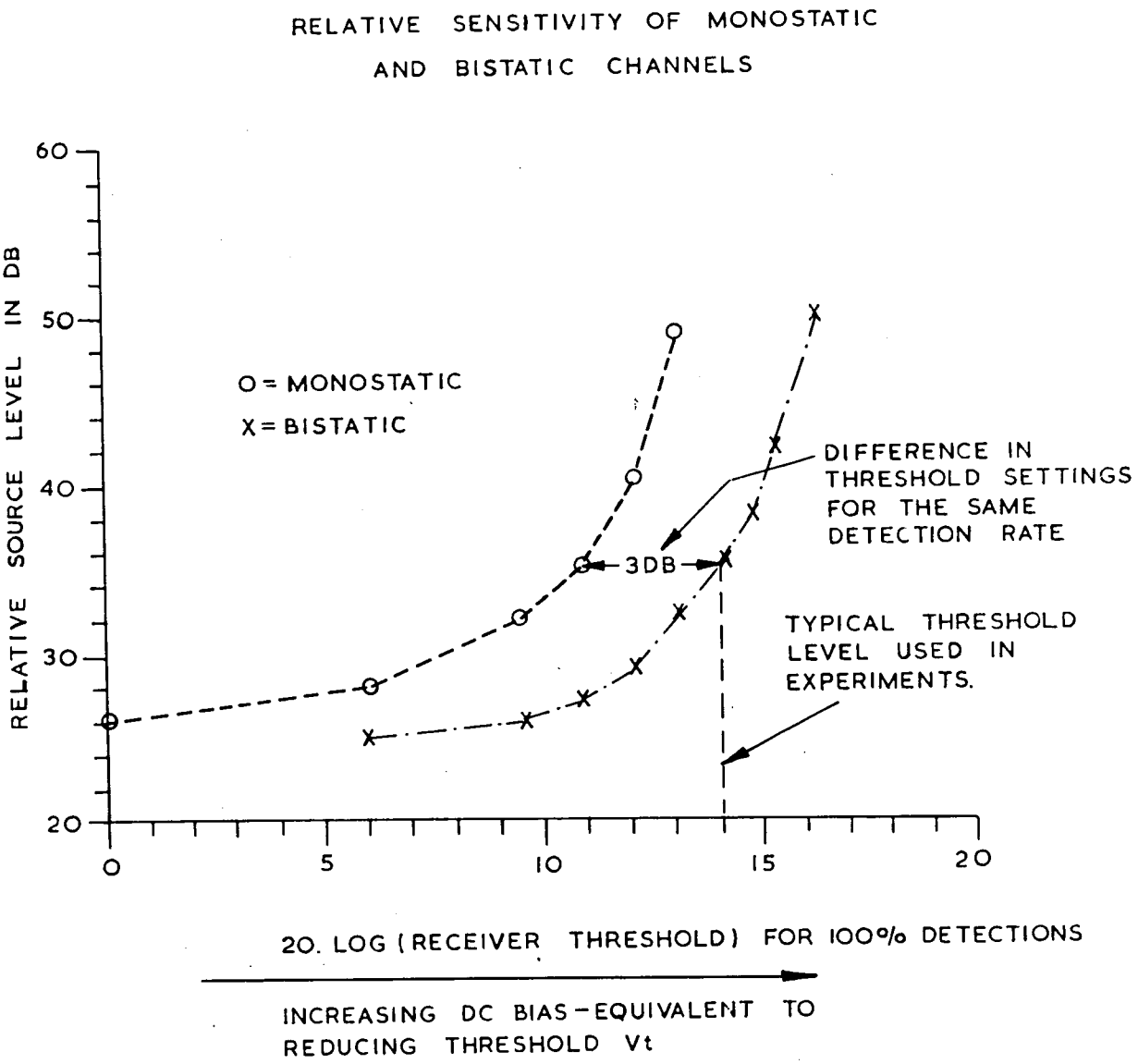

FIG. 4.4 A GRAPH SHOWING THE SENSITIVITY OF THE MONOSTATIC AND BISTATIC CHANNELS AT TYPICAL RECEIVER THRESHOLD SETTINGS.

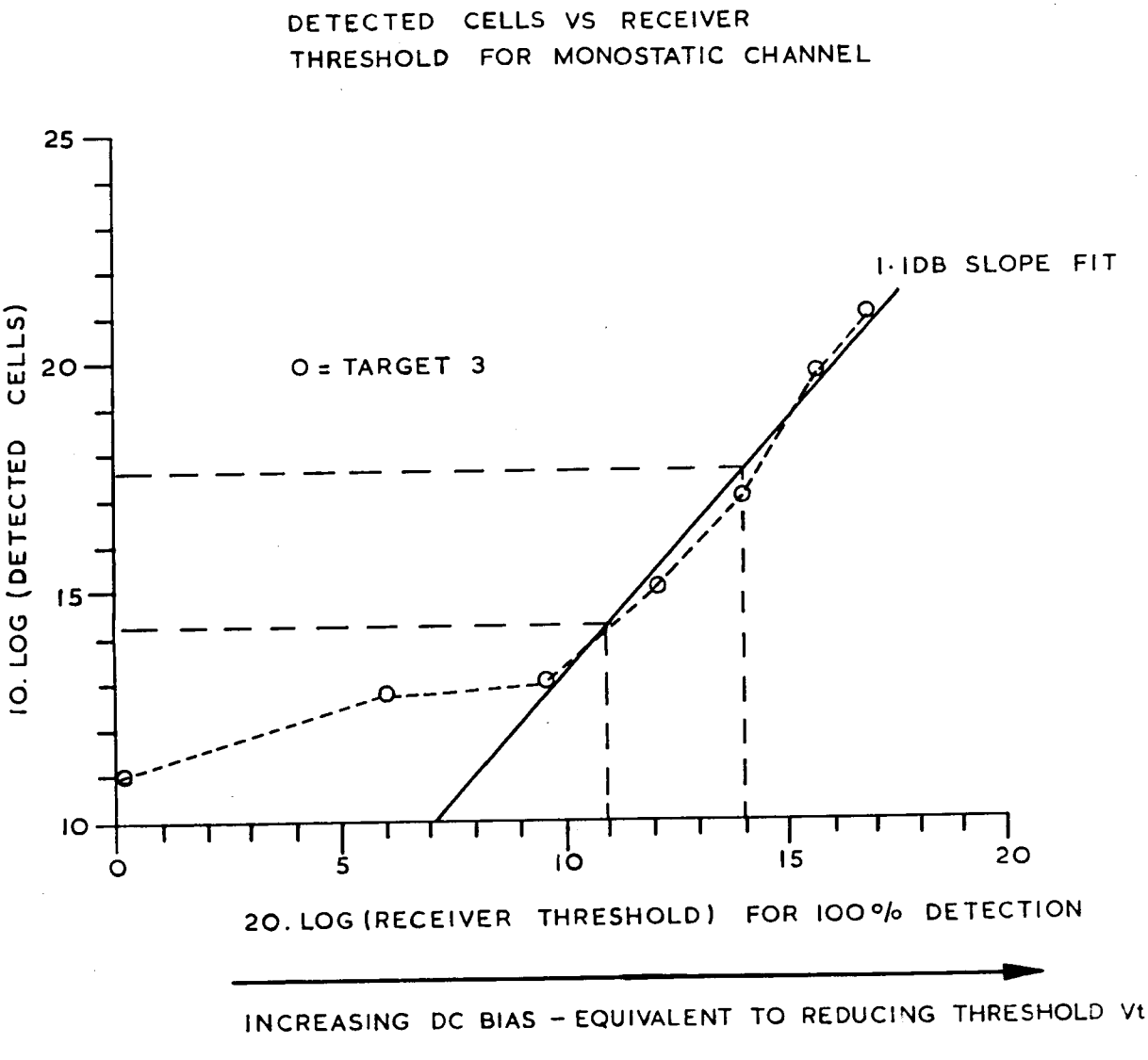

FIG.4·5 A GRAPH SHOWING THE CHANGE IN THE NUMBER OF DETECTED CELLS AS THE RECEIVER THRESHOLD WAS VARIED IN THE MONOSTATIC CHANNEL

under conditions of constant source level and with this particular receiver threshold range.

In order to estimate the change in the loss factor, as defined in CHAPTER II, which would result from this imbalance, reference was made to figure 4.5 at two log thresholds separated by the above figure of 3 dB. It can be seen that from about 9-16 dB of threshold, the rate of change of the number of data points expressed in dB units was roughly constant at 1.1 dB per dB of threshold change. Therefore a 3 dB reduction in the monostatic receiver threshold to equalise the receivers could be expected to result in a +3.4 dB change in the calculated loss factor. Consequently this derived value was used to correct the results of the next chapter where this was necessary.

It must be emphasised however, that the basis of this experiment was an average situation regarding the choice of orientation and position of the target, which was intended to be representative of the geometry used in the other runs. The resulting correction figure was a sampled quantity which was considered typical of the differences between the monostatic and bistatic systems which could be expected, and which was valid within the threshold band quoted.

4.5 Setting up a data run and calibrating the equipment

A data run was defined as the sequence of events comprising choosing and positioning the target in the surveillance area, setting up the required system geometry in terms of transmitter-receiver separation, calibrating the analogue sonar, scanning and obtaining an echo pattern in the computer, and finally dumping the stored echo co-ordinates for subsequent study and further processing.

The position and orientation of the target in the surveillance area was intended to provide a set of results for the system under various operating conditions and system geometries. Table 4.1 is a list of the

runs performed which are presented in the next chapter and which were designed to validate the concept of the multistatic sonar system. It can be seen that a variety of orientations and positions along the receiver plane were evaluated. This was an attempt to obtain quantitative data relating to the average or expected improvement in target shape portrayal provided by the system.

TABLE 4.1 LIST OF EXPERIMENTAL RECORDS TAKEN

RECORD NUMBER	TARGET	ORIENTATION	APPROXIMATE AV X-COORD OF TARGET	RESOLUTION PARAMETERS	COMMENTS
208	1	0 Deg	352 cells	1 cell, 0.5 Deg	CPU overload correction required
209	1	-40 Deg	354 cells	1 cell, 0.5 Deg	CPU overload correction required
214	1	0 Deg	498 cells	1 cell, 0.1 Deg	
215	1	-40 Deg	498 cells	1 cell, 0.1 Deg	CPU overload correction required
216	1	-90 Deg	403 cells	1 cell, 0.1 Deg	CPU overload correction required
220	1	0 Deg	891 cells	1 cell, 0.1 Deg	
219	1	-40 Deg	891 cells	1 cell, 0.1 Deg	
218	1	-90 Deg	897 cells	1 cell, 0.1 Deg	
222	2	-20 Deg	220 cells	1 cell, 0.1 Deg	
202	3	0 and 60 Deg	Variable	1 cell, 0.1 Deg	Experiment to measure co-ords as fn of X
203	1	0 Deg		1 cell, 0.1 Deg	Experiment to measure co-ords as fn of threshold

TABLE 4.1 LIST OF EXPERIMENTAL RECORDS TAKEN

Calibration of the system prior to gathering data proper consisted of adjustment of the parameter measuring circuits to ensure a correspondence between the analogue voltages and the physical separation of transmitter and receivers. This was followed by a quick look at the echo pattern to ensure that large specular echoes from one receiver were not overloading the cpu.

The method of calibrating the system was straightforward and is described briefly below.

By pointing the transmitter directly at the hydrophones, ie zero azimuth degrees, the time of arrival and consequent triggering of the corresponding receiver channel represented the time of direct transmission between transmitter and receiver. The sampled sweep waveform (trace C in figure 3.6) was monitored on an oscilloscope together with the PAM output (trace M in figure 3.6) for that channel. It was necessary to check that the PAM output voltage was equal to the sampled sweep-waveform to ensure calibration of the transmitter - receiver separation measurements in terms of the sweep-waveform. This voltage was adjusted by means of the preset potentiometers shown in the circuit diagram included in APPENDIX A.

After calibrating the analogue sonar and taking an initial look at the echo pattern, the display program was restarted and the appropriate parameters controlling the display resolutions (number of range and bearing bins) entered. The software was controlled remotely as described in the previous chapter and the control switch was initially set to zero. This resulted in the real-time display of echoes, and after setting the position and orientation of the target, the display was observed to ensure that no new echoes were being displayed, apart from noise spikes, and that a steady state condition existed. The control switch was then set to position 2 which caused the data being currently displayed to be simultaneously deposited into display store 1. The control switch was then set to position 3 which gave a refreshed display from this

previously loaded store 1. This allowed a critical examination of the stored echo pattern to determine its suitability as a reference display for noise reduction. This examination was mainly to ensure that overload of the cpu due to transmitter side-lobes was not obscuring echoes which should have been received had this not occurred. It was of necessity a qualitative assessment and the display usually included an acceptable number of false echoes.

The control was then switched to position 1. This presented a real-time display which was the result of correlating incoming echoes with the pattern in store 1. In addition the correlated echoes were simultaneously deposited into store 2. The scan was continued until such time as it was judged that no new echoes were being added to the display which was then considered to be saturated. The system was then switched to refresh the display from store 2 only and the scanner and transmitter switched off.

This completed the data gathering phase and after deciding on suitable limits of arc which encompassed the target echo pattern, these limits were entered into the computer via the keyboard. When these had been typed in, the program then proceeded to output a record of all non zero echo co-ordinates between these limits onto paper tape. All the display records were preserved in this way for later re-processing by a non real-time display program.

Some problems to do with the display processor bandwidth were encountered during the experimental phase for reasons which were described in the previous chapter. In order to minimise the effects of this system artifact, most runs were divided into separate data records for each channel, as well as for the combined three channel system. In other words, initially, only channel one was enabled in the system and a data record obtained in the manner described above, then channel

two was enabled followed by channel three and records obtained for each in turn. Finally all three channels were switched on and a record of the combined display obtained. This method of obtaining display records enabled the non real-time display program, described in the next chapter, to compare the effects of enabling all three channels simultaneously with the separate response from each channel.

The procedure outlined briefly above was followed for all the runs and the results obtained using the system are presented in the next chapter.

CHAPTER V

ECHO PATTERNS OBTAINED WITH THE SONAR SYSTEM

5.1 Introduction

In this chapter a selection of the ppi display results obtained with the experimental system used to investigate the multistatic sonar concept are presented and briefly discussed.

The basis of these results were data sets obtained from a number of experimental runs performed with the system, a run being defined as in CHAPTER IV. Each data set comprised a number of groups of X, Y co-ordinate pairs, representing the output of the digital computer which was fed to the ppi display, and constituted an echo pattern from the target. Each group of co-ordinates was derived from either the output of one receiver channel or any combination of channels as detailed in Table 4.1.

Having initially punched out the results for each run onto paper tape, the data was in a form which could be easily and rapidly retrieved for subsequent processing, and all the displays of echo patterns shown in this chapter were obtained from this data stored on paper tape. This facility, to be able to reprocess the data without the need for real-time speed, was merely a convenience which enabled some additional procedures to be added to the real-time display program which was briefly described in CHAPTER III. For example, this improved program incorporated a better display routine with the ability to display both the echo patterns and a reference outline for comparison, also a system geometry picture showing the layout of the system was available at the start of the reprocessing run.

5.2 The method of reprocessing the results

The basic function of the reprocessing program was to re-display the echo patterns on a grid representing the surveillance area. This was achieved in a noise and interference free environment which was suitable for good reproduction and further study of the echo patterns.

The form of the data which was input to the program is shown in figure 5.1, which is a part of the data set recorded from run number 209. Each data set had exactly this format so that dealing with each run merely entailed reassigning a different data set to the program data input channel. A further reference input channel was used to input a data set comprising the X,Y co-ordinate pairs of the projected plan outline of each of the targets used. This data set was obtained by placing a full sized plan projection of the target (see figure 4.4, CHAPTER IV) onto a graphical digitising machine and then sampling its outline. This contour, comprising a set of X,Y co-ordinates relative to some arbitrary zero point on the digitiser, was then input to a reference processing program. The function of this program was to perform a linear interpolation between points on the non-uniformly sampled contour, and to resample and rescale the data so as to produce a reference display which was correctly scaled to the 1024 x 1024 bit display of the surveillance area.

This reference display was stored in a two-dimensional data array, set aside in the display processing program, where it could be quickly retrieved for use in the manner described below.

Depending on the combination of channels recorded, the display program enabled a separate display of the output of each receiver channel to be obtained. In addition, all channels could be combined into an overlayed display which was compared with the combined multichannel output obtained with the real-time system. This enabled the loss of data due to the 'processor busy' condition described in CHAPTER III to be estimated, and a simulation of a non-processor limited display to be obtained. The next phase in processing the results entailed a manual alignment of the reference display with the measured echo patterns. The program enabled the reference display to be rotated, and moved along the X,Y axes relative to the surveillance area, and thus allowed this reference display to be accurately positioned over the echo patterns.

FIG 5.1

DATA	EXPLANATION
209	RECORD NUMBER
1	RUN NUMBER
1	TARGET NUMBER
-40	RELATIVE ORIENTATION IN DEGREES
5	ANGULAR RESOLUTION PARAMETER IN 10ths DEGREE
1	RANGE RESOLUTION PARAMETER IN CELLS
200	MINIMUM RANGE ACCEPTED BY PROCESSOR
400 600	ANGULAR SECTOR ACCEPTED BY PROCESSOR (40-60)
8	SEPARATION BETWEEN TRANSMITTER AND ACTIVE RECEIVER
01 06 00 00 00 00 00 00 00 00 00 00	NUMBER OF RECEIVER ACTIVE, THRESHOLD, ATTENUATOR SETTING
0404 0448	START OF XY DATA
0402 0454 0397 0457 0393 0460 0389 0463 0330 0400 0324 0400 0325 0409 0320 0409 0318 0415 0313 0416 0311 0420 0282 0410 0277 0411 0273 0413 0271 0418 0268 0420	X CO-ORDINATE, Y CO-ORDINATE IN RANGE CELLS
9999 9999	END OF SCAN LIMIT
1	STORE NUMBER OUTPUT
209	START OF NEXT SCAN IN SEQUENCE
1	
4	

FIG 5.1 PART OF THE DATA COMPRISING THE RESULTS OF RECORD 209 IN THE FORMAT INPUT TO THE DISPLAY PROCESSING PROGRAM

For example, run 219 was made with the target at 40 degrees orientation, and the reference display was sampled at zero degrees relative, so before correct alignment could be achieved it was necessary to perform a 40 degree rotation of the target contour. In addition X and Y offsets were required before the reference was aligned with the echo pattern. These X and Y offsets were a matter of judgement on the part of the author, and the echo pattem and reference display were observed simultaneously in order to ascertain the magnitude and sign for each offset.

When a satisfactory alignment was obtained a command was given to the program calling a sub-routine which performed a two-dimensional spatial comparison between the stored reference and the echo pattern being displayed. The binary nature of both sets of data enabled a simple logical AND to be performed across the display between the reference and measured patterns. The result of the AND process for each separate display group was stored in a new area set aside for the purpose, enabling both the original and processed data to be examined separately.

Because of the possibility of errors being introduced into the echo patterns by the sonar system and to a lesser degree by the display formatting program itself, a parameter was passed to this sub-routine in the form of a cell tolerance which allowed an area of uncertainty to be defined around the target reference contour.

Let $C_t = (X_1Y_1, X_2Y_2, X_3Y_3, ...)$ be the reference contour,

and $E_t = (X_{t1}\ Y_{t1}, X_{t2}\ Y_{t2}, ...)$ be the echo pattern,

then for each reference co-ordinate pair X_q, Y_q, the calculation

$$R_p = (X_q - X_{tp})^2 + (Y_q - Y_{tp})^2 \quad ^{\frac{1}{2}}, \text{ for } 1 < p < P,\ 1 < q < Q$$

where Q = total number of co-ordinates in the reference contour C_t,

and P = total number of co-ordinates in the measured echo pattern, was performed. R_p represents the magnitude of the vector difference between each individual reference and measured echo pattern co-ordinate pairs, and its value was compared with a display tolerance, T, allowed for errors. If the magnitude of R_p was greater than T, the echo co-ordinates X_t, Y_t were rejected and not placed in the processed data store. At the end of this masking operation, what remained of the raw echo patterns were those co-ordinates which corresponded to the reference outline co-ordinates to within the tolerance T.

The filtering of the echo patterns by this means was specifically to remove, as far as possible, echoes due to either noise or side-lobes of the main beam. The resulting cell counts output by the program for each echo group were considered to be better estimates of the independent information rates from the system, than from the raw unfiltered data.

The value of the tolerance T was based on the analysis of errors described in CHAPTER III and corresponded to an area of uncertainty of $\pm$ 3 display cells around each target echo co-ordinate.

All the experimental echo pattern results obtained with the system were processed in this way by this program. Each complete set of display results therefore comprised:-

(a) The unprocessed outputs from each echo pattern together with the reference display (not aligned yet),

(b) The X,Y co-ordinate counts for each echo pattern measured when the run was originally performed,

(c) The computer real-time combined display and the simulated combined display so that a data processing rate could be estimated and losses due to processor rejection of echoes evaluated,

(d) The filtered outputs from each echo pattern,

and (e) The final X,Y co-ordinate counts for each filtered display.

In order to help clarify the procedures used to process the results, an example of the sequence of events is described for run number 220, this being a typical run.

Four separate data sets were obtained for this run, being assigned as follows:-

display 1 - monostatic, channel 1 only

display 2 - bistatic, channel 2 only

display 3 - bistatic, channel 3 only

display 4 - combined display, channels 1, 2 and 3.

The geometry for this run is shown in figure 5.2(a) which is a plan outline of the experimental tank together with the relative locations of the target and bistatic channels as measured by the computer display formatting program. The target was thus at a range of approximately 0.8m from the monostatic position (shown as '$\emptyset$'). The box marked surveillance area in this figure corresponds to the expanded display area shown in the accompanying display records for run 220. Thus, with reference to figure 5.2(b), which shows the first of these, the co-ordinates of the corner nearest the sound projector, in figure 5.2(a), are X = 741 = 0.74m and Y = 353 = 0.35m. When studying these display results, therefore, reference can be made to figure 5.2(a) to see the geometrical relationship between the target and the multistatic system. The box marked 'insonified area of target' in figure 5.2(a) refers to a line-of-sight vector representation of the directly insonified regions of the target as 'seen' by an idealised transmitter with no side-lobes and situated at the origin 'O'. It was included as an aid to indicate the target outline which would be displayed under conditions of detections from each insonified resolution cell and no ambiguous responses from beam side-lobes or system noise. A similar plan showing system geometry

and insonified area was provided for every run.

Actual display records for run 220 show the details of the echo patterns obtained within the surveillance area. This area is shown in an expanded format depicting a region of 250 by 180 display cells calibrated in 10 cell increments. These cells represented the accuracy of the output X,Y data channels from the computer to the display drive (10 bits), and do not represent the resolution available from the sonar system itself. The actual display area was chosen to encompass all the echo patterns obtained during the run, hence the sometimes non-rational choice of values for X_{min} and Y_{min}. In figure 5.2(b), (display 1), the echo pattern due to the monostatic channel is shown with the reference display adjusted for optimum matching of the two, however, normally the appearance would be with the reference displaced to allow the ensemble of echoes to be seen without being confused by the target reference contour.

After matching with the reference display to remove side-lobes and any other spurious responses the appearance of display 1 is as per figure 5.2(c) where it can be seen that the number of points displayed has been reduced from 82 to 49; a 40 percent reduction. Note particularly, that the side-lobe echoes with co-ordinates 930X, 383Y, have been completely removed from the display.

Figures 5.2(d) and (e) show a similar situation for display 3, now with only channel 3 of the system in the active receive mode. Again in figure 5.2(e) side-lobes have been removed and the number of echo co-ordinates reduced by about 60 percent. With reference to figure 5.2(d), it can be seen that the echoes corresponding to the projection at about X = 920, appear to be unsymmetrical with respect to the corner from which they originate. This was because the side-lobe echoes at X,Y co-ordinates 880, 393, caused a 'processor busy' condition

to lock out echoes which would have occurred to correct this unsymmetrical aspect of the display.

A similar procedure was followed for the other data sets for this run. For brevity, only the real-time combined display, and the simulated combined display are shown here to illustrate the detrimental effects on the echo patterns caused by the limited data processing speed of the computer system. Figure 5.2(f) shows the processed version of display 4, obtained when all three channels were receiving simultaneously, and should be compared with figure 5.2(g) which shows the processed and simulated version of display 4.

This limitation prompted a change in experimental procedures, where appropriate, from the situation where the receiver channels were switched on accumulatively, ie channel 1, then channel 1 + channel 2, then channel 1 + channel 2 + channel 3, to the situation where the channels were operated selectively, ie channel 1, then channel 2, then channel 3, then channel 1 + channel 2 + channel. This procedure was followed where initial results for the run indicated that overloading of the computer was occurring; the penalty being a greatly increased time required to complete a run. In order to utilise results from some runs in which this procedure was not followed however, corrections were applied to the data which were based on an estimate of the percentage of data rejected by the computer. This aspect is discussed further in CHAPTER VI.

The above set of display figures constituted a selection of the experimental results obtained for this particular run, and were presented in raw and processed form to show the options available with the off-line processing program. In the results which follow, only the echo patterns obtained after the comparison process are presented, mainly in the interests of brevity, but also because the results discussed in

THE METHOD OF PROCESSING THE RESULTS

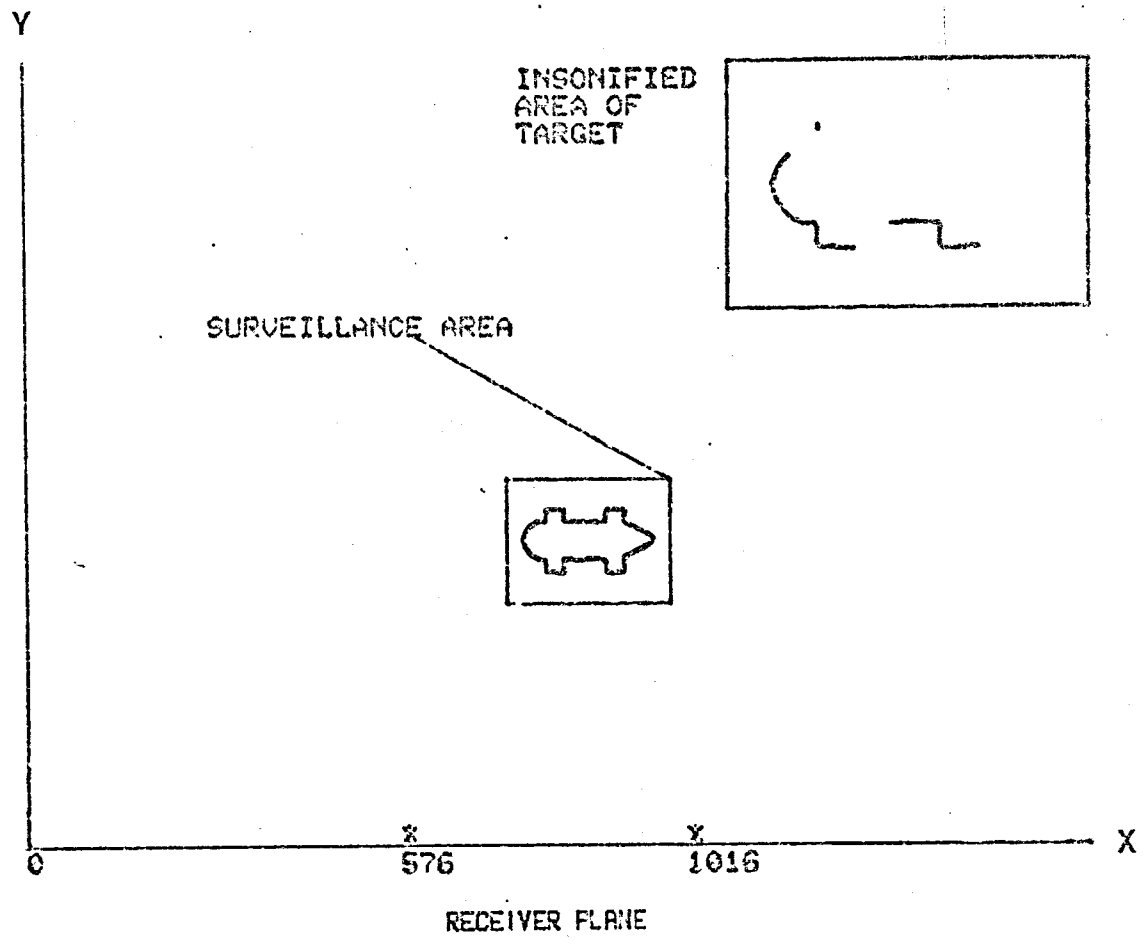

FIG 5.2(A) SYSTEM GEOMETRY FOR RECORD 220 SHOWING THE RELATIONSHIP BETWEEN THE TARGET AND THE MULTI -STATIC SYSTEM.

THE METHOD OF PROCESSING THE RESULTS

SURVEILLANCE AREA

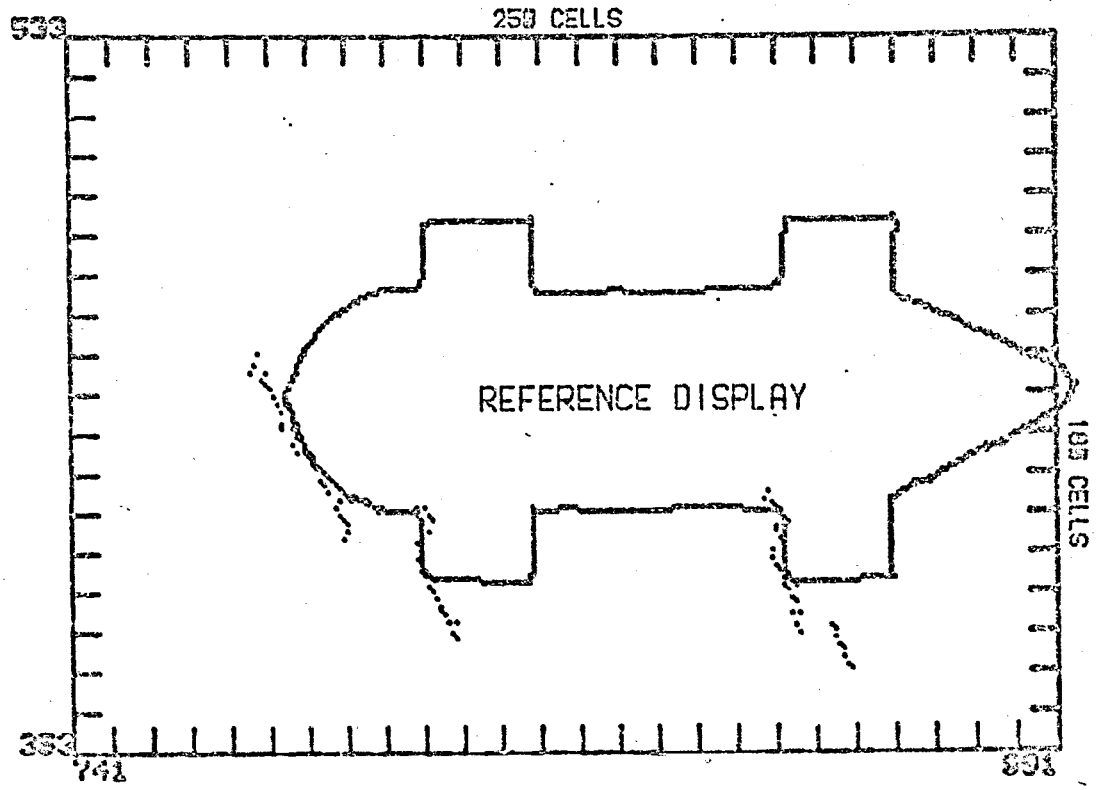

PPIREC 0220 0 PNTS DISPLAYED 02

RANGE QUANTISING = 01 CELLS
ANGULAR QUANTISING = 0.1 DEG
TARGET ORIENTATION = 00 DEG
REFERENCE DISPLAY OFFSET IN CELLS = 00(X),00(Y)

FIG 5.2(B) PPI DISPLAY OBTAINED WITH THE MONOSTATIC SYSTEM BEFORE PROCESSING TO REMOVE SIDE-LOBE ECHOES.

THE METHOD OF PROCESSING THE RESULTS

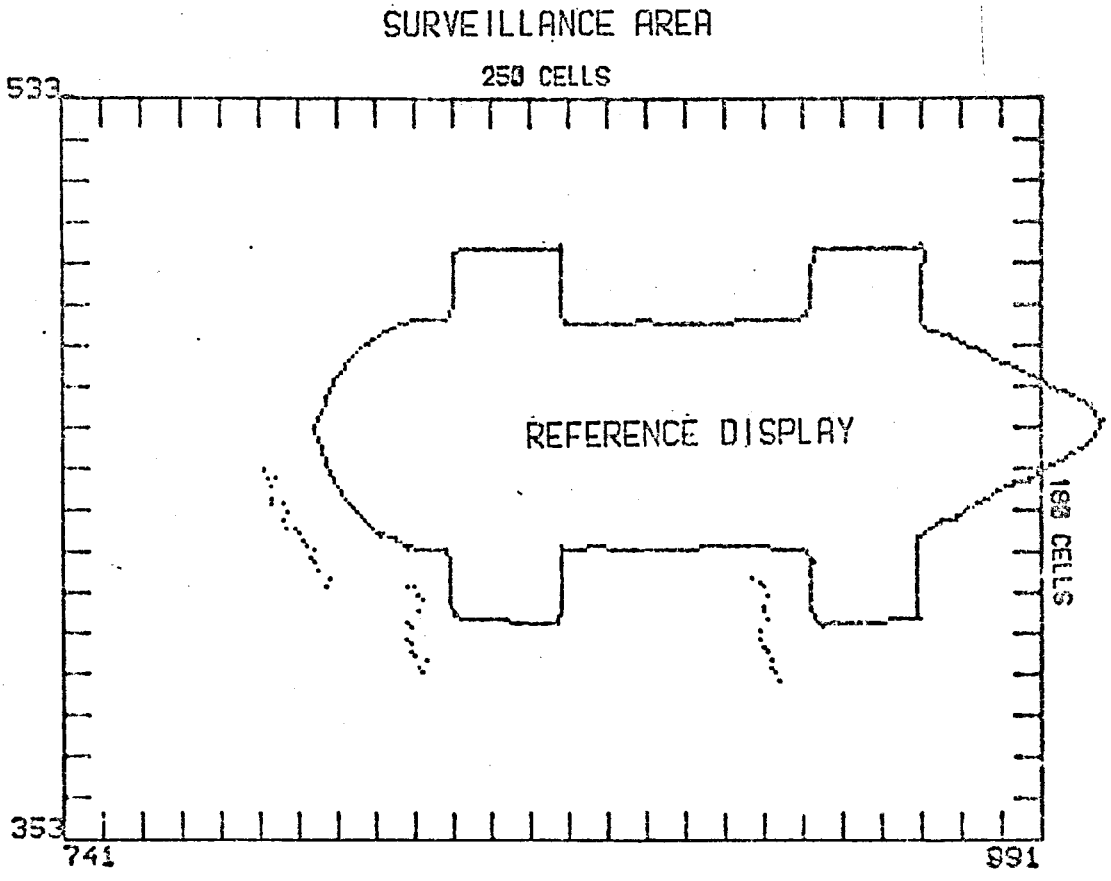

FIG 5.2(C) PPI DISPLAY OBTAINED WITH THE MONOSTATIC SYSTEM AFTER PROCESSING TO REMOVE SIDE-LOBE ECHOES.

THE METHOD OF PROCESSING THE RESULTS

SURVEILLANCE AREA

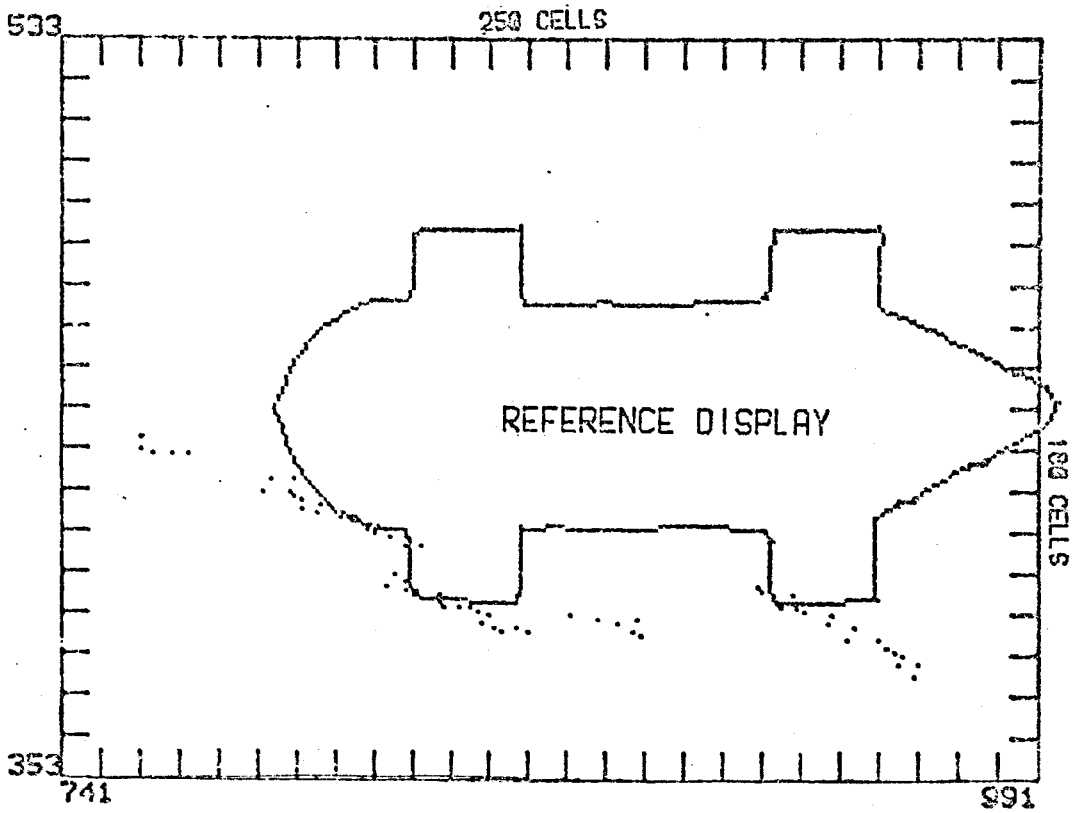

PPIREC $220 # PNTS DISPLAYED 62
RANGE QUANTISING = 01 CELLS
ANGULAR QUANTISING = 0.1 DEG
TARGET ORIENTATION = 00 DEG
REFERENCE DISPLAY OFFSET IN CELLS = 00(X),00(Y)

FIG 5.2(D) PPI DISPLAY OBTAINED WITH THE BISTATIC RECEIVER AT X-COORD. 1016 BEFORE PROCESSING TO REMOVE SIDE-LOBE ECHOES.

THE METHOD OF PROCESSING THE RESULTS

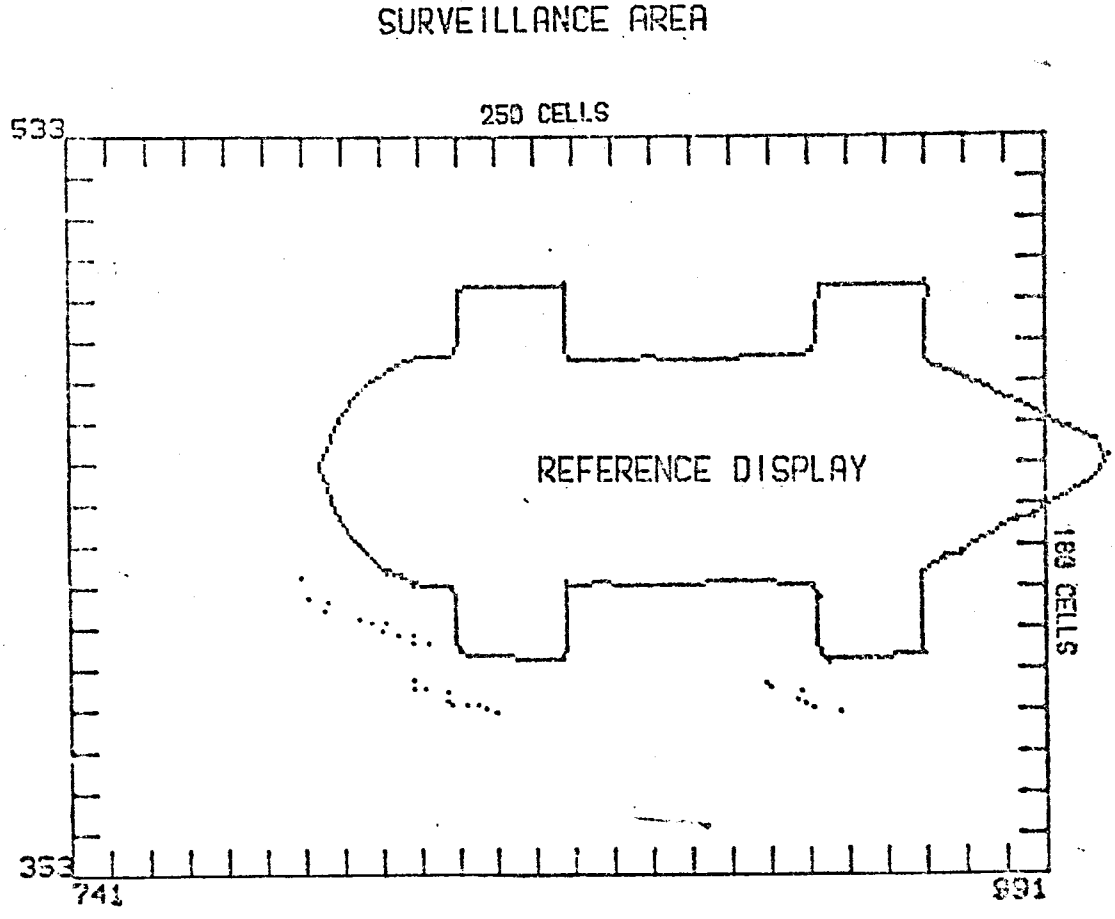

FIG 5.2(E) PPI DISPLAY OBTAINED WITH THE BISTATIC RECEIVER AT X-COORD. 1016 AFTER PROCESSING TO REMOVE SIDE-LOBE ECHOES.

THE METHOD OF PROCESSING THE RESULTS

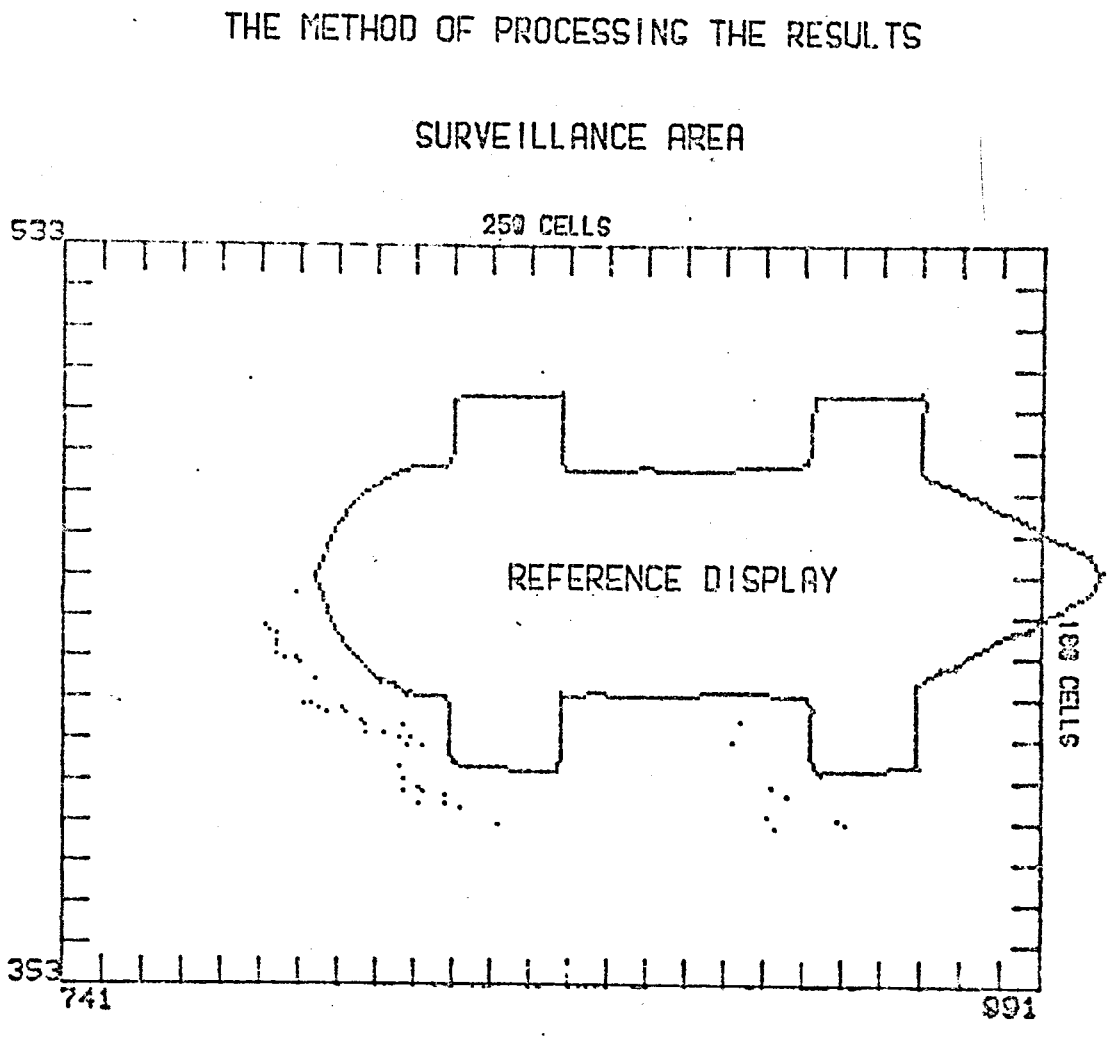

FIG 5.2(F) REAL-TIME DISPLAY OBTAINED WITH ALL THREE RECEIVERS AFTER PROCESSING TO REMOVE SIDE-LOBE ECHOES.COMPARE WITH (C) TO SEE THE IMPROVEMENT DUE TO MULTISTATIC OPERATION!

THE METHOD OF PROCESSING THE RESULTS

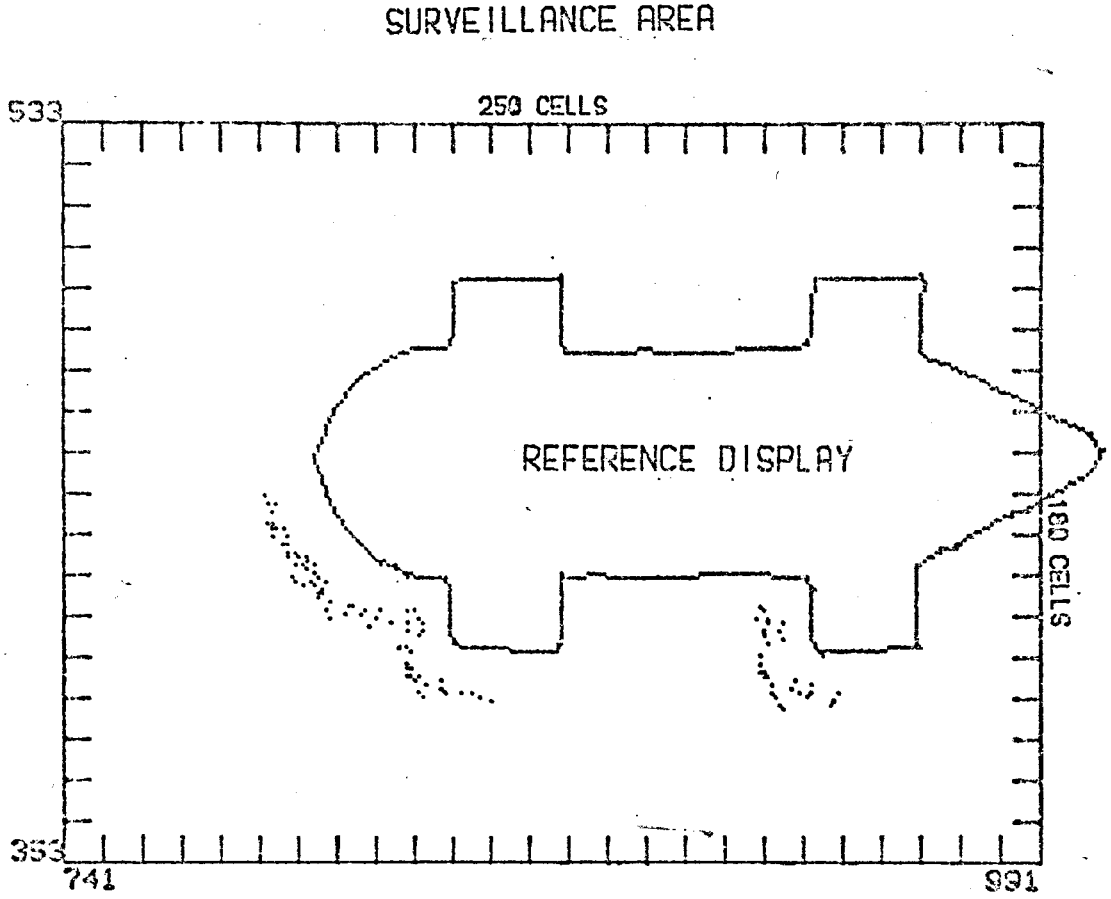

PPIREC 2220 # PNTS DISPLAYED 108
RANGE QUANTISING = 01 CELLS
ANGULAR QUANTISING = 0.1 DEG
TARGET ORIENTATION = 00 DEG
REFERENCE DISPLAY OFFSET IN CELLS = 10(X),10(Y)

FIG 5.2(G) SIMULATED REAL-TIME DISPLAY OBTAINED BY COMBINING INDIVIDUAL REAL-TIME DISPLAYS.COMPARE WITH (C) TO SEE THE IMPROVEMENT DUE TO MULTISTATIC OPERATION.

CHAPTER VI were obtained exclusively from the processed echo patterns, and not the raw echo patterns.

5.3 Selected PPI display results for target 1

A selection of the echo patterns obtained from the target designated as number 1 and shown in figure 4.2 in CHAPTER IV are presented first. This was considered the most important set of results because this was the most convoluted target shape, the other two targets used being simple linear geometric shapes. This target provided the opportunity to observe and compare the performance of the multistatic and monostatic systems under conditions of varying target contours including specularly reflecting surfaces, corners and target contour boundaries.

It was the opinion of the author that an equally representative set of results could be obtained by using a complex target contour, as would be obtained by using a succession of basic geometrical shapes. Particularly since it was the average performance improvement for various target orientations and positions in the surveillance area which was being studied and measured.

In general three aspects were used:-

(a) Zero degrees relative to the receiver plane (see figure 5.4(a) for run 214).

(b) 90 degrees relative to the receiver plane (see figure 5.8(a) for run 218).

and (c) approximately 40-50 degrees relative to the receiver plane (see figure 5.3(a) for run 209).

Thus, in sonar parlance, a set of results at beam, bow and quarter aspects were obtained for a number of positions along the receiver plane, with the object of observing the effects of X position and aspect relative to the receiver plane on the number of echo co-ordinates produced and the target shape portrayal performance of the system.

The first of these results shows the ppi displays for run 209, which was a 30 degree, quarter aspect run with respect to the transmitter. In addition, for this chronologically early run, the angular accuracy parameter for the computer program was changed from the default value of 0.1 degrees to 0.5 degrees azimuth. This was still better than the nominal transmitter beamwidth by a factor of three, but it meant that only 180 bearing bins were available to store echo co-ordinates. The problems to do with co-ordinate overwrite in the display stores mentioned in CHAPTER III, meant that some echoes were lost for this reason and later runs were performed with 901 bearing bins covering the 90 degree sector. The results were nevertheless included in the analysis in the next chapter by making appropriate changes in the value of 'display magnification' m, used in the calculations.

The insonified area included most of the front curved portion of the target in addition to the two projections nearest the receiver plane. However, the flat surface joining these projections was in an acoustic shadow zone. It should be noted also that although the upper curved front portion of the target was insonified, it still presented a very shallow angle of incidence to the projector and was shielded from the bistatic receivers by the other insonified areas. Figure 5.3(b) shows the echo pattern due to the monostatic system and echoes can be seen corresponding to the specular region on the curved front portion and from discontinuities at the projections and from the corner reflector nearest the source. Figure 5.3(c) shows the echo pattern obtained with the bistatic receiver at location 572, and figure 5.3(d) shows that obtained with the bistatic receiver at location 1028. In both cases the specular echoes from surfaces tangential to the constant path length ellipses of the bistatic channels were detected, and corner and discontinuity echoes can be seen in figure 5.3(d) and figure 5.3(c), respectively. Figure 5.3(e) shows the echo pattern obtained when all

channels were outputting data simultaneously, and the absence of echoes from some regions where echoes were detected with the individual receivers was due to the overloading of the system computer program. It was stated in CHAPTER III that measurements with the real-time display program indicated a response time of approximately 180 μs, which meant that echoes closer together than about 13 cms in time could not both be displayed. Only the first echo would be processed, the second would be rejected by a 'system busy' condition. Side-lobes of the main transmission did occasionally cause false echoes to occur prior to the reception of the true echoes on a particular bearing, and the resulting system busy condition meant that these echoes were lost.

Finally figure 5.3(f) shows the echo pattern by combining figures 5.3(b) and (d) in the manner described above. Comparison of this display with figure 5.3(b) shows the improvement due to the multistatic environment. The curvature of the front of the target can now be seen together with the discontinuity echoes due to the projections on the target contour.

FIG 5.3(A)

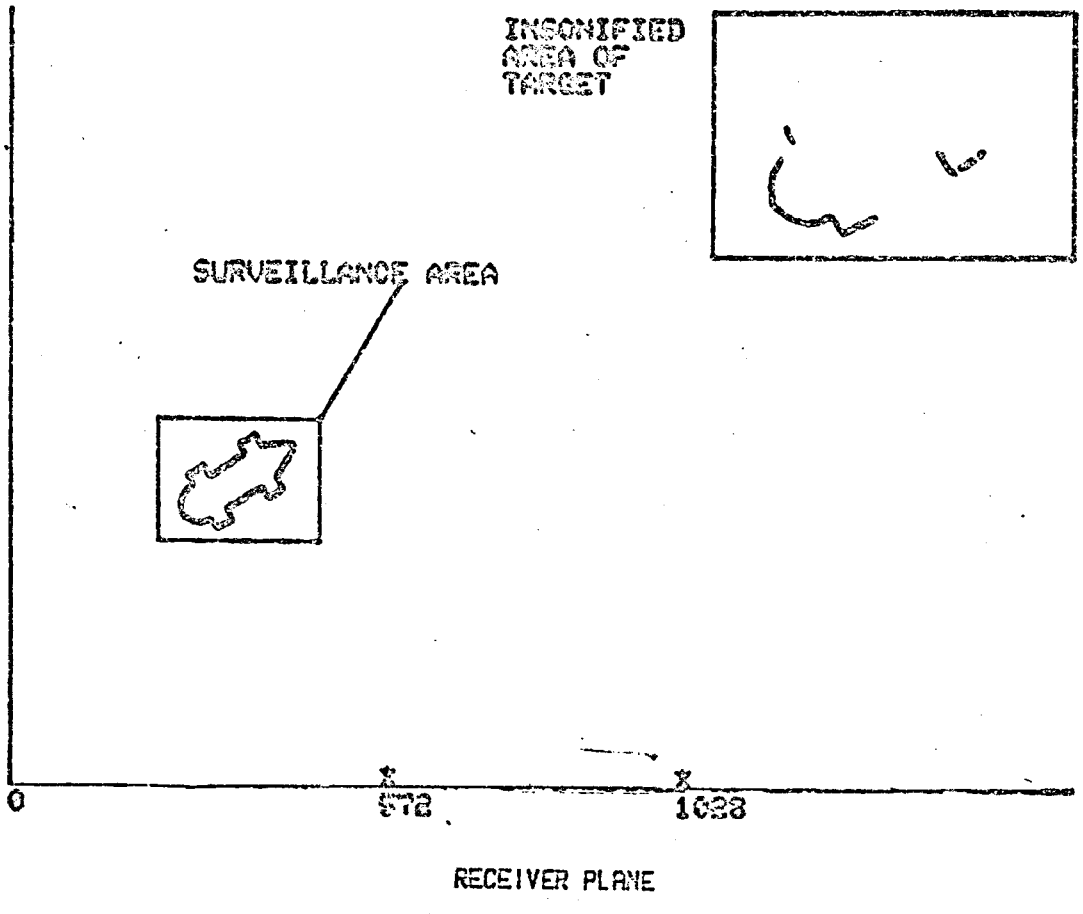

FIG 5.3(A) SYSTEM GEOMETRY FOR RECORD 209 SHOWING THE RELATIONSHIP BETWEEN THE TARGET AND THE MULTISTATIC SYSTEM.

FIG 5.3(B)

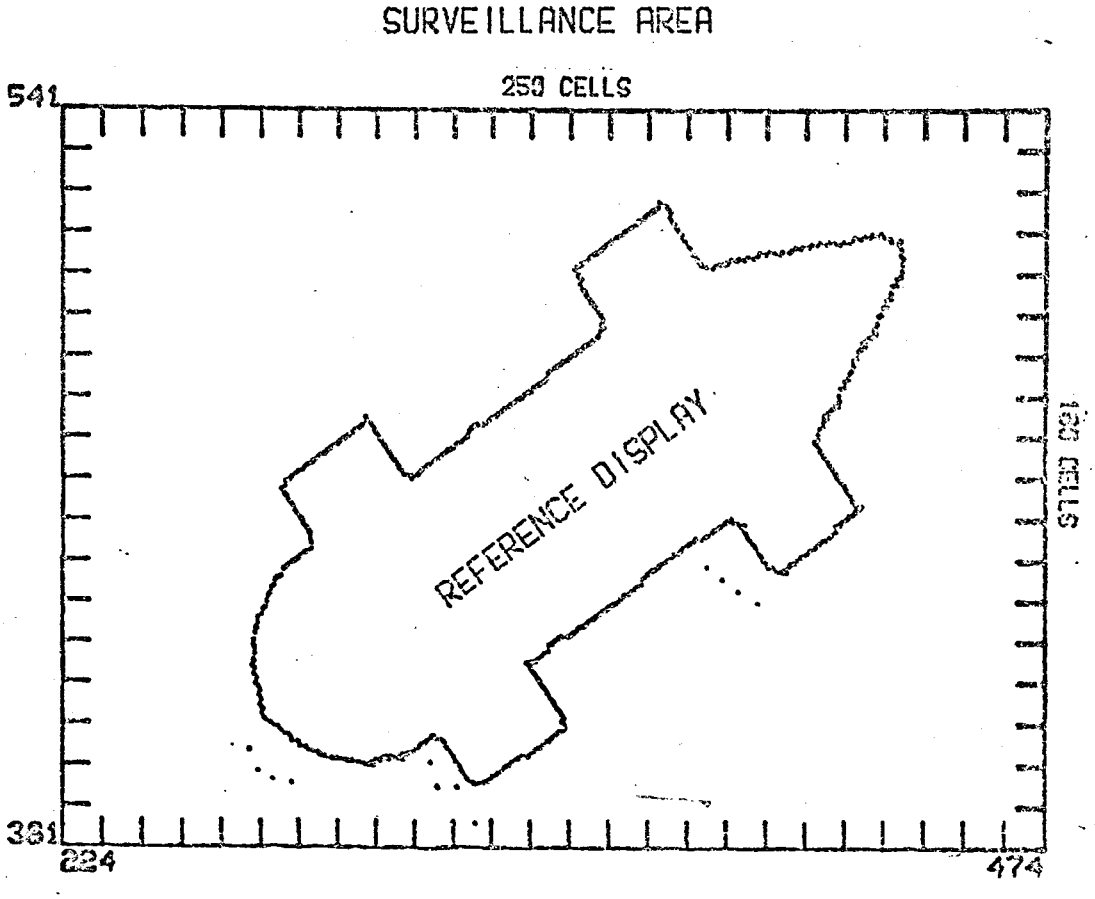

PPIREC 0209 8 PNTS DISPLAYED 13
RANGE QUANTISING = 01 CELLS
ANGULAR QUANTISING = 0.5 DEG
TARGET ORIENTATION = 40 DEG
REFERENCE DISPLAY OFFSET IN CELLS = 03(X),10(Y)

FIG 5.3(B) PPI DISPLAY OBTAINED WITH THE MONOSTATIC SYSTEM.

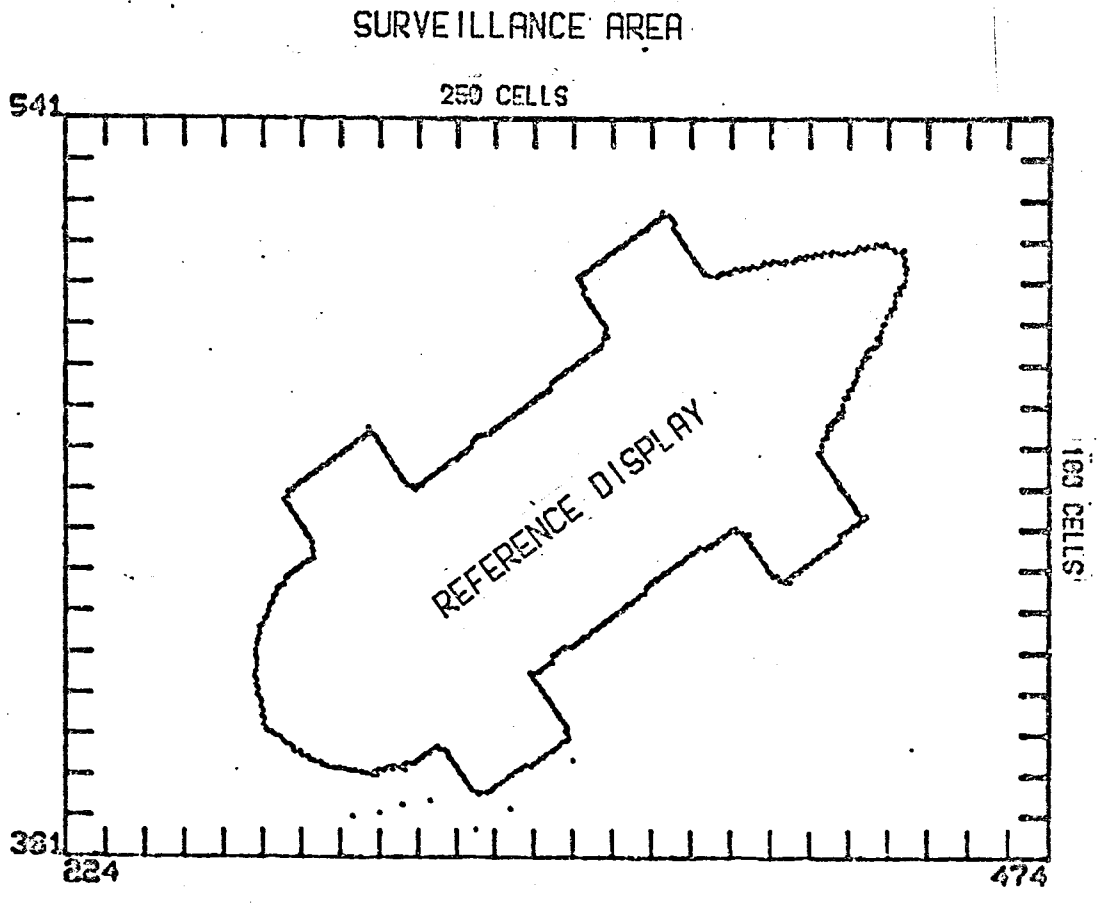

PPIREC 0209 8 PNTS DISPLAYED ?
RANGE QUANTISING = 01 CELLS
ANGULAR QUANTISING = 0.5 DEG
TARGET ORIENTATION = 40 DEG
REFERENCE DISPLAY OFFSET IN CELLS = 00(X),10(Y)

FIG 5.3(C) PPI DISPLAY OBTAINED WITH THE BISTATIC RECEIVER AT X-COORD. 572.

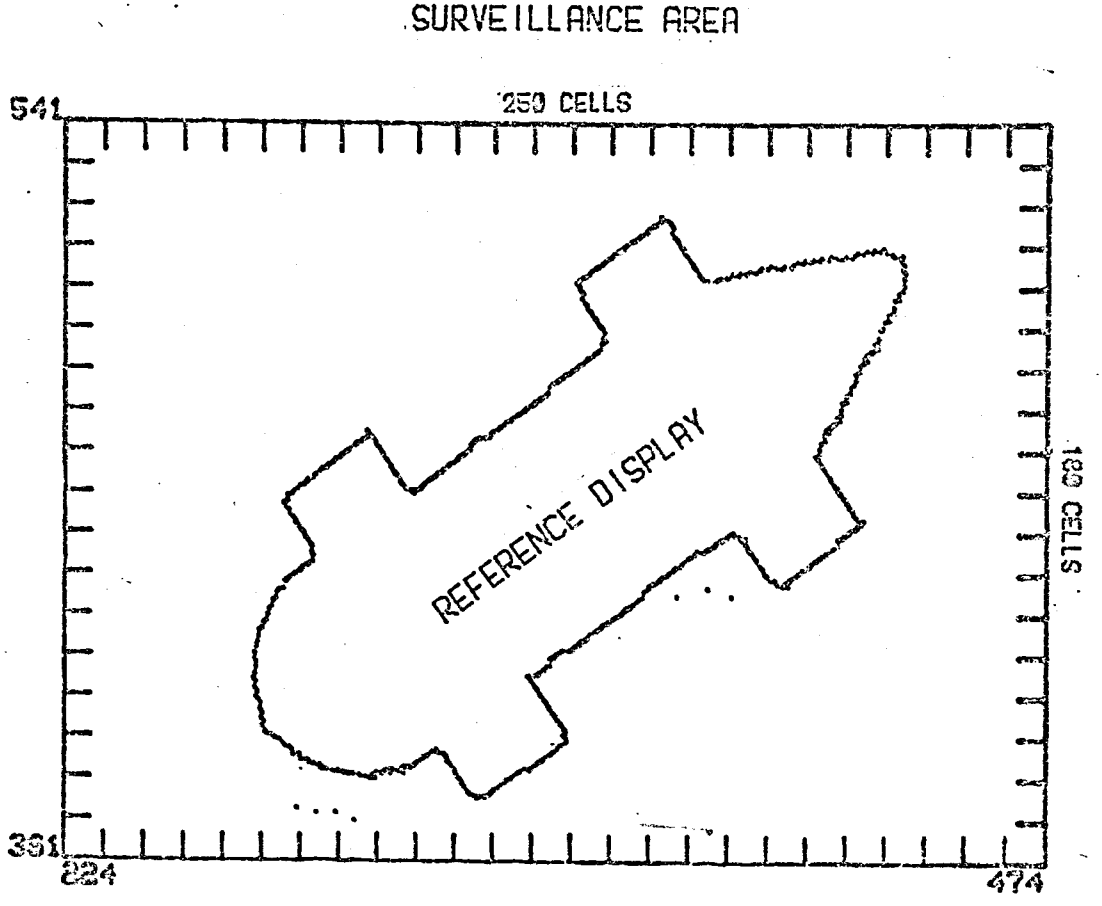

PPIREC 0303 8 PNTS DISPLAYED ?
RANGE QUANTISING = 01 CELLS
ANGULAR QUANTISING = 0.5 DEG
TARGET ORIENTATION = 40 DEG
REFERENCE DISPLAY OFFSET IN CELLS = 03(X),10(Y)

FIG 5.3(D) PPI DISPLAY OBTAINED WITH THE BISTATIC RECEIVER AT X-COORD. 1028.

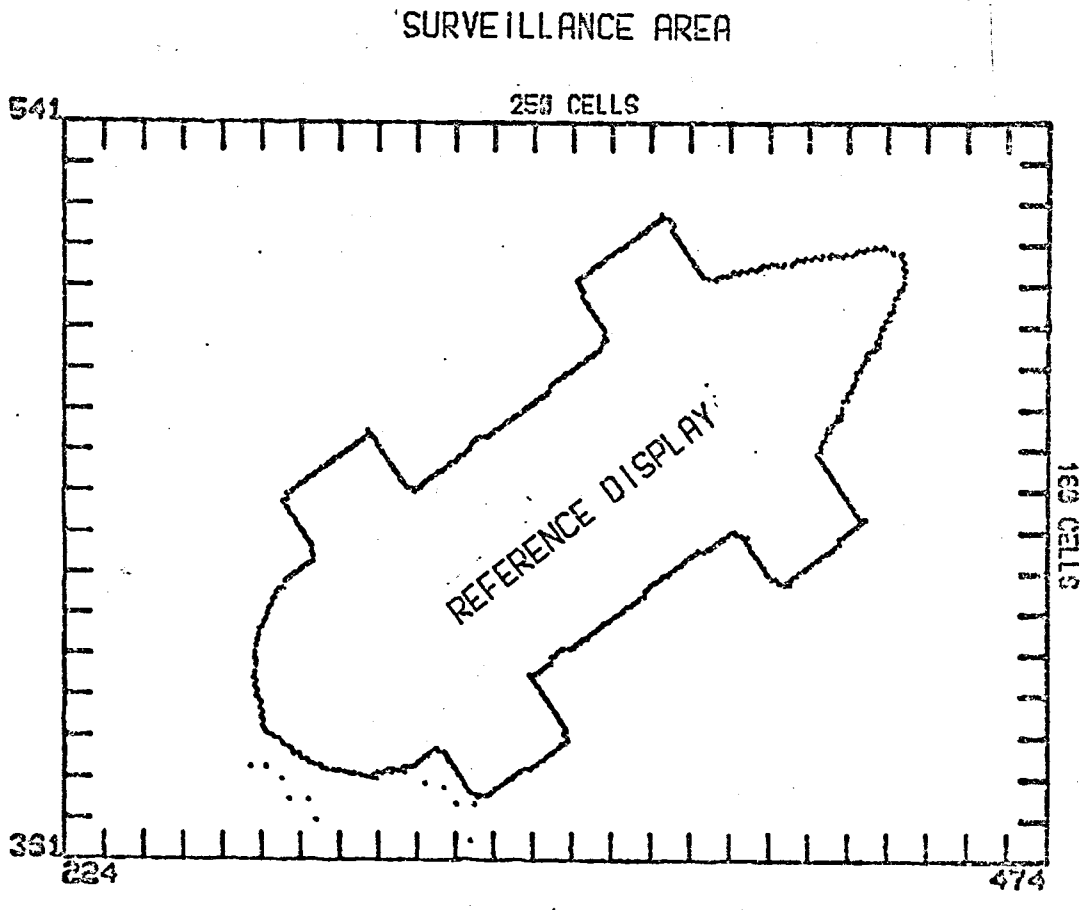

PPIREC 0009 8 PNTS DISPLAYED 11
RANGE QUANTISING = 01 CELLS
ANGULAR QUANTISING = 0.5 DEG
TARGET ORIENTATION = 40 DEG
REFERENCE DISPLAY OFFSET IN CELLS = 00(X),10(Y)

FIG 5.3(E) REAL-TIME PPI DISPLAY OBTAINED WITH ALL THREE RECEIVERS.

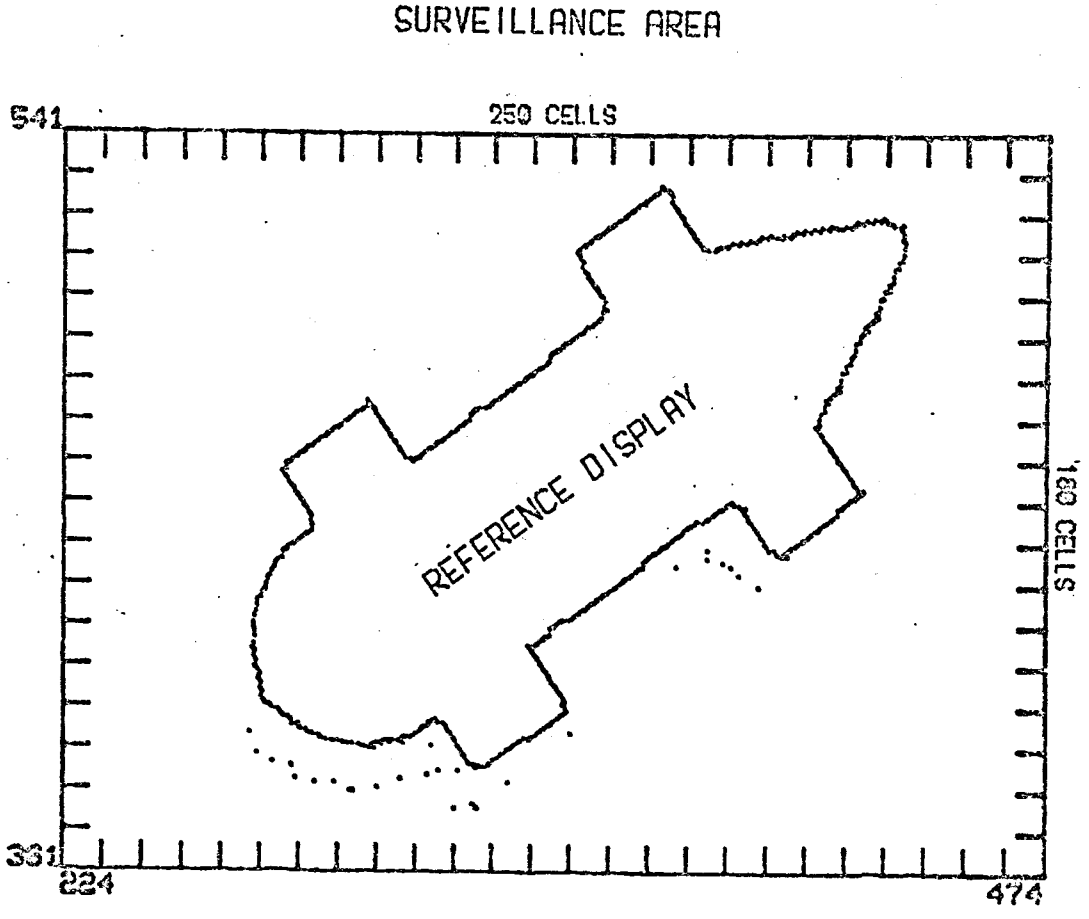

FIG 5.3(F) SIMULATED REAL-TIME PPI DISPLAY OBTAINED BY COMBINING (B),(C) AND (D).COMPARE WITH (B) TO SEE THE IMPROVEMENT DUE TO MULTISTATIC OPERATION.

For run 214, the target was orientated and located along the X axis as shown in figure 5.4(a). In this and subsequent runs, the angular accuracy parameter in the display program was set to 0.1 degrees. This meant that all 901 separate bearing bins were available in the X-Y co-ordinate store, in contrast with the previous run presented in which only 181 were available. It was found that an apparently more complete picture of the target contour was obtained as a result, although the bearing accuracy then exceeded that available at the transmitter in terms of its beam pattern. This was an averaging effect due to the high transmission rate. There was more than one ping within the azimuth resolution defined by the beam patterns, and consequently as the transmitter beam was scanned, each returning echo was stored in a slightly different bearing bin, thus reducing the problem of overwriting of previous echoes and presenting a more detailed echo pattern. Figure 5.4(b) shows the display obtained with the monostatic system only. Echoes were obtained from the area at the front of the target which provided a specular surface normal to the insonifying beam and also from the internal corner reflector. Additional echoes can be seen from the corners formed by the projections on the target and from the internal corner reflector which is insonified at the rear of the target. Figure 5.4(c) shows the echo pattern obtained from the receiver located at X co-ordinate 572 in figure 5.4(a) and more of the front curved surface of the target is now displayed together with echoes arising due to the finite detection arc at the corners of the projections. Figure 5.4(d) shows the echo pattern obtained with the receiver at X co-ordinate 1028. This echo pattern corresponds to the specular echoes received from the flat surface interconnecting the two projections on the target. It was expected that two other traces would be obtained from the two parallel flat surfaces of the projections, but no such echoes were detected.

The author made a mental note at the time to return to this configuration and conduct an investigation of why these echoes were missing, but for various reasons this was never done. However, on reconsidering possibilities the most likely explanation was that the method of data storage in the computer again caused overwriting of echoes from these positions, which were on nearly equal azimuth bearings. Figure 5.4(e) shows the echo patterns obtained when all three channels were active simultaneously and illustrates the degree to which the software and hardware limitations of the system degraded the performance. For this reason figure 5.4(e) should be compared with figure 5.4(f) which shows the combined output of figures 5.4(b), (c) and (d). A comparison of the number of points displayed shows that the display loss is about 4 dB using the definition in equation 2.3 of CHAPTER II. Figure 5.4(f) shows the improvement in target shape portrayal obtained with the multistatic environment and should be compared with figure 5.4(b). A recognisable outline is emerging at this stage, conforming to the insonified areas of the target except for the upper portion of the curved front and the missing echoes from the projections mentioned above.

FIG 5.4(A)

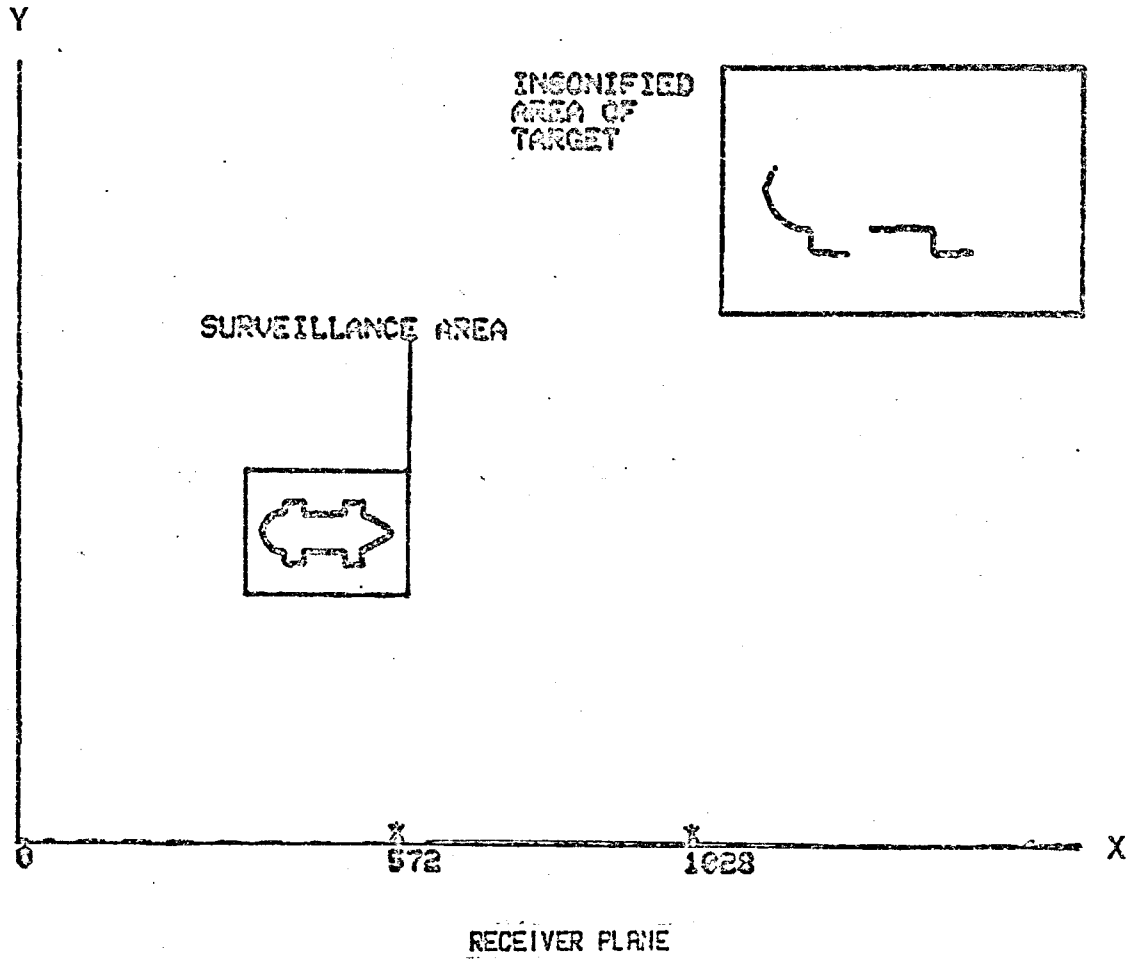

FIG 5.4(A) SYSTEM GEOMETRY FOR RECORD 214 SHOWING THE RELATIONSHIP BETWEEN THE TARGET AND THE MULTISTATIC SYSTEM.

FIG 5.4(B)

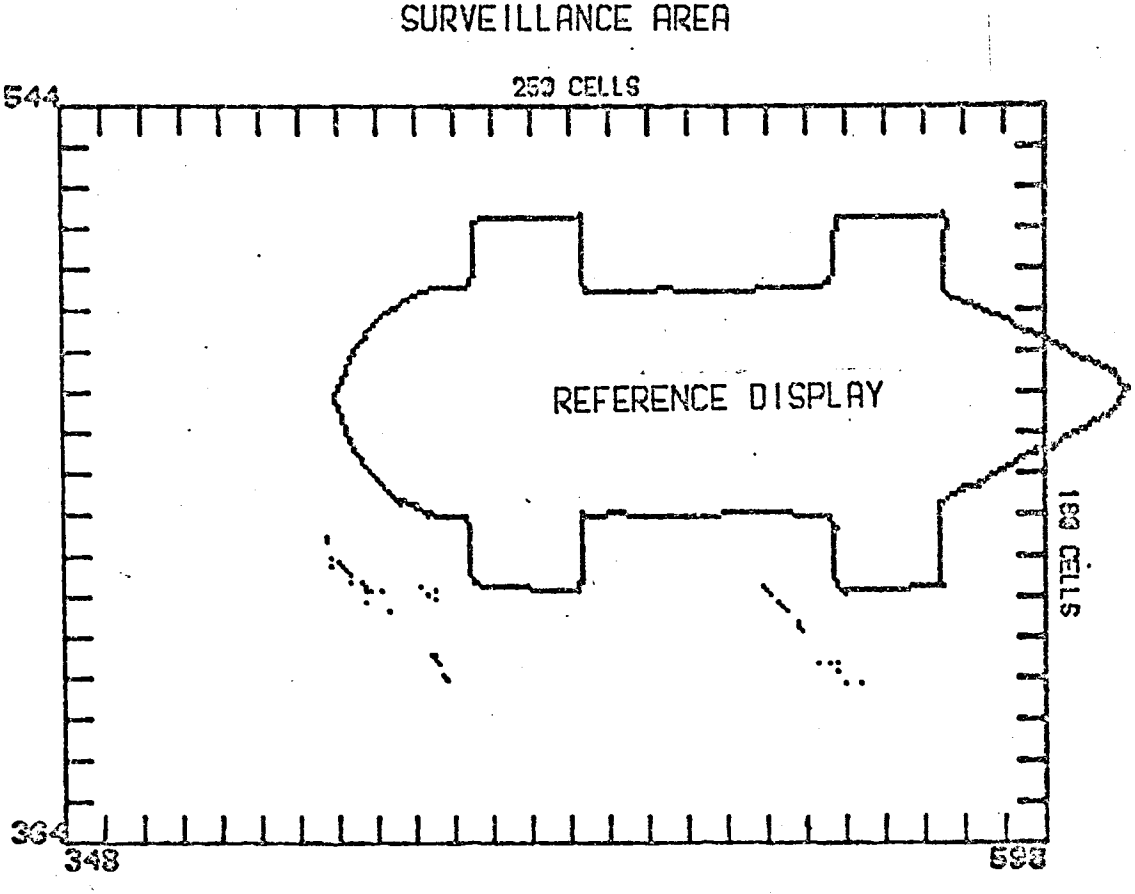

PPIREC 8214 8 PNTS DISPLAYED 42
RANGE QUANTISING = 01 CELLS
ANGULAR QUANTISING = 0.1 DEG
TARGET ORIENTATION = 03 DEG
REFERENCE DISPLAY OFFSET IN CELLS = 10(X),20(Y)

FIG 5.4(B) PPI DISPLAY OBTAINED WITH THE MONOSTATIC SYSTEM.

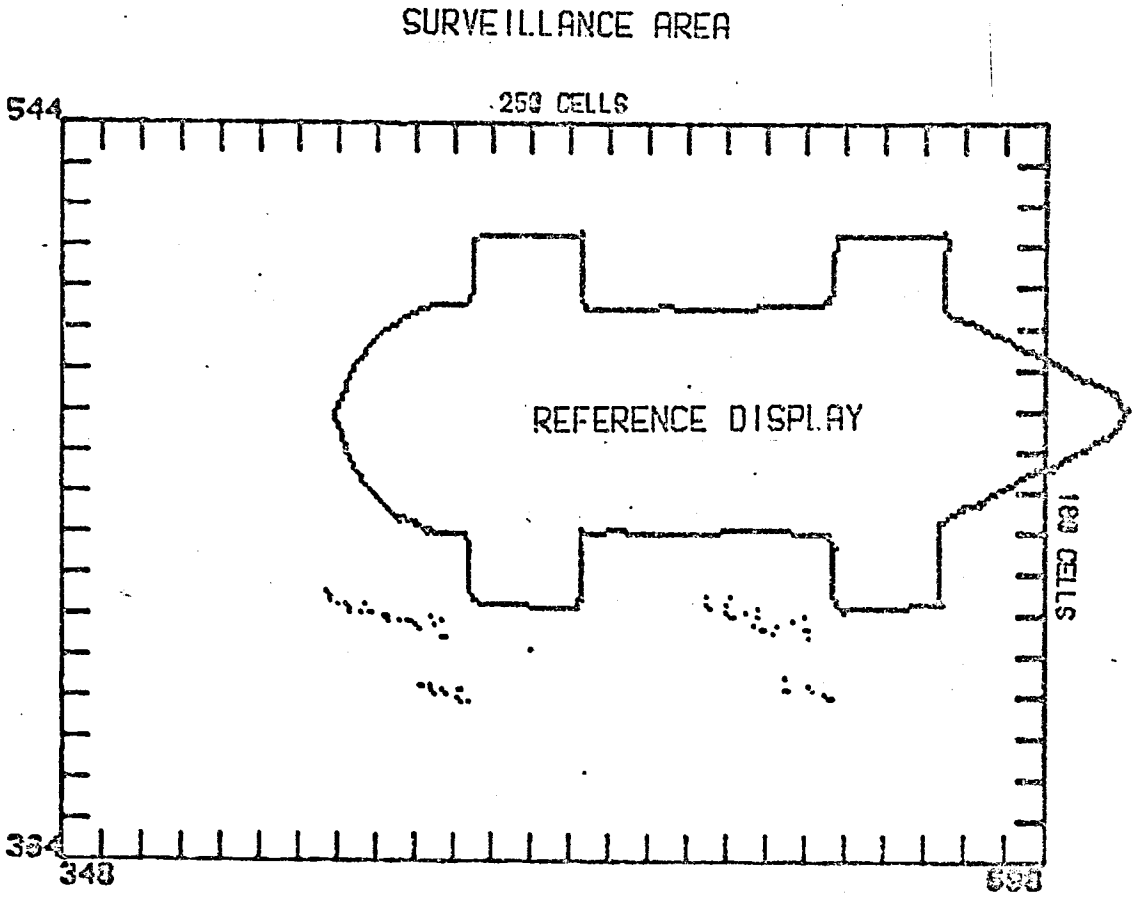

PPIREC 0214 0 PNTS DISPLAYED 66

RANGE QUANTISING = 01 CELLS

ANGULAR QUANTISING = 0.1 DEG

TARGET ORIENTATION = 03 DEG

REFERENCE DISPLAY OFFSET IN CELLS = 10(X),20(Y)

FIG 5.4(C) PPI DISPLAY OBTAINED WITH THE BISTATIC RECEIVER AT X-COORD. 572..

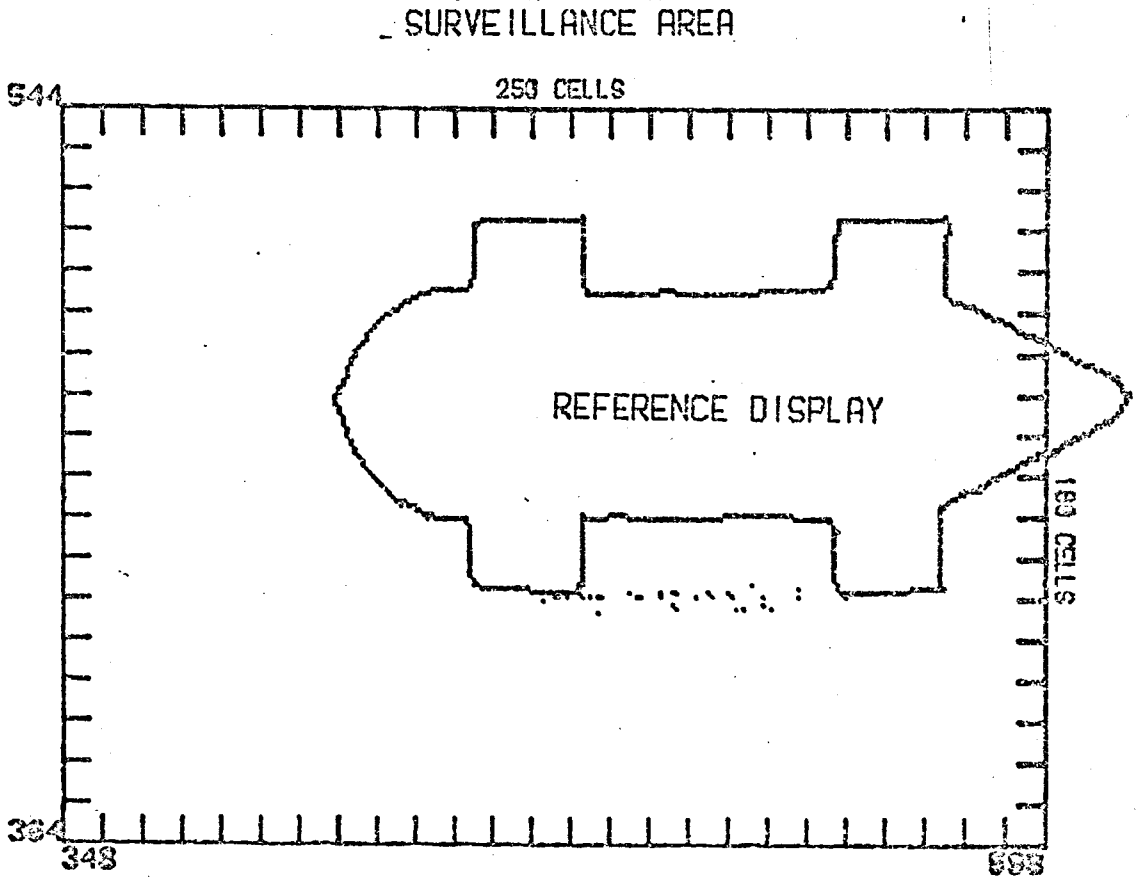

PPIREC 0214 & PNTS DISPLAYED 32
RANGE QUANTISING = 01 CELLS
ANGULAR QUANTISING = 0.1 DEG
TARGET ORIENTATION = 00 DEG
REFERENCE DISPLAY OFFSET IN CELLS = 10(X),20(Y)

FIG 5.4(D) PPI DISPLAY OBTAINED WITH THE BISTATIC RECEIVER AT X-COORD. 1028.

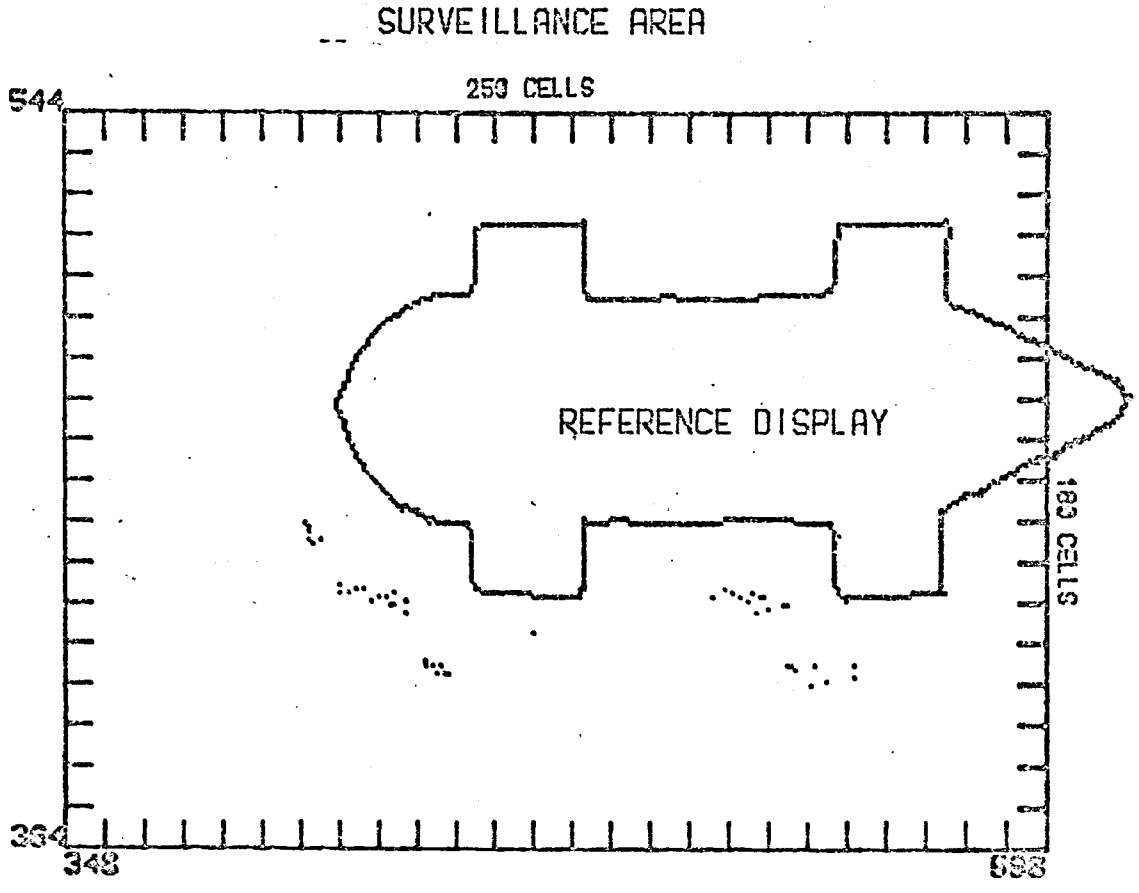

PPIREC 8214 8 PNTS DISPLAYED 54
RANGE QUANTISING = 01 CELLS
ANGULAR QUANTISING = 0.1 DEG
TARGET ORIENTATION = 03 DEG
REFERENCE DISPLAY OFFSET IN CELLS = 10(X),20(Y)

FIG 5.4(E) REAL-TIME DISPLAY OBTAINED WITH ALL THREE RECEIVERS.

FIG 5.4(F)

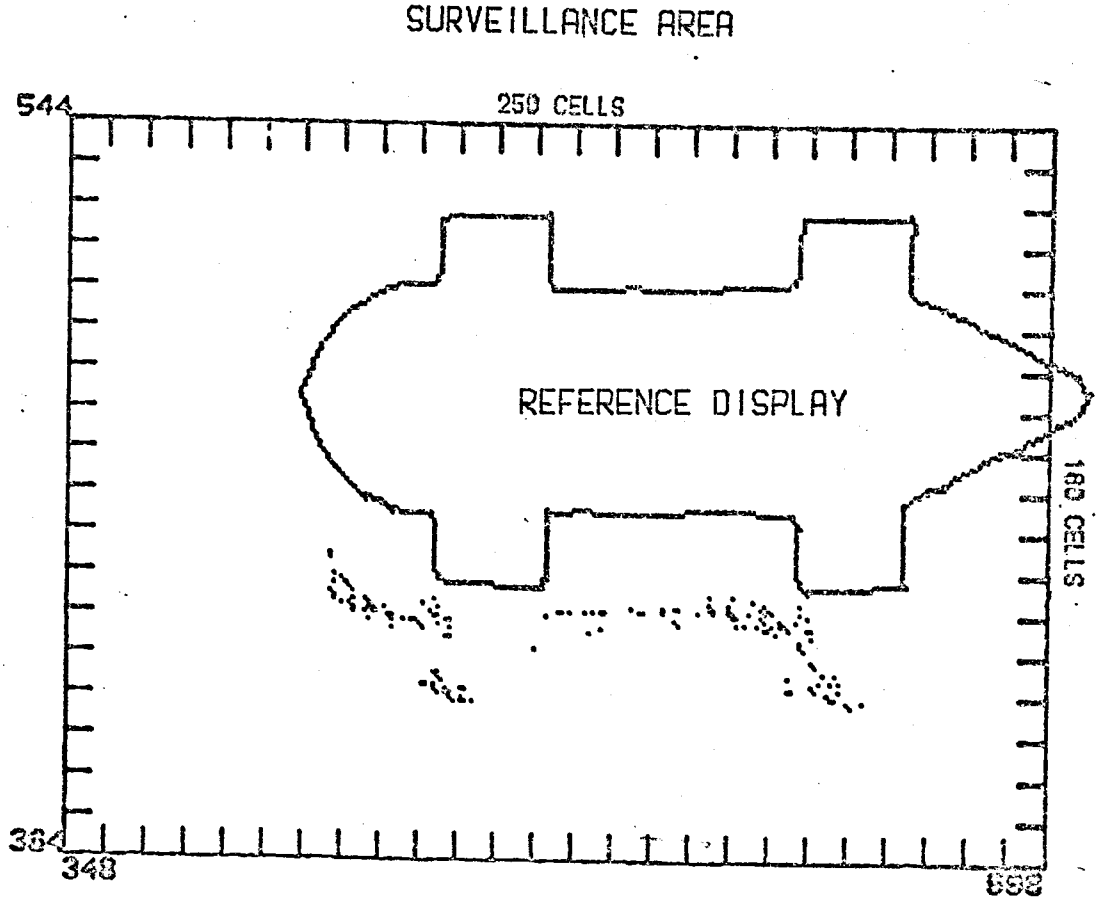

PPIREC 0214 # PNTS DISPLAYED 151

RANGE QUANTISING = 01 CELLS

ANGULAR QUANTISING = 0.1 DEG

TARGET ORIENTATION = 00 DEG

REFERENCE DISPLAY OFFSET IN CELLS = 00(X),20(Y)

FIG 5.4(F) SIMULATED REAL-TIME PPI DISPLAY OBTAINED BY COMBINING (B),(C) AND (D).COMPARE WITH (B) TO SEE THE IMPROVEMENT DUE TO MULTISTATIC OPERATION.

For run 215, the target was rotated by 40 degrees to present a bow quarter-aspect to the receiver plane as shown in figure 5.5(a). The predicted line-of-sight insonified area shown on this figure highlights the inadequate coverage of the target obtained at this aspect. The bistatic coverage is even more restricted in that the upper portions of the insonified area are not acoustically visible at the bistatic positions. The expectation was therefore that the improvement in target shape portrayal by the multistatic system would be minimal, with a small number of additional points being displayed by each hydrophone. Consequently, in order to save time the procedure adopted for this run was to switch on the receivers successively, rather than each one individually. Figure 5.5(b) shows the monostatic echo pattern, displaying two specular echoes from the normal incidence surfaces of the projections, and the discontinuity echo from the front of the target. Figure 5.5(c) shows the accumulative display including the output of the hydrophone at X co-ordinate 512 in figure 5.5(a). It can be seen that no specular echo trace from the curved portion has been added to the echo pattern. Figure 5.5(d) shows the cumulative display from all three receivers and the curvature of the target is now more evident. The combined display shown in figure 5.5(e) was obtained by summing the outputs of figures 5.5(b), (c) and (d) and showed that even in the case of a predicted small degree of improvement in shape portrayal, system overloading still occurred to the level of about 3 dB equivalent display loss.

FIG 5.5(A)

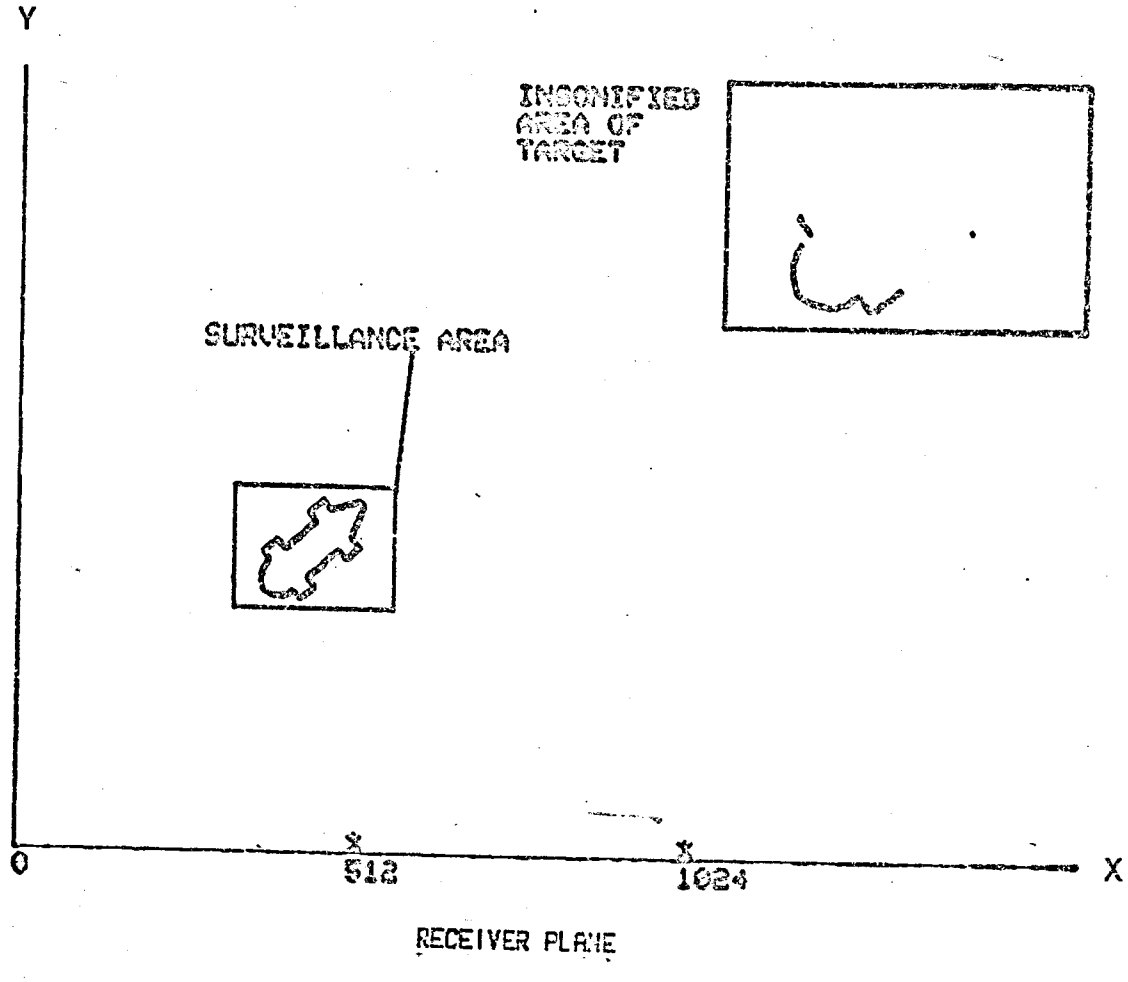

FIG 5.5(A) SYSTEM GEOMETRY FOR RECORD 215 SHOWING THE RELATIONSHIP BETWEEN THE TARGET AND THE MULTISTATIC SYSTEM.

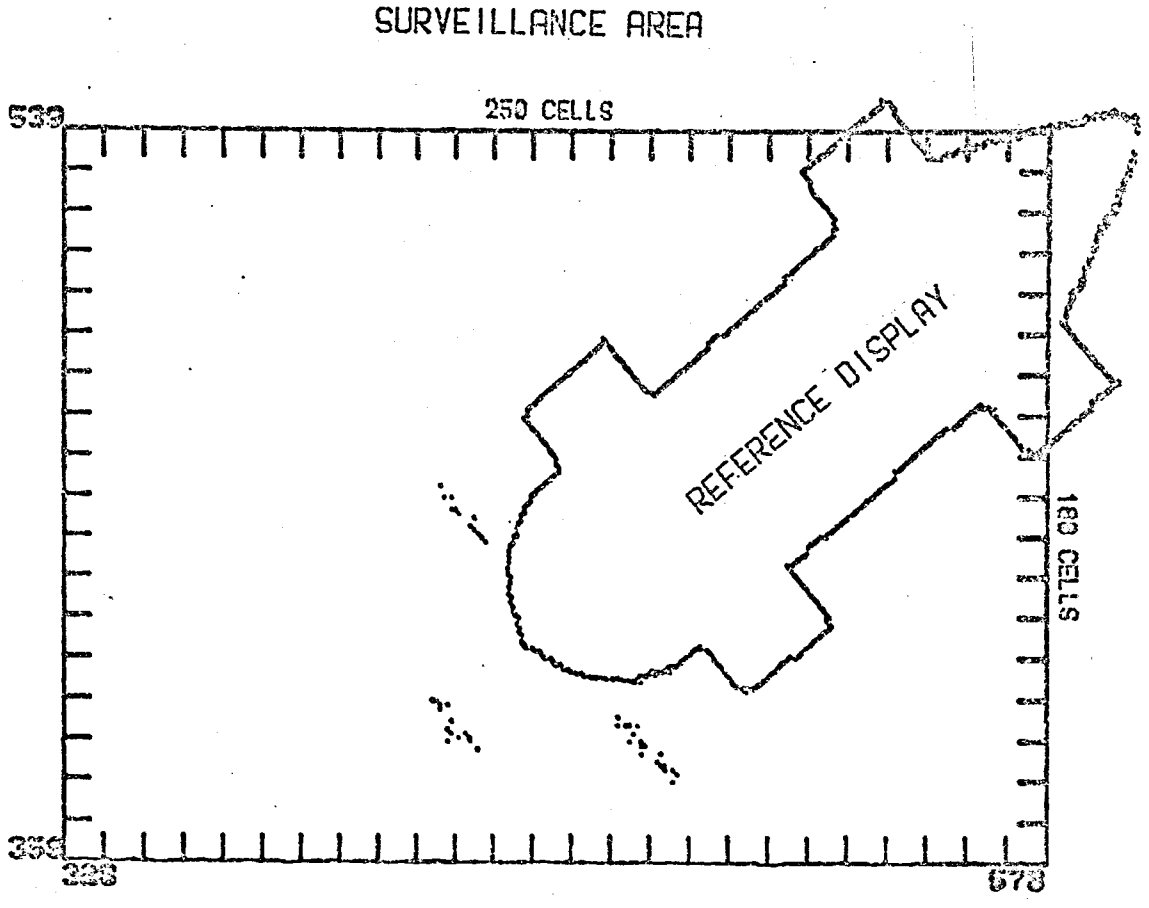

FPIREC 3815 8 PNTS DISPLAYED 45
RANGE QUANTISING = 01 CELLS
ANGULAR QUANTISING = 0.1 DEG
TARGET ORIENTATION = 40 DEG
REFERENCE DISPLAY OFFSET IN CELLS = 20(X),20(Y)

FIG 5.5(B) PPI DISPLAY OBTAINED WITH THE MONOSTATIC SYSTEM.

FIG 5.5(C)

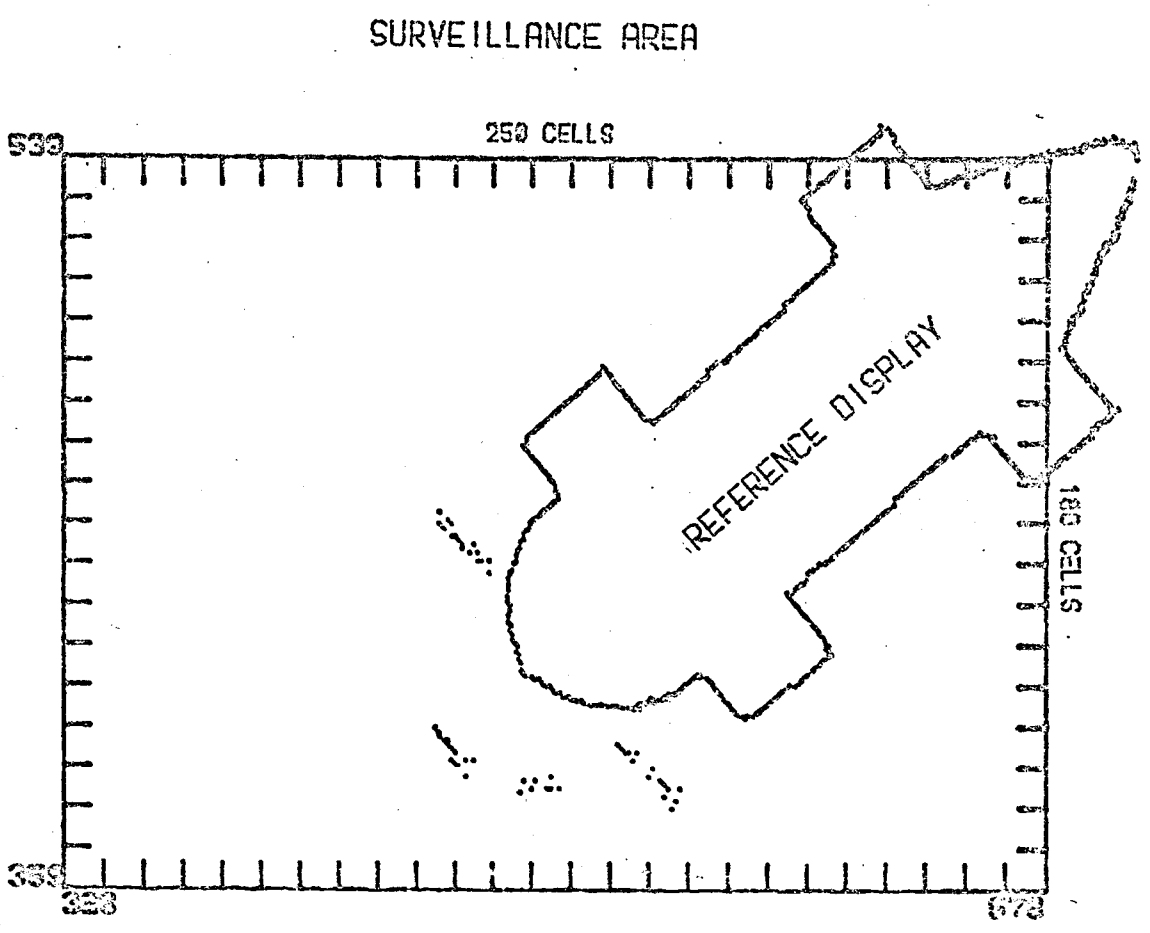

PPIREC 8215 8 PNTS DISPLAYED 55

RANGE QUANTISING = 01 CELLS
ANGULAR QUANTISING = 0.1 DEG
TARGET ORIENTATION = 40 DEG
REFERENCE DISPLAY OFFSET IN CELLS = 20(X),20(Y)

FIG 5.5(C) REAL-TIME PPI DISPLAY OBTAINED WITH THE MONOSTATIC SYSTEM AND THE BISTATIC RECEIVER AT X-COORD. 512.

FIG 5.5(D)

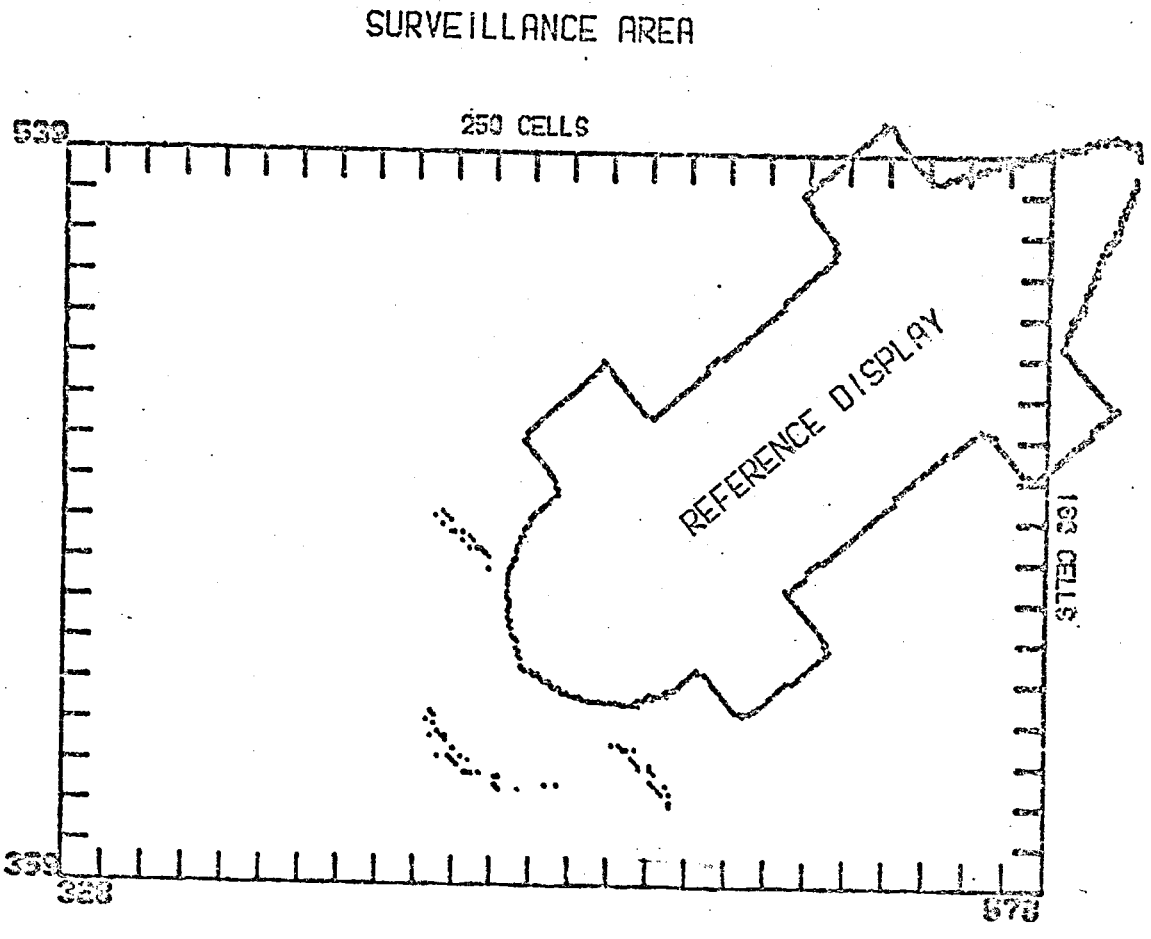

FIG 5.5(D) REAL-TIME PPI DISPLAY OBTAINED WITH ALL THREE RECEIVERS.

FIG 5.5(E)

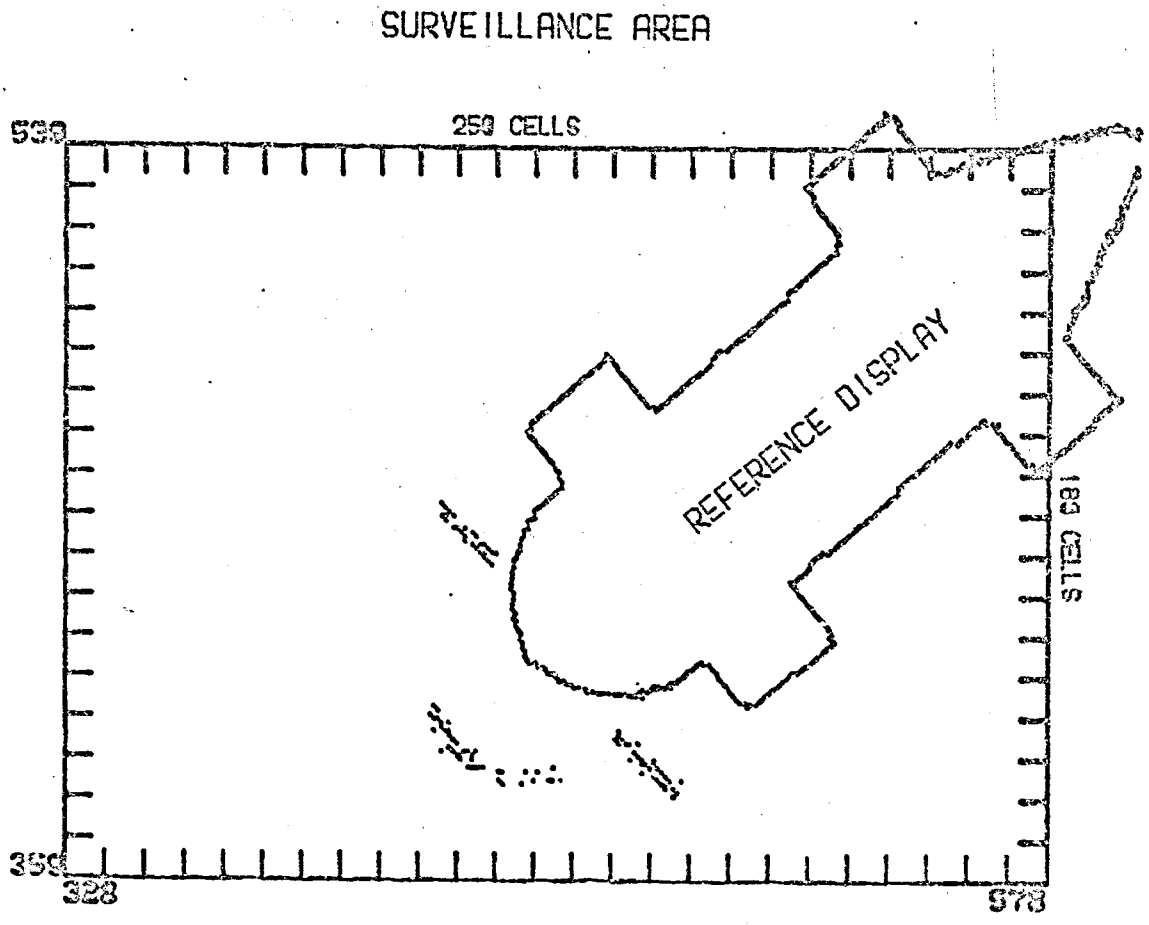

PPIREC 8816 8 PNTS DISPLAYED 161
RANGE QUANTISING = 01 CELLS
ANGULAR QUANTISING = 0.1 DEG
TARGET ORIENTATION = 40 DEG
REFERENCE DISPLAY OFFSET IN CELLS = 20(X),20(Y)

FIG 5.5(E) SIMULATED REAL-TIME PPI DISPLAY OBTAINED BY COMBINING (B),(C) AND (D).COMPARE WITH (B) TO SEE THE IMPROVEMENT DUE TO MULTISTATIC OPERATION.

For run 220 the target was moved to a new X position further away from the projector as shown in figure 5.6(a). The insonified area and geometry for this run can be compared with that shown in figure 5.4(a), run 214. The receiver at position 576 in run 220 will receive backscattered echoes whilst that at X position 1076 will receive forward scattered echoes. In run 214, however, both receivers were in the forward scatter zone with respect to echoes from the target, the point being that the receiver at position 576 in run 214 had moved through a subtended angle of about 80 degrees with respect to the target and was now in a position where it would be detecting echoes propagating in the general direction of the monostatic receiver. The angular separation between the monostatic and bistatic receiver was approximately 25 degrees and the geometry was approaching a configuration in which echoes from contour boundaries (wide angular scattering) would probably be detected simultaneously by both monostatic and bistatic receivers. Figure 5.6(b) shows the monostatic display obtained with the target in this new position. As expected, it did not differ greatly from that obtained in run 214 (shown in figure 5.4(b)). Figure 5.6(c) shows the output of the receiver at X co-ordinate 576, and figure 5.6(d) that of the receiver at X co-ordinate 1016. The combined output of all three receivers is shown in figure 5.6(e) and can be compared with figure 5.4(f) which showed the combined output of run 214 which was performed with the target at the same orientation, but with a smaller X co-ordinate. The difference between these two echo patterns was that in run 214 more of the contour between the projections was detected, whereas in run 220 more of the curvature of the front of the target was detected.

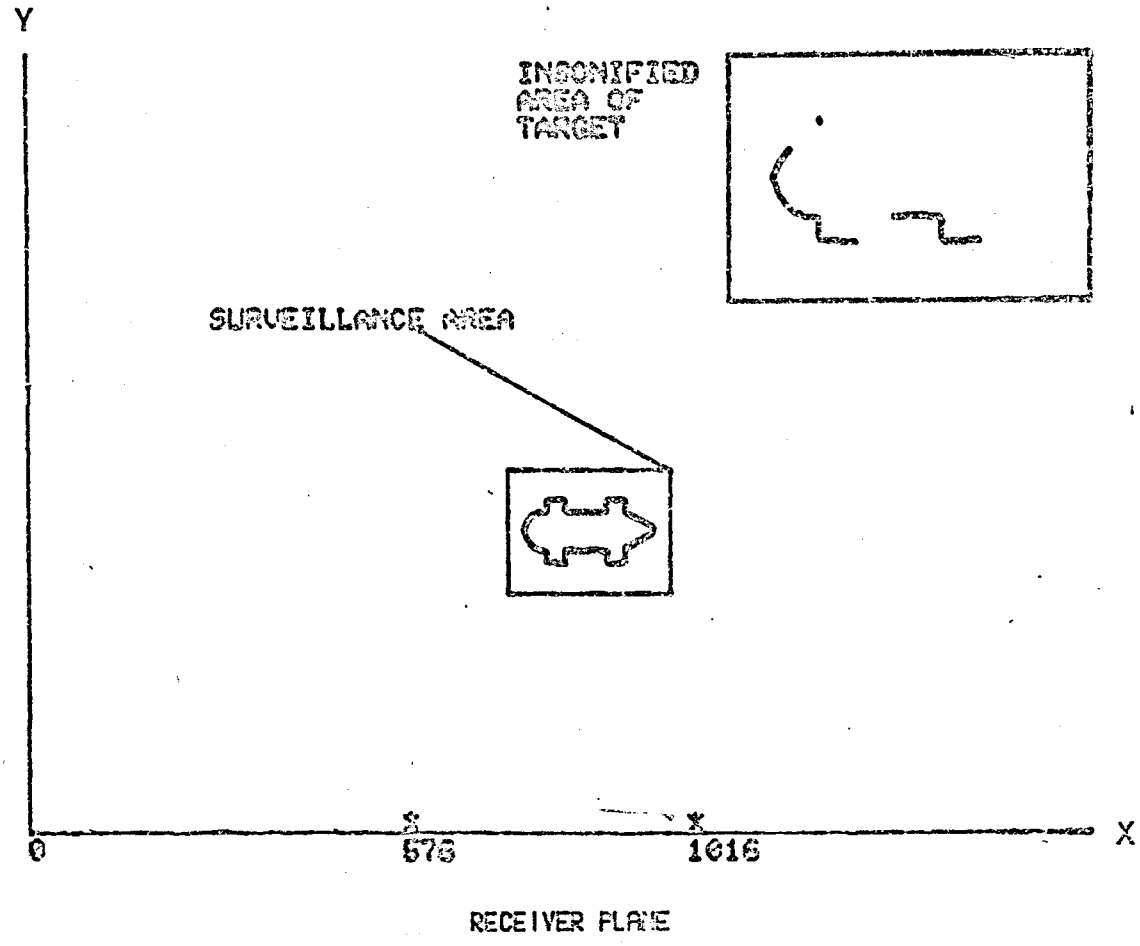

FIG 5.6(A) SYSTEM GEOMETRY FOR RECORD 220 SHOWING THE RELATIONSHIP BETWEEN THE TARGET AND THE MULTISTATIC SYSTEM.

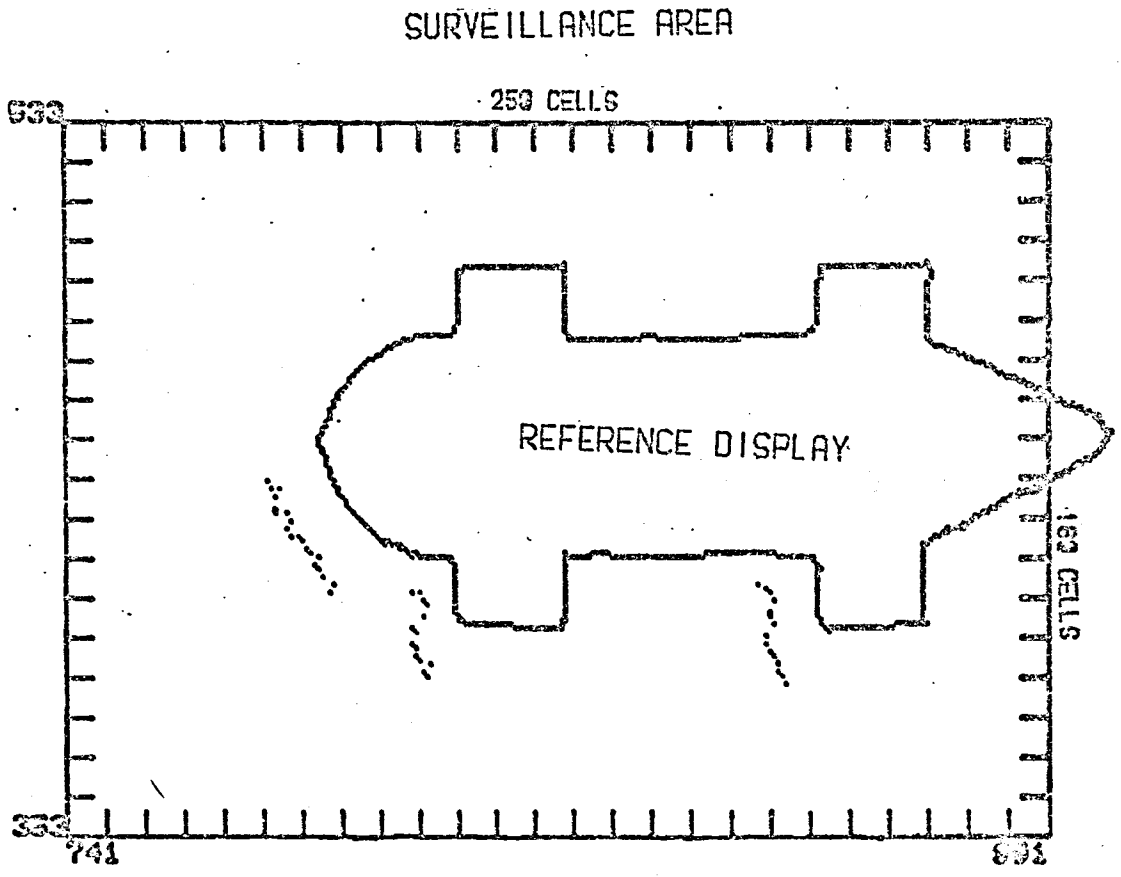

PPIREC 0220 8 PNTS DISPLAYED 49
RANGE QUANTISING = 01 CELLS
ANGULAR QUANTISING = 0.1 DEG
TARGET ORIENTATION = 00 DEG
REFERENCE DISPLAY OFFSET IN CELLS = 10(X),10(Y)

FIG 5.6 (B) PPI DISPLAY OBTAINED WITH THE MONOSTATIC SYSTEM.

FIG 5.6(C)

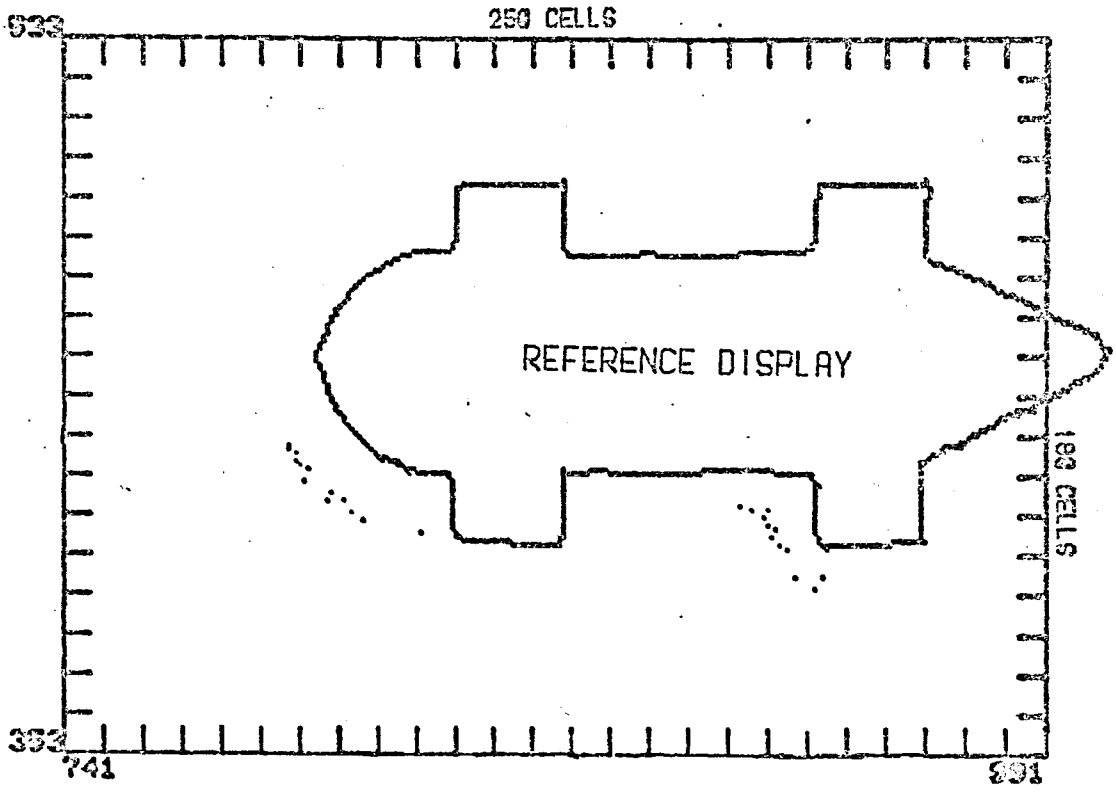

FIG 5.6(C) PPI DISPLAY OBTAINED WITH THE BISTATIC RECEIVER AT X-COORD. 576.

FIG 5.6(D)

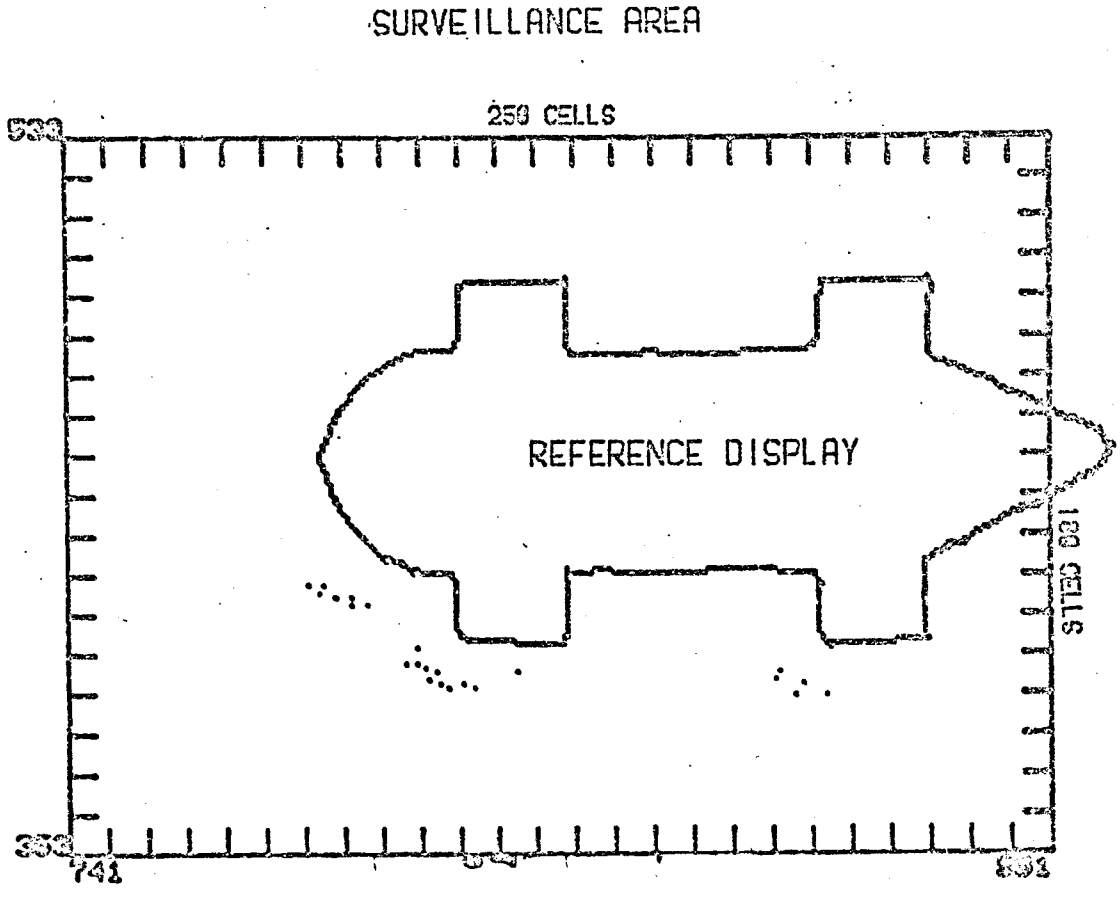

PPIREC 3220 0 PNTS DISPLAYED 22
RANGE QUANTISING = 01 CELLS
ANGULAR QUANTISING = 0.1 DEG
TARGET ORIENTATION = 00 DEG
REFERENCE DISPLAY OFFSET IN CELLS = 10(X),10(Y)

FIG 5.6(D) PPI DISPLAY OBTAINED WITH THE BISTATIC RECEIVER AT X-COORD. 1016.

FIG 5.6(E)

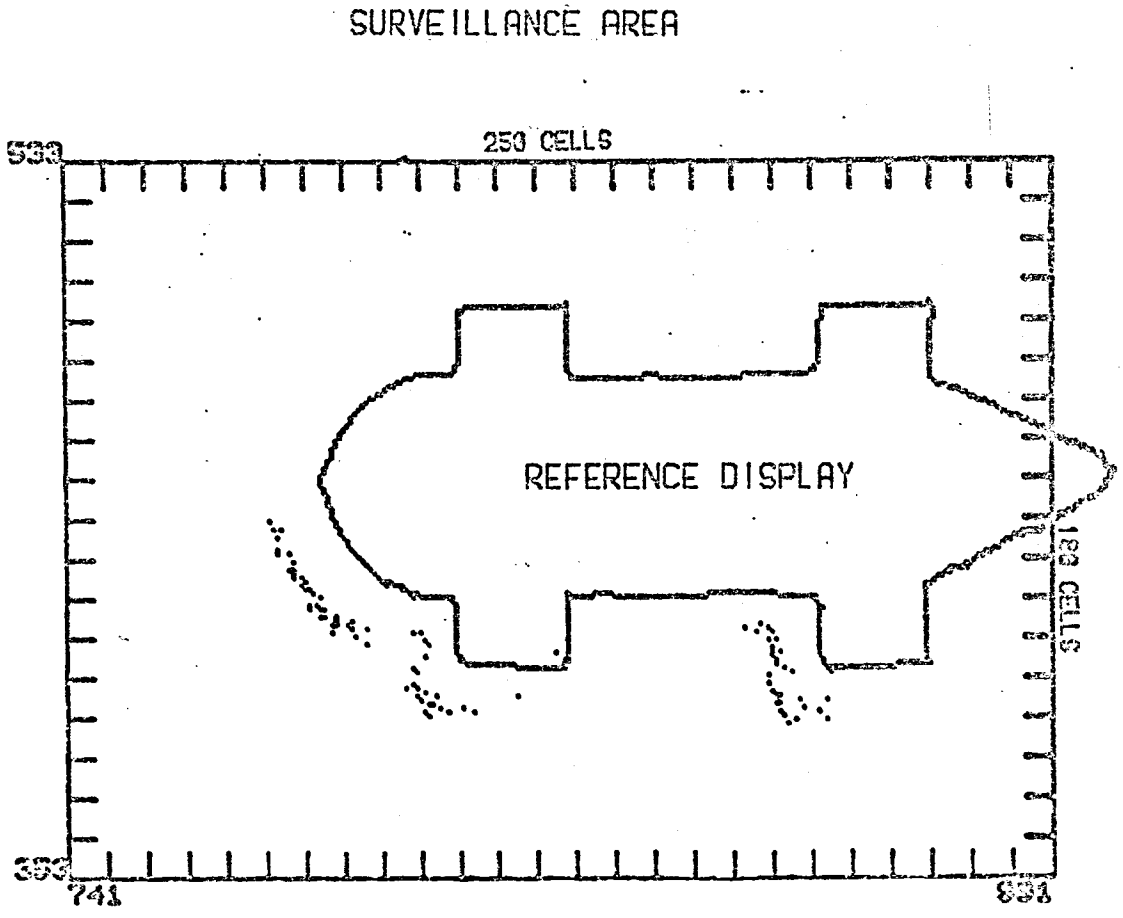

PPINSC 0220 0 PNTS DISPLAYED 05
RANGE QUANTISING = 01 CELLS
ANGULAR QUANTISING = 0.1 DEG
TARGET ORIENTATION = 03 DEG
REFERENCE DISPLAY OFFSET IN CELLS = 10(X),10(Y)

FIG 5.6(E) SIMULATED REAL-TIME PPI DISPLAY OBTAINED BY COMBINING (B),(C) AND (D).COMPARE WITH (B) TO SEE THE IMPROVEMENT DUE TO MULTISTATIC OPERATION!

Run 219 was performed with the target rotated to present a quarter bow aspect to the X axis. The geometry is shown in figure 5.7(a), and it can be seen that the insonified region of the contour only included the front curvature and projections. The upper part of this region was in shadow when viewed from the bistatic receivers and only a small number of additional co-ordinates were expected under these conditions. Figure 5.7(b) shows the monostatic echo pattern with specular echoes from the front curvature normal to the incident beam, and also from the flat surfaces of the projections. An echo was also detected from the rear projection which was first insonified at this orientation. Figures 5.7(c) and (d) show the contribution from the bistatic channels individually, and in particular figure 5.7(c) shows that no new co-ordinates were detected by this receiver. Figure 5.7(e) is the echo pattern obtained by combining figures 5.7(b), (c) and (d). Only a fragmented representation of the target contour can be seen due partly to the restricted region of insonification and partly to the additional shadowing at the bistatic positions, with the result that only a small contribution was made to the target shape portrayal by the bistatic receivers.

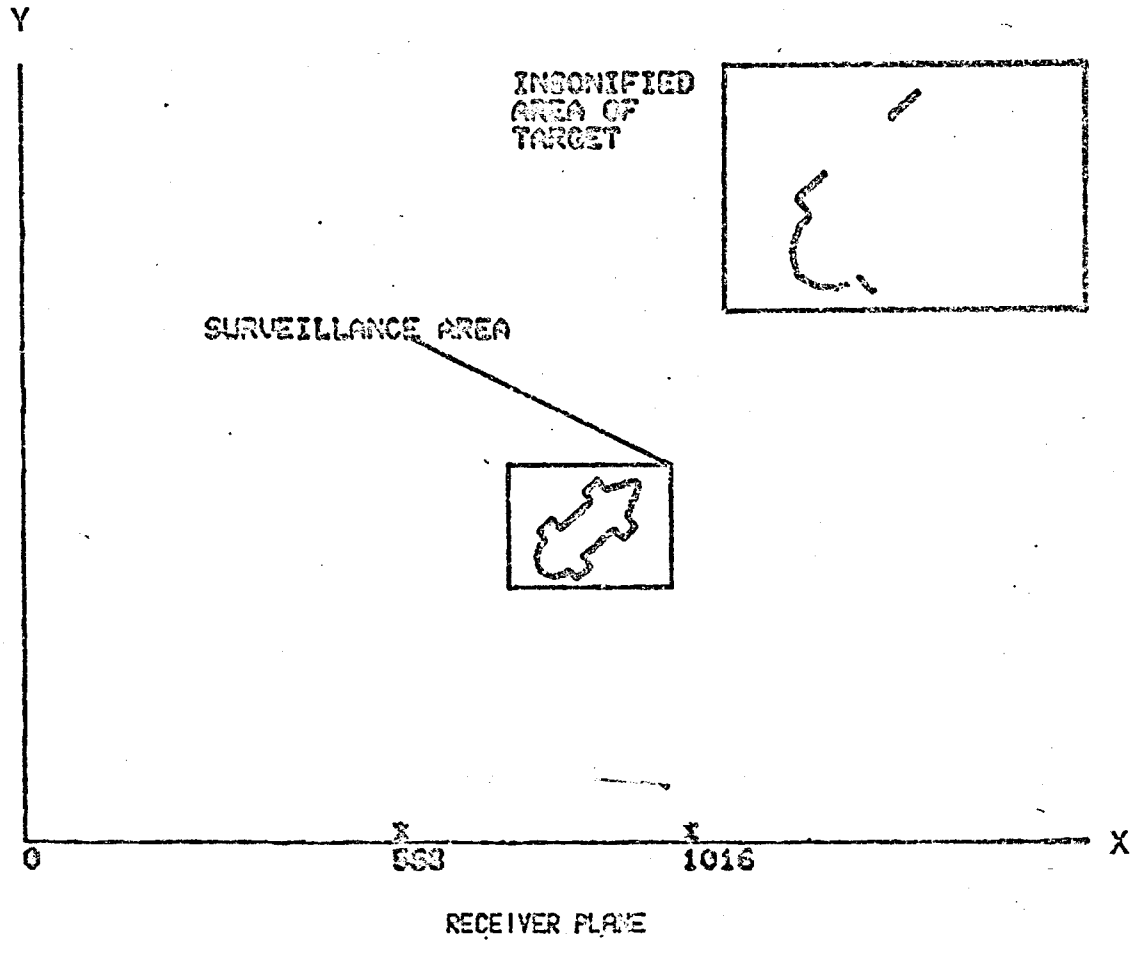

FIG 5.7(A) SYSTEM GEOMETRY FOR RECORD 219 SHOWING THE RELATIONSHIP BETWEEN THE TARGET AND THE MULTISTATIC SYSTEM.

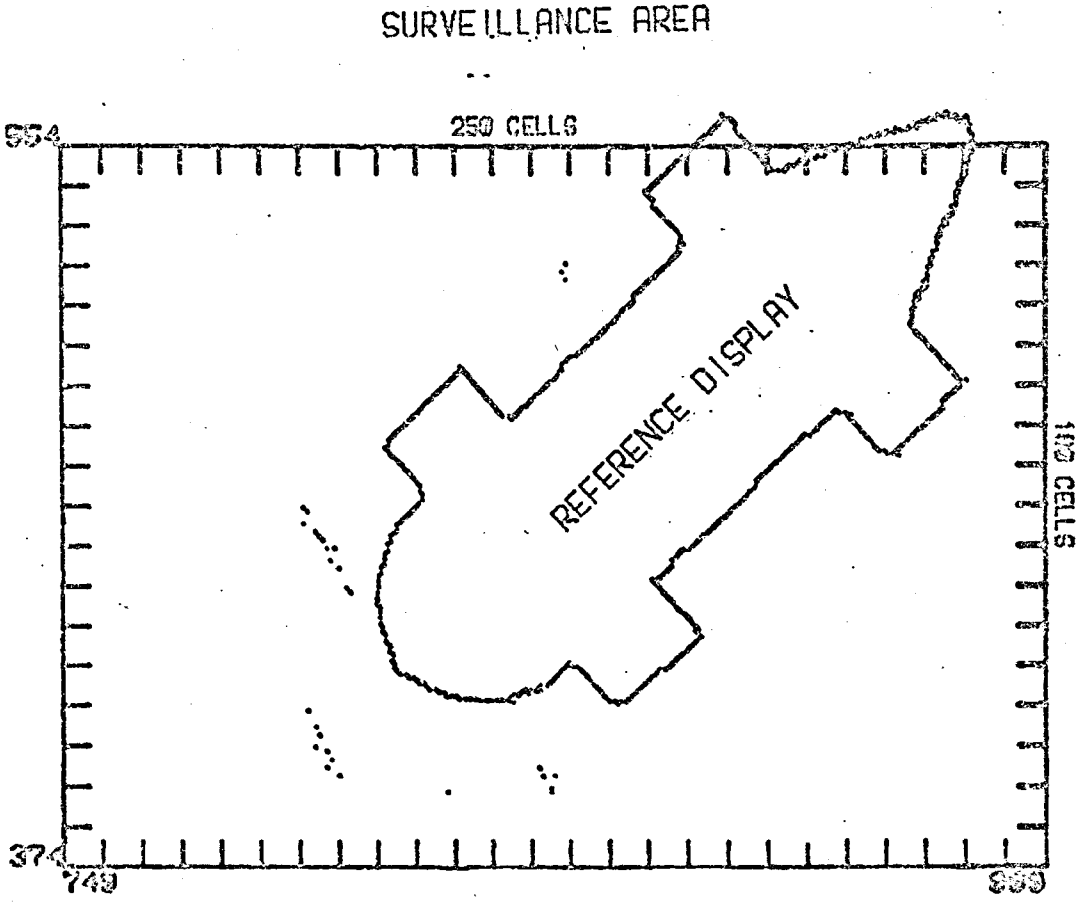

PPIREC 0219 0 PNTS DISPLAYED 89
RANGE QUANTISING = 01 CELLS
ANGULAR QUANTISING = 0.1 DEG
TARGET ORIENTATION = 40 DEG
REFERENCE DISPLAY OFFSET IN CELLS = 20(X),10(Y)

FIG 5.7(B) PPI DISPLAY OBTAINED WITH THE MONOSTATIC SYSTEM.

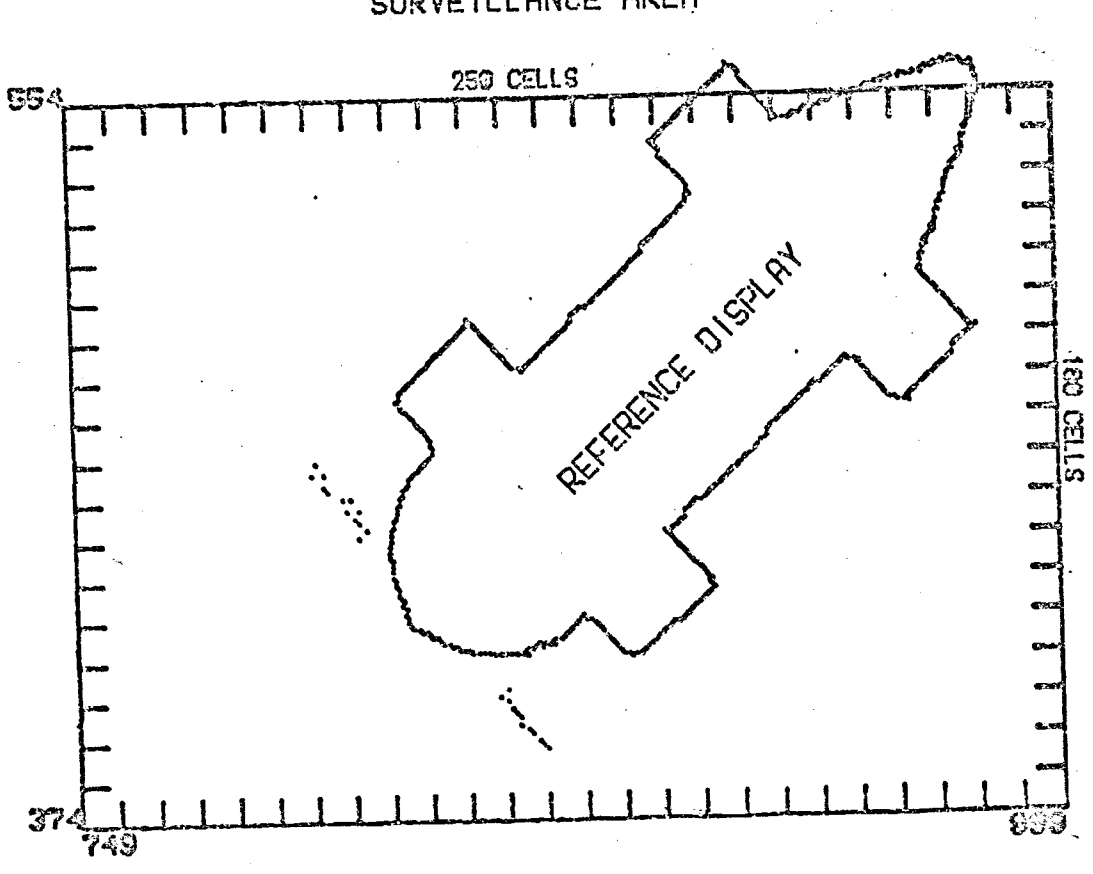

PPIREC 0819 8 PNTS DISPLAYED 65
RANGE QUANTISING = 01 CELLS
ANGULAR QUANTISING = 0.1 DEG
TARGET ORIENTATION = 40 DEG
REFERENCE DISPLAY OFFSET IN CELLS = 20(X),20(Y)

FIG 5.7(C) PPI DISPLAY OBTAINED WITH THE BISTATIC RECEIVER AT X-COORD. 568.

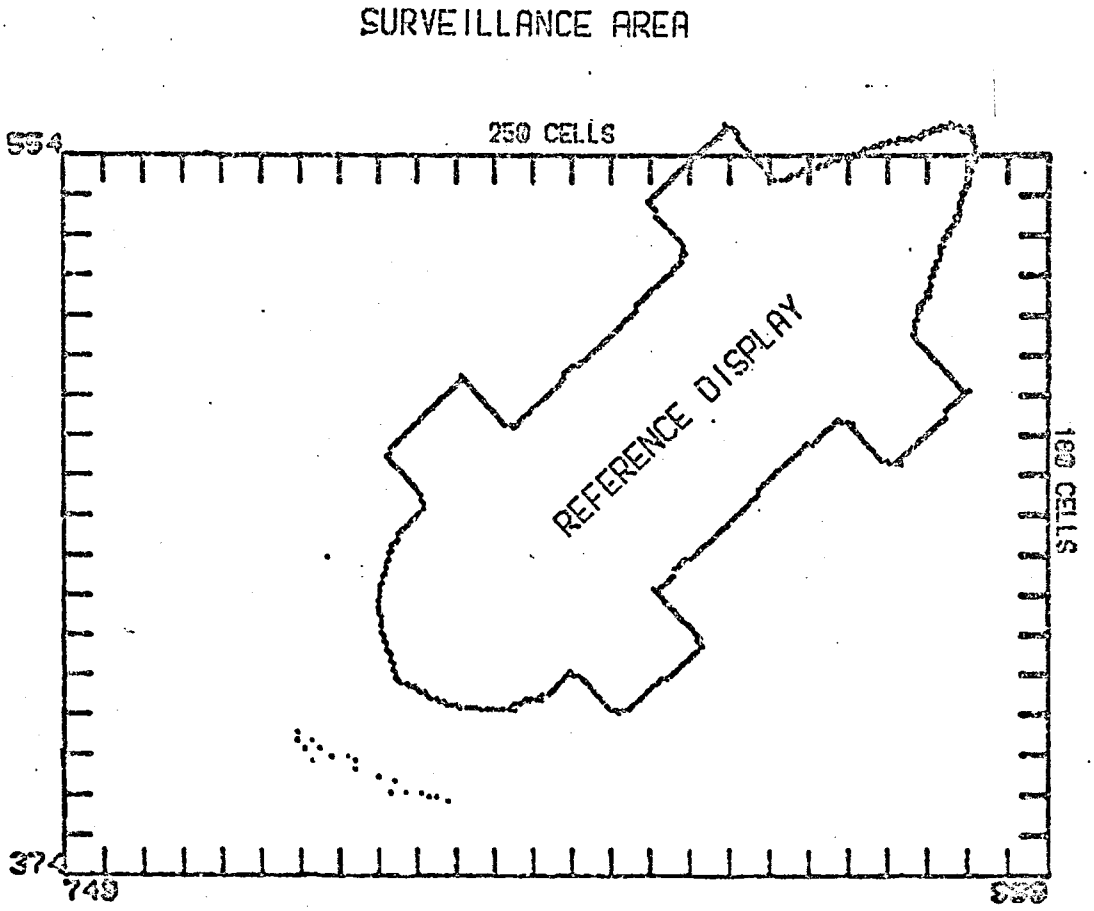

PPIREC 8219 8 PNTS DISPLAYED 19
RANGE QUANTISING = 01 CELLS
ANGULAR QUANTISING = 0.1 DEG
TARGET ORIENTATION = 40 DEG
REFERENCE DISPLAY OFFSET IN CELLS = 20(X),20(Y)

FIG 5.7(D) PPI DISPLAY OBTAINED WITH THE BISTATIC RECEIVER AT X-COORD. 1016.

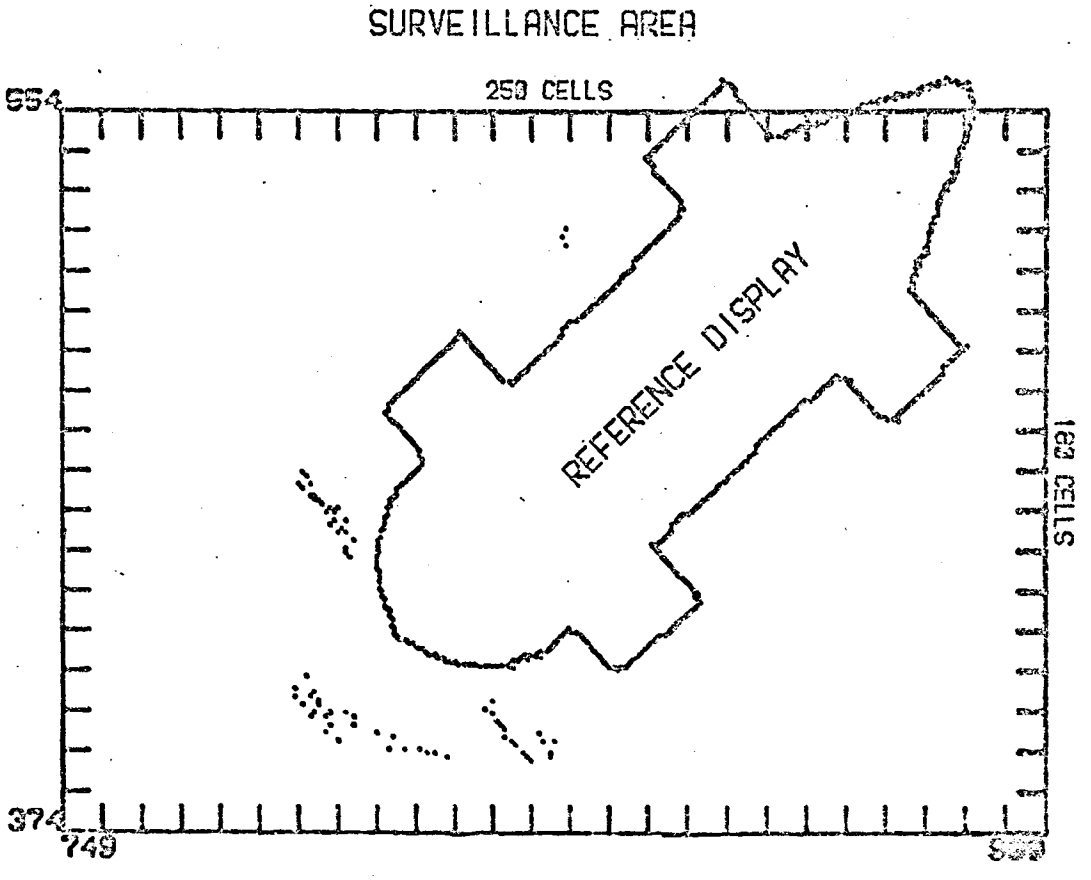

PPIREC 0219 0 PNTS DISPLAYED 71
RANGE QUANTISING = 01 CELLS
ANGULAR QUANTISING = 0.1 DEG
TARGET ORIENTATION = 40 DEG
REFERENCE DISPLAY OFFSET IN CELLS = 20(X),20(Y)

FIG 5.7(E) SIMULATED REAL-TIME PPI DISPLAY OBTAINED BY COMBINING (B),(C) AND (D).COMPARE WITH (B) TO SEE THE IMPROVEMENT DUE TO MULTISTATIC OPERATION!

Run 218 was performed with the target rotated 90 degrees with respect to the X-axis, presenting a frontal aspect to the receiver plane. The geometry for this run is shown in figure 5.8(a). Note that the insonified region has increased from the previous run, but the region visible from the receiver at X co-ordinate 1024 is still restricted.

Figure 5.8(b) shows the monostatic echo pattern and echoes were detected from the normally incident surface at the front and from the internal corner reflectors formed by the projections. A non-specular echo from the external corner on the front projection was also detected.

The echo pattern from the receiver at X co-ordinate 568 is shown in figure 5.8(c). This was not expected to be very different from the monostatic picture because the change in relative aspect of the target at this receiver was small with respect to the monostatic position. However, it can be seen that additional co-ordinates corresponding to a different specular region of the frontal curvature were detected. Figure 5.8(d) shows the output of the receiver X co-ordinate 1024 and only the specular echo from the corresponding region of the contour was added to the echo pattern as independent data.

Finally, figure 5.8(e) shows the combined outputs from all three receivers produced by the display program. The contribution from the bistatic receivers can be seen by comparing figures 5.8(b) and 5.8(e). The contribution in this case amounts to filling in more of the contour corresponding to the curved insonified region.

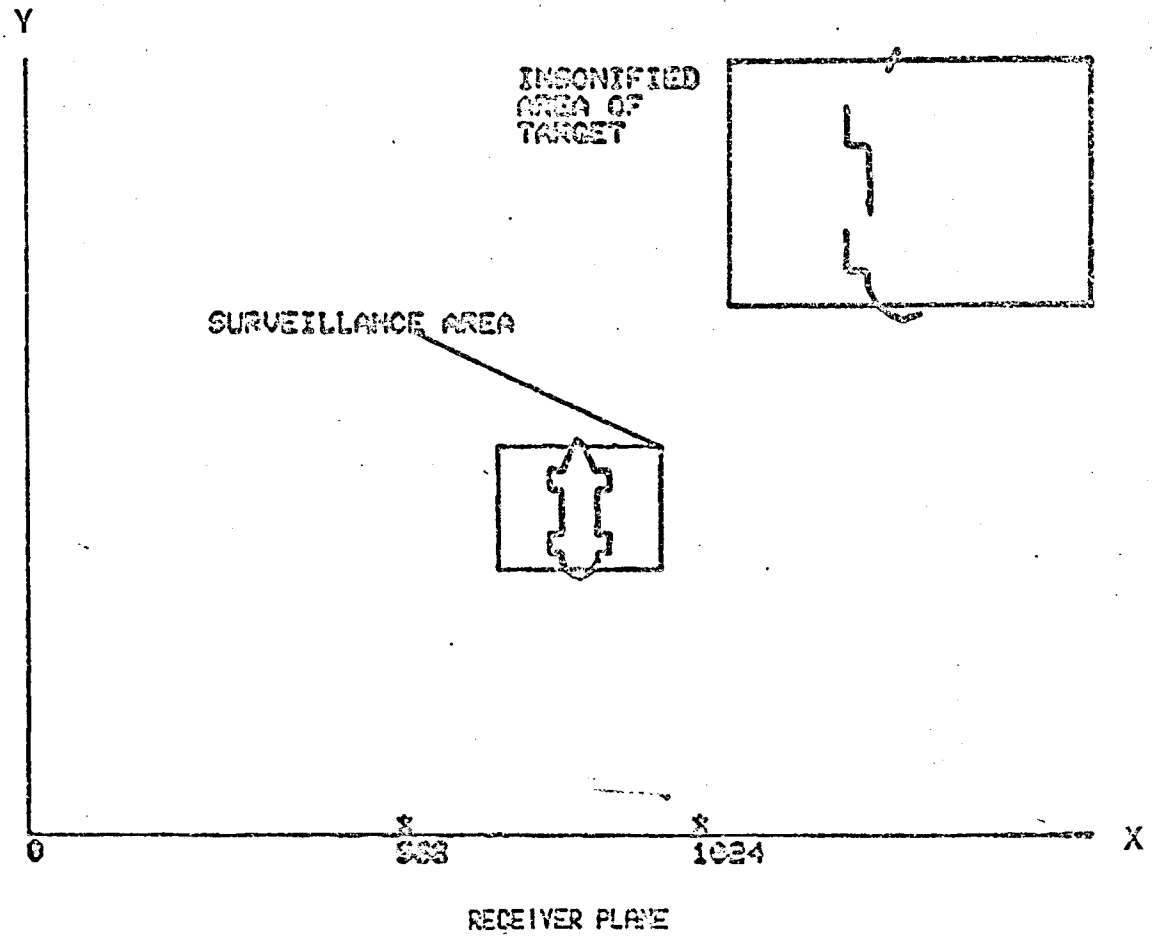

FIG 5.8(A) SYSTEM GEOMETRY FOR RECORD 218 SHOWING THE RELATIONSHIP BETWEEN THE TARGET AND THE MULTISTATIC SYSTEM.

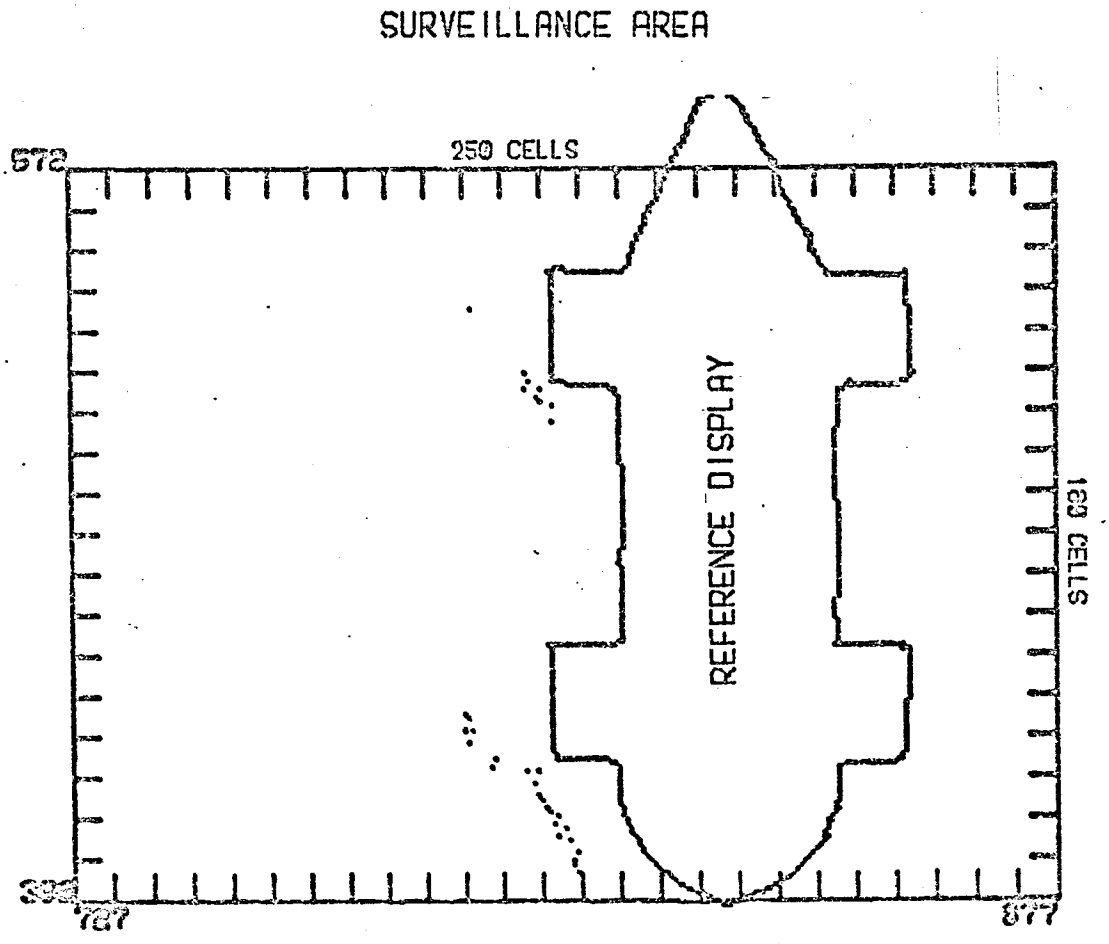

PPIREC 3818 8 PNTS DISPLAYED 33
RANGE QUANTISING = 01 CELLS
ANGULAR QUANTISING = 0.1 DEG
TARGET ORIENTATION = 90 DEG
REFERENCE DISPLAY OFFSET IN CELLS = 20(X),00(Y)

FIG 5.8(B) PPI DISPLAY OBTAINED WITH THE MONOSTATIC SYSTEM.

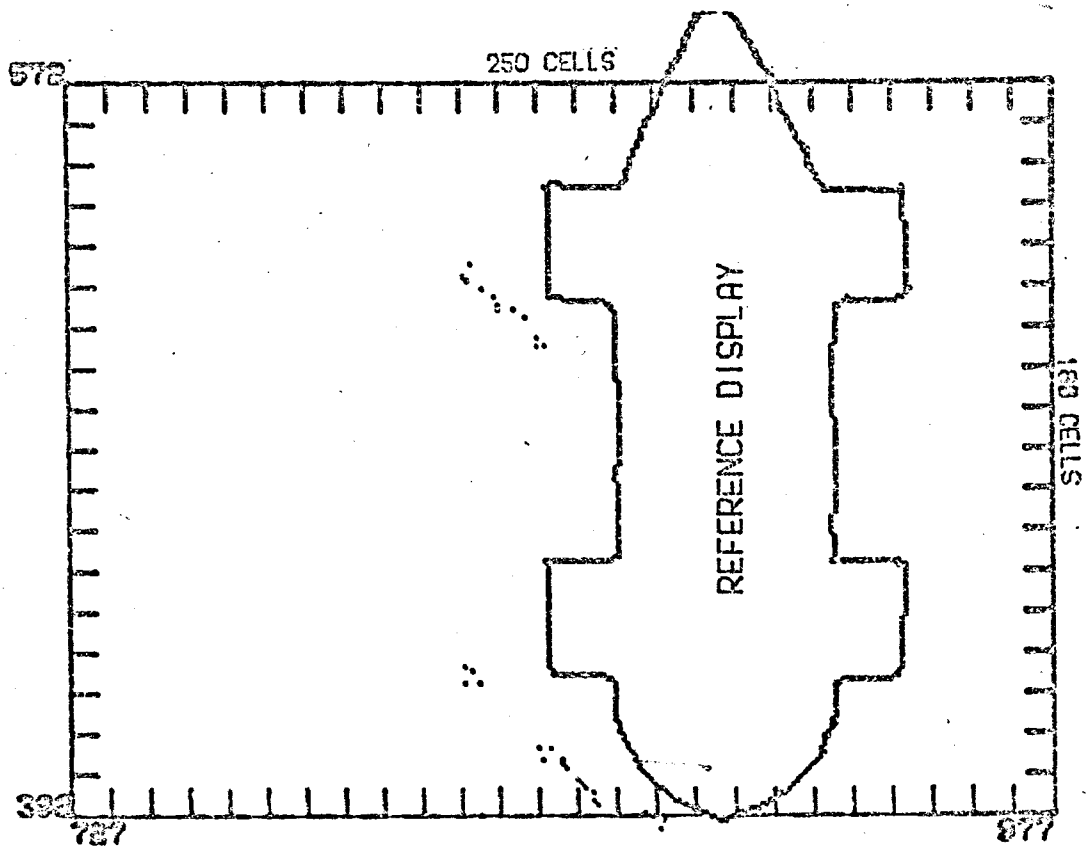

PPIREC 8810 8 PNTS DISPLAYED 22
RANGE QUANTISING = 01 CELLS
ANGULAR QUANTISING = 0.1 DEG
TARGET ORIENTATION = 90 DEG
REFERENCE DISPLAY OFFSET IN CELLS = 20(X),00(Y)

FIG 5.8(C) PPI DISPLAY OBTAINED WITH THE BISTATIC RECEIVER AT X-COORD. 568.

FIG 5.8(D)

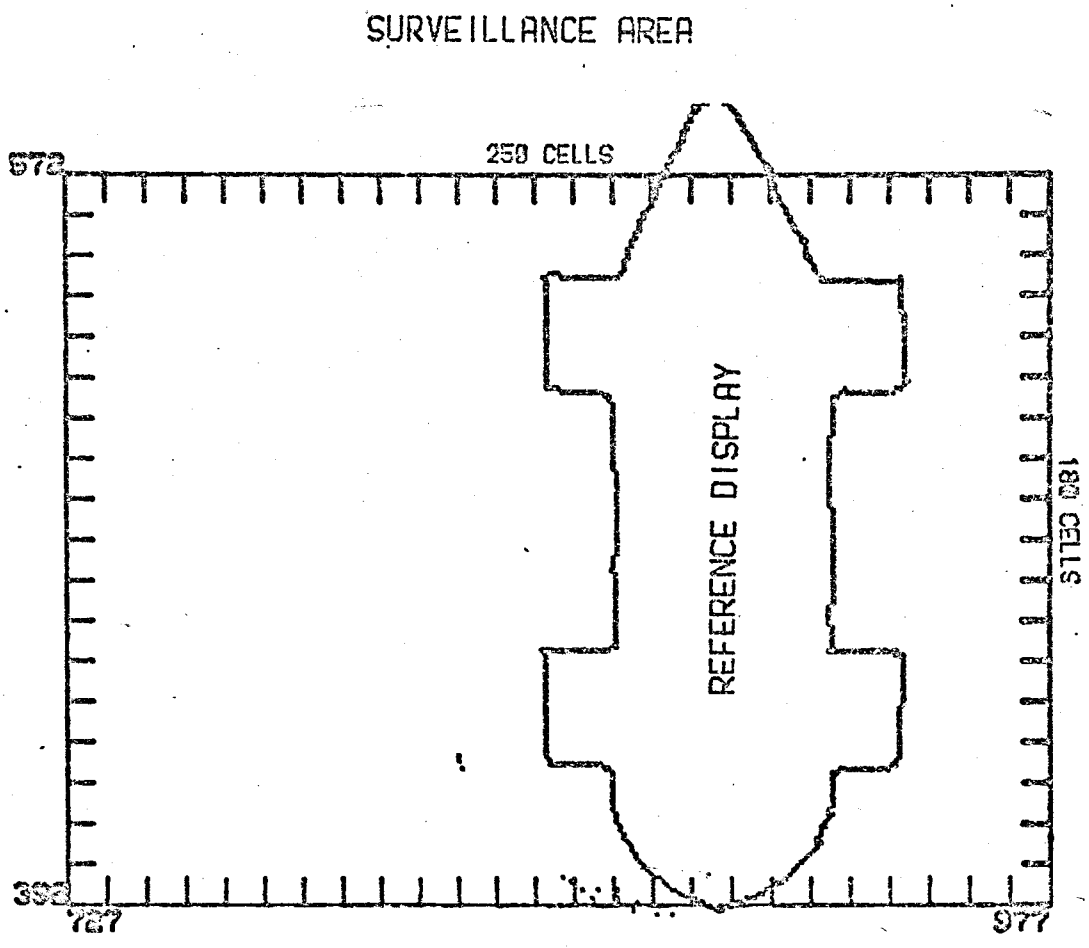

PPIREC 0818 8 PNTS DISPLAYED 15
RANGE QUANTISING = 01 CELLS
ANGULAR QUANTISING = 0.1 DEG
TARGET ORIENTATION = 90 DEG
REFERENCE DISPLAY OFFSET IN CELLS = 23(X),00(Y)

FIG 5.8(D) PPI DISPLAY OBTAINED WITH THE BISTATIC RECEIVER AT X-COORD. 1024.

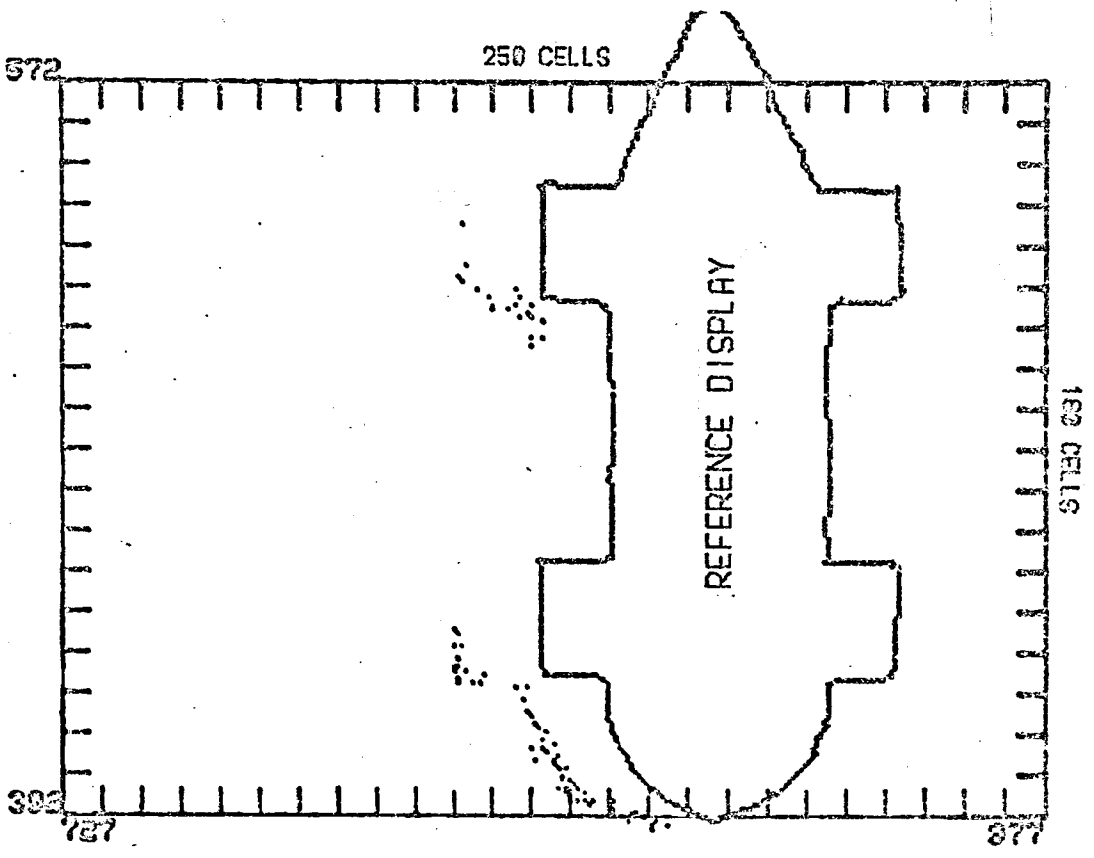

PPIREC 8818 8 PNTS DISPLAYED 80
RANGE QUANTISING = 01 CELLS
ANGULAR QUANTISING = 0.1 DEG
TARGET ORIENTATION = 90 DEG
REFERENCE DISPLAY OFFSET IN CELLS = 20(X),00(Y)

FIG 5.8(E) SIMULATED REAL-TIME DISPLAY OBTAINED BY COMBINING (B),(C) AND (D).COMPARE WITH (B) TO SEE THE IMPROVEMENT DUE TO MULTISTATIC OPERATION.

5.4 PPI display results for target 2

A typical set of displays obtained with this target are shown in figures 5.9(a) to (e). The system geometry is depicted in figure 5.9(a) and shows the target at approx 40 degrees orientation relative to the X-axis at a position midway between the monostatic receiver and bistatic receiver at X co-ordinate 588. Figure 5.9(b) shows the output of the monostatic recevier and the characteristic discontinuity echoes can be clearly seen at the corresponding discontinuities in the contour formed at the target boundaries and the right angle formed by the intersection of the two planes.

Figure 5.9(c) shows the output from the bistatic receiver at X co-ordinate 588. The discontinuity echo from the right angle has been detected at this receiver because of the large angular distribution of the sound reflected from this position. An example of echo formation under similar conditions was discussed in CHAPTER II. An echo was also detected from the bistatically visible contour boundary, but the reduced sensitivity of the bistatic channels compared with the monostatic channel was thought to be the cause of the reduced number of echo co-ordinates displayed. An experiment designed to measure these differences was described in CHAPTER IV and suggested that on average about 3.4 dB of display loss difference could be attributed to this cause. Figure 5.9(a) shows the echo pattern obtained with the receiver at X co-ordinate 1036. Only the specular echo from the flat area with respect to the bistatic receiver position was detected, again this was thought to be the result of different sensitivities in the bistatic and monostatic channels.

The combined display corresponding to all three channels operating is shown in figure 5.9(e), and no significant improvement over figure 5.9(b) is evident. This was because only one channel at X co-ordinate 1036 contributed any new co-ordinates to the echo pattern.

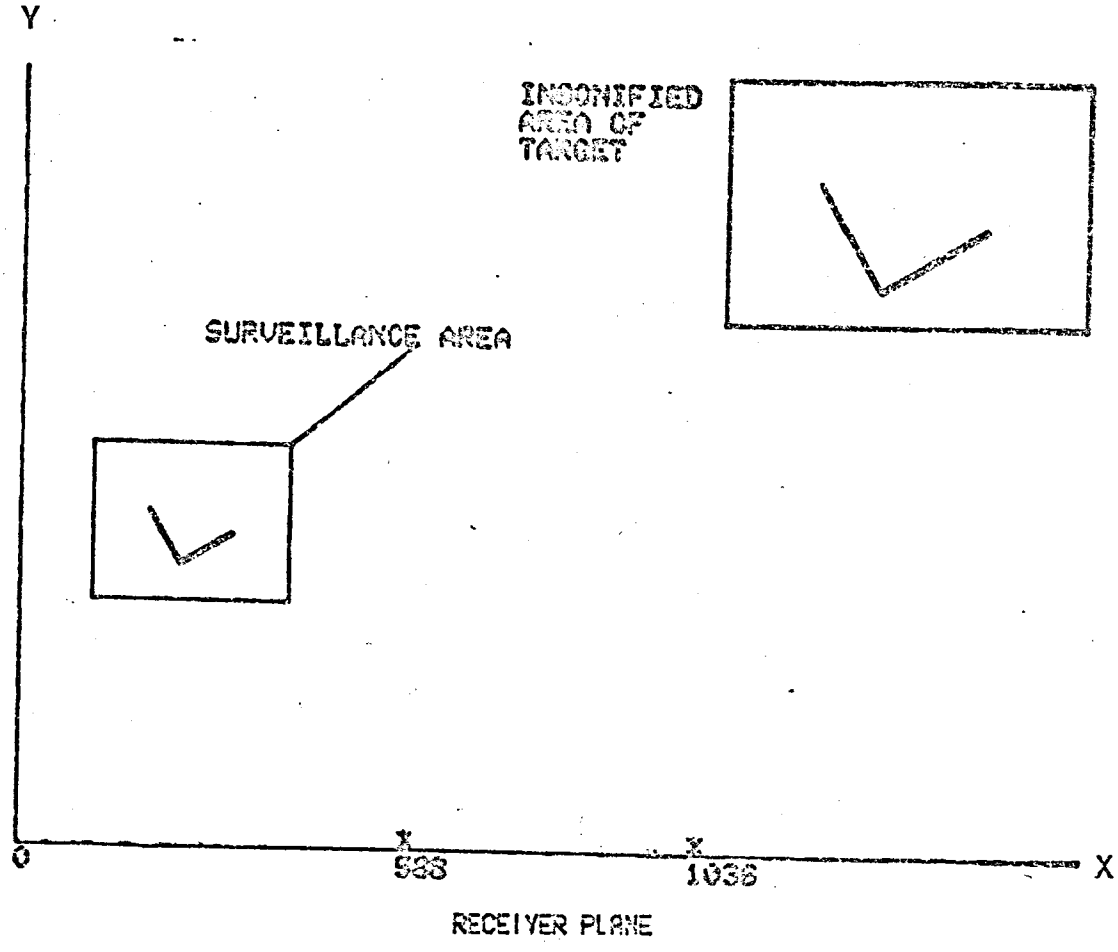

FIG 5.9(A) SYSTEM GEOMETRY FOR RECORD 222 SHOWING THE RELATIONSHIP BETWEEN THE TARGET AND THE MULTISTATIC SYSTEM.

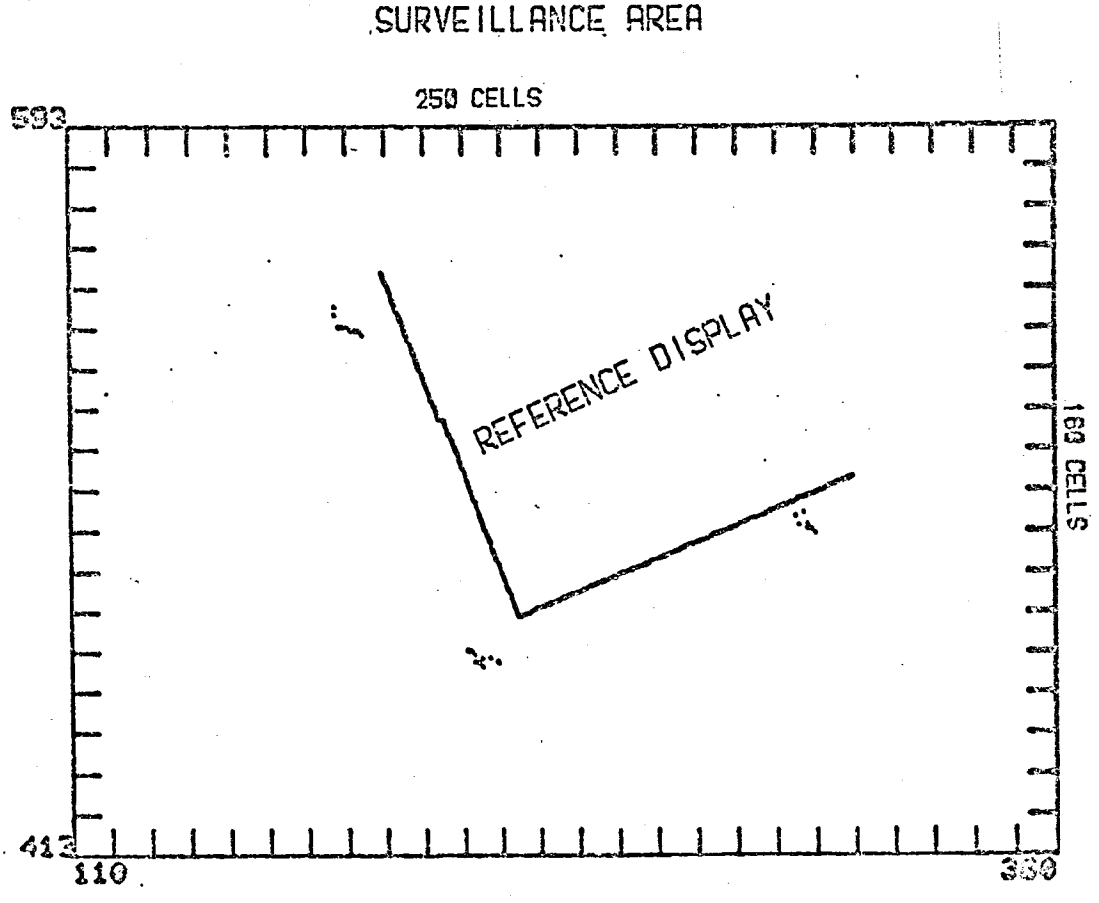

FPIREC 0222 8 PNTS DISPLAYED 25
RANGE QUANTISING = 01 CELLS
ANGULAR QUANTISING = 0.1 DEG
TARGET ORIENTATION = 20 DEG
REFERENCE DISPLAY OFFSET IN CELLS = 10(X),10(Y)

FIG 5.9(B) PPI DISPLAY OBTAINED WITH THE MONOSTATIC SYSTEM.

FIG 5.9(C)

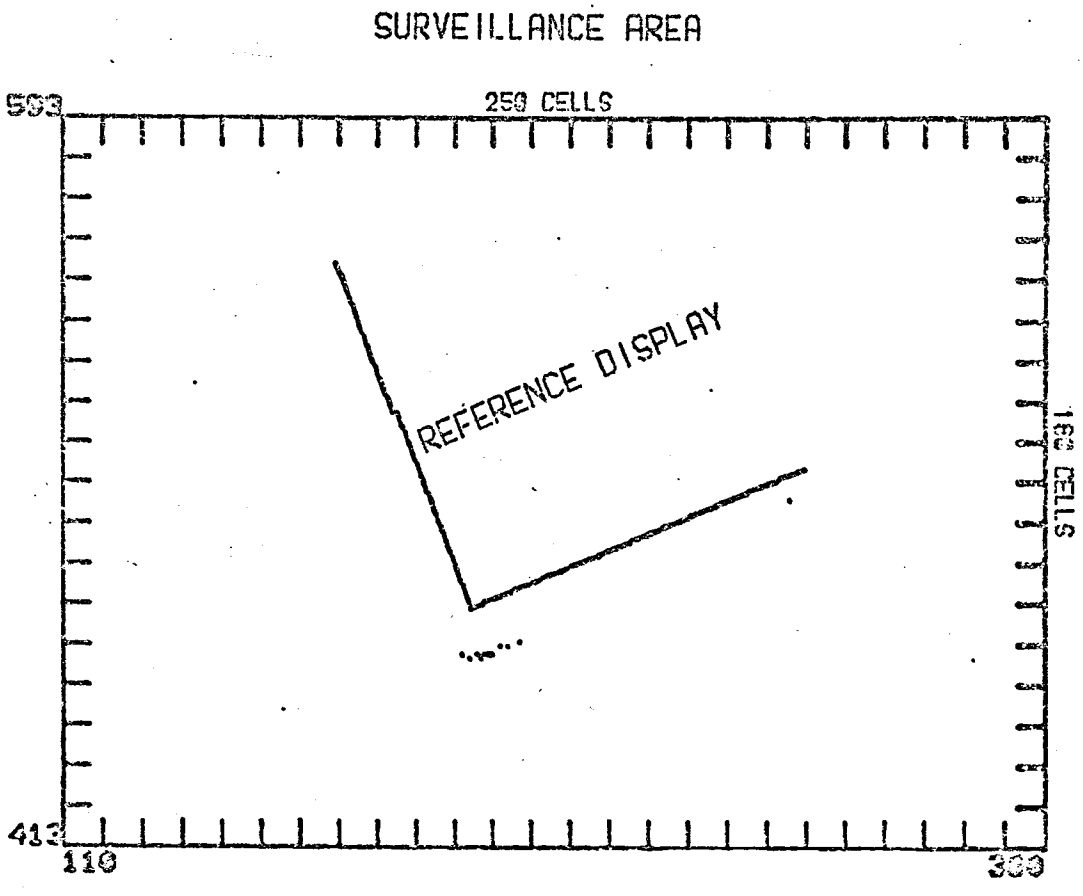

PPIREC 0222 8 PNTS DISPLAYED 11
RANGE QUANTISING = 01 CELLS
ANGULAR QUANTISING = 0.1 DEG
TARGET ORIENTATION = 23 DEG
REFERENCE DISPLAY OFFSET IN CELLS = 03(X),10(Y)

FIG 5.9(C) PPI DISPLAY OBTAINED WITH THE BISTATIC RECEIVER AT X-COORD. 588.

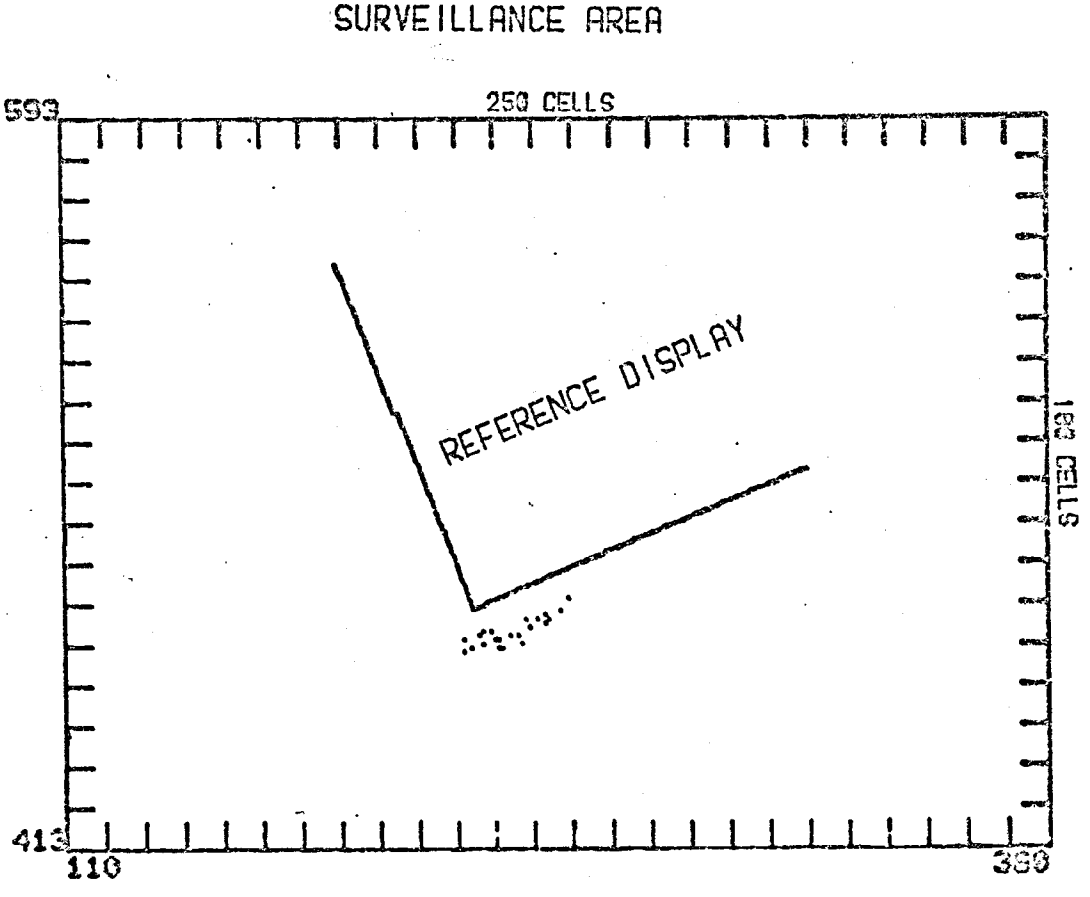

PPIREC 0222 8 PNTS DISPLAYED 22
RANGE QUANTISING = 01 CELLS
ANGULAR QUANTISING = 0.1 DEG
TARGET ORIENTATION = 20 DEG
REFERENCE DISPLAY OFFSET IN CELLS = 03(X),10(Y)

FIG 5.9(D) PPI DISPLAY OBTAINED WITH THE BISTATIC RECEIVER AT X-COORD. 1036.

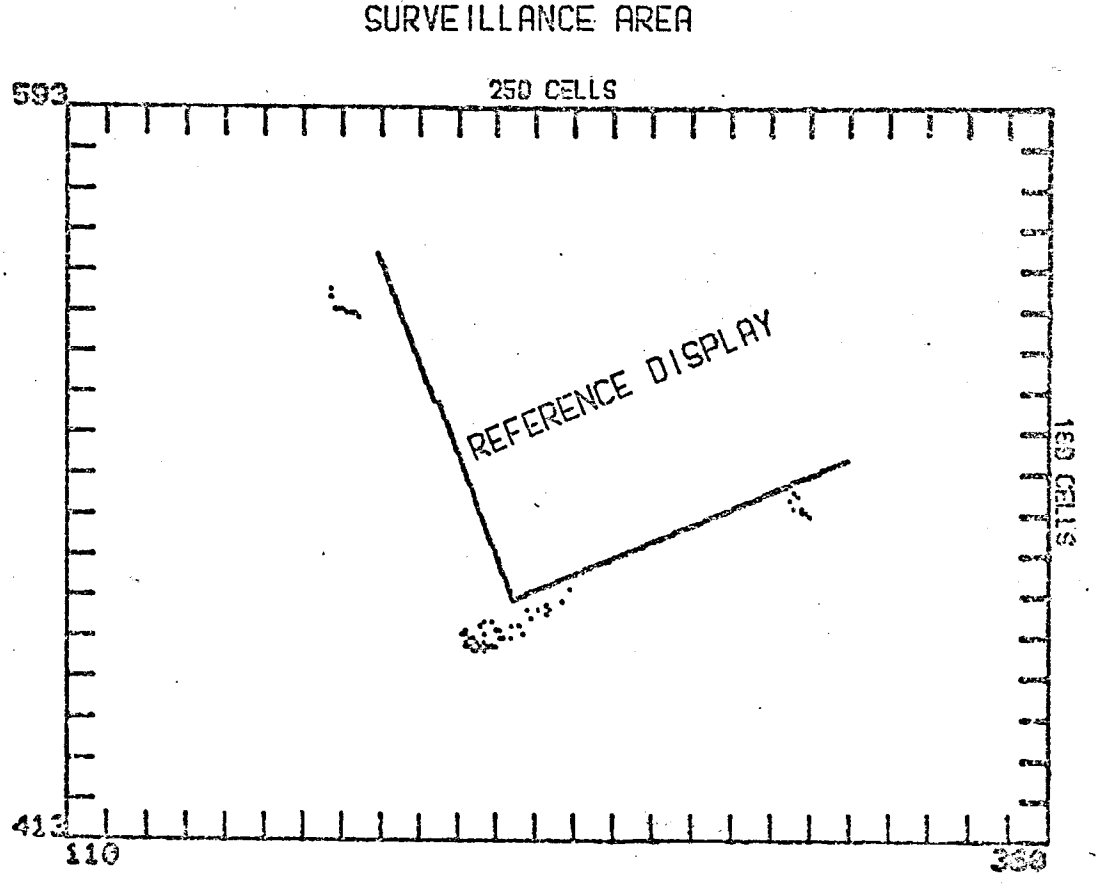

FIG 5.9(E) SIMULATED REAL-TIME PPI DISPLAY OBTAINED BY COMBINING (B),(C) AND (D).COMPARE WITH (B) TO SEE THE IMPROVEMENT DUE TO MULTISTATIC OPERATION.

This particular target and the echo patterns it produced did highlight the extremely specular nature of the echoes and pointed to the fact that even more bistatic channels would be required to adequately define the shape of the target contour. Nevertheless the performance curve shown in the next chapter for this particular target indicated that from a display loss viewpoint the echo patterns were equivalent to those obtained for target 1, but the fact that the value of 'display magnification' m, for this target was less than for target 1, meant that poorer target shape portrayal was obtained.

In conclusion however, it was felt that notwithstanding the different results obtained with target 2, the concept of the multistatic system had been adequately demonstrated and validated by the sum total of the results, and that sufficient data was available for an analysis of performance to be obtained. Further interpretation of these results in terms of an evaluation of the display loss as a function of position and the number of receivers is dealt with in the next chapter.

CHAPTER VI

ANALYSIS OF THE RESULTS OBTAINED

6.1 The effect of system errors on the results

Before undertaking a more quantitative assessment of the experimental results presented in the previous chapter, it is useful to first re-consider the likely type and magnitude of errors which occurred during the experiments. The intention being to apply such corrections as are necessary to the data during the analysis of the results.

The factors which affected the results can be discussed under the general headings which were first mentioned in CHAPTER III. These were,

(a) the rejection of echoes due to the limited system throughput rate,

and (b) the errors introduced into the echo co-ordinates by the finite accuracy of the hardware and software.

Regarding the first of these headings, the finite response time of the system from receiving a data input clock pulse to the output of the corresponding echo co-ordinates was observed to degrade the performance by causing less than the actual number of echoes detected at the receivers to be displayed. This problem was most acute when all three receiver channels were simultaneously inputting data to the cpu. An average figure relating to this loss was estimated by comparing the real-time combined displays with the simulated combined displays, obtained by combining the outputs from each separate receiver. The number of echoes detected on-line when all three channels were receiving and outputting data simultaneously was expressed as a fraction of the sum total of all echoes produced by the system when each channel was operating alone. Thus,

$$\text{data loss due to system response time} = \frac{\Sigma\,(\text{echoes for real-time combined display})}{\Sigma\,(\text{echoes for all channels separately})}$$

By using this definition, and appropriate runs in which both the individual channel outputs and the combined outputs were recorded, a figure for this data rejection was calculated. Table 5.1 lists these runs and an average loss of 3.2 dB was obtained from them. In other words, in those runs where only the real-time combined display was recorded, on average only 52 percent of the total number of detected echoes were displayed.

Therefore, in calculating the display loss factor for each run, if the display was cumulative and not presented on an individual channel basis, 3.2 dB was added to the resulting calculated display loss factor to account for this data defficiency.

The accuracy of the system software program was discussed in CHAPTER III, and was summarised by specifying a mean error in the X,Y directions, plus standard deviations about these means.

These resulted in an error figure of $\pm$ 1.3 cells in the X direction and $\pm$ 1 cell in the Y direction. Of greater importance were the hardware produced errors, including errors in the measurement of the three variables necessary to compute the echo co-ordinates. An analysis of the sensitivity of the range equations was performed and the results of this discussed in CHAPTER III, where it was shown that in general errors in the azimuth bearing would produce relatively large errors in the echo co-ordinates. To a lesser degree errors in the measured separation of transmitter and receiver transducers were also shown to produce errors in the X and Y co-ordinates.

It can be seen from observation of the run geometry diagrams presented with each set of display figures shown above, that the nominal position of the two bistatic hydrophones, as measured by the system, varied from run to run. This was despite careful calibration before each run and the fact that the probes were carefully repositioned before each

TABLE 6.1: CALCULATION OF AVERAGE DATA LOSS

DUE TO SYSTEM BANDWIDTH LIMITATIONS

Run No	Number of XY Pairs Produced				Loss %
	Channel 1	Channel 2	Channel 3	Chs 1+2+3 Total	
209	17	17	12	20	56.5
214	75	33	98	113	45.1
218	83	48	88	121	44.7
219	57	32	55	85	40.9
220	83	62	54	95	52.2

Average Loss = 48%

= 3.2 dBs

Standard Deviation = 0.063

run. The differences were attributed in part to drift in the analogue circuits used to measure this parameter, and noise pickup on the long data transmission path between the sonar and the computer. Time did not permit a more detailed examination of this source of error and the conclusion was that such errors as were attributable to this source could not be properly compensated for.

This necessitated the introduction of a tolerance or area of uncertainty which was included in the correlation of the echo patterns with the reference display, and the details have already been mentioned in the previous chapter.

Although not strictly under the heading of hardware and software accuracy, another correction was applied to the results which arose due to the nature of the divergent sound beam from the transmitter. It was observed that as the target was moved along parallel to the receiver plane, the number of echo co-ordinates produced by the same target with constant receiver threshold settings varied. This was due to the increase in width of the resolution cells as the range to the target increased, which in turn meant that the target was overlayed by fewer resolution cells. This was likely to affect the results of the analysis because a constant value for m, the 'display magnification' was assumed for each target irrespective of its range from the transmitter.

In order to correct for this effect an experiment was performed with target 3 (see table 4.1) to evaluate the change in display loss in dBs as the target X position was increased. Two separate orientations were evaluated with other factors such as receiver threshold kept constant. The results of this measurement are shown in figure 6.1 in which the display loss for m = 6 is shown for various target positions along the receiver plane. The figure shows the individual measurements and the best fit linear regression line which resulted. Using this

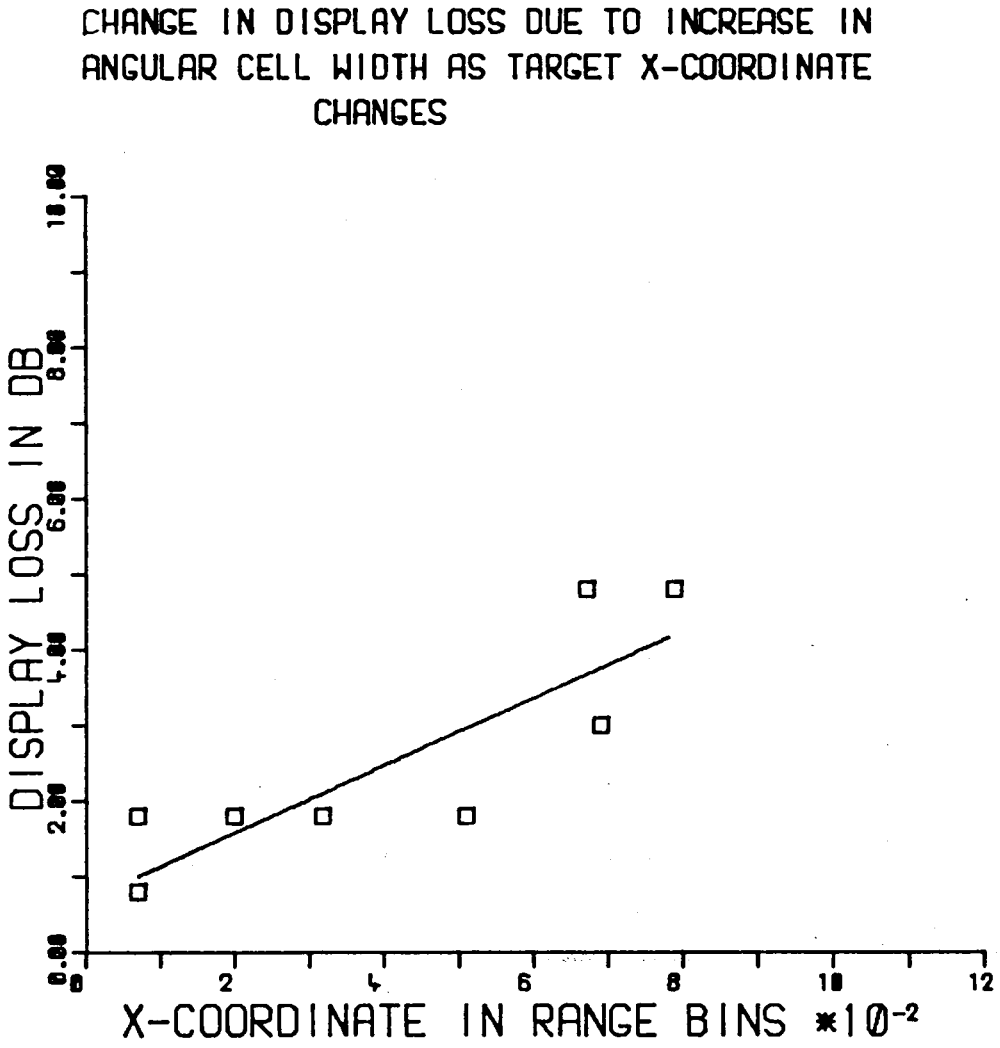

FIG 6.1 A GRAPH OF THE CHANGE IN DISPLAY LOSS AS A FUNCTION OF TARGET X-COORDINATE.

figure the results of the analysis of system performance were corrected for relative X co-ordinate differences by reading off the change in display loss resulting from any particular position with respect to the origin at X = 0. For instance, in comparing two display outputs for a target at X = 200 and X = 400 say, then a change of 1 dB could be expected due to this effect. Applying this correction meant that the results at each position were normalised to the same value of display loss maximum given by + 10 log (m). In addition, any improvements in system performance in terms of display loss as the target position changed in the scanned area would not be obscured by this particular effect.

6.2 Performance curves obtained from the results

In order to make comparisons between the actual results obtained, and the simulated results of the performance of a multistatic system discussed in CHAPTER II, the echo patterns were analysed in terms of the display loss factor defined in CHAPTER II. Two separate evaluations of performance were made. The first was to relate the position of the surveillance area with respect to its position along the receiver plane, to the display loss factor for both monostatic and multistatic operation. The second was an evaluation of the loss factor at each position of the target along the receiver plane, and averaged with respect to orientation, to obtain data for extrapolation of the results.

For the first of these evaluations figure 6.2 shows a scatter plot of the actual numbers of echo co-ordinates produced at each position along the X axis for both monostatic and multistatic systems. These results have been averaged over the different orientations used and thus represent the mean performance at each position. Where necessary the results have been adjusted by the 3.2 dB correction calculated to compensate for the loss of echo co-ordinates due to the limited bandwidth of the system. Figure 6.3 was derived from this data and shows the results plotted on a normalised display loss basis as per CHAPTER II and with the maximum display taken as + 27 dB. Two sets of curves are shown corresponding to the monostatic and multistatic systems. Each set is in turn shown in corrected and uncorrected form as labelled in the figure. In the case of the corrected curves, figure 6.1 was used as explained above to correct for movement of the targets parallel to the X axis. With reference to these corrected curves, the monostatic system shows an almost flat display level to within 0.5 dB throughout the range with the mean level at + 7.4 dB. The corresponding curve for the

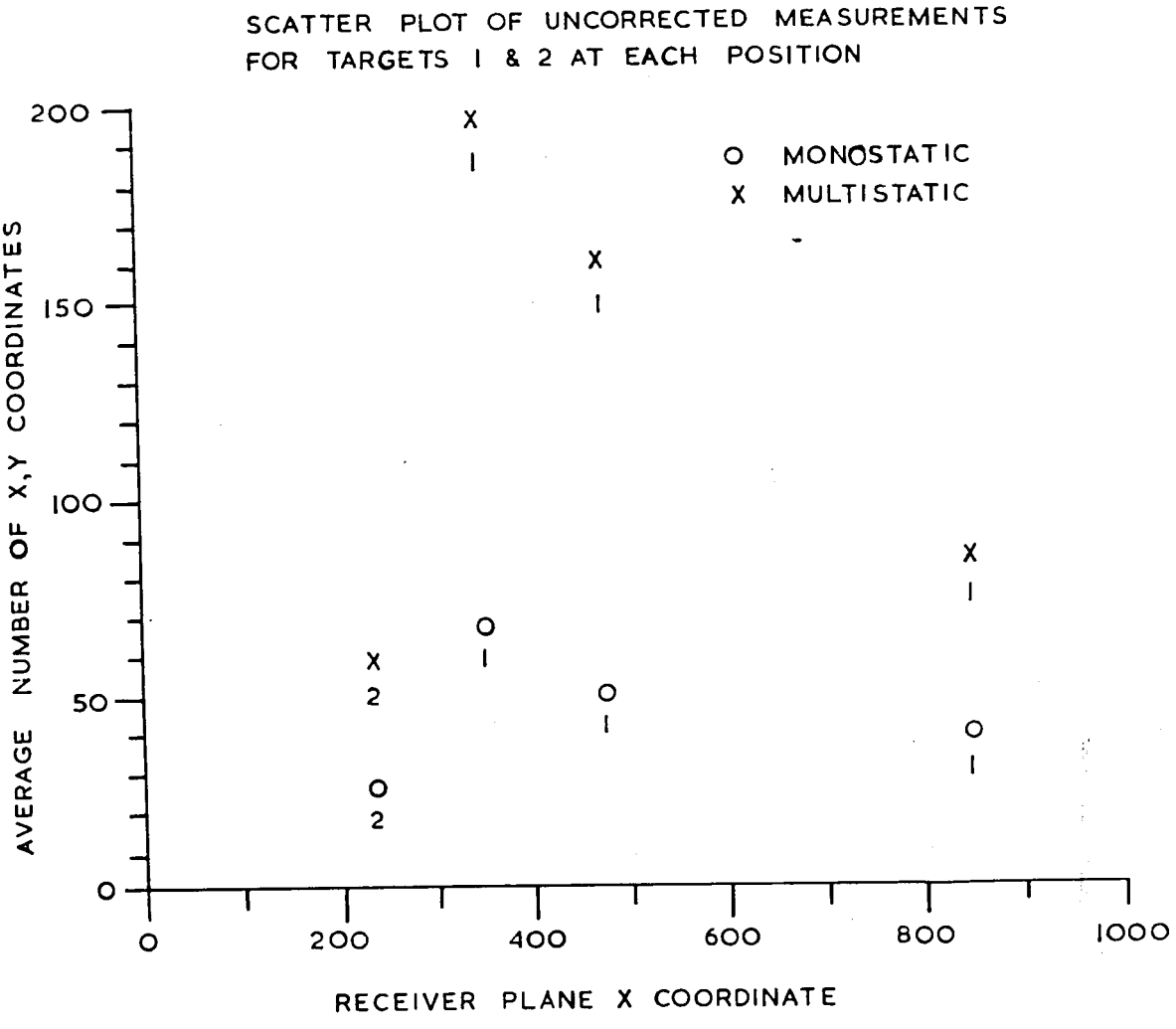

FIG 6·2 UNCORRECTED MEASUREMENTS OBTAINED FROM THE PPI DISPLAYS BY AVERAGING EACH SET OF ORIENTATIONS OF THE TARGET AT A CONSTANT X VALUE.

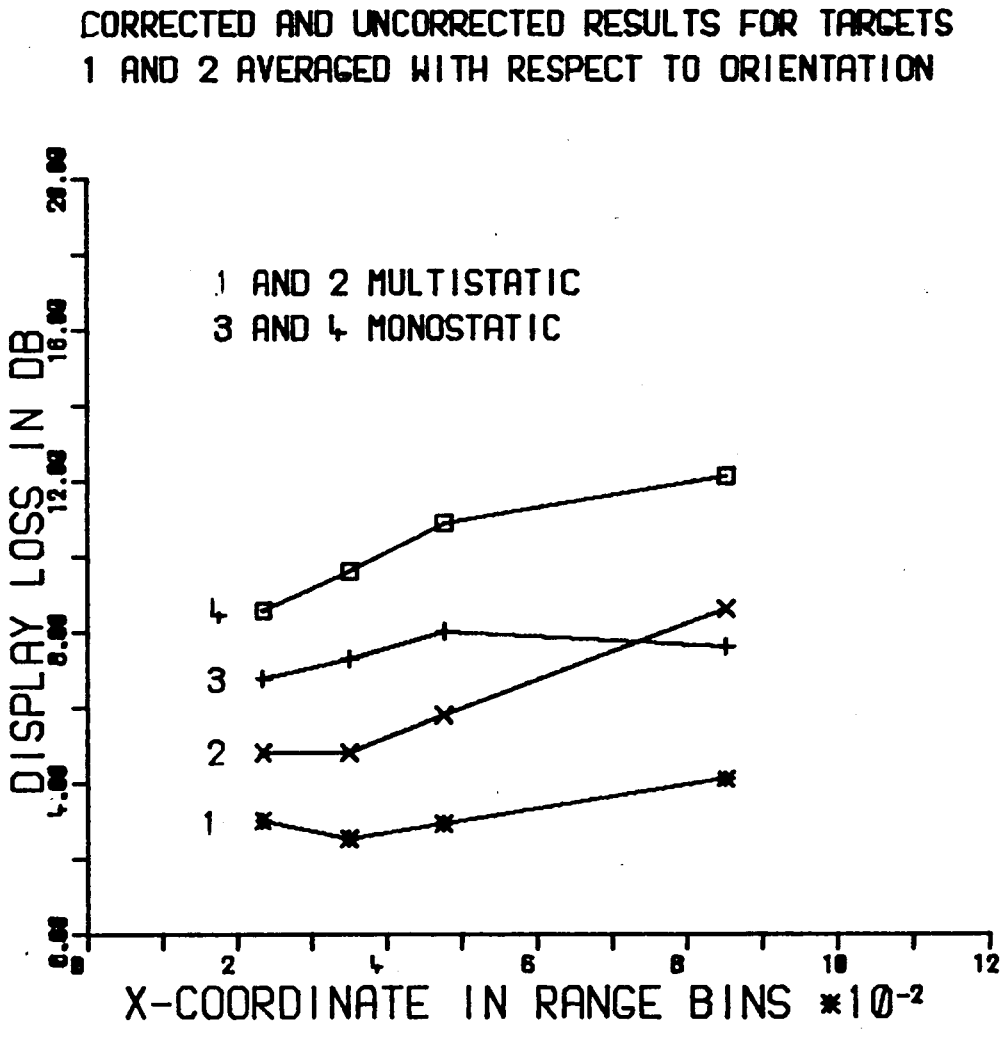

FIG 6.3 A COMPARISON BETWEEN MONOSTATIC AND MULTISTATIC SYSTEM PERFORMANCE AS A FUNCTION OF TARGET X-COORDINATE.

multistatic system shows a mean level of + 3.1 dB with a standard deviation of 0.65 dB. This corresponds to a mean improvement of 4.3 dB for the multistatic system. The best improvement occurred at about X = 480 units with the difference being 5 dB and the minimum improvement occurred at X = 850 units and was 3.5 dB.

This particular graph demonstrates that, when properly corrected for changes in the resolution cell size with range, (due to beam divergence), the loss factor for both monostatic and multistatic systems is independent of the position of the surveillance area. The results at each position of the surveillance area can therefore be grouped together into one data set representing the performance of the system as a whole.

Before grouping the data in this way however, the individual results obtained at each position are shown in figures 6.4 to 6.7. These show the display loss in dB as a function of the number of receivers used, for targets 1 and 2. To produce these graphs the display loss was calculated for each orientation and each receiver combination. A data point on the graphs was obtained by averaging the results for that receiver combination with respect to orientation. All the plots show a lower limiting value of display loss labelled 'insonified area limit', which represents the theoretical best performance in that configuration. It was calculated by assuming a fixed value for m for the target, then averaging the number of cells calculated to be detected by the line-of-sight vector mentioned in CHAPTER V, with respect to orientation again. In this sense it is an average performance, but nevertheless, the actual measured loss values must be assymptotic to this limit as the number of receivers is increased.

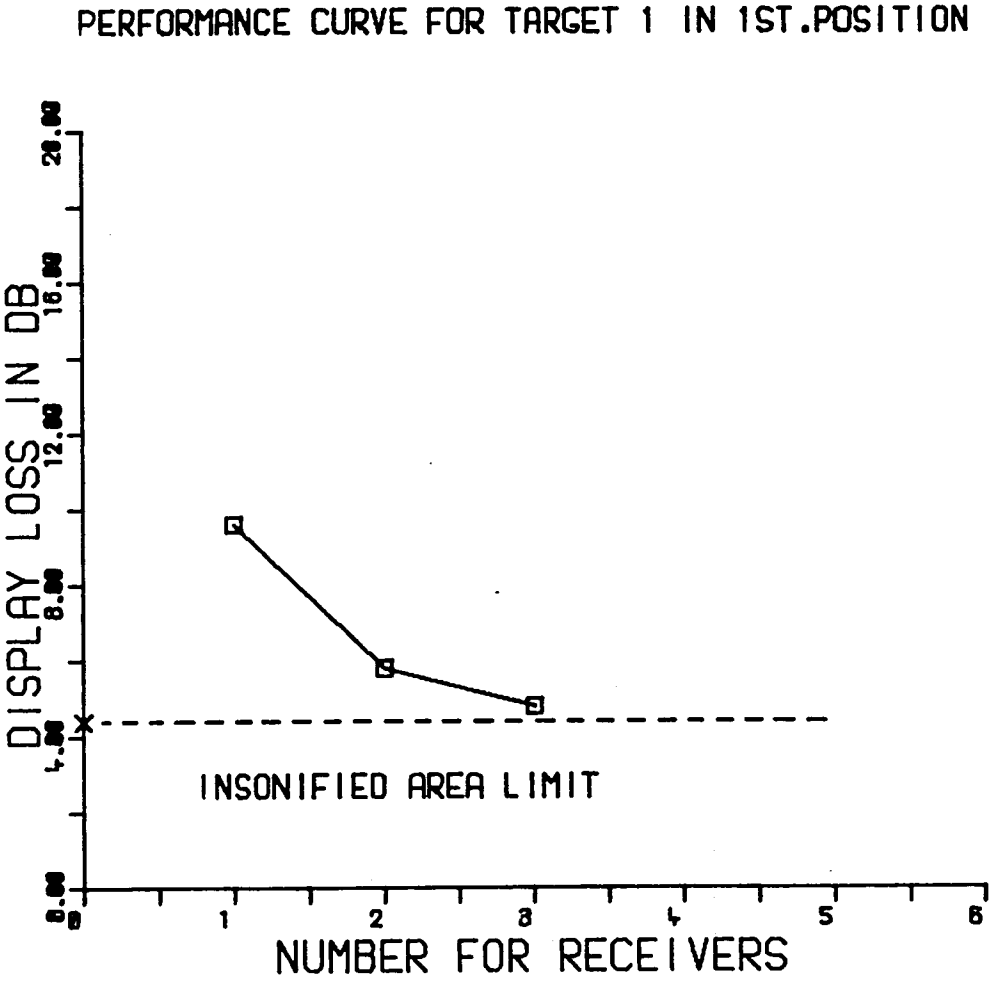

FIG 6.4 A GRAPH OF THE AVERAGE DISPLAY LOSS FOR TARGET 1 CALCULATED FROM THE CORRESPONDING PPI DISPLAYS.

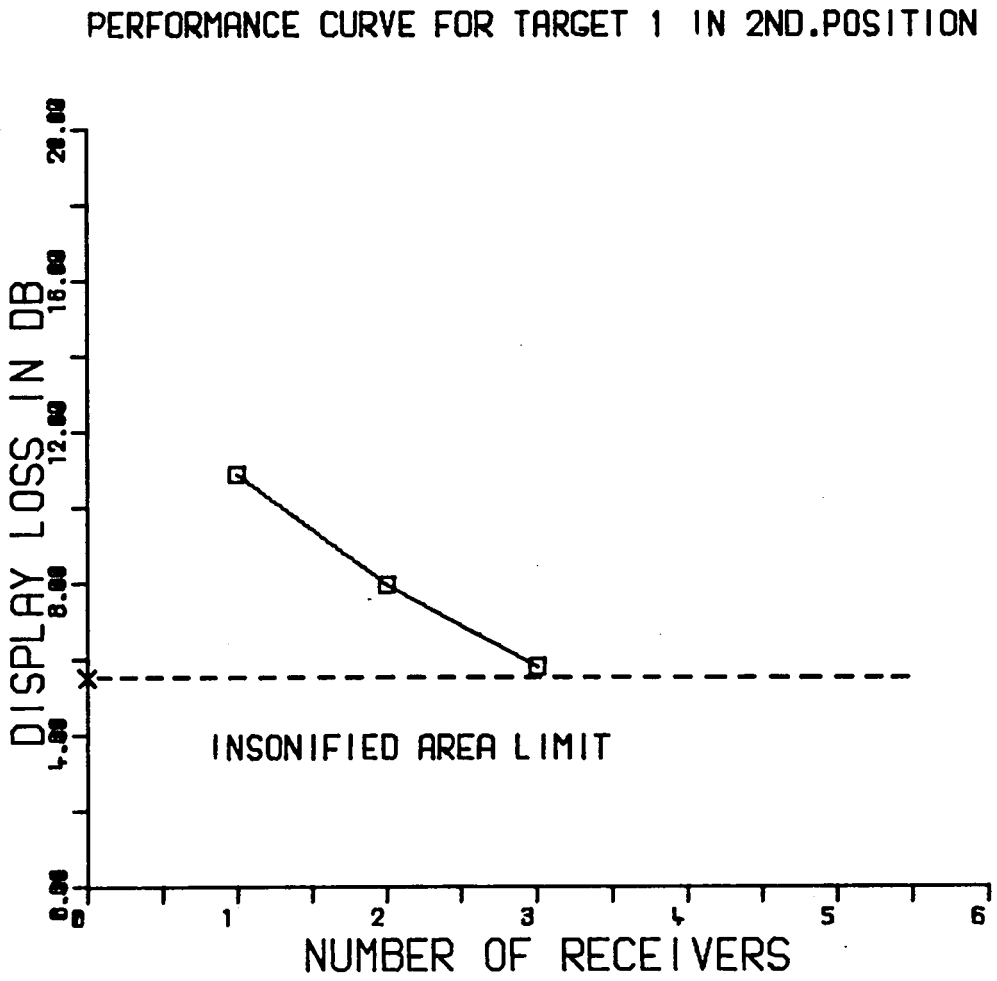

FIG 6.5 A GRAPH OF THE AVERAGE DISPLAY LOSS FOR TARGET 1 CALCULATED FROM THE CORRESPONDING PPI DISPLAYS.

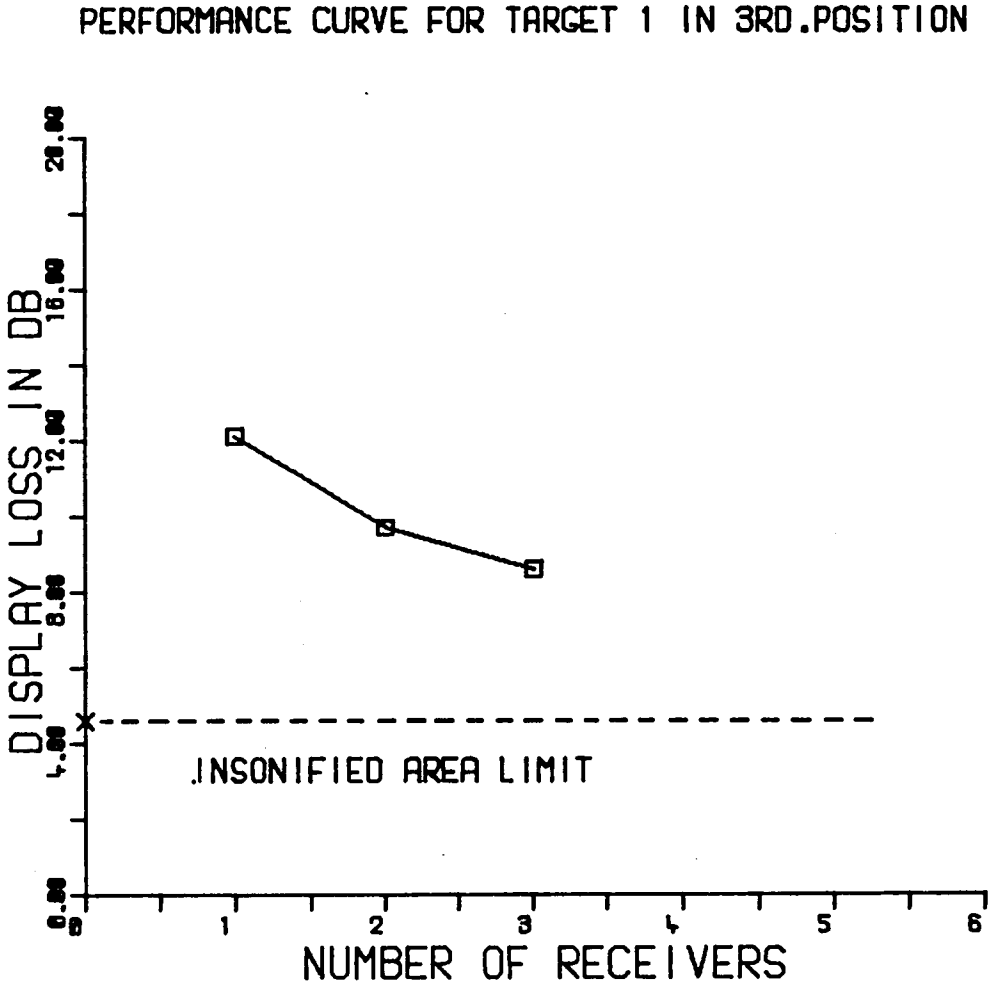

FIG 6.6 A GRAPH OF THE AVERAGE DISPLAY LOSS FOR TARGET 1 CALCULATED FROM THE CORRESPONDING PPI DISPLAYS.

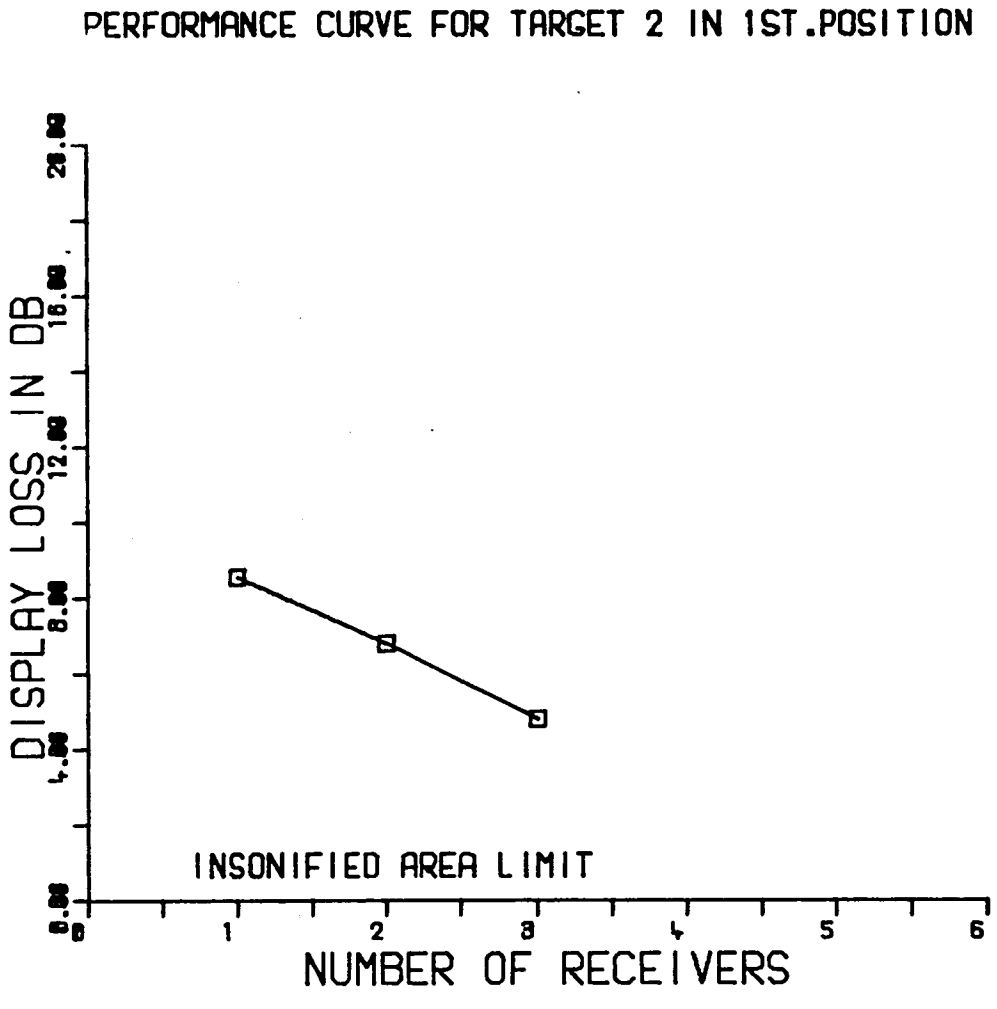

FIG 6.7 A GRAPH OF THE AVERAGE DISPLAY LOSS FOR TARGET 2 CALCULATED FROM THE CORRESPONDING PPI DISPLAYS.

Figure 6.4 shows the result for target 1 in the first position nearest the transmitter and it can be seen that almost maximum performance was obtained when three receivers were employed to detect echoes. Figure 6.5 shows the result when the target was repositioned along the receiver plane away from the projector and it can be seen by comparison with the other figures that this was the best improvement obtained with the multistatic system. The performance with three receivers approached the limiting value to within 1 dB and this graph corresponds to the maximum improvement situation referred to previously in figure 6.3. The final result with this target is shown in figure 6.6. In this case it can be seen that the performance does not approach the insonified area limit closer than 4 dB, and the improvement obtained with the 3 channel multistatic system is also at a minimum in this position.

Figure 6.7 shows the performance curve for target 2 in a position closest to the transmitter. In this case the total target contour was insonified, hence the 0 dB insonified area limit. It can also be seen that the three receiver system was still approximately 4.5 dB above this and a simple linear extrapolation of this data indicated that about five receivers would be necessary to improve the performance to within a dB or so of this limit.

A particular feature of the above figures 6.4 to 6.7, was that uncorrected data was taken directly from the display results to calculate the data points, but it was shown above that a change in the display loss occurs which was a function of the range of the target relative to the transmitter. When corrections, taken from figure 6.1, were applied to the curves to compensate for this effect, a more uniform picture of system performance emerged, with less spread than the individual uncorrected results. Figure 6.8 is a plot of all the results after corrections were applied and shows that the data points all lie within

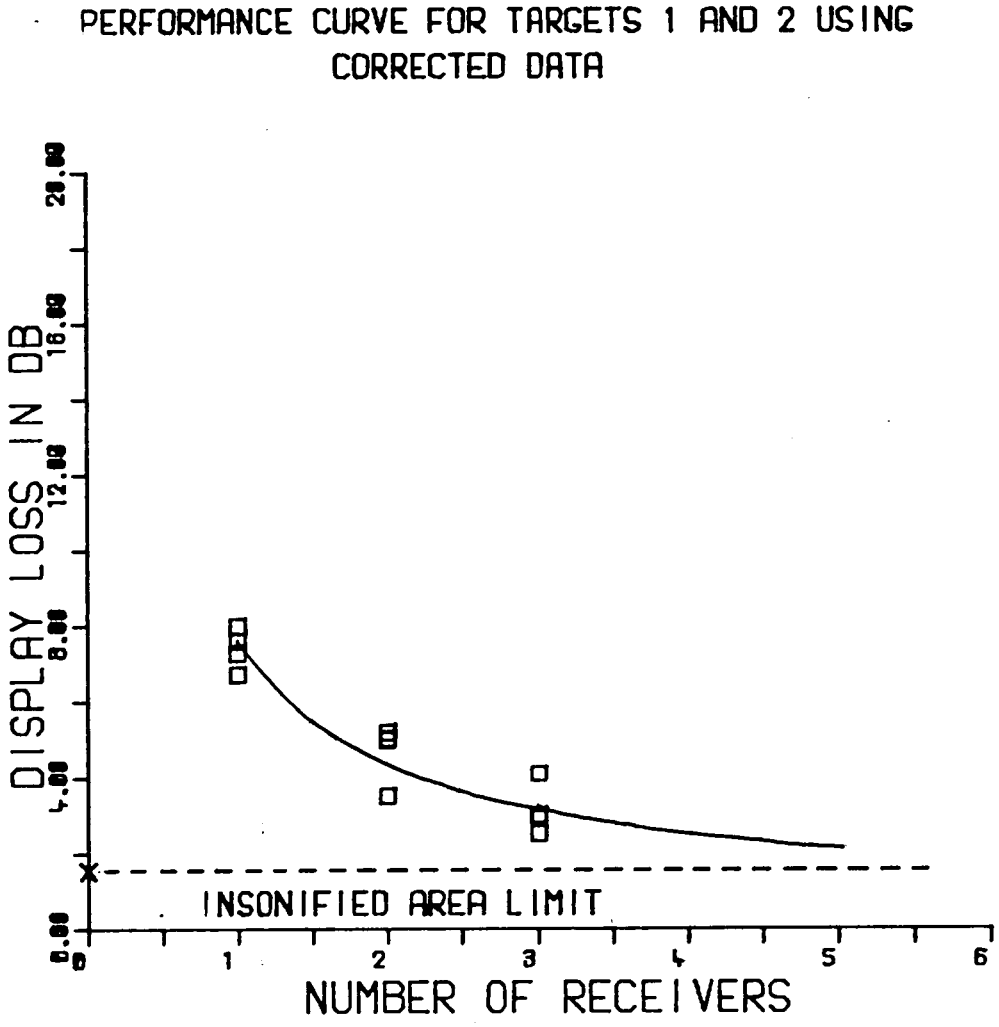

FIG 6.8 SYSTEM PERFORMANCE CURVE USING DATA FROM FIGS 6.4-6.7 CORRECTED FOR POSITION ALONG THE RECEIVER PLANE.

± 1 dB of the power law regression line fitted to the data. A power law regression line was chosen because an intuitive approach to extrapolation of the data suggested a 3 dB doubling law. The actual least squares fit was,

$$\text{Display loss in dB} = 7.55\ (N)^{-0.79}, \quad \ldots\ldots\ldots\ldots \quad 6.1$$

where N = 1, 2, 3 . . . . . , ie an integer representing the number of receivers in the system.

A difficulty arose in adding an insonified area limit to this graph. Simply averaging the limits shown on figures 6.4 to 6.7 results in an estimate for this constant which would be exceeded when N was about 2.5. This is not possible by definition, and the difficulty is resolved if the insonified area limits are corrected by the same amounts as the actual data points. This is reasonable since the insonified area limit was calculated in each case based on a fixed number of approximately square resolution cells overlaying the reference contour C_t, and took no account of the change in width of cells due to the divergent nature of the transmit beams. The insonified area limit shown was therefore calculated by averaging the corrected limits obtained from figures 6.4 to 6.7. It can be seen that the regression line fit is approximately assymptotic to this estimate and this bodes well that this is a sensible estimate of performance limit in this situation.

Equation 6.1 therefore emerges as a quantitative measure of performance for this system and as the basis for the design of a multistatic sonar with similar parameters and a similar requirement in terms of target definition on the final display.

6.3 Comparison of the results with the simulation discussed in CHAPTER II

In CHAPTER II the performance of the sonar system as a target shape portrayal device was linked to the amount of information on the binary output display. This meant that performance could be shown graphically and independently of the observer. It was also shown via a simple example that the echo excess which existed at the receiver partly determined the degree of improvement possible with multistatic operation. A trade-off between this dynamic range and the monostatic system performance existed which could be compensated by multistatic operation. In the results obtained a particular set of parameters prevailed which included a fixed dynamic range for the monostatic system. As a consequence only one curve showing performance as a function of the number of receivers was obtained, in contrast to the family of such curves shown in figure 2.7 of CHAPTER II. Nevertheless, the results demonstrate that a relationship of the form shown in CHAPTER II describes the performance of the system. Difficulties to do with modelling a complex target shape in the simulation prevented a more exact correspondence between the simulated and actual results, but there is no reason to doubt that a similar family of curves exists for the system used here.

An important difference between the simulated performance and the measured results was the assumption of equal directivity indices, and overall sensitivities for all receivers made in the simulation. This was not the case in the experimental system, and the monostatic receiver differed in both directivity index and sensitivity with respect to the other two receivers.

In CHAPTER IV, a set of measurements was presented from which a correction figure of 3.4 dB was derived which represented the change in display loss between the monostatic and bistatic channels to account for this difference in overall sensitivity. When this final correction was applied to the data by reducing the contribution from the monostatic receiver by a corresponding amount, a different average performance curve for the system resulted and is shown in figure 6.9. By noting that the ppi displays using the monostatic receiver showed the first side-lobes of the transmit beam (see figure 5.2(b)), and with reference to the transmitter beam pattern shown in the appendix, it can be seen that for the monostatic system about 25 dB of echo excess existed. This assumed that the side-lobes on the display from the transmit-receive product beam were about 25 dB down on the main lobe. Curve 4 in figure 2.7 has therefore been extracted and plotted in figure 6.9 for comparison since this corresponded to a 30 dB echo excess in the example of CHAPTER II. At the monostatic position the curves differ by about 2 dB, which can be attributed to the fact that more discontinuity echoes were received from the experimental targets than from the simple linear target used in CHAPTER II. This tended to improve the measured monostatic performance, and this improvement increases to about 3 dB from the 2 receiver point onwards. But apart from a mean offset between the curves of about 2.5 dB, the overall trend is the same. The least squares fit for the measured data was now,

$$\text{Display loss in dB} = 11.45\ (N)^{-0.73}, \quad \ldots\ldots\ldots \quad 6.2$$

Where the terms are as per equation 6.1.

Whether the correction applied here is valid because it reduces the directivity index which is already available in the common transmit/receive transducer is open to criticism, but it is justified when the object is to remove all possible variables except those connected with the multistatic sonar concept.

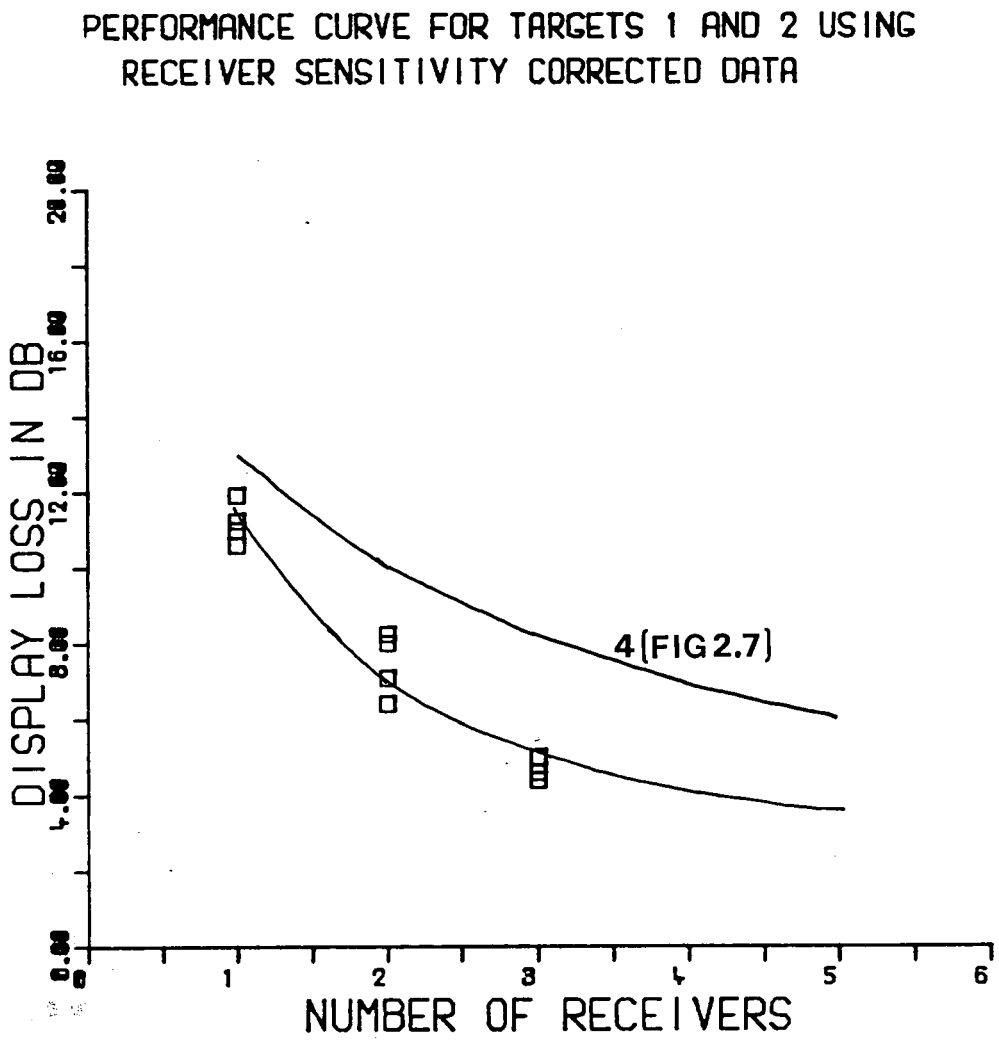

FIG 6.9 SYSTEM PERFORMANCE CURVE SHOWN IN FIG 6.8 AFTER CORRECTIONS TO ACCOUNT FOR THE DIFFERENCE IN SENSITIVITY OF THE BISTATIC AND MONOSTATIC RECEIVERS.

In any event, the overall conclusion was that the performance of the multistatic system did follow the trends described in CHAPTER II with regard to the display loss plots, even when a more complex target shape was examined.

Using equation 6.1, the predicted performance for the system was that a maximum of four bistatic receivers in addition to the monostatic channel represented the useful upper limit on performance with the particular targets and value of m chosen. Beyond this number, a state of diminishing returns is to be expected as the curve is assymptotic to the limit set by the insonified area.

An attempt to incorporate these findings into a set of design guidelines is made in the next chapter.

CHAPTER VII

CONCLUSIONS AND SUGGESTIONS FOR FUTURE WORK

7.1 General conclusions

The work described in this thesis addressed the problem of improving target shape portrayal in high resolution sonar systems. The results shown in previous chapters, in the form of echo pattern displays and in graphical form, showed that shape portrayal was improved when the target was placed in a multistatic environment. Such an environment proved to be an efficient means of utilising the angular distribution of energy reflected by the target. In this sense a multistatic sonar does not provide something for nothing because the energy already exists due to simply 'pinging' at the target, a fact which seems to have been neglected in the past.

A difficulty which was met at the outset in dealing with this topic however, concerned the qualitative and subjective nature of the problem as briefly outlined in CHAPTER I. This necessitated the introduction of a quantitative measuring technique designed specifically to cope with the binary type of display used here. This was developed in CHAPTER II and related the information on the display to the parameters of the system, including the detection arc of reflected echoes determined by the echo excess at each receiver. The concept of the detection arc was an important aspect. Its angular extent determined the number of cells detected by a receiver working with a particular echo excess, and also a minimum desirable angular separation between receivers, which if violated, reduced the effectiveness of the receivers in the system.

The measure of performance mentioned above was called the display loss and was defined in equation 2.1. It was a useful, normalised, performance index which enabled curves to be constructed showing the degree of improvement as the number of receivers in the system was increased. It also meant that in addition to a visual comparison of ppi

echo pattern displays, a quantitative comparison could also be made. The amount of improvement possible, measured in dBs, depended on the intrinsic display loss level for the monostatic system before the addition of any bistatic receivers. This minimum point on the performance curve, corresponding to the monostatic system alone, depended on the echo excess and the number of discontinuity and specular echoes detected by the monostatic receiver. A family of curves could be drawn, each representing a different echo excess, and the existence of such a family enabled an important trade-off between the number of receivers and the available echo excess, if so desired. For example, this meant that a constant performance level could be maintained if the echo excess was reduced, by increasing the number of receivers and moving along the performance curve for the new echo excess.

The worth of this property of multistatic systems relates to a problem with high resolution systems mentioned in CHAPTER I. Namely, that when employing a monostatic system alone, a large dynamic range of about 80-100 dB is required in the receiver sub-system. This is a consequence of the narrowband nature of the reflected angular spectrum $F_R(S)$, and the fact that only under certain conditions is the maximum response directed towards the receiver. Expressed in the terminology used here, this is equivalent to saying that an echo excess of 80-100 dB is required in the system; it is tacitly assumed that detection of this range of echoes occurs, which in turn means that the maximum response echoes, ie specular, are about 80-100 dB above the minimum detectable level. This seems a stringent requirement, and means that most of the transmit beam side-lobes will appear as false echoes on the display in situations where the target strength approaches the target strength of a normally incident, specularly reflecting resolution cell.

The multistatic system provides the means to attack both of these difficulties at once. Firstly, by employing the trade-off discussed above, the requirement to be able to detect a large dynamic range of echoes is removed or at least drastically reduced. Secondly, and hand in hand with this benefit, as a result of reducing the dynamic range the side-lobe problem is also reduced by a corresponding amount. The system can in theory be adjusted to operate within the dynamic range of the first side-lobes of the transmit beam, thereby removing them altogether from the display. With reference to figures 5.2(b) and (d), which show unprocessed results, only the first side-lobes are visible and these echo patterns were wholly representative of the results obtained. The system was therefore operating with a dynamic range of only about 25 dB, yet still producing recognisable target outlines.

The performance curves shown in CHAPTER II, indicated that a less than 3 dB improvement in the display loss per doubling of the number of receivers was to be expected. The exception to this rule was a special limiting case when the monostatic performance level coincided with the upper maximum value of display loss, which by definition was given by,

$$L_{max} = 10 \log_{10} (m),$$

Where m was the chosen value of 'display magnification'.
This special situation was unlikely to occur in practice since it corresponded to the absolute minimum value of echo excess required to just detect a specular echo at the monostatic receiver, ie zero dB.

The experimental performance curves derived from the results shown in CHAPTER V, also showed a less than 3 dB law in the case of the averaged results of figures 6.8 and 6.9. Remember that the exponents of both fitted curves had magnitudes less than unity, which corresponded to the situation in the simulation described in CHAPTER II. Because only

curves at one value of echo excess were obtained experimentally, no verification of the expected changes with different echo excesses was obtained, however, there seemed no reason to doubt that a similar family of curves would be obtained as per the examples in CHAPTER II. In the author's opinion, the experimental results sufficiently confirm the prediction methods discussed in CHAPTER II, to enable them to be used in the design of a multistatic system.

The multistatic sonar is conceptually simple, a factor which augurs well for any proposed improved system. But a closer and more detailed examination reveals that the improvements possible are dependent upon a number of system parameters, and a law of diminishing returns eventually prevails. The system described here was the simplest configuration, but was still considerably more complex than its monostatic counterpart and needed the services of a powerful computer to operate successfully. These factors must be taken into account when considering the improvements in system performance obtainable. Nevertheless real improvements can be obtained, and the results presented here show only a 'first cut' attempt at the proper utilisation of the concept.

During the course of the study, a number of questions emerged which remain unresolved. One of these concerned the subjective nature of the definition level on the display chosen to enable recongition of different targets. This manifested as the initial choice for m, the 'display magnification', which was decided on an empirical basis. Figure 1.1 showed this choice in display definition terms relative to some relevant previous studies. Having chosen m for the likely target contours to be portrayed, the problem studied here could be succinctly put as that of maximising the value of b in equation 2.1. The unresolved aspect is how m should be chosen to maximise the chances of an observer correctly recognising and classifying a target contour, and at the same time to choose the minimum value so that the system is not overspecified.

Relating this problem more closely to the display loss curves presented in the results, it remains an objective to be able to quantitatively specify the display loss level at which a line parallel to the X axis is drawn and labelled 'target recognition level'. The system could then be designed to reach this level of display loss in the most economical way.

In a similar vein concerning the subjective aspects of any echo pattern studies, it can be argued that echo co-ordinates 'painted' on the display do not all convey the same or equal information to the observer, and that some echoes in a fragmented display might be more significant than others. Whether this is the case or not will depend on the a priori knowledge of the observer. In this work all echo co-ordinates were given equal weighting in constructing the display loss curves. Since subjective studies were outside the aims and scope of this work, this was the only approach which made sense.

What the display loss curves did not show or infer was the actual geometrical arrangement of the system. Taken in isolation they only indicated the amount of improvement as a function of the number of receivers in the system, and they were derived from a fixed geometrical relationship between the transmitter and receivers called the receiver plane. This particular geometry was merely a convenience from the point of view of both implementing the experimental system and simulating the performance. Other geometrical arrangements of the receiver plane are possible, but their effect on performance would only be to further reduce the variability in response which necessitated averaging a number of target orientations in the experimental phase described. Two similar alternative geometries can be proposed, being either two receiver planes at right angles, with the transmitter at the intersection of the two or a semicircular or quadrant arrangement of receivers with the transmitter again in the centre of arc. During the course of the experiments it was

apparent that reduced coverage of the target was occurring due to shadowing of areas of contour from both the transmitter and bistatic receiver points of view. For these situations additional receivers on a receiver plane at right angles to the existing one would contribute echo co-ordinates which would tend to compensate for the display loss due to shadowing at the other plane. This arrangement would smooth out fluctuations in the system performance even more than observed here, and in the author's opinion provide almost constant target shape portrayal performance independent of orientation.

For example, consider the multistatic display shown in figure 5.8(e) which depicts the target at 90 degrees relative to the receiver plane. The contribution to improved target portrayal from the bistatic receivers was minimal in this case because only a small part of the insonified target contour was also acoustically visible at the bistatic receivers. With reference to the run geometry shown in figure 5.8(a) it can be seen that most of the bistatic echoes were being deflected towards the Y axis and not the X axis. A similar receiver plane orientated along this axis would have produced a response similar to that of figure 5.4(f) and the combined output from 5 receivers would then have more closely approached the insonified area limit for the target.

The maximum receiver density limit, which arose as a consequence of the idea of a finite detection arc for the echo, was never approached in this work. In all likelihood the limit on performance caused by the insonified area limit will be reached before this in most cases, but the system designer ought to be aware that such a limit exists, if only to ensure that in all geometrical configurations, no two bistatic receivers subtend an angle at the target less than this limit.

7.2 Steps in designing a multistatic system

In order to further highlight the findings of this work and to illustrate some of the points made, a sequence of stages describing the

design of a hypothetical system is set out below. Each case of target portrayal has specific problems due in part to the variability of the sonar environment and the description given is therefore in qualitative terms only. Nevertheless, a systematic approach along these lines will, in the author's opinion, result in a sensible working solution to the target shape portrayal problems studied here despite the discussion being unavoidably vague about certain aspects.

(a) Given a particular target shape or class of targets to be portrayed with maximum classification potential and minimum display loss, then the first step would be to carefully consider the value of 'display magnification' m, which was necessary. The circumstances of this choice have been briefly discussed above. No generally accepted method exists to the author's knowledge to help in making this choice and it will be currently based on the judgement of the observer who decides that the target can be classified with a particular definition. The final correct choice for m with respect to the target shapes to be portrayed is probably 50 percent of the problem of pattern recognition which is implied here.

(b) Having made this initial choice, then with some a priori knowledge of the target contour a resolution cell size can be estimated using this value for m and making some assumptions about the likely range from the transmitter to the surveillance area. In this way the two most basic parameters of the system can be calculated, ie the angular width or resolution of the scanning sound beam and the bandwidth or range resolution required.

(c) Using these resolution cell parameters, the range, and corresponding propagation losses, a suitable working frequency band can be chosen using well known methods.

(d) With some knowledge of the target contour and resolution cell size, the dimensions of the reflecting aperture in wavelengths can be determined. Note that provided the bandwidth required for a particular range resolution is small enough, and the system Q factor greater than 10, then it was shown in CHAPTER II that changes in aperture size due to changes in wavelengths at each end of the frequency band can be neglected. The estimated aperture size then determines the reflected angular spectrum bandwidth under conditions of straightforward reflection from the target; there being no complex phase shading or amplitude tapers at the target - medium interface. At this point the effects of scanning across target boundaries and discontinuities can be investigated by using a Fourier transform relationship as described in CHAPTER II. The purpose of this investigation would be to obtain data on the expected angular spread of reflection. This can be presented in the form of a polar diagram or S-plane response so that the effect of different echo excesses on the detection arc can be seen.

In most cases only a limited source level will be available finally and the extent of the detection arc at discontinuities can be estimated for different source levels. The angular extent of the detection arc will also fix an upper limit on receiver density which can be borne in mind and related later to performance predictions, if necessary.

(e) The next important stage concerns the estimation of the average number of discontinuity and specular echoes detectable by the monostatic receiver. In this sense discontinuity echoes

includes those originating on target boundaries where aperture limiting effects occur with a consequently wide angular spectrum; specular echoes occur from normally incident surfaces in this context. For this purpose it is suggested that a minimum of three separate orientations of the target are considered with the object of obtaining an average prediction. This stage will be the most difficult and the validity of the subsequent performance predictions will depend upon a sensible estimate being made here. In making this estimate the existence of the previously determined detection arc for a particular echo excess must be taken into account in deciding how many resolution cells either side of a normally incident specularly reflecting cell will be detected by the monostatic receiver. The final result will then be a realistic estimate of the display loss in dB's for the monostatic system working with a particular echo excess. The first point on the performance curve can now be drawn representing the upper limit from which the prediction starts.

Information regarding the lower limit of the display loss due to the insonified area can also be estimated at each of the orientations considered above. In this work a simple line of sight vector to the target was used. This is valid provided no significant diffraction occurs at the target to cause insonification of shadow zones. Since the performance prediction is itself an average obtained from all the orientations of the target used, the lower limit due to the insonified area can also be averaged to give a working lower limit to which the prediction curve will be approximately asymptotic. When this lower limit is approached to within a specified tolerance, optimum system performance has been reached.

(f) The penultimate stage requires that a performance curve is superimposed on the display loss graph such that it intersects the upper limit estimated previously for the monostatic system. It was shown in the previous chapter that a power law fitted the observed data well and it is proposed that equation 6.1 is used with the appropriate constant. Adjustment up or down the Y axis can then be made to intersect the monostatic point and the resulting curve will then represent current knowledge as recorded by this work. The resulting graph is now an estimate of system performance for one echo excess, and a family of curves can be built up by recalculating the detection arc for each new echo excess. The final picture will then depict how echo excess can be traded with the number of receivers to maintain the same performance level for example. Alternatively, if the initial objective was the best target shape portrayal, as was the case here, then a sensible choice can be made regarding the number of receivers required for optimum performance with due regard to the lower limits set by the insonification of the target. In this way a multistatic sonar can be built with a priori knowledge of the likely performance of the system with the chosen class of targets.

The above description of events was necessarily qualitative because there remain areas where the right course of action is unclear and knowledge is incomplete. Nevertheless, it has been shown in previous chapters how most of the above steps in the design can be undertaken or approached.

7.3 Possible uses of the present system

In its present form, the system described really requires a fixed scenario for both target and sonar system, but this does not preclude applications where a fixed geometrical relationship of the required sort is not available. For example, where improved shape portrayal of fixed underwater structures is required for surveying or maintenance purposes, then a fixed arrangement of transmitter and receivers could be manoeuvred into position. The transmitter and associated bistatic receivers would remain in a fixed geometrical relationship to each other by virtue of their being mounted rigidly to a receiver plane. It is, of course, possible to determine the positions of each receiver by using an echo location technique as a prelude to multistatic operation, but this would complicate the setting up procedure and might not be justified if rapid results were required. Some interesting possibilities exist in the medical ultrasonic scanning field for an improved diagnostic tool which does not require repositioning and rescanning after each transmission to achieve total subject cover. For this type of application a more conformal receiver plane might be a better choice and would not present any difficulties regarding range computation provided suitable provision was made in the display formatting software to allow for the different, but fixed, angular offsets of each receiver with respect to the transmitter.

With regard to the anti-submarine warfare (A.S.W.) field of activity, then a fundamental difference exists with respect to the work discussed. The number of resolution cells covering the surveillance area and target, and the likely range to the target, differ greatly from those used in the experiments conducted here. Even though modern sonars working in the kHz range of frequencies employ very narrow beams, the requirement for initial detection at long ranges always means that the target is overlayed by one or at most a few resolution cells. Because of this often marginal mode

of operation the emphasis changes from improved target shape portrayal to whether improved initial detection can be obtained with multistatic operation.

If it is assumed that the ASW sonar works in a surface reverberation limited environment with submarine targets at moderate depths, and if it is further assumed that the backscattered sound comprising this reverberation is distributed uniformly in a spatial sense, then each bistatic receiver should intercept approximately the same reverberation energy. In general, even targets overlayed by a few resolution cells tend to have complex polar reflection diagrams with usually beam-aspect being the strongest return. Changes in the target strength do occur with target aspect changes, but it has been shown that multistatic operation tends to smooth out such fluctuations by providing many more data samples as the aspect of the target changes. If the reverberation energy at each receiver is approximately the same and if equal signal energy is received at each bistatic station, then a maximum 3 dB doubling in signal to noise ratio could be expected for each doubling in the number of receivers. Thus with four stations, including the monostatic one, a 6 dB improvement in signal to noise ratio, and consequently the initial detection performance, should be possible using a within cell integration method. This would be achieved without any increase in source level or transmitter directivity, and is a worthwhile improvement.

Of course only a principle has been outlined here and the argument pays no attention to either the logistics of multi-ship working arrangements or to the likely cost of such a scheme. Bearing in mind the typical separations between transmitter and receivers, which must be of the same order as the target range, then such a scheme would not be without technical problems regarding navigation and the determination of receiver locations etc. However such considerations are outside the scope of this work.

7.4 Improvements to the experimental sonar system

The digital nature of both the display output and formatting and the actual range computation provided all the advantages associated with the use of a digital computer as opposed to special purpose dedicated hardware. These included the ease of modifying the software and program functions together with the ease of data storage and retrieval. This work could not have progressed along these lines without such facilities, or if alternative equivalent analogue computations had been employed. The use of a digital computer introduced new possibilities for display processing which were not possible with more conventional equipment employing long persistence phosphor tubes for instance. The next logical step is therefore to replace the remaining analogue circuitry in the system with an all digital design along the lines suggested below, so that improved compatibility with the computer is achieved. This would mean that the interface between the cpu and the sonar was in a digital form and many of the problems concerning the accuracy of the data generated by the analogue circuits would then be removed.

The range measuring ramp waveform which provided the voltage proportional to elapsed time after transmission was an obvious candidate for replacement by a digital range counter. The magnitude of the count and the number of bits used would determine the number of range increments possible during a sweep. For example, a 10 bit counter would provided a thousand range increments. In a similar manner, the measurement of relative bearing of the transmission can be performed using a digital bearing encoder. A third digital word would be required to encode the location and distance of the particular receiver outputting data at any particular instant.

The parameters required to localise the detected echoes would now be encoded into the three digital words in a precise manner and with known fixed precisions. The use of these digital words in place of the

previous analogue data would enable a direct memory access (DMA) method to be employed to deposit the data directly into the cpu memory. Inputting data in this way would be controlled by the threshold detectors in the receivers as before, which would cause latching and sequential gating of the digital data instead of initiating a sample and hold process. The advantage of DMA is that it can be made to operate completely independently of the cpu and therefore represents a considerable time saving in terms of computer operations. The software must of course be restructured to take advantage of this by processing data on an interrupt or queue basis in an asynchronous fashion. This would greatly ease the data loss problem with the system due to the processor being busy when new data was available, and which adversely affected the results. The only real limitation would then be the size of the stack or queue allowed in the computer to store unprocessed data. Although the actual display output would lag behind the real time scan during periods of high data input rates, catching up would occur at the ends of the scan when little or no echoes were being detected. The interrupt polling and DMA facilities needed for this mode of operation were not available on the cpu used in the experiments, but they are now common features of most mini-computers suitable for this work.

The method of storing the echo co-ordinates in the computer was wasteful of memory, and the binary nature of the final display means that a more efficient data storage scheme can be proposed. In this more efficient scheme each resolution cell in the surveillance area has an associated unique 'bit' of storage. For example, a 512 x 512 cell surveillance area, considered adequate for this work, comprises 262, 144 cells, or 'bits' using this new scheme. If a word is 16 bits long then each 512 bit line of the surveillance area requires 32 words of storage. The total requirement is therefore 512 x 32 words, and occupies 16K words (K = 1024) of 16 bit memory, a figure well within the capacity of most

modern computers. The advantage of this different method of storing the data for display is that there is now no possibility of data being overwritten by echoes occurring on the same bearing but at a later time, as was the case here. The disadvantage with this method is that increased complexity is required in both the software and hardware necessary to transfer the data to and from the bit map format and encode and decode it into X,Y co-ordinates.

The final choice in this matter would probably depend on the size and access speed of any mass storage device available. If a rotating disc store were used, then a 512 x 512 surveillance area would use up 512K words of data per scan if stored in the X,Y co-ordinate pair format used here. The average disk memory provides about one million words of 16 bit word storage, but with an access time of typically 10 μs per word. A refresh display would be working with a 5 second cycle time, which might be unacceptable. Eventually a compromise must be chosen which suits the requirements of the display and the system.

Figure 7.1 shows a schematic diagram of an improved experimental system which embodies all of the changes discussed above, and it is recommended that improvements along these lines form the starting point of any future experimental work.

The other area where some improvement to the system used here would be desirable is in the design of transducer beam patterns. In this work a high frequency transmission was used, and the transducers presented their own special problems concerning beam pattern design due to their extremely small size. However techniques do exist for tailoring beam patterns in small transducers, and S. Ying [20] describes one such method which utilises collimators to shape the main lobe response and reduce the side lobes to about 40 dB below axial response.

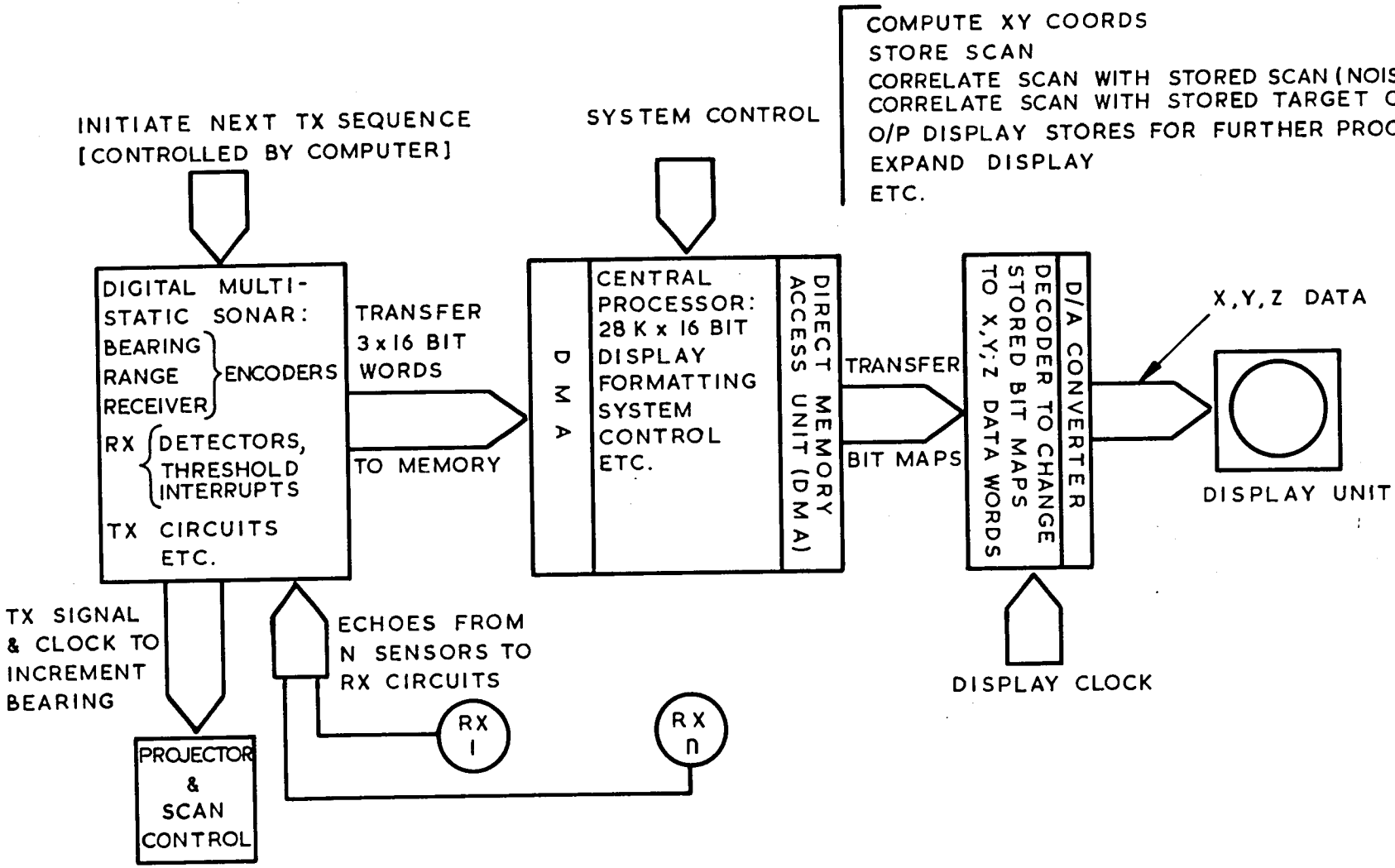

FIG. 7·1 SCHEMATIC OF IMPROVED MULTISTATIC RESEARCH SONAR

FIG. 7·1

In particular the design of the bistatic hydrophones meant that their receive beam patterns were omnidirectional in the horizontal plane and in the vertical plane covered a wider arc than was necessary to encompass the target. It would be more sensible to confine their horizontal directional response to the region corresponding to the surveillance area. This would help to offset the differences in overall sensitivity which existed between the monostatic and bistatic receivers.

7.5 Suggestions for future work

7.5.1 Computer modelling

Having implemented the changes which were considered the immediate priorities regarding the overall system, further studies in what the author feels is an interesting research area might begin with an extension of the work done to model the system. Only the basic concepts concerned with describing the reflection process for a resolution cell were investigated and modelled in this work. A more complete model which encompassed and enabled all aspects of the multistatic scenario to be studied would be of great value, since such a system model would allow rapid assessment of many schemes involving changes in the number and location of the receive sensors, and changes in other important system parameters such as echo excess, for example.

One possible approach to the problem of implementing such a model is suggested by an extension of the method discussed in CHAPTER II, which was used to describe the echo formation process in the resolution cell.

The complete environment, including the surveillance area and the projector and receiver area, can be described in terms of a set of resolution cells mapped out on an X-Y plane for convenience. The actual surveillance area is now a subset of the total number of cells, and the target outline contour C_t, is represented by a finely quantised set of co-ordinates within this area. Within each resolution cell which overlays the contour C_t a straight line approximation to the contour at that point can be developed. The position of the projector can be defined by its location in a particular resolution cell at some range from the target. The scanning beam would be represented by discreet changes in the bearing and at each change the position of the insonified resolution cell

overlaying the contour C_t can be found by ray geometry. Shadow zones created by the beam could also be approximated by this means, at least initially. The straight line approximation for the contour C_t within this insonified cell would be retrieved and an amplitude and phase aperture function calculated from the beam pattern and the slope of the line relative to the beam. Arbitrary beam patterns can be specified for the projector and incorporated into the aperture function at this point in the simulation.

An angular spectrum can now be computed for the insonified cell as described in CHAPTER II, and the far field response in those resolution cells specified as containing receive sensors computed by using the equations given in CHAPTER II which describe the far field response.

When the response is thus computed and checked for possible shadowing of the receiver by simple ray theory, the output of the receiver can be simulated by specifying a sensitivity in the direction of the incoming ray. A detection would be made if the signal vector, plus any noise term if desired, exceeded some realistic preset amplitude.

Incorporating specific signal types other than simple pulsed CW is not easily done in such a model, although the angular spectrum can be computed for individual components of the signal frequency spectrum and recombined at the far field point as outlined in CHAPTER II. In any case, if the resolution cell size is specified in terms of a range and bearing ambiguity diagram then signal bandwidth at least, is implicit in the range resolution.

A display of the detected signals, in a binary format as used in this work, and some interactive features and control such as the number and position of sensors and the specification of the target contour C_t, would be desirable and would complete the computer model. But it should be noted that although such an extension to the existing model is conceptually straightforward, the changes suggested constituted an ambitious project in its own right in the author's opinion. This was partly why only a limited system model was developed here.

As pointed out at the start of this chapter, the present system provided a biased, one-sided look at the target. The field of insonification was limited by shadow zones which allowed only one side of the target to be displayed.

The fact that increased system complexity would be needed prevented experiments from being performed with alternative arrangements of receivers. There is an upper bound to the improvement which can be expected of course, which was described in CHAPTER II and confirmed in CHAPTER V, but this was certainly not reached in this project, and it would seem a worthwhile exercise to prove that this limit exists for a given resolution cell size and known target contour.

There are a number of possible arrangements of projector and receiver stations which will increase the field of view of the target. One such arrangement, consisting of two receiver planes at right angles has already been mentioned, but it must be borne in mind that the geometrical relationships between receivers and projector affects the number of independent resolution cells containing detected echoes. In this thesis an attempt has been made to quantify these interactions and it is hoped that the results obtained so far will provide a guide for a 'first out' look at least.

No progress towards determining either some principles or ground rules for the choice of the 'display magnification' m has been made because it was considered outside the scope of the work at the outset. Further work in this respect is needed, and would be useful if a proper framework can be decided for such a study, which was not itself of a subjective nature.

Since the target has been described here by its two-dimensional contour C_t, it would seem sensible to consider employing a two-dimensional version of the sampling theorem in some way, so as to relate the value of m to target definition. Picture transforms using a two-dimensional version of the well known Fast Fourier transform algorithm could be performed, with the object of defining a two-dimensional bandwidth for a given set of targets which was the analogue of the familiar Nyquist rate definition in the frequency domain. With the target contours in an equivalent transform space, changes in the target aspect may become more easily recognisable, although it should be remembered that no new information would be presented, merely the same information in a different form. If a high speed computer was utilised in the system then the echo data will already be in memory and a transform could perhaps be performed in real-time. However, irrespective of such sophisticated display processing, if a two-dimensional bandwidth can be defined for the class of target contours to be displayed, then a calculation in terms of sampling rate can be made which will determine the number of cells and the value of m required.

7.5.2 Coherent processing of the receiver outputs

The signals received at each receiver due to reflections from the target were processed independently and incoherently in the sense that each receiver was essentially a simple energy

detector. What are the likely gains which might be achieved by coherent processing of the receiver outputs? By this is meant the recording of relative phase with respect to a reference at each receiver in addition to the signal amplitude.

In simple terms the use of signal phase introduces another degree of freedom into the system, but it is not immediately obvious how this extra dimension would be used. Two cases can be considered,

(a) when more than one receiver detects an echo from the same cell,

and (b) when only one echo is detected per resolution cell by one receiver.

In the first case, by utilising the property of range resolution to localise the signals to a particular resolution cell, what is achieved is a sampling of the far field response of a particular resolution cell. In other words, depending on how many receivers are simultaneously detecting the echo field, a number of discrete samples of the reflecting aperture beam pattern is obtained.

The aperture to far field transformation described in CHAPTER II is of course invertable and the aperture function can be synthesised from sufficient samples of the far field response. If only the amplitude is available in the far field, only the autocorrelation function of the aperture can be obtained, but if phase is included in the inverse transform then, theoretically, a reconstruction can take place. In the experimental environment of this work the phase coherence of the medium and propagation effects appeared to be very good and the implication is that provided sufficient samples are available, and can properly be localised to one range cell,

some form of within cell bandlimited reconstruction of the reflecting aperture might be envisaged. The object of this would be to try to improve the definition at discontinuities and regions where wide angular spectrum reflection takes place, this condition being a pre-requisite for multiple detection from the same resolution cell.

Although this within cell reconstruction seems attractive, there are a number of obvious problems. Firstly the assumption of completely coherent transmission through the medium may not be true in other environments and multipath propagation for instance would destroy this necessary property. Secondly, only a very few samples would be obtained unless large numbers of receivers were employed and consequently only a very band-limited estimate of the aperture obtained.

For the second case where only one echo per cell is detected, the best use of signal phase is even less obvious. However, one line of approach is to consider all the samples of the target contour obtained during one scan as the target response. Instead of an attempt to reconstruct the aperture within a resolution cell, the aperture is now given the wider meaning of covering the whole target. Again the introduction of phase would result in a set of vectors representing the target response which would be transformed into the two-dimensional angular frequency space mentioned before. In this different form possible effects of small aspect changes which can dramatically change the ppi echo pattern (which cannot implicitly display phase) might be more recognisable as such.

The phase simply introduces another degree of freedom again and the transform is suggested only as a way of incorporating that phase into an information format which might be more easily presented, for example in the form of a quasi-three-dimensional display.

Little more can be said on this approach and the brief discussion above is no more than the collected thoughts of the author on the subject after many interesting discussions with colleagues working in the field of acoustic holography, where of course phase is of paramount importance.

7.5.3 Acoustic holography and echo ranging

The final comments on future studies are concerned with the field of acoustic holography and its aspirations to target shape portrayal as per this project. The objectives of both spheres of activity come under the general heading of acoustic imaging, and both seek to present a recognisable image to the observer. If coherence is somehow introduced into the processing of signals obtained with a multistatic type of sonar then the gap between the two otherwise separate activities seems to narrow. Perhaps techniques and processes from the two disciplines could be usefully combined, for example the inclusion of echo ranging techniques into the hologram or, (even more speculatively) the replacement of bistatic receivers with holographic imaging devices.

7.6 Summary of the work

Past studies of echo pattern formation from underwater acoustic targets have been mainly concerned with the formulation of models which relate the image formed on a display by a monostatic system, to the target. A feature of such studies is the large variability of the echoes received from the target. How can a display designed to present the pattern of echoes from the target convey this variability of 100 dB or so in echo strength when it only possesses 10-12 dB of dynamic range itself? Dynamic range compression is one answer, but is the observer able to comprehend the now subtle changes in the echo patterns and relate them to features on the target? It seems to the author that until the human observer is able to 'see' acoustically in the manner of say a dolphin, and has the kind of pattern recognition 'equipments' which these animals possess, the task which he must perform is very difficult even for a highly informed observer.

In this project, a different approach was made to the problem of displaying echo patterns. An attempt was made to add more information to the display in terms of the outline and structure of the echo patterns, and the subtlety of amplitude variation was deliberately removed. It was believed that this was more in keeping with the tasks the observer does well, ie recognising outlines and structure. All echoes were given equal significance on the binary display and emphasis was placed on the geometrical aspects of the echo patterns.

This approach resulted in some new insight concerning the general problem area, and in particular a more objective measurement of the performance of the sonar was formulated. However, it would be wrong to criticise methods of display analysis which used human observers to make value judgements. After all, the system is designed to interface with an observer in the final instance.

It was simply that in order to put the problem into a framework which could be more easily studied and understood, a move towards the objective end of the scale was considered desirable and therefore attempted. Complete objectivity was not achieved, but it is the opinion of the author that the technique of display evaluation used here provides a useful tool for further work in this area of research.

The computer model described briefly in CHAPTER II was founded on the assumption that since this work used high frequencies and relatively large, smooth surfaced, specular reflectors, the analogy was with the 'physical optics' region. This meant that reflection mechanisms could be assumed to be well behaved and not subject to complications such as surface roughness causing shadow zones within a resolution cell for example. This was a valid assumption as far as it went, and the results confirmed this mode of behaviour. It also meant that a manageable computer model could be developed, but this was not without its limitations. For example, it was only possible to study simple linear target contours with the model, and an extension of this part of the work to cover a more comprehensive situation has been suggested.

The design of the experimental sonar presented problems. Probably the most severe of these was the restricted bandwidth of the digital processor which was sometimes insufficient to handle the data input rate from the sonar. However, all of the problems encountered can be overcome and ways to do this have been suggested in this and other chapters. These difficulties are not considered as any kind of stumbling block to an improved system's proper operation.

Setting up the system before a data run occupied a considerable amount of time as a result of some of these shortcomings in the equipment. Nevertheless a comprehensive set of results was obtained, from which a high degree of confidence in the validity of both the simulation and the basic concept was gained. The ppi displays shown in CHAPTER V were representative of the performance of the system and showed improvements in shape portrayal to the point where a recognisable outline of the target was emerging. This subjective assessment was confirmed on further analysis of the results in terms of the display loss and measurable improvement was obtained. The correspondence between the simulated performance curves and the measured results, with regard to the shape of the curves and the degree of improvement, gave confidence in the empirical relationship derived from the results. This was used to predict the performance of the system beyond the three receiver limit imposed by the experimental system constructed.

Returning to an earlier point about the large dynamic range of echo strengths observed during such studies, an important aspect of multistatic system operation was the much reduced overall dynamic range required in the system to achieve comparable or improved performance compared with the monostatic counterpart. Some control over this dynamic range requirement was available through a trade-off between the number of receivers in the system and the echo excess required to achieve a particular level of display loss. This was considered a valuable property which could be used to advantage when dealing with display ambiguities due to side-lobes for example.

A number of things remain outstanding in the authors opinion. There is a need to formulate procedures for determining the display definition required to classify different target shapes. In other

words, the system designer must firstly decide what type of targets are likely to be encountered in a particular scenario. Then, a method of deciding how many resolution cells need to overlay the target shapes to make them distinguishable from one another must be available. On this subject, which at the moment involves subjective judgements by the designer, some suggestions have been made here based on an extension of one-dimensional sampling theory to the two-dimensional spatial sampling used in this work. The author believes that this is the best way to tackle this problem. A need to explore different system geometries and in particular to extend the number of receivers in the system also remains. Initially, it would be desirable to do this work with the improved system model suggested, in the belief that this is the easiest way.

In conclusion, encouraging results were obtained and the author believes that an avenue of investigation which is largely unexplored has been highlighted. In the author's opinion, there is no logical reason to confine investigations in this area to monostatic systems, despite the increased complexity and cost of multistatics. Multistatic sonar systems seem to offer new possibilities for enhancing the target shape portrayal performance of high resolution systems.

APPENDIX A

ANALOGUE SONAR CIRCUIT DIAGRAMS AND TRANSMITTER BEAM PATTERN

In this section, the detailed circuit diagrams of the various functional parts of the analog sonar which was described briefly in CHAPTER III are given. A brief explanation of the design criteria and operation of each circuit is also given for completeness, the purpose being to indicate how the various functions were implemented in this particular case. Figure A13 showing the measured transmitter beam pattern is also included for reference purposes.

A1.1 The master timing oscillator

The operation of the sonar was controlled by the master timing oscillator which generated a pericdic square wave signal. This timing waveform was used to initiate the sequence of events starting with the transmission of a C.W. pulse of sound into the water, and ending a fixed time interval later when all echoes of interest had been received.

The final design was based on a temperature compensated Schmitt trigger type SN7413N, and is shown in figure A1. An RC feedback network was used to cause the device to oscillate between the logic zero and one states, and by adjusting the value of C a control range for the period of this oscillation of approximately 0.5-5 ms was obtained. Assuming that when power was applied, the output was at logic one, this voltage was fed back via the resistor (430 ohms) and charged up the capacitor connected to the input. When the voltage across the capacitor reached the upper trigger level the output changed to logic zero. This in turn allowed the capacitor to discharge through the output stage of the device until the lower trigger point was

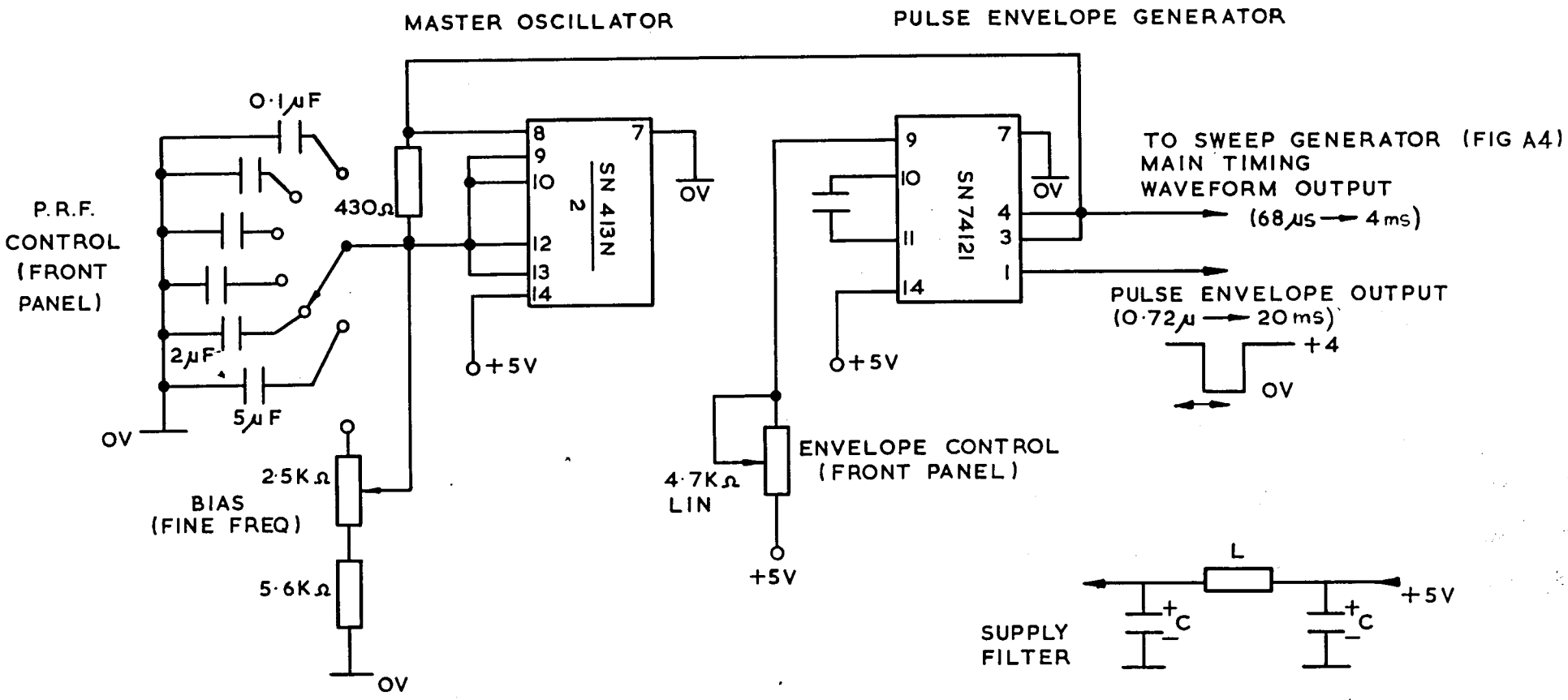

FIG. A1

FIG A1. MASTER TIMING OSCILLATOR
PULSE ENVELOPE CONTROL.

reached and the cycle repeated. A hysteresis of about 800 mV was built into the device and therefore caused the voltage at the input to follow an exponential charge and discharge curve whose time constant was controlled by the R and C values in the feedback loop. The upper and lower trigger voltages were quoted as 1.7V and 0.8V, respectively for the device and using this information, a calculation could be made to determine the values of capacitance needed for a particular frequency of oscillation. With no additional components, the circuit was made to oscillate with an approximately equal mark-space ratio and with a stability adequate for this purpose. A bias voltage was applied to the input via a variable resistance as shown, and this had the effect of causing the capacitor to charge more slowly to the upper trigger point and to discharge quickly through the lower impedance formed by the parallel combination of feedback and bias resistors and by this means the mark-space ratio could be adjusted to ensure that the correct sweep time was obtained. A calibration of approximately, 1 range cell = 1.1 millimetres, was used in the results obtained, which with a sweep voltage of 5V meant a sweep time of about 0.75 ms.

The output of this oscillator controlled the sweep generator and also triggered the pulse envelope control shown. This pulse envelope control was simply a gating circuit whose output was used to enable and disable the 2.5 MHz transmitter oscillator. This gating circuit was based on an SN74121 monostable multivibrator used as a pulse stretcher to give an output variable between approximately 1 μs to 20 ms. This range was achieved by using two switched capacitors in the circuit. Fine control of the pulse width was obtained via a variable resistor as shown.

A1.2 The transmitter oscillator

The transmitter oscillator generated a square wave tone burst at a fixed frequency of 2.5 MHz which was used to drive the class A transmitter power amplifier. The duration of the tone burst was controlled by the pulse length generator described above. In order to produce controlled oscillations, one of the four logic AND function inputs of the SN7413 was fed by an inverter as shown (itself the other half of the dual Schmitt trigger device) to obtain the correct polarity of signal. Oscillations were only possible when this input was in the logic zero state and the duration at logic zero determined the length of the tone burst and resulting transmitted signal. The output of the oscillator was fed via an impedance matching transformer to the power amplifier. This transformer employed a small toroidal core type FERALEX MM 263 which was wound in a 2:1 ratio. The input impedance of the class A transmitter was approximately 30 ohms, comprised of 6 ohms base spreading resistance, and 25 ohms forward biased emitter junction resistance. The output impedance of the SN7413 device was about 120 ohms so that a 2:1 ratio effectively transformed the 30 ohms input impedance into 120 ohms, and improved performance was obtained with the more optimum loading of the Schmitt trigger.

A1.3 The 2.5 MHz class A transmitter

The requirements for the transmitter were that it should be capable of driving the piezoelectric transducer and co-axial cable load. At resonance the type of transducer used presented an approximate equivalent load of about 100 ohms in parallel with about 1000 pF capacitance. This presented a total impedance of about 50 ohms at the resonant frequency of 2.5 MHz. A simple class A amplifier was designed to drive this load, and is shown in figure A3. The proved

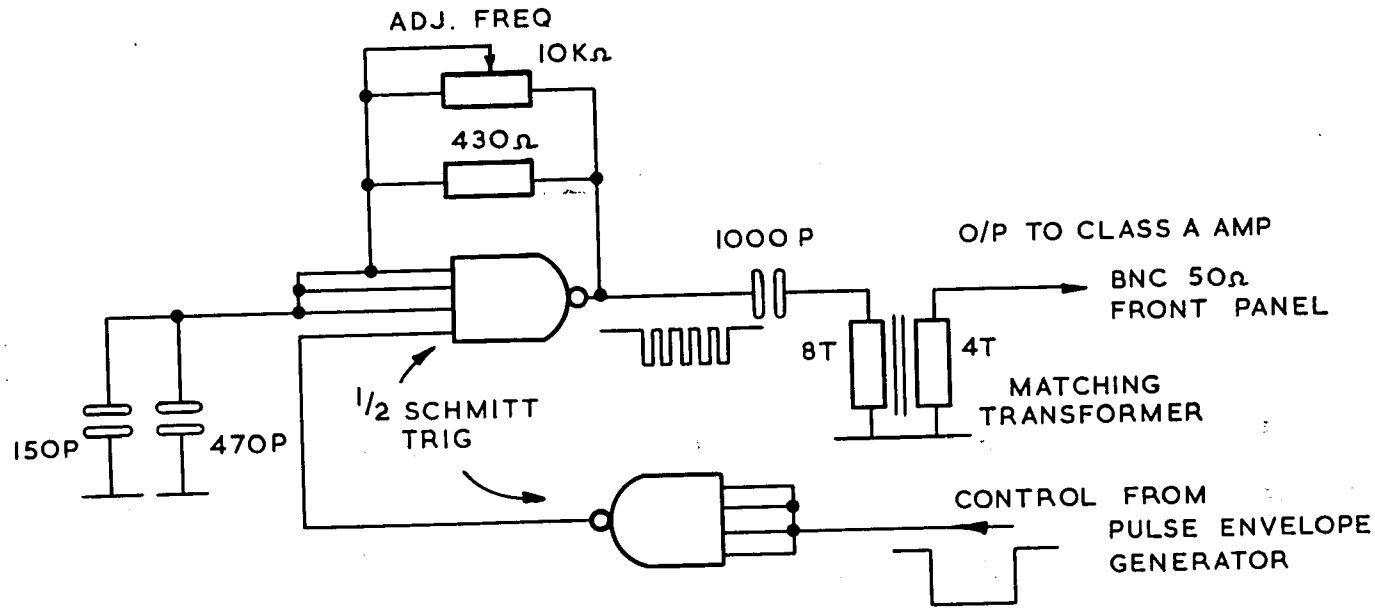

FIG. A2 TRANSMITTER OSCILLATOR

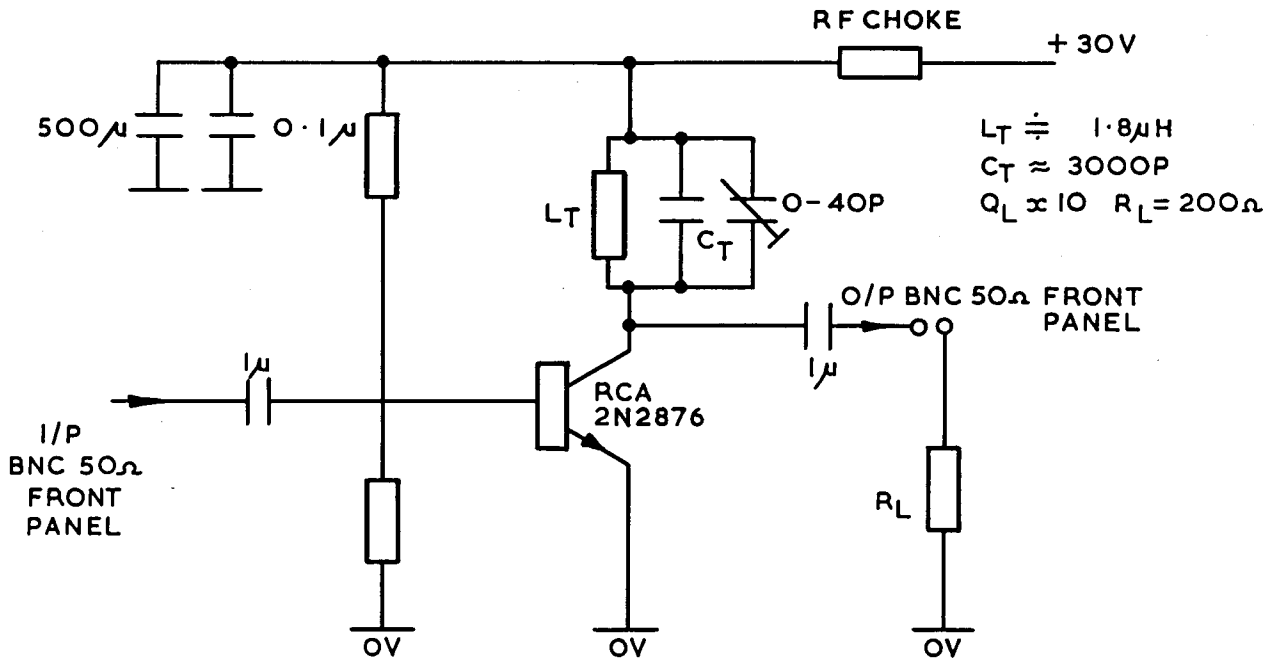

RESPONSE AT 2·5MHz

0·9V PK–PK I/P, 40V PKPK O/P INTO 50Ω

0·28V PK–PK I/P, 40V PKPK O/P INTO 220Ω

FIG. A3 2·5MHz CLASS A TRANSMITTER AMPLIFIER

adequate for the purpose, if not the most efficient design, and was capable of about 8 watts peak power into 50 ohms at 2.5 MHz. A voltage gain of approximately 33 dB was obtained with this circuit and the source level was varied when necessary by inserting a 50 ohms attenuator into the feed cable to the transducer. Note that no tuning of the transducer was attempted to neutralise the capacitance load.

A1.4 The linear sweep generator path length (PL)

An analogue voltage proportional to the elapsed time after transmission was provided by the sweep generator. At the instant when an echo was detected, this voltage was sampled and passed to the digital computer to enable a calculation of echo range to be performed. Because this signal was input to the ADC peripheral attached to the computer, the sweep characteristics were designed to be compatible with the ADC characteristics given in Table 3.1 of CHAPTER III. A maximum sweep amplitude of 5V was provided, with a duration controlled by the master timing oscillator of approximately 0.75 ms. A sweep error of less than 5 mV was required to be compatible with the least significant bit value of the ADC. This translated into a displacement error (defined as the maximum departure from a linear sweep) of 0.1 per cent, and a transmission error (defined as the maximum deviation from the design value of the sweep voltage at the end of the sweep) of 0.1 per cent.

The sweep reset time was not important because the PRF of transmissions could be adjusted to suit.

Using these parameters a standard operational amplifier integrator circuit was designed using the LM709C amplifier. This circuit was based on a similar design given in SGS,UK, Applications of linear IC's, 1970 and is shown in figure A4. A balanced FET input stage was employed to reduce offset currents and the sweep errors associated with these.

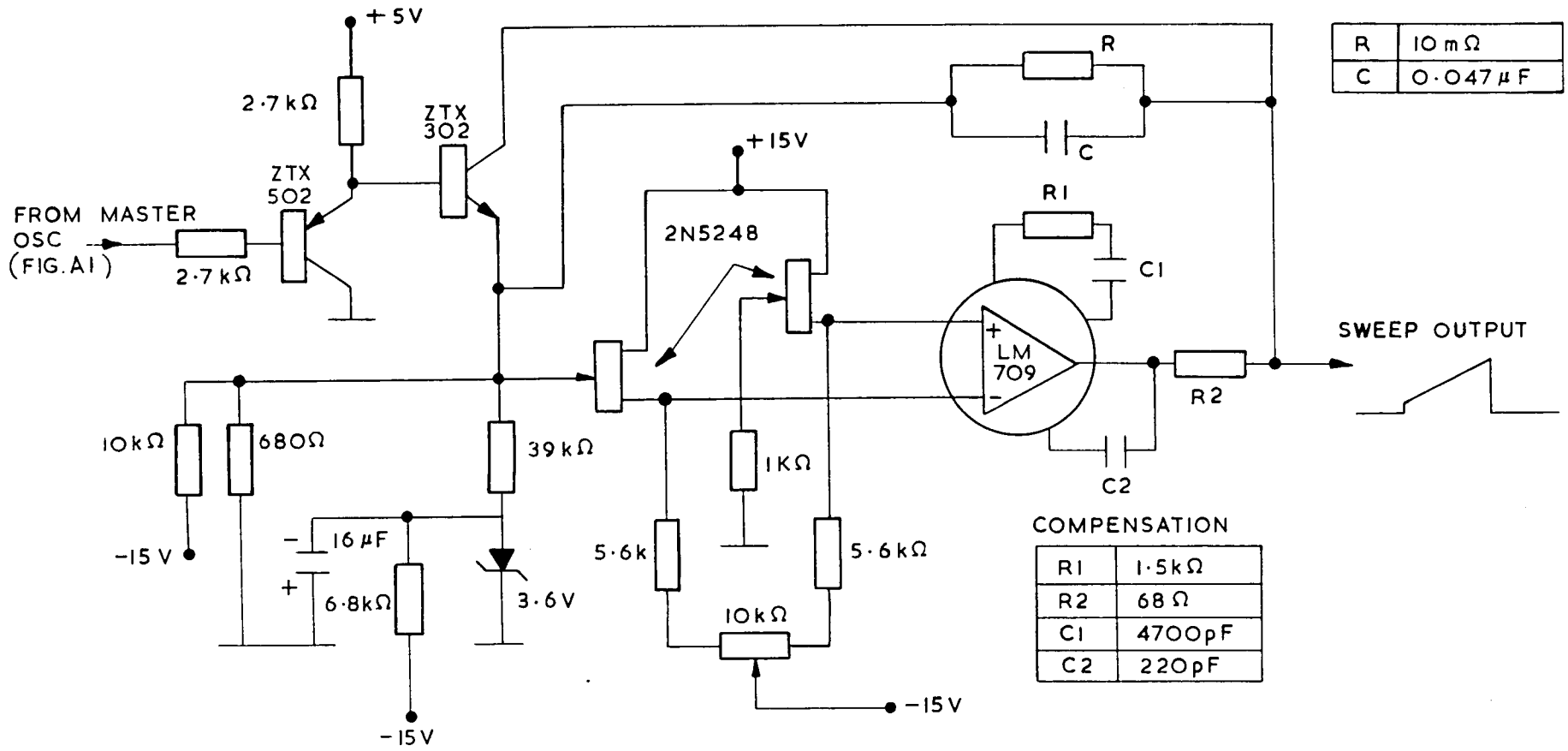

R	10 mΩ
C	0·047 μF

COMPENSATION

R1	1·5kΩ
R2	68 Ω
C1	4700pF
C2	220pF

FIG. A4 LINEAR SWEEP GENERATOR

FIG. A4

A ZTX302 transistor switch was employed to discharge the circuit back to zero volts.

The sweep was started when the correct polarity pulse was applied to the ZTX502 input stage. This open-circuited the ZTX302 switch and allowed the capacitor to charge linearly from an equivalent constant current source. The reference voltage required by this circuit was provided by a 3.6V zener diode as shown, and the sweep output fed via a buffer amplifier to the sample and hold circuit described below.

A1.5 The sweep sample and hold circuit

The specification for the ADC interface to the computer indicated that the total time required to scan the four data input channels under program control would be about 70 μs. Allowing for tolerances and signal setting times a figure of 80 μs was taken as being representative of the total time. During this period the sweep output described above could change by a maximum which was equivalent to approximately 12 cms of range, and because of this unacceptable situation a track and hold circuit was incorporated into the system. The output of the sweep generator was therefore fed to the track and hold circuit shown in figure A5.

The specification for the circuit required that during a hold time of 80 μs that the sampled voltage did not decay by more than 5 mV. From this requirement, and a maximum holding voltage of 5V, a hold capacitor of 0.1 μF was chosen. With this value of capacitor, the circuit reset time from the hold to track mode was about 8 μs, which effectively increased the latency in the data input phase to approximately 90 μs. The output of the holding capacitor was input to a high impedance, non-inverting, LM709C buffer amplifier which also incorporated voltage offset control which was used to null the small

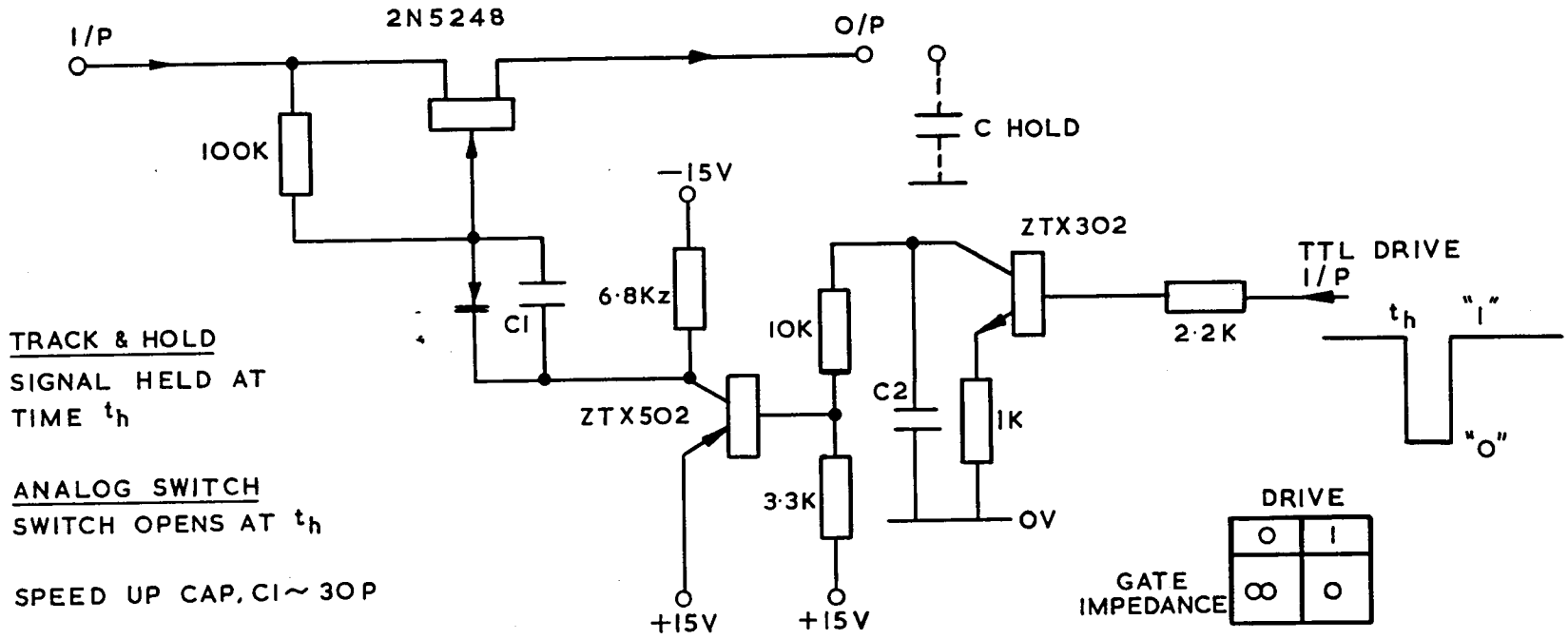

FIG A5. ANALOG FET GATE CIRCUIT

positive offset voltage associated with the sweep generator. Note that this buffer amplifier is not shown.

A1.6 The pulse amplitude modulator (data base DB)

The function of this circuit was to generate a set of amplitude weighted pulses of 80 μs duration whose amplitudes were proportional to the separation between the transmitter and the particular receiver which triggered the channel selector. The duration of each pulse was fixed by the channel selector monostables and corresponded to the track and hold circuit specification.

The circuit is shown in figure A6, and consisted of an operational weighting network using an LM709C amplifier. The inputs to this circuit were the logic pulse outputs of the channel selector circuit. These pulses were amplitude scaled by the preset potentiometers shown to correspond to the separation of each receiver, and this adjustment formed part of the calibration procedure described in CHAPTER IV. Independence of each adjustment was ensured by using the LM709C to form a virtual earth point at the junction of all the potentiometer outputs and in addition offset and gain controls were provided to enable the output to be properly scaled with respect to the ADC interface in the computer. The actual output of the circuit was first fed to a unity gain power amplifier described below, which provided sufficient power to transmit the signal down the data link cable to the remote computer suite. The accuracy of the amplitude scaling of each pulse was better than 5 mV in accordance with the requirement of the ADC least significant bit value.

A1.7 The channel selector circuit

The channel selector logic is shown in figure A7, and the circuit was designed to provide four output pulses as follows:-

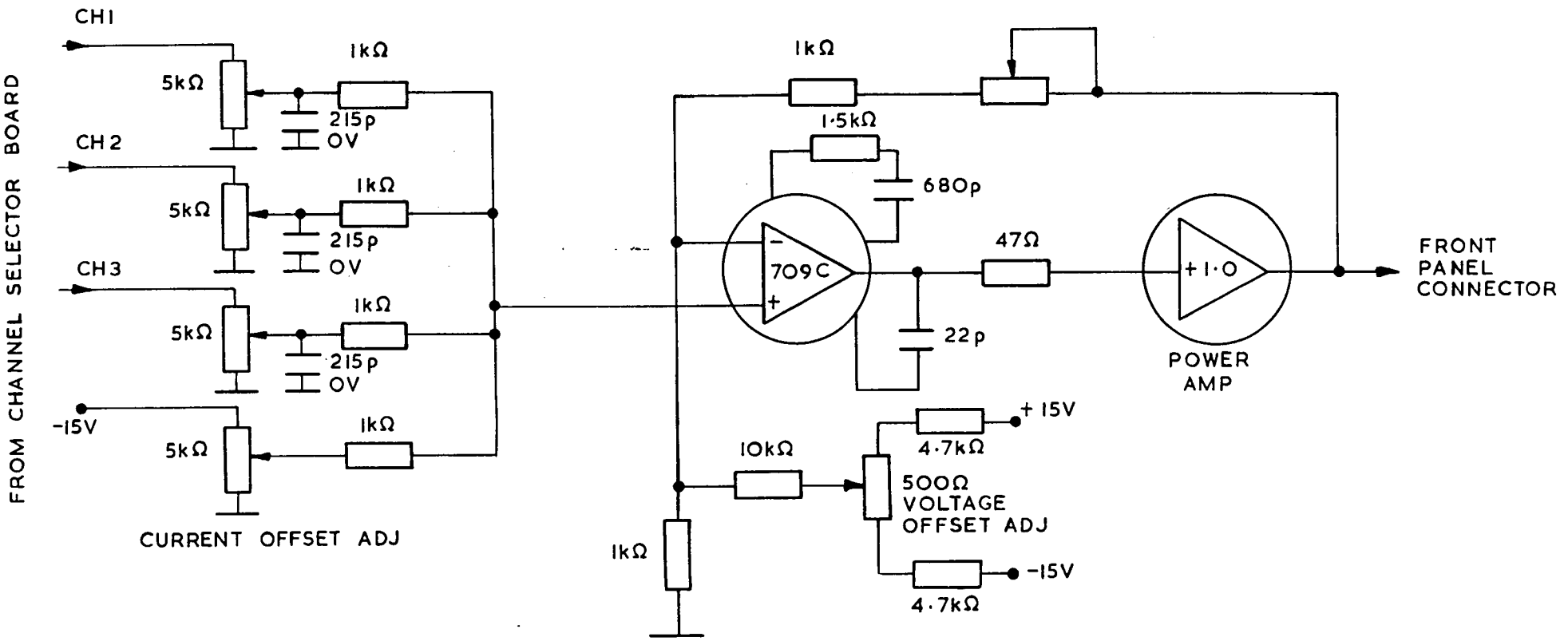

FIG. A6 DB GENERATOR (P.A.M.)

FIG. A6

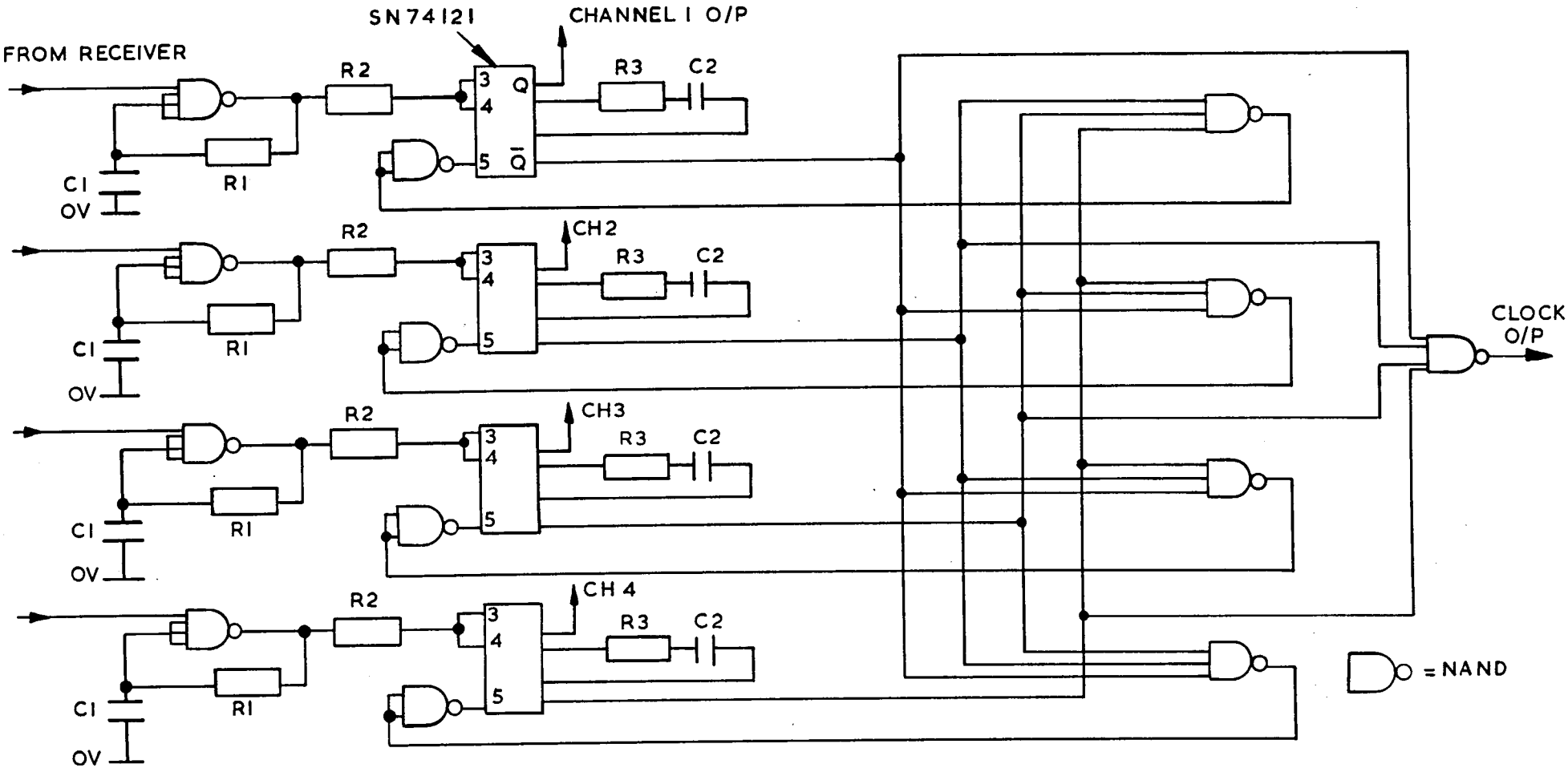

FIG. A7 (BOARD 2) CHANNEL SELECTOR

FIG. A7

(a) The clock pulse used to drive the sample and hold circuit described above,

and (b) A unique logic pulse, one for each of three receivers.

The pulses were all of 80 μs duration, controlled by the monostables incorporated in each input stage, and were generated whenever the input signals from the receiver outputs exceeded the upper trigger level of the Schmitt trigger circuits in the inputs. The clock pulse was the logical 'OR' of the other pulses. Feedback to pin 5 of the monostables (SN74121) ensured that if any one channel was triggered by a received echo, then for a period of 80 μs thereafter no other output pulse could occur until the original monostable had reset. Since these pulses were input directly to the pulse amplitude modulator, this ensured that no ambiguities concerning which receiver had detected the echo could result.

The Schmitt trigger circuits which formed the input stage of the circuit received the bandpass filtered and dc biased signals from the receiver circuits and the consistency of the detection process therefore relied upon the constancy of the temperature controlled Schmitt trigger level.

A1.8 The azimuthal bearing measurement and scaling circuit

The mechanical scanner was driven at approximately 14 revs/min by the 50 Hz ac supply used. This meant that for a 90 degree sector scan, the time for a complete sweep was about 1.08 seconds.

The data input scan at the ADC interface took 80 μs, and this corresponded to a bearing change of approximately $0.64.10^{-2}$ degrees at the scanner. Since the bearing voltage was also the first signal digitised, this further reduced the bearing change during digitisation and no sample and hold was necessary to preserve the bearing at the instant of echo detection.

The actual bearing was generated by a linear potentiometer driven by the scanner and fed from a +5 volts stabilised supply. Provided the potentiometer wiper was not loaded, then a voltage directly proportional to angle would be obtained at this point. The wiper output was consequently connected to the buffer circuit shown in figure A8(a), which consisted of an FET front end to ensure minimal loading of the potentiometer, and an LM709C amplifier to provide offset and scale adjustments. For a 0-90 degree sector scan, the output was adjusted to a voltage range of 0-4.5 volts, which in turn gave a 0.1 degree accuracy after digitisation. The output of the operational amplifier was connected to a unity gain power amplifier described below, and the output of this connected on to the data link to the computer.

Calibration of the system consisted of a check that the scanner was traversing a 90 degrees sector, then a gain adjustment to ensure a corresponding 0-4.5 volt sweep and an offset adjustment to ensure that the sweep started at 0 volts. Fig A8(b) shows the result of a calibration in which the circuit output was connected to the Y axis of an XY recorder. It can be seen that linearity was maintained throughout the range and consistent results obtained for this highly sensitive measurement.

A1.9 The receivers

The outputs of each receiver transducer were input to the corresponding receivers shown in figure A9. The function of each receiver was to bandpass filter and amplify the echoes received, and then add the resulting ac waveform to a variable dc bias. The resulting signal was then input to the Schmitt trigger channel selector circuits described above. The bias voltage was controlled by a potentiometer on the front panel of each receiver, and allowed the echo excess (above the background) needed to trigger the channel selector to be varied.

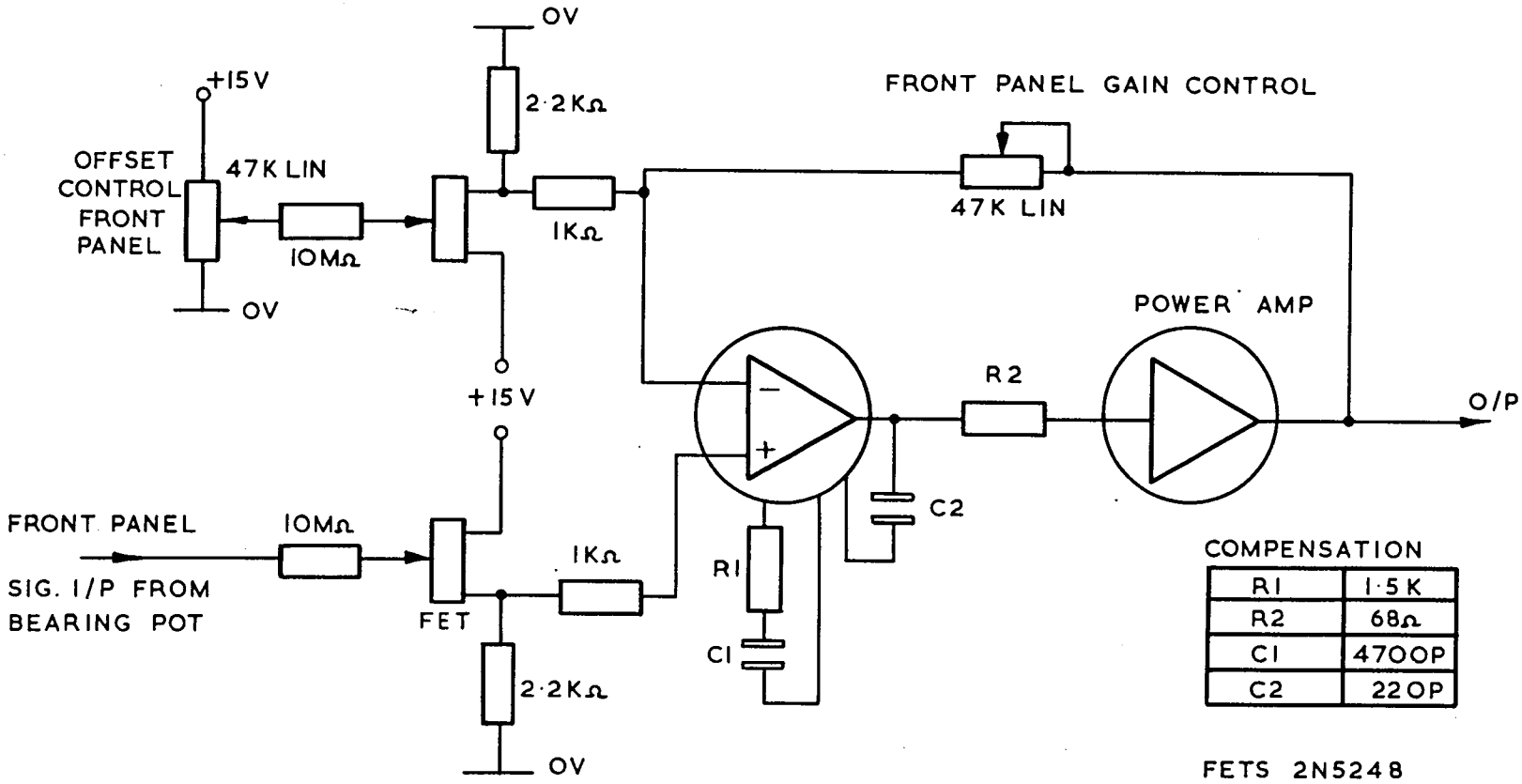

FIG. A8(a) BEARING SCALING & BUFFER AMP.

FIG. A8(a)

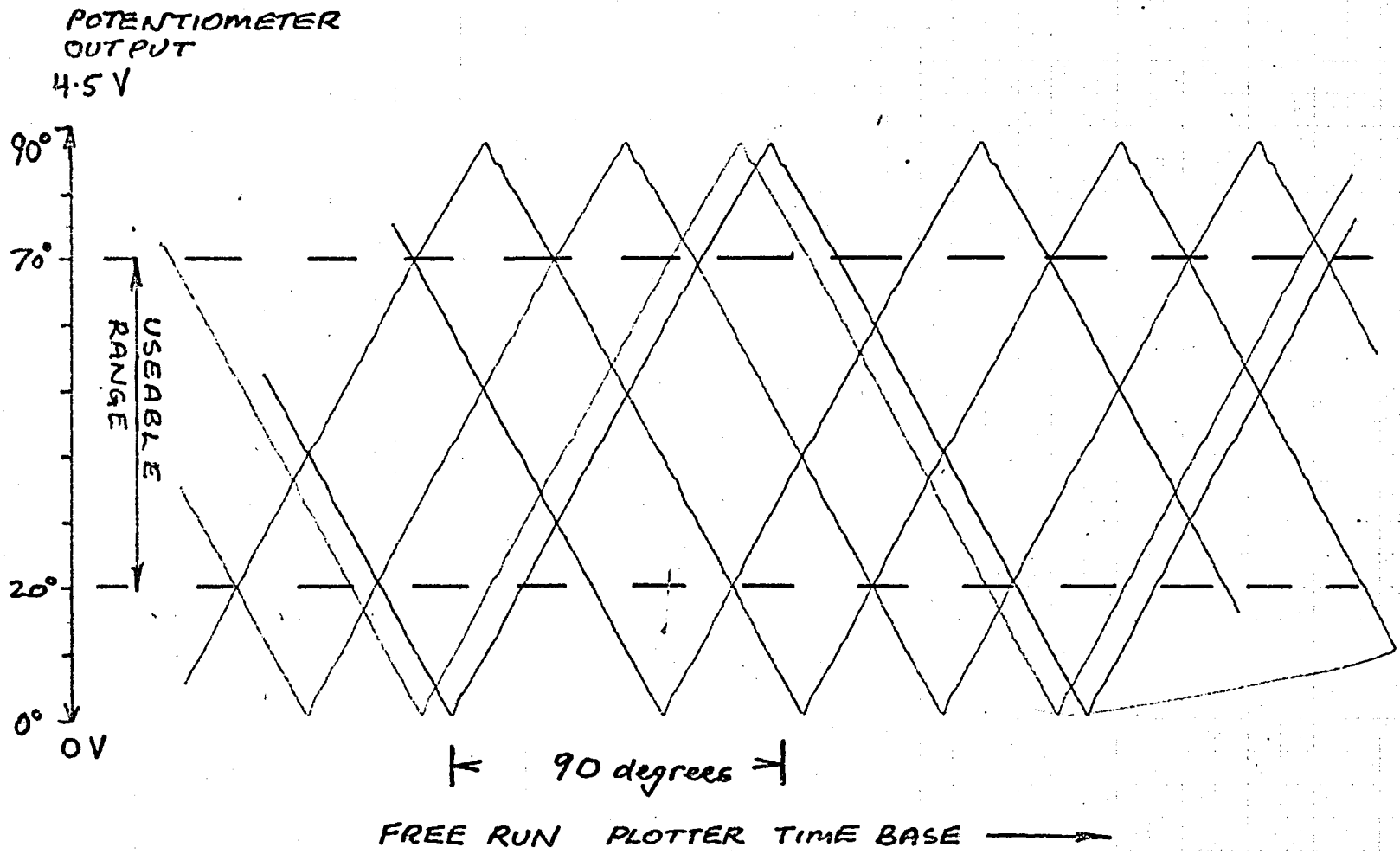

FIG A8(8) LINEARITY TEST

FIG A8(b)

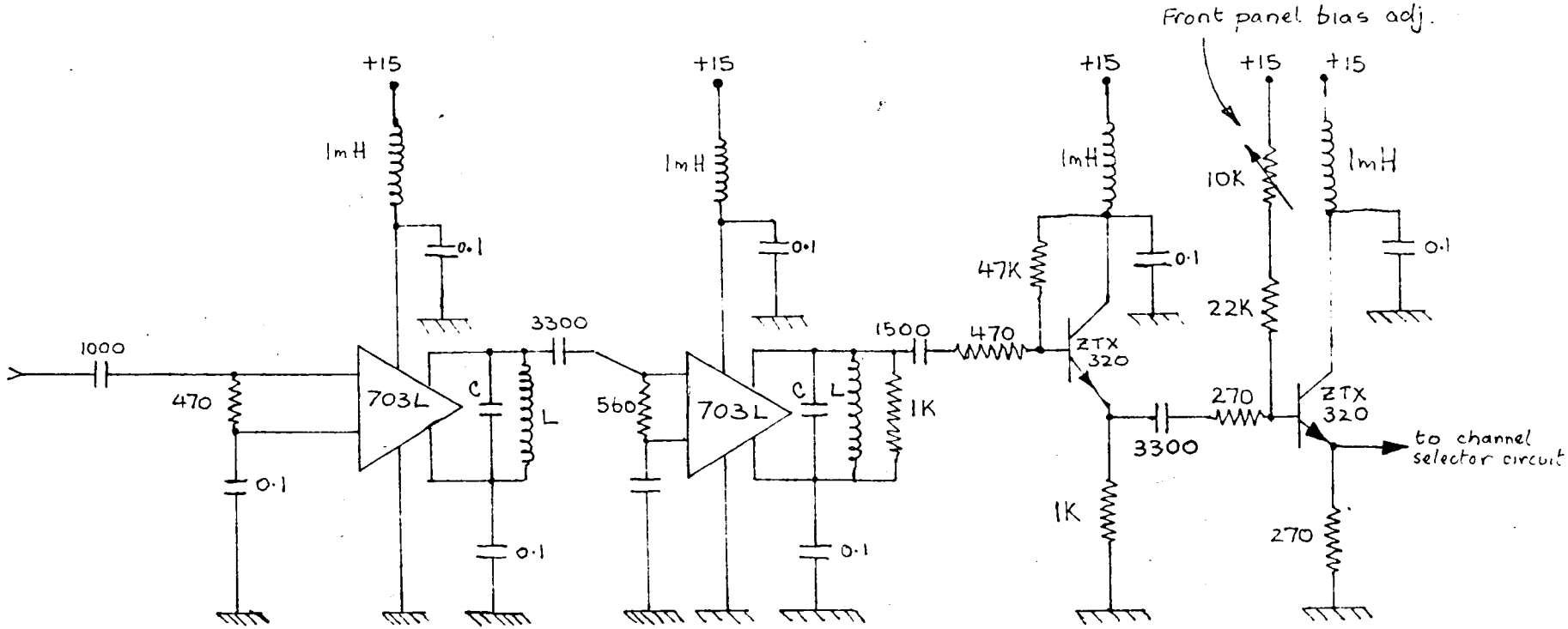

NOISE LEVEL AT OUTPUT WHEN CONNECTED TO TRANSDUCERS = 60 mV pk to pk.
MINIMUM RELIABLE SCHMITT TRIGGER LEVEL ≃ 50 mV pk (+Ve going)
Power gain ≃ 16 dB
C ≃ 1047 pF
L ≃ 3·9 μH

FIG A9 THE RECEIVER

FIG A9

Each stage of the two stage receiver was a simple class A tuned amplifier which used an LM703L RF amplifier as the active device. The tuned circuits were designed with a Q-factor of approximately 10 at 2.5 MHz and the voltage gain of the complete receiver was approximately 30 dB. The output of the final tuned stage was buffered with an emitter-follower to provide isolation from the bias network. The addition of a dc bias to the output was achieved by using another emitter-follower stage with a variable base resistor to adjust the quiescent current through the emitter resistor.

Precautions were necessary with the receiver circuits regarding decoupling of each stage, and L and C components were included in the power supply to prevent feedback via this path. It was also found initially that because of the close proximity of each receiver board, cross coupling between the circuits was occurring. This necessitated the mounting of screening cans around each board.

A1.10 The hydrophone pre-amplifiers

The hydrophone amplifier shown in figure A10 was used in each of the bistatic receivers to provide an initial voltage gain of approximately 14 dB. The requirement was for a high input impedance so that minimal loading of the capacitive source would occur, and a low output impedance to drive the long co-axial cable link to the receivers described above. The design used employed an FET input stage to provide a high input impedance, and was followed by a single stage amplifier and finally an emitter follower output stage. The frequency response of the circuit is shown in figure A10 and was rolled off at about 3 MHz by the RC filter in the emitter circuit of the voltage amplifier stage.

A1.11 Scanner drive motor controller

The controller shown in figure A11 changed the direction of rotation in the appropriate sense at the ends of the 90 degree

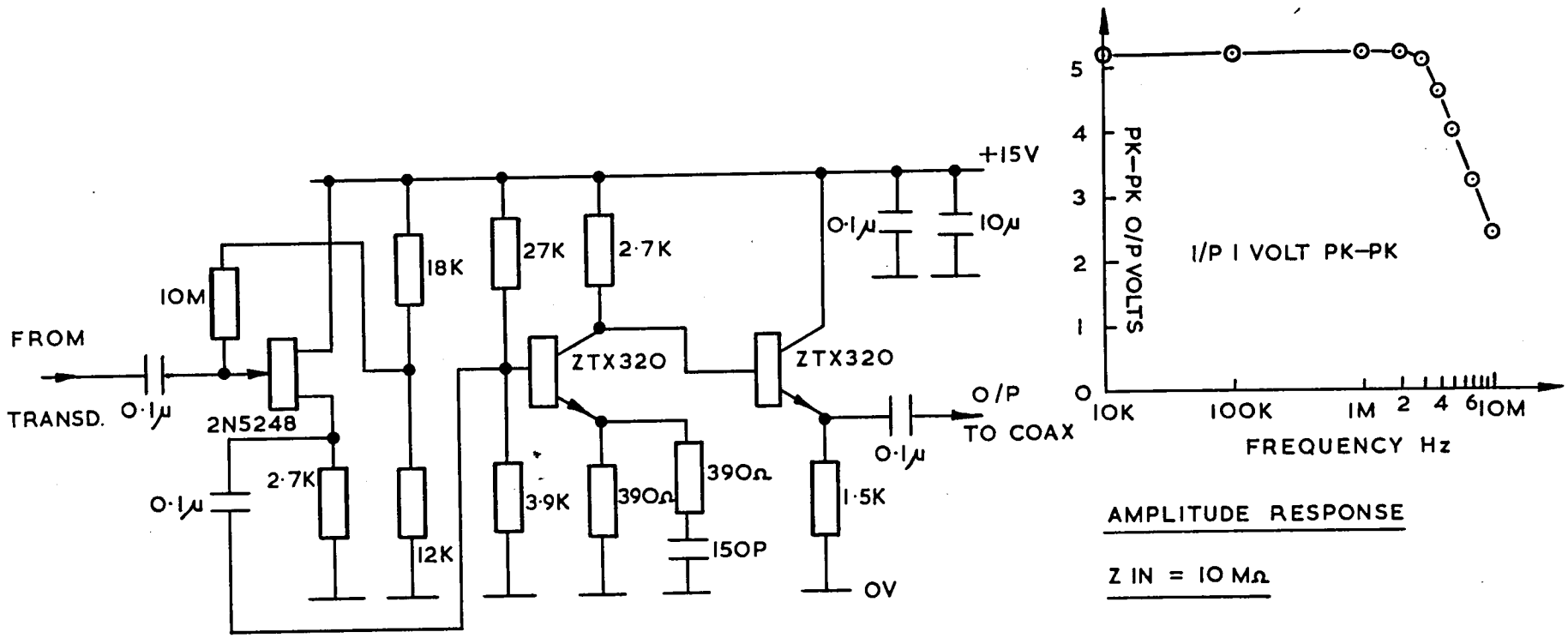

FIG.AIO. HYDROPHONE PROBE AMPLIFIER

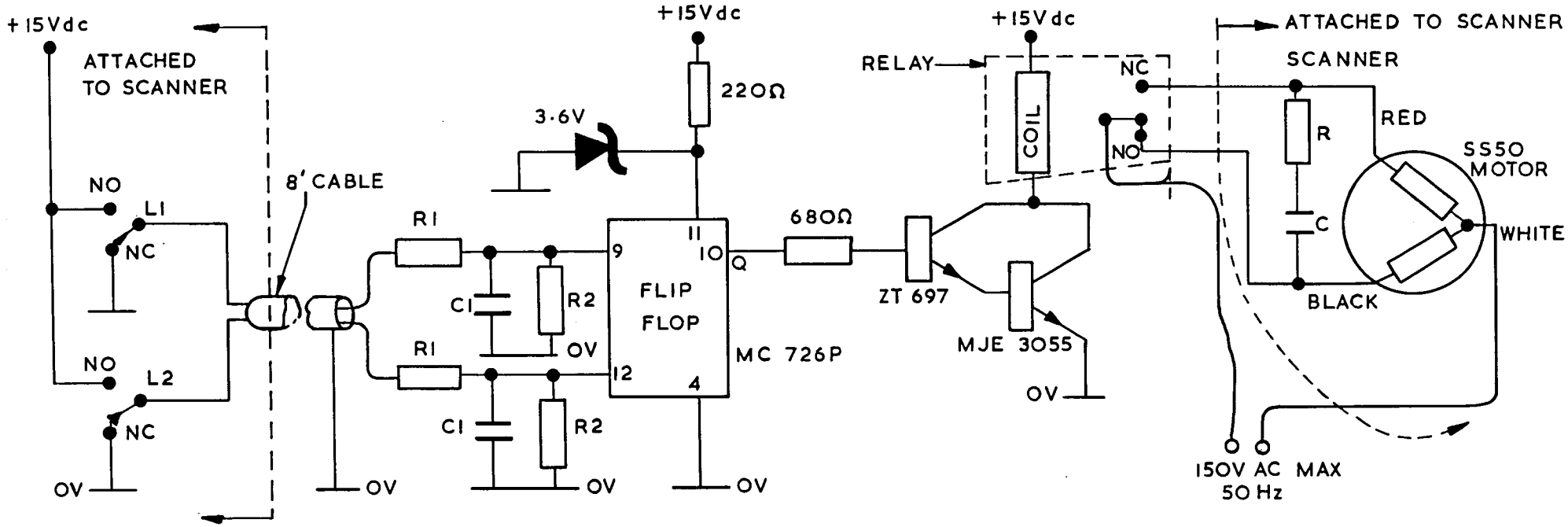

FILTER
R1 = 8·2kΩ
R2 = 1kΩ
C1 = 0·1μF

NC = NORMALLY CLOSED
NO = NORMALLY OPEN
PINS 2, 3 AND 13 GROUNDED

FIG A11. SS50 STEPPING MOTOR CONTROLLER

sector scan. This was achieved by using a bistable circuit to control the motor relay shown. The bistable circuit was set and reset by the limit switches attached to the mechanical scanner shown in figure 3.2 of CHAPTER III. These limit switches were spaced 90 degrees apart and were operated by a cam fixed to the scanner shaft.

The output of the bistable was used to change the state (off to on) of the MJE 3055 power transistor, which in turn, energised and de-energised the relay. The relay was connected up in such a way that operation of the contacts changed the direction of rotation of the stator field in the SLO-SYN type SS50 stepping motor which was employed to drive the scanner. Reversing the stator field caused reversal of the rotor and the transmitter-receiver transducer was thus scanned through a 90 degrees sector.

Because the cable linking the controller to the limit switches was long, a simple RC filter arrangement was used at the input to the bistable to prevent spurious noise spikes from triggering the bistable.

A1.12 Data link power amplifier

The analogue sonar equipment and the remote digital computer required a data link comprising approximately 300 feet of multicored telephone cable. The main difficulty, concerned with transmitting signals down this cable without attenuation and distortion, was providing sufficient drive current to charge and discharge the cable capacitance. It was found that each signal had to be buffered through a power amplifier before transmission down the cable. This power booster was incorporated inside the feedback loop of the operational amplifier circuit, and the design shown in figure A12 was based on a published design in SGS UK, Applications of Linear IC's, Volume I, 1970. This circuit was capable of giving $\pm$ 100 mA into a 100 ohms load and was adequate for the purpose. The frequency response is shown inset in figure A12 and was flat up to 100 kHz.

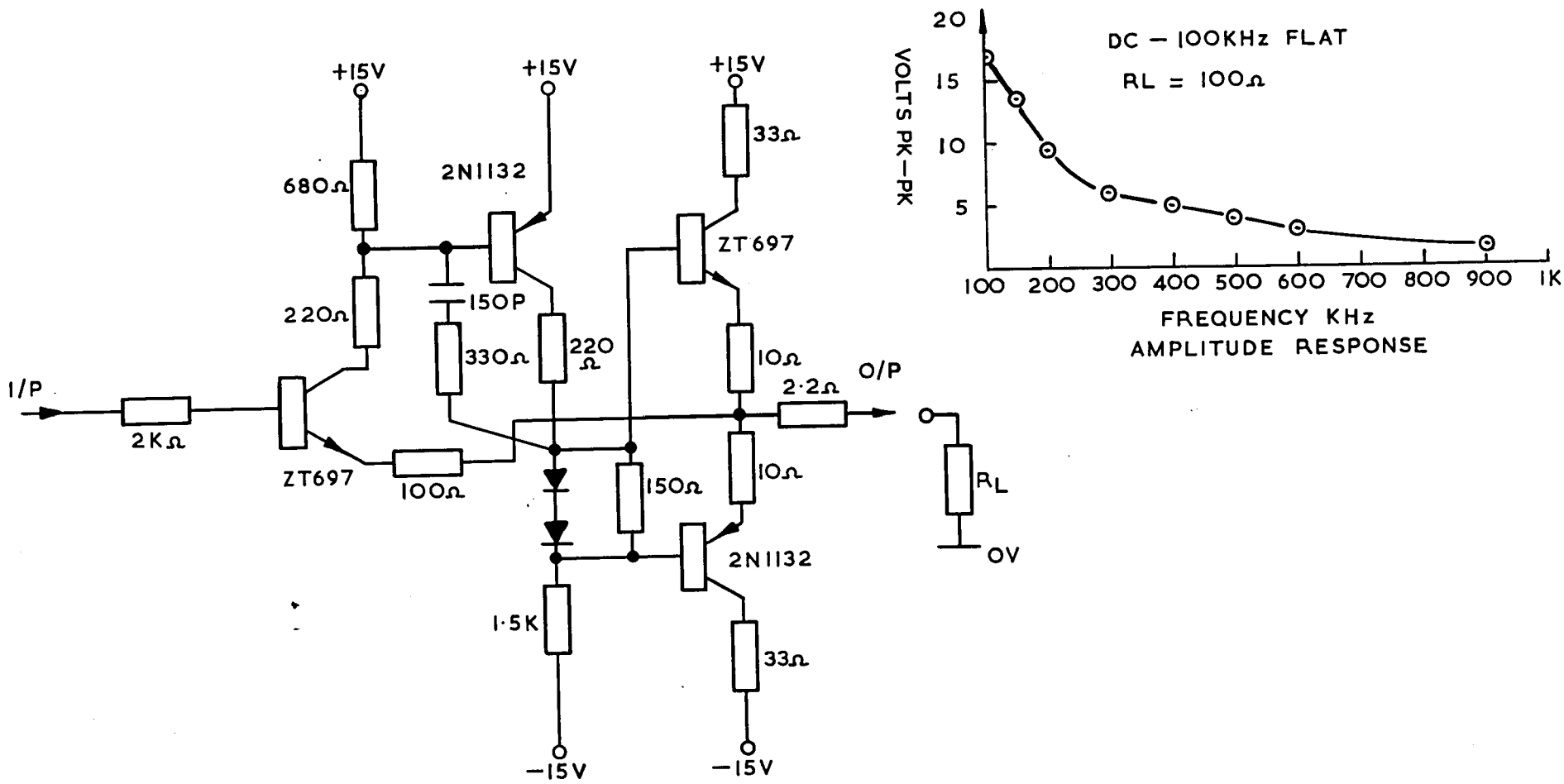

FIG A12 UNITY GAIN POWER AMPLIFIER CIRCUIT

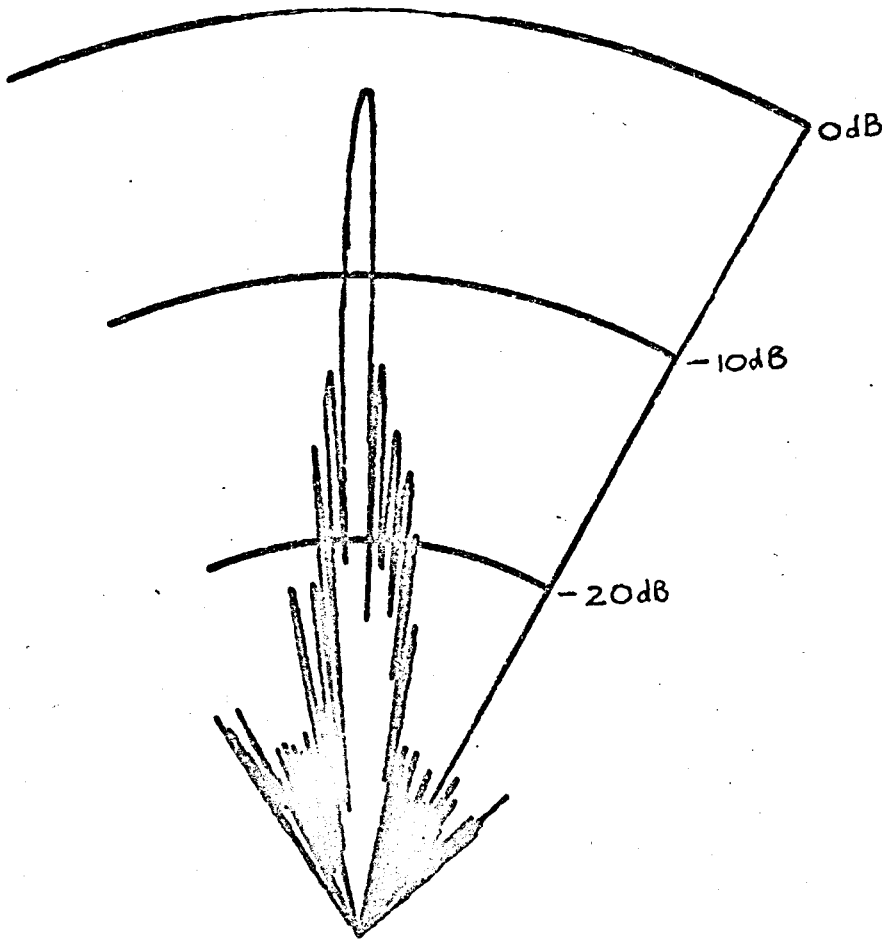

FIG A13 THE MEASURED TRANSMITTER BEAM PATTERN

REFERENCES

1. A D Dunsiger, A study of underwater acoustic target recognition using simple geometric shapes,
   Ph D thesis submitted to the University of Birmingham, 1968.
2. T H Glisson, C I Beach, A P Page, On sonar signal analysis, IEEE Transactions on Aerospace and Electronic Systems, Vol AES-6, No 6, 1970.
3. A D Dunsiger, High-frequency acoustic echoes received from simple geometric shapes with possible application to target recognition, Journal of Sound and Vibration, Vol 13, No 3, 1970.
4. A Freedman, A mechanism of acoustic echo formation, Acoustica, Vol 12, No 2, 1962.
5. A Freedman, The high-frequency echo structure of some simple body shapes, Acoustica, Vol 12, No 2, 1962.
6. A Freedman, The portrayal of body shape by a sonar or radar system, Journal of British IRE, January 1963.
7. A D Dunsiger, A study of acoustic echoes from solid cylindrical targets, Journal of Sound and Vibration, Vol 8, No 2, 1968.
8. G Toraldo di Francia, Resolving power and information, Acoustic Society of America, Vol 45, No 7, 1955.
9. J A Ratcliffe, Some aspects of diffraction theory and their application to the ionosphere, Reports on Progress in Physics, Vol XIX, 1956.
10. J Parker, Reflection of plane sound waves from an irregular surface, Journal of the Acoustic Society of America, Vol 28, No 4, 1956.
11. W C Meecham, Fourier transform method for the treatment of the problem of the reflection of radiation from irregular surfaces, Journal of the Acoustic Society of America, Vol 28, No 1, 1956.

12. W C Meecham, On the use of the Kirchoff approximation for the solution of reflection problems, Journal of Rational Mechanical Analysis, Vol 5, No 2, 1956.

13. P Beckmann, A Spizzichino, Scattering of EM waves from rough surfaces, Pergammon Press, 1963.

14. H G Booker, P C Clemmow, The concept of an angular spectrum of plane waves and its relation to that of polar diagram and aperture distribution, Proceedings of the IEEE, Vol 97, No 3 1950.

15. T H Glisson, C I Black, A P Page, The digital computation of discrete spectra using the fast fourier transform, IEEE transactions on Audio and Electroacoustics, Vol AU-18, No 3, 1970.

16. J W Cooley, P D Welch, Application of the FFT to computation of fourier integrals, Fourier series, and convolution, IEEE Transactions on Audio and Electroacoustics, Vol AU-15, No 2, 1967.

17. G L Turin, An introduction to matched filters, IRE Transactions on Information Theory, June 1960.

18. M Schwartz, Information Transmission Modulation and Noise, McGraw-Hill, 1970.

19. M I Skolnik, An analysis of bistatic radar, IRE Transactions on Aerospace and Navigational Electronics, Vol ANE-8, 1961.

20. S Ying, Single narrow beam ultrasonic transducer with conical and wedge-shaped collimators, IEEE Transactions on Sonics and Ultrasonics, Vol SU-14, No 2, 1967.